

INFRARED PHOTODISSOCIATION SPECTROSCOPY
OF PROTONATED COMPLEXES

By

TIMOTHY CALEB CHENG

(Under the Direction of Michael A. Duncan)

ABSTRACT

Protonated complexes are produced via arc discharge in a molecular beam apparatus and probed using infrared photodissociation spectroscopy. The effects of protonation on the relative energies of the cis and trans configurations of protonated glyoxal are investigated with theoretical calculations. Upon protonation, the cis configuration is lower in energy than the trans configuration. Protonated hydrogen clusters are studied, and the spectra are assigned with the help of anharmonic theory. The structure of H_5^+ is a shared proton between two hydrogen molecules, while larger hydrogen clusters have a H_3^+ center solvated by neutral hydrogen. The effects of solvation, such as charge delocalization and polarization, in mixed protonated benzene-water clusters are also investigated.

INDEX WORDS: Infrared Spectroscopy, Protonation, Proton Transfer, Solvation, Physical Chemistry, Laser Spectroscopy

INFRARED PHOTODISSOCIATION SPECTROSCOPY
OF PROTONATED COMPLEXES

By

TIMOTHY CALEB CHENG

B.A., Ouachita Baptist University

A Dissertation Submitted to the Graduate Faculty of the University of Georgia

In Partial Fulfillment of the Requirements for the Degree

DOCTOR OF PHILOSOPHY

ATHENS, GEORGIA

2012

© 2012

Timothy Caleb Cheng

All Rights Reserved

INFRARED PHOTODISSOCIATION SPECTROSCOPY
OF PROTONATED COMPLEXES

By

TIMOTHY CALEB CHENG

Major Professor:

Michael A. Duncan

Committee:

Geoff Smith
Henning Meyer

Electronic Version Approved:
Maureen Grasso
Dean of the Graduate School
The University of Georgia
May 2012

DEDICATION

I dedicate this dissertation to my mother. You will always be remembered.

Angie Liu Cheng: November 15, 1948 – May 7, 2011

ACKNOWLEDGEMENTS

I had the privilege to work and make memories with many people throughout my graduate career. There are far too many people to thank, and I like keeping things short.

To my family, thanks for always supporting me, helping me, and giving me advice all these years. I could not have done it without your support. Trying to teach scientific principles to my niece and nephews in simple ways that they can understand is both challenging and funny.

I wouldn't be at this stage of my life without the help of my advisor, Mike. Even if I forget all principles of spectroscopy and chemistry later in life, you have taught me life lessons I will always remember. I am a better person today compared to when I first got to graduate school because of you. Your passion for what you love and in helping others is something I strive for.

To all the Duncan graduate students, thanks for putting up with me all these years, it was fun. You made working at lab enjoyable. You guys were the reason I stayed 30 minutes longer than I planned every day, always talking for a while after saying "I'll be leaving soon." Special thanks are required to all the App 2 people that I collaborated with during my time, especially Biswajit. Taking the midnight shift on the App is something I never have to do again, but even that was interesting in its own way.

To my other friends, thank you for keeping me sane throughout the years.

TABLE OF CONTENTS

	Page
ACKNOWLEDGEMENTS.....	v
CHAPTER	
I. INTRODUCTION.....	1
References.....	5
II. EXPERIMENTAL SETUP.....	22
References.....	31
III. INFRARED PHOTODISSOCIATION SPECTROSCOPY OF GLYOXAL CATION AND THEORETICAL CALCULATIONS OF PROTONATED GLYOXAL.....	42
Abstract.....	43
Introduction.....	44
Experimental Setup.....	45
Results and Discussion.....	47
Conclusion.....	53
References.....	54
IV. INFRARED PHOTODISSOCIATION SPECTROSCOPY OF PROTONATED HYDROGEN CLUSTERS.....	72

Abstract.....	73
Introduction.....	74
Experimental Setup.....	77
Results and Discussion.....	78
Conclusion.....	88
References.....	90
V. INFRARED PHOTODISSOCIATION SPECTROSCOPY OF PROTONATED BENZENE-WATER CLUSTERS.....	109
Abstract.....	110
Introduction.....	111
Experimental Setup.....	113
Results and Discussion.....	115
Conclusion.....	127
References.....	128
VI. CONCLUSIONS.....	159
APPENDIX.....	161

CHAPTER I

INTRODUCTION

The addition of a proton to a molecule, known as protonation, is integral to many aspects of Chemistry and Biology. Protonation is involved in acid-base reactions, atmospheric reactions, biological reactions, electrochemistry, and a plethora of other areas.¹⁻⁴ Structural changes upon protonation lead to changes in reactivity, solubility, etc.⁵⁻¹⁰ The focus of this dissertation lies in understanding the structural changes that occur upon protonation, especially in proton-shared complexes and the effects of solvation on these systems.

There have been many studies focusing on the infrared spectroscopy of gas phase protonated molecules.¹¹⁻³⁹ Gas-phase studies are performed to understand the fundamental nature of a protonated complex without the influence of the environment. Infrared spectroscopy examines the vibrational modes of these complexes, and is used to identify the structure of these complexes. The effects of protonation include structural changes to favor one configuration over another.

Neutral glyoxal has two stable isomers that have been observed in nature corresponding to a cis-trans isomerization.⁴⁰⁻⁴¹ The *trans*-glyoxal structure is the primary structure observed in nature, and is 3.2 kcal/mol lower in energy than *cis*-glyoxal.⁴²⁻⁴³ Theory predicts that the protonated *cis* structure is lower in energy than the *trans* structure.⁴⁴ This is because an intramolecular shared proton, where the proton is shared between the two oxygen atoms, is

possible in the cis configuration. These shared proton complexes are key structures for studying the dynamics of proton transfer reactions.⁴⁵⁻⁴⁷

One of the most famous shared proton molecules is the Zundel ion, whose structure has an equally shared proton between two water molecules.⁴⁸⁻⁴⁹ Protonated water clusters have been studied extensively because of their various isomeric structures and importance in numerous chemical and biological processes.⁵⁰⁻⁵⁶ Work by Saykally and coworkers included the first high resolution infrared spectrum of hydronium, and larger protonated water clusters have been studied extensively.⁵⁷⁻⁵⁹ Asmis and coworkers studied the low frequency modes of the protonated water dimer using a free-electron laser, and assigned the spectrum obtained to be the Zundel ion.⁶⁰ The O-H bond positions of various protonated water cluster sizes have been investigated by Lee and coworkers.⁶¹⁻⁶² Our research group in collaboration with Johnson and coworkers has studied protonated water complexes up to 22 water molecules.⁶³⁻⁶⁷ Isotopic effects on hydronium and protonated water were studied by Johnson and coworkers, and our group has continued that work with larger protonated water clusters up to n=5.

The smallest shared proton complex is H_5^+ , which has been the focus of many theoretical investigations.⁶⁸⁻⁹⁴ Shared proton complexes are hard to model accurately using harmonic calculations because of anharmonicity coming from the high amplitude motion of the proton in a shallow well. H_5^+ is a model system because of its small size, so high level anharmonic calculations are possible. The interaction of H_3^+ and neutral hydrogen is believed to form H_5^+ .⁷² Oka and coworkers measured the infrared spectrum of H_3^+ , which has now been identified in the interstellar medium. H_3^+ plays a key role in many interstellar reactions.⁹⁵⁻⁹⁸ Due to the abundance of both H_3^+ and H_2 in space, there is interest in the infrared spectrum of H_5^+ , since it may also be present in space. The infrared spectrum of H_5^+ was obtained by Lee and coworkers

in the mid infrared region, and was assigned to the shared proton dimer structure of H_5^+ .⁹⁹⁻¹⁰⁰ Larger hydrogen clusters, such as H_7^+ and H_9^+ , have also been studied. The structures of larger protonated hydrogen clusters are predicted to contain H_3^+ solvated by neutral hydrogen molecules.

The shared proton stretch has been measured for protonated symmetric and asymmetric dimers. A comparison between the difference in proton affinity (ΔPA) and the location of the shared proton stretch was studied by Johnson and coworkers.¹⁰¹ By looking at seventeen different proton-shared dimers, a trend was found where the higher the difference in proton affinity, the higher the frequency of the shared proton stretch. Some protonated dimers with high dipole moments are predicted not to follow this trend. One such example is protonated water-acetonitrile, measured by Johnson and coworkers, where the proton favors water even though it has the lower proton affinity.¹⁰²

There are previous investigations on the spectroscopy of protonated mixed benzene-water clusters.¹⁰³⁻¹⁰⁵ Neutral benzene-water clusters have been studied by Zwier and coworkers while benzene-water cation clusters has been studied by Mikami and coworkers.¹⁰⁶⁻¹¹³ The interest in the structure of protonated benzene-water clusters is applicable especially in biology, where charge is predicted to be located near liquid-gas interfaces. Infrared spectroscopy of protonated biological complexes includes work by Williams, Rizzo, and McMahon.¹¹⁴⁻¹²⁵

In this present work, the infrared spectrum of glyoxal cation is observed using infrared photodissociation spectroscopy. This technique has already been used to study many protonated complexes in our research group.¹²⁶⁻¹³⁹ The effects of protonation on glyoxal is investigated using a variety of theoretical methods. Glyoxal is an ideal system to study the effects of

protonation on energetics because two different stable isomers are known to exist: *cis*-glyoxal and *trans*-glyoxal. The spectra of small protonated hydrogen clusters and their deuterated isotopologues are also measured using the same technique. A full infrared spectrum is obtained above the dissociation limit, while infrared multiphoton dissociation spectroscopy was performed using a FEL for H_5^+ . The bands are assigned with new anharmonic calculations. Larger protonated hydrogen clusters are also studied. Solvation effects are investigated in protonated mixed clusters of benzene and water. These clusters involve a shared proton stretch vibration between two different molecules. Trends in charge delocalization, polarization and the shared proton stretch frequency are investigated by comparing the infrared spectra of subsequent benzene addition on protonated water and on protonated water dimer.

References

1. R P. Bell, *The Proton in Chemistry*, Chapman & Hall, London, 1973.
2. E. Caldin and V. Gold, eds., *Proton Transfer Reactions*, Chapman and Hall, London, 1975.
3. J. T. Hynes, J. P. Klinman, H.-H. Limbach, R. L. Schowen, eds., *Hydrogen-Transfer Reactions*, Vols. 1-4, Wiley-VCH Publishers, Weinheim, 2006.
4. Bertini, H. B. Gray, E. I. Stiefel and J. S. Valentine, *Biological Inorganic Chemistry*, University Science Books, Sausalito, CA, 2007.
5. E. E. Ferguson, F. C. Fehsenfeld and D. L. Albritton, *Gas Phase Ion Chemistry*, edited by M. T. Bowers, Vol. 1, Academic Press, New York, 1979, p. 45.
6. S. T. Ceyer, P. W. Tiedemann, B. H. Mahan, and Y. T. Lee "Energetics of gas-phase proton solvation by NH_3 ," *J. Chem. Phys.* **70**, 14 (1979).
7. H. C. Chang, J. C. Jiang, I. Hahndorf, S. H. Lin, and Y. T. Lee "Migration of an excess proton upon asymmetric hydration: $\text{H}^+[(\text{CH}_3)_2\text{O}](\text{H}_2\text{O})_n$ as a model system," *J. Am. Chem. Soc.* **121**, 4443 (1999).
8. K. Wu, M. J. Iedema, and J. P. Cowin "Ion penetration of the water-oil interface," *Science* **286**, 2482 (1999).
9. C.-T. Chiang, K. S. Shores, M. Freindorf, T. Furlani, R. L. DeLeon, and J. F. Garvey "Size-Restricted Proton Transfer within Toluene-Methanol Cluster Ions," *J Phys. Chem. A* **112**, 11559 (2008).

10. H. P. Cheng, "The motion of protons in water-ammonia clusters," *J. Chem. Phys.* **105** 6844 (1996).
11. Y.-S. Wang, J.-C. Jiang, C.-L. Cheng, S. H. Lin, Y. T. Lee, H.-C. Chang, "Identifying 2-, 3-coordinated H₂O in protonated ion-water clusters by vibrational pre-dissociation spectroscopy, *ab initio* calculations," *J. Chem. Phys.* **107**, 9695 (1997).
12. J.-C. Jiang, Y.-S. Wang, H.-C. Chang, S. H. Lin, Y. T. Lee, G. Niedner-Schatteburg, H.-C. Chang, "Infrared spectra of H⁺(H₂O)₅₋₈ clusters: Evidence for symmetric proton hydration," *J. Am. Chem. Soc.* **122**, 1398 (2000).
13. H.-C. Chang, J.-C. Jiang, I. Hahndorf, S. H. Lin, Y. T. Lee, H.-C. Chang, "Migration of an excess proton upon asymmetric hydration: H⁺[(CH₃)₂O](H₂O)_n as a model system," *J. Am. Chem. Soc.* **121**, 4443 (1999).
14. D. W. Boo, Y. T. Lee, "Infrared spectroscopy of the molecular hydrogen solvated carbonium ions, CH₅⁺(H₂)_n (n=1-6)," *J. Chem. Phys.* **103**, 520 (1995).
15. D. W. Boo, Y. T. Lee, "Vibrational spectroscopy and dynamics of ionic complexes of CH₅⁺ and CH₅⁺(A)_x(B)_y (A, B = Ar, N₂, CH₄; x, y = 0-5)," *Int. J. Mass Spectrom. Ion Processes* **159**, 209 (1996).
16. A. R. W. McKellar and J. K. G. Watson, "The infrared spectrum of H₃⁺ revealed," *J. Mol. Spec.* **191**, 215 (1998).
17. H. Linnartz, T. Speck, J. P. Maier, "High-resolution infrared spectrum of the ν₃ band in Ar-HCO⁺," *Chem. Phys. Lett.* **288**, 504 (1998).

18. H. Linnartz, D. Verdes and T. Speck, "High resolution infrared direct absorption spectroscopy of ionic complexes," *Rev. Sci. Instrum.* **71**, 1811 (2000).
19. F. Dong, D. Uy, S. Davis, M. Child and D. J. Nesbitt, "Supersonically cooled hydronium ions in a slit-jet discharge: High-resolution infrared spectroscopy and tunneling dynamics of HD_2O^+ ," *J. Chem. Phys.* **122**, 224301 (2005).
20. S. A. Nizkorodov, O. Dopfer, T. Ruchti, M. Meuwly, J. P. Maier, E. J. Bieske, "Size effects in cluster infrared spectra: The ν_1 band of $\text{Ar}_n\text{-HCO}^+$ ($n=1-13$)," *J. Phys. Chem.* **99**, 17118 (1995).
21. S. A. Nizkorodov, O. Dopfer, M. Meuwly, J. P. Maier, E. J. Bieske, "Mid- infrared spectra of the proton-bound complexes $\text{Ne}_n\text{-HCO}^+$ ($n=1,2$)," *J. Chem. Phys.* **105**, 1770 (1996).
22. O. Dopfer, S. A. Nizkorodov, M. Meuwly, E. J. Bieske, J. P. Maier, "The ν_3 infrared spectrum of the He-NH_4^+ complex," *Chem. Phys. Lett.* **260**, 545 (1996).
23. O. Dopfer, S. A. Nizkorodov, M. Meuwly, E. J. Bieske, J. P. Maier, "Microsolvation of the ammonium ion in argon: Infrared spectra of $\text{NH}_4^+\text{-Ar}_n$ complexes," *Int. J. Mass Spectrom. Ion. Proc.* **167-168**, 637 (1997).
24. R. V. Olkhov, S. A. Nizkorodov, O. Dopfer, "Hindered internal rotation in ion-neutral molecular complexes: The ν_1 vibration of $\text{H}_2\text{-HCO}^+$ and $\text{D}_2\text{-DCO}^+$," *J. Chem. Phys.* **107**, 8229 (1997).
25. O. Dopfer, R. V. Olkhov, D. Roth, J. P. Maier, "Intermolecular interaction in proton-bound dimers: Infrared photodissociation spectra of Rg-HOCO^+ ($\text{Rg}=\text{He, Ne, Ar}$) complexes," *Chem.*

- Phys. Lett.* **296**, 585, (1998). R. V. Olkhov, S. A. Nizkorodov, O. Dopfer, "Infrared photodissociation spectra of $\text{CH}_3^+ \text{-Ar}_n$ complexes ($n=1-8$)," *J. Chem. Phys.* **108**, 10046 (1998).
26. N. Solca and O. Dopfer, "Infrared Spectra of the Phenol-Ar and Phenol- N_2 Cations: Proton-bound versus π -bound structures," *Chem. Phys. Lett.* **325**, 354 (2000).
27. O. Dopfer, D. Roth, J. P. Maier, "Potential energy surface and infrared spectrum of the $\text{Ar-H}_2\text{Cl}^+$ ionic complex," *J. Chem. Phys.* **114**, 120 (2000).
28. N. Solcà, O. Dopfer, "Protonated benzene: IR spectrum and structure of C_6H_7^+ ," *Angew. Chem. Int. Ed.* **41**, 3628 (2002). 1) N. Solca and O. Dopfer, "Protonation of aromatic molecules: Competition between ring and oxygen protonation of phenol (Ph) revealed by IR spectra of $\text{PhH}^+ \text{-Ar}_n$," *Chem. Phys. Lett.* **342**, 191 (2001).
29. N. Solca, O. Dopfer, "IR spectrum of the benzene-water cation: Direct evidence for a hydrogen-bonded charge-dipole complex," *Chem. Phys. Lett.* **347**, 59 (2001).
30. N. Solca, O. Dopfer, "Interaction of the benzenium ion with inert ligands: IR spectra of $\text{C}_6\text{H}_7^+ \text{-L}_n$ cluster cations ($\text{L}=\text{Ar}, \text{N}_2, \text{CH}_4, \text{H}_2\text{O}$)," *Chem. Eur.* **9**, 3154 (2003).
31. N. Solca, O. Dopfer, "Protonation of gas phase aromatic molecules: IR spectrum of the fluoronium isomer of protonated fluorobenzene," *J. Am. Chem. Soc.* **125**, 1421 (2003).
32. N. Solca, O. Dopfer, "Isomer-selective detection of microsolvated oxonium and carbenium ions of protonated phenol: IR spectra of $\text{C}_6\text{H}_7\text{O}^+ \text{-L}_n$ clusters ($\text{L}=\text{Ar}, \text{N}_2, n \leq 7$)," *J. Chem. Phys.* **120**, 10470 (2004).

33. N. Solca, O. Dopfer, "IR spectrum and structure of protonated ethanol dimer: implications for the mobility of excess protons in solution," *J. Am. Chem. Soc.* **126**, 9520 (2004).
34. N. Solcà and O. Dopfer, "Hydrogen-bonded networks in ethanol proton wires: IR spectra of $(\text{EtOH})_q\text{H}^+ - \text{L}_n$ clusters ($\text{L} = \text{Ar}/\text{N}_2$, $q \leq 4$, $n \leq 5$)," *J. Phys. Chem. A* **109**, 6174 (2005).
35. F. M. Pasker, N. Solca, O. Dopfer, "Spectroscopic identification of carbenium and ammonium isomers of protonated aniline (AnH^+): IR spectra of weakly bound $\text{AnH}^+ - \text{L}_n$ clusters ($\text{L} = \text{Ar}, \text{N}_2$)," *J. Phys. Chem. A* **110**, 12793 (2006).
36. K. R. Asmis, Y. Yang, G. Santambrogio, M. Brümmer, J. R. Roscioli, L. R. McCunn, M. A. Johnson, O. Kühn, "Gas phase infrared spectroscopy and multi-dimensional quantum calculations of the protonated ammonia dimer N_2H_7^+ ," *Ang. Chem. Int. Ed.* **46**, 8691 (2007).
37. T. D. Fridgen, L. MacAleese, P. Maitre, T.B. McMahon, P. Boissel, J. Lemaire, "Infrared spectra of homogeneous and heterogeneous proton-bound dimers in the gas phase," *Phys. Chem. Chem. Phys.* **7**, 2747 (2005).
38. T. D. Fridgen, L. MacAleese, T. B. McMahon, J. Lemaire, P. Maitre, "Gas phase infrared multiple-photon dissociation spectra of methanol, ethanol, propanol proton-bound dimers, protonated propanol and the propanol/water proton-bound dimer," *Phys. Chem. Chem. Phys.* **8**, 955 (2006).
39. O. Asvany, P. Kumar, B. Redlich, I. I. Hegemann, S. Schlemmer, D. Marx, "Understanding the infrared spectrum of bare CH_5^+ ," *Science* **309**, 1219 (2005).

40. F. Wittrock, A. Richter, H. Oetjen, J. Burrows, M. Kanakidou, S. Myriokefalitakis, R. Volkamer, S. Beirle, U. Platt and T. Wagner, "Simultaneous global observations of glyoxal and formaldehyde from space," *Geophys. Res. Lett.* **33**, L16804 (2006).
41. J. D. Blando and B. J. Turpin, "Secondary organic aerosol formation in cloud and fog droplets: a literature evaluation of plausibility," *Atmosph. Env.* **34**, 1623 (2000).
42. R. W. Larsen, F. Pawlowski, F. Hegelund, P. Jorgensen, J. Gauss and B. Nelander, "The equilibrium structure of trans-glyoxal from experimental rotational constants and calculated vibration-rotation interaction constants," *Phys. Chem. Chem. Phys.* **5**, 5031 (2003).
43. K. W. Butz, D. J. Krajnovich and C. S. Parmenter, "An experimental potential energy surface for internal rotation in glyoxal," *J. Chem. Phys.* **93**, 1557 (1990).
44. E. L Coitino and J. Tomasi, "Solvent effects on the internal rotation of neutral and protonated glyoxal," *Chem. Phys.* **204**, 391 (1996).
45. C. T. J. de Grotthuss, "Sur la décomposition de l'eau et des corps qu'elle tient en dissolution à l'aide de l'électricité galvanique," *Ann. Chim.* **58**, 54 (1806)
46. P. B. Petersen and R. J. Saykally, "Evidence for an enhanced hydronium concentration at the liquid water surface," *J. Phys. Chem. B* **109**, 7976 (2005).
47. P. B. Petersen and R. J. Saykally, "Is the liquid water surface basic or acidic? Macroscopic vs. molecular-scale investigations," *Chem. Phys. Lett.* **458**, 255 (2008).
48. G. Zundel, H. Z. Metzger, "Energy bands of excess tunneling protons in fluid acids. IR spectroscopy of H_5O_2^+ groups," *Z. Phys. Chem. (N.F. Frankfurt)* **58**, 225 (1968).
49. G. Zundel, "Hydrogen bonds with large proton polarizability and proton transfer processes in electrochemistry and biology," *Adv. Chem. Phys.* **111**, 1 (2000).

50. D.-L. Liu, T. Oka, "Experimental determination of the ground-state inversion splitting in H_3O^+ ," *Phys. Rev. Lett.* **54**, 1787 (1985).
51. J. Tang, T. Oka, "Infrared spectroscopy of H_3O^+ : The ν_1 fundamental band," *J. Mol. Spec.* **196**, 120 (1999).
52. M. Miyazaki, F. Asuka, T. Ebata, N. Mikami, "Infrared spectroscopic evidence for protonated water clusters forming nanoscale cages," *Science* **304**, 1134 (2004).
53. T. D. Fridgen, T. B. McMahon, L. MacAleese, J. Lemaire, P. Maitre, "Infrared spectrum of the protonated water dimer in the gas phase," *J. Phys. Chem. A* **108**, 9008 (2004).
54. C.-K. Lin, C.-C. Wu, Y.-S. Wang, Y. T. Lee, H.-C. Chang, J.-L. Kuo, Klein, M. L. "Vibrational predissociation spectra, hydrogen-bond topologies of $\text{H}^+(\text{H}_2\text{O})_{9-11}$," *Phys. Chem. Chem. Phys.* **7**, 938 (2005).
55. H.-C. Chang, C.-C. Wu, J.-L. Kuo, "Recent advances in understanding the structures of medium-sized protonated water clusters," *Int. Rev. Phys. Chem.* **24**, 553 (2005).
56. C.-C. Wu, C.-K. Lin, H.-C. Chang, J.-C. Jiang, J.-L. Kuo and M. L. Klein, "Protonated clathrate cages enclosing neutral water molecules: $\text{H}^+(\text{H}_2\text{O})_{21}$ and $\text{H}^+(\text{H}_2\text{O})_{28}$," *J. Chem. Phys.* **122**, 074315 (2005).
57. M. H. Begemann, C. S. Gudeman, J. Pfaff, R. J. Saykally, "Detection of the hydronium ion (H_3O^+) by high-resolution infrared spectroscopy," *Phys. Rev. Lett.* **51**, 554 (1983).
58. C. S. Gudeman, M. H. Begeman, J. Pfaff, R. J. Saykally, "Velocity-modulated infrared spectroscopy of molecular ions: The ν_1 band of HCO^+ ," *Phys. Rev. Lett.* **50**, 727 (1983).

59. M. H. Begemann, R. J. Saykally, "A study of the structure, dynamics of the hydronium ion by high-resolution infrared laser spectroscopy. I. The ν_3 band of $\text{H}_3^{16}\text{O}^+$," *J. Chem. Phys.* **82**, 3570 (1985).
60. K. R. Asmis, N. L. Pivonka, G. Santambrogio, M. Brümmer, C. Kaposta, D. M. Neumark, L. Wöste, "Gas-phase infrared spectrum of the protonated water dimer," *Science* **299**, 1375 (2003).
61. L. I. Yeh, M. Okumura, J. D. Myers, J. M. Price, Y. T. Lee, "Vibrational spectroscopy of the hydrated hydronium cluster ions $\text{H}_3\text{O}^+(\text{H}_2\text{O})_n$ ($n=1,2,3$)," *J. Chem. Phys.* **91**, 7319 (1989).
62. L. I. Yeh, Y. T. Lee, J. T. Hougen, "Vibration-rotation spectroscopy of the hydrated hydronium ions H_5O_2^+ , H_9O_4^+ ," *J. Mol. Spec.* **164**, 473 (1994).
63. J. M. Headrick, J. C. Bopp, M. A. Johnson, "Predissociation spectroscopy of the argon-solvated H_5O_2^+ "zundel" cation in the 1000-1900 cm^{-1} region," *J. Chem. Phys.* **121**, 11523 (2004).
64. E. G. Diken, J. M. Headrick, J. R. Roscioli, J. C. Bopp, M. A. Johnson, A. B. McCoy, "Fundamental excitations of the shared proton in the H_3O_2^- , H_5O_2^+ complexes," *J. Phys. Chem. A* **109**, 1487 (2005).
65. N. L. Hammer, E. G. Diken, J. R. Roscioli, M. A. Johnson, E. M. Myshakin, K. D. Jordon, A. B. McCoy, X. Huang, J. M. Bowman, S. Carter, "The vibrational predissociation spectra of the $\text{H}_5\text{O}_2^+\text{RG}_n$ ($\text{RG}=\text{Ar}, \text{Ne}$) clusters: Correlation of the solvent perturbations in the free OH, shared proton transitions of the Zundel ion," *J. Chem. Phys.* **122**, 244301 (2005).

66. L. R. McCunn, J. R. Roscioli, M. A. Johnson, A. B. McCoy, "An H/D isotopic substitution study of the $\text{H}_5\text{O}_2^+\text{Ar}$ vibrational predissociation spectra: exploring the putative role of Fermi resonances in the bridging proton fundamentals," *J. Phys. Chem. B.* **112**, 321 (2008).
67. L. R. McCunn, J. R. Roscioli, B. M. Elliott, M. A. Johnson, A. B. McCoy, "Why does argon bind to deuterium? Isotope effects, structures of ArH_5O_2^+ complexes," *J. Phys. Chem. A* **112**, 6074 (2008).
68. T. Oka, *Molecular Ions: Spectroscopy, Structure, and Chemistry*, eds Miller T. A. , Bondybey V. E. (North-Holland, Amsterdam), pp 73–90. (1983)
69. P. H. Dawson and A. W. Tickner, "Detection of H_5^+ in the hydrogen glow discharge," *J. Chem. Phys.* **37**, 672-673 (1962)
70. K. Buchheit and W. Henkes, "Mass spectra of energy-analyzed hydrogen cluster ions," *Z. Angew. Phys.* **24**, 191 (1968).
71. R. Clampitt and L. Gowland, "Clustering of cold hydrogen gas on protons," *Nature*, **223**, 816 (1969).
72. S. L. Anderson, T. Hirooka, P. W. Tiedemann, B. W. Mahan, and Y. T. Lee, "Photoionization of $(\text{H}_2)_2$ and clusters of O_2 molecules," *J. Chem. Phys.* **73**, 4779 (1980).
73. A. van Lumig and J. Reuss, "Collisions of hydrogen cluster ions with a gas target at 250-900 eV energy," *Int. J. Mass Spectrom. Ion Phys* **25**, 137 (1977).
74. A. van Lumig and J. Reuss, "Collisions of hydrogen cluster ions with a gas target at 200-850 eV energy," *Int. J. Mass Spectrom. Ion Phys.* **27**, 1197 (1978).

75. K. Giles, N. G. Adams and D. Smith, "A study of the reactions of H_3^+ , H_2D^+ , and D_3^+ with H_2 , HD and D_2 using a Variable-temperature Selected Ion Flow Tube," *J. Phys. Chem.* **96**, 7645-7650 (1992).
76. W. Paul, S. Schlemmer, B. Lücke and D. Gerlich, "Deuteration of Positive Hydrogen Cluster ions H_5^+ to H_{17}^+ at 10K," *Chem. Phys.* **209**, 265-274 (1996).
77. M. Cordonnier, D. Uy, R. M. Dickson, K. E. Kerr, Y. Zhang and T. Oka, "Selection rules for nuclear spin modifications in ion-neutral reactions involving H_3^+ ," *J. Chem. Phys.* **113**, 3181-3193 (2000).
78. E. Hugo, O. Asvany and S. Schlemmer, " $\text{H}_3^+ + \text{H}_2$ isotopic system at low temperatures: Microcanonical model and experimental study," *J. Chem. Phys.* **130**, 164302 (2009).
79. B. A. McGuire, Y. Wang, J. M. Bowman and S. I. Widicus-Weaver, "Do H_5^+ and its isotopologues have rotational spectra?" *J. Phys. Chem. Lett.* **2**, 1045-1047 (2011).
80. R. Prosmiti, P. Villarreal and G. Delgado-barrio, "Structures and Energetics of H_n^+ Clusters (n=5-11)," *J. Phys. Chem. A.* **107**, 4768-4772 (2003).
81. A. Aguado, P. Barragan, R. Prosmiti, G. Delgado-Barrio, P. Villarreal and O. Roncero, "A new accurate and full dimensional potential energy surface of H_5^+ based on a triatomics-in-molecules analytic functional form," *J. Chem. Phys.* **133**, 24306 (2010).
82. P. Barragan, R. Prosmiti, O. Roncero, A. Aguado, P. Villarreal and G. Delgado-Barrio, "Towards a realistic density functional theory potential energy surface for the H_5^+ cluster," *J. Chem. Phys.* **133**, 54303 (2010).

83. G. M. e Silva, R. Gargano, W. B. da Silva, L. F. Roncaratti and P. H. Acioli, "Quantum monte carlo and genetic algorithm study of the potential energy surface of the H_5^+ molecule," *Int. J. Quantum Chem.* **108**, 2318-2325 (2007).
84. Y. Ohta, K. Ohta and K. Kinugawa, "Quantum effect on the internal proton transfer and structural fluctuation in the H_5^+ cluster," *J. Chem. Phys.* **121**, 10991-10999 (2004).
85. H. Chermette and I. V. Ymmund, "Structure and stability of hydrogen clusters up to H_{21}^+ ," *Phys. Rev. B* **63**, 165427 (2001).
86. W. P. Kraemer, V. Spirko and O. Bludsky, "Extended Ab Initio study of the Vibrational Dynamics of H_5^+ and D_5^+ including all vibrational modes," *J. Mol. Spec.* **165**, 500-509 (1994).
87. V. Spirko, T. Amano and W. P. Kraemer, "Vibrational predissociation of H_5^+ ," *J. Chem. Phys.* **124**, 244303 (2006).
88. M. Barbatti, G. Jalbert and M. A. C. Nascimento, "The structure and the thermochemical properties of the $H_3^+(H_2)_n$ clusters ($n=8-12$)," *J. Chem. Phys.* **114**, 7066-7072 (2001).
89. M. Barbatti and M. A. C. Nascimento, "Vibrational analysis of small H_n^+ hydrogen clusters," *J. Chem. Phys.* **119**, 5444 (2003).
90. E. Herbst and W. Klemperer, "Formation and Depletion of Molecules in Dense Interstellar Clouds," *Astrophys. J.* **185**, 505-533 (1973).
91. L. Trafton, D. F. Lester, K. L. Thompson, "Unidentified Emission-Lines in Jupiter's Northern and Southern 2-micron Aurorae," *Astrophys. J.* **343**, L73 (1989).

92. M. Goto, T. Usuda, T. Nagata, T. R. Geballe, B. J. McCall, N. Indriolo, H. Suto, T. Henning, C. P. Morong and T. Oka, "Absorption line survey of H_3^+ towards the Galactic Center sources. II. Eight Infrared sources within 30 pc of the Galactic Center," *Astrophys. J.* **688**, 306 (2008).
93. S. Miller, J. Tennyson, S. Lepp, and A. Dalgarno, "Identification of features due to H_3^+ in the Infrared spectrum of Supernova 1987A," *Nature* **355**, 420 (1992).
94. H. Suzuki, *Towards Interstellar Chemistry* University of Tokyo Press, Tokyo 1989
95. T. Oka, "Observation of the Infrared Spectrum of H_3^+ ," *Phys. Rev. Lett.* **45**, 531 (1980).
96. T.R. Geballe and T. Oka, "Detection of H_3^+ in interstellar space," *Nature* **384**, 334 (1996).
97. B.J. McCall and T. Oka, " H_3^+ - an Ion with Many Talents," *Science* **287**, 1941 (2000).
98. C.M. Lindsay and B.J. McCall, "Comprehensive Evaluation and Compilation of H_3^+ Spectroscopy," *J. Mol. Spec.* **210**, 60 (2001).
99. M. Okumura, L. I. Yeh, Y. T. Lee, "The vibrational predissociation spectroscopy of hydrogen cluster ions," *J. Chem. Phys.* **83**, 3705 (1985).
100. M. Okumura, L. I. Yeh, Y. T. Lee, "Infrared spectroscopy of the cluster ions hydrogen triatomic monopositive ion(molecular hydrogen)_n ($\text{H}_3^+-(\text{H}_2)_n$)," *J. Chem. Phys.* **88**, 79 (1988).
101. J. R. Roscioli, L. R. McCunn, and M. A. Johnson, "Quantum structure of the intermolecular bond," *Science*, **316**, 249 (2007).

102. G. H. Gardenier, J. R. Roscioli and M. A. Johnson, "Intermolecular proton binding in the presence of a large electric dipole: Ar-tagged vibrational predissociation spectroscopy of the $\text{CH}_3\text{CNH}^+\text{OH}_2$ and $\text{CH}_3\text{CNH}^+\text{OD}_2$ complexes," *J. Phys. Chem. A* **112**, 12022 (2008).
103. N. Solca and O. Dopfer, "Interaction of the benzenium ion with inert ligands: IR spectra of $\text{C}_6\text{H}_7^+\text{-L}_n$ cluster cations ($\text{L} = \text{Ar}, \text{N}_2, \text{CH}_4, \text{H}_2\text{O}$)," *Chem. Eur. J.* **9**, 3154 (2003).
104. N. Solca and O. Dopfer, "Protonated benzene: IR spectrum and structure of C_6H_7^+ ," *Angew. Chem. Int. Ed.* **41**, 3628 (2002).
105. N. Solca, and O. Dopfer, "IR spectrum of the benzene-water cation: direct evidence for the hydrogen-bonded charge-dipole complex," *Chem. Phys. Lett.* **347**, 59 (2001).
106. R. N. Pribble, and T. S. Zwier "Size-specific infrared-spectra of benzene- $(\text{H}_2\text{O})_n$ clusters ($n=1$ through 7) – evidence for noncyclic $(\text{H}_2\text{O})_n$ structures," *Science* **265**, 75 (1994).
107. T. S. Zwier "The spectroscopy of solvation in hydrogen-bonded aromatic clusters," *Annu. Rev. Phys. Chem.* **47**, 205 (1996).
108. J. D. Augspurger, C. E. Dykstra, and T. S. Zwier, "Model study of the structures and stabilities of benzene- $(\text{H}_2\text{O})_{2-12}$ Complexes," *J. Phys. Chem.* **97**, 980 (1993).
109. S. Y. Fredericks, K. D. Jordan, and T. S. Zwier, "Theoretical characterization of the structures and vibrational spectra of Benzene- $(\text{H}_2\text{O})_{(n)}$ ($n=1-3$) clusters," *J. Phys. Chem.* **100**, 7810 (1996).
110. T. Ebata, A. Fujii, and N. Mikami, "Vibrational spectroscopy of small-sized hydrogen-bonded clusters and their ions," *Int. Rev. Phys. Chem.* **17**, 331 (1998).

111. M. Miyazaki, A. Fujii, T. Ebata, and N. Mikami, "Infrared spectroscopy of hydrated benzene cluster cations, $[\text{C}_6\text{H}_6\text{-(H}_2\text{O)}_n]^+$ (n=1-6): Structural changes upon photoionization and proton transfer reactions," *Phys. Chem. Chem. Phys.* **5**, 1137 (2003).
112. M. Miyazaki, A. Fujii, and N. Mikami, "Binding energy of the benzene-water cluster cation: an Ar-mediated IR photodissociation study," *J. Phys. Chem. A.* **108**, 8272 (2004).
113. M. Miyazaki, A. Fujii, T. Ebata, and N. Mikami, "Infrared spectroscopy of size-selected benzene-water cluster cations $[\text{C}_6\text{H}_6\text{-(H}_2\text{O)}_n]^+$ (n=1-23): hydrogen bond network evolution and microscopic hydrophobicity," *J. Phys. Chem.* **108**, 10656 (2004).
114. J. S. Prell, E. R. Williams, "Structure of thermal, mass-selected water clusters probed with hydrophobic ion tags and infrared photodissociation spectroscopy," *J. Am. Chem. Soc.* **131**, 4110 (2009).
115. J. T. O'Brien, J. S. Prell, J. D. Steill, J. Oomens, E. R. Williams, "Changes in binding motif of protonated heterodimers containing valine and amines investigated using IRMPD spectroscopy between 800 and 3700 cm^{-1} and theory," *J. Am. Chem. Soc.* **131**, 3905 (2009).
116. S. R. Mercier, O. V. Boyarkin, A. Kamariotis, M. Guglielmi, I. Tavernelli, M. Cascella, U. Rothlisberger, T. R. Rizzo, "Microsolvation effects on the excited-state dynamics of protonated tryptophan," *J. Am. Chem. Soc.* **128**, 16938 (2006).
117. A. Kamariotis, O. V. Boyarkin, S. R. Mercier, R. D. Beck, M. F. Bush, E. R. Williams, T. R. Rizzo, "Infrared spectroscopy of hydrated amino acids in the gas phase: protonated and lithiated valine," *J. Am. Chem. Soc.* **128**, 905 (2006).

118. O. V. Boyarkin, S. R. Mercier, A. Kamariotis, T. R. Rizzo, "Electronic spectroscopy of cold, protonated tryptophan and tyrosine," *J. Am. Chem. Soc.* **128**, 2816 (2006).
119. J. A. Stearns, S. Mercier, C. Seaiby, M. Guidi, O. V. Boyarkin, T. R. Rizzo, "Conformation-specific spectroscopy and photodissociation of cold, protonated tyrosine and phenylalanine," *J. Am. Chem. Soc.* **129**, 11814 (2007).
120. J. A. Stearns, O. V. Boyarkin, T. R. Rizzo, "Spectroscopic signatures of gas-phase helices: Ac-Phe-(Ala)₅-Lys-H⁺, Ac-Phe-(Ala)₁₀-Lys-H⁺," *J. Am. Chem. Soc.* **129**, 13820 (2007).
121. J. A. Stearns, M. Guidi, O. V. Boyarkin, T. R. Rizzo, "Conformation-specific infrared, ultraviolet spectroscopy of tyrosine-based protonated dipeptides," *J. Chem. Phys.* **127**, 154322 (2007).
122. R. Wu, T. B. McMahon, "Infrared multiple photon dissociation spectra of proline and glycine proton-bound dimers. Evidence for zwitterionic structure," *J. Am. Chem. Soc.* **129**, 4864 (2007).
123. R. Wu, T. B. McMahon, "Infrared multiple photon dissociation spectroscopy as structural confirmation for GlyGlyGlyH⁺ and AlaAlaAlaH⁺ in the gas phase. Evidence for amide oxygen as the protonation site," *J. Am. Chem. Soc.* **129**, 11312 (2007).
124. R. Wu, T. B. McMahon, "Structures, energetics and dynamics of gas phase ions studied by FITCR and HPMS," *Mass Spectrom. Rev.* **28**, 546 (2009).
125. R. Wu, T. B. McMahon, "Protonation sites and conformations of peptides of glycine (Gly₁₋₅H⁺) by IRMPD spectroscopy," *J. Phys. Chem. B* **113**, 8767 (2009).

126. K. LaiHing, P. Y. Cheng, T. G. Taylor, K. F. Wiley, M. Peschke, and M. A. Duncan, "Photodissociation in a reflectron time-of-flight mass-spectrometer – A novel mass-spectrometry mass-spectrometry configuration for high-mass systems," *Anal. Chem.* **61**, 1458 (1989).
127. D. S. Cornett, M. Peschke, K. LaiHing, P. Y. Cheng, K. F. Wiley, and M. A. Duncan, "Reflectron time-of-flight mass-spectrometer for laser photodissociation," *Rev. Sci. Instrum.* **63**, 2177 (1992).
128. B. Bandyopadhyay, T. C. Cheng and M. A. Duncan, "Proton sharing in hydronium-nitrogen clusters probed with infrared spectroscopy," *Int. J. Mass Spectrom.* **297**, 124 (2010).
129. A. M. Ricks, G. E. Douberly and M. A. Duncan, "Infrared spectroscopy of proton-bridged nitrogen dimers: Complex vibrational dynamics of the shared proton," *J. Chem. Phys.* **131**, 104312 (2009).
130. G.E. Douberly, A.M. Ricks, B.W. Ticknor and M.A. Duncan, "Infrared spectroscopy of protonated acetone and its dimer," *Phys. Chem. Chem. Phys.* **10**, 77 (2008).
131. G.E. Douberly, A.D. Ricks, B.W. Ticknor and M.A. Duncan, "The structure of protonated carbon dioxide clusters: Infrared photodissociation spectroscopy and ab initio calculations," *J. Phys. Chem. A* **112**, 950 (2008).
132. G.E. Douberly, A.M. Ricks, B.W. Ticknor, W.C. McKee, P.v.R. Schleyer and M.A. Duncan, "Infrared photodissociation spectroscopy of protonated acetylene and its clusters," *J. Phys. Chem. A* **112**, 1897 (2008).

133. A. M. Ricks, G. E. Douberly, P. v. R. Schleyer and M. A. Duncan, "The infrared spectrum of gas phase $C_3H_3^+$: The cyclopropeny and propargyl cations," *J. Chem. Phys.* **132**, 051101 (2010).
134. A. M. Ricks, G. E. Douberly, P. v. R. Schleyer and M. A. Duncan, "Infrared spectroscopy of protonated ethylene: The nature of proton binding in the non-classical structure," *Chem. Phys. Lett.* **480**, 17 (2009).
135. A. M. Ricks, G. E. Douberly and M. A. Duncan, "The infrared spectroscopy of protonated naphthalene and its relevance for the unidentified infrared bands," *Astrophys. J.* **702**, 301 (2009).
136. G.E. Douberly, A.M. Ricks, B.W. Ticknor, P.v.R. Schleyer and M.A. Duncan, "Infrared spectroscopy of gas phase benzenium ions: Protonated benzene and protonated toluene from 750 to 3400 cm^{-1} ," *J. Phys. Chem. A* **112**, 4869 (2008).
137. G.E. Douberly, A.M. Ricks, P.v.R. Schleyer and M.A. Duncan, "Infrared spectroscopy of gas phase $C_3H_5^+$: The allyl and 2-propenyl cations," *J. Chem. Phys.* **128**, 021102 (2008).
138. G.E. Douberly, A.M. Ricks, B.W. Ticknor, W.C. McKee, P.v.R. Schleyer and M.A. Duncan, "Infrared photodissociation spectroscopy of protonated acetylene and its clusters," *J. Phys. Chem. A* **112**, 1897 (2008).
139. G.E. Douberly, A.M. Ricks, B.W. Ticknor, P.v.R. Schleyer and M.A. Duncan, "The infrared spectrum of the tert-butyl cation in the gas phase," *J. Am. Chem. Soc.* **129**, 13782 (2007).

CHAPTER II

EXPERIMENTAL SETUP

Protonated hydrocarbons of interest are produced in a home-made molecular beam apparatus with a pulsed arc discharge source configuration coupled with a time of flight mass spectrometer. The experimental setup used to produce these clusters has been described in detail previously.¹⁻⁵ While other configurations have been used to study a variety of different molecules, there are no differences that occur besides what is in the source chamber.

Figure 1 shows a schematic of the apparatus with the arc discharge source used to study many other protonated systems such as carbonyl clusters, water clusters, and other protonated hydrocarbons.⁶⁻¹⁸ The apparatus consists of two differentially pumped chambers, with the front chamber known as the “source” chamber, while the second chamber is known as the “mass spec” chamber. These two chambers are connected with a gate valve in between so that they can be isolated when needed. Typically, the mass spec chamber is kept under vacuum while the source chamber is pumped down to vacuum in the morning and brought back to atmospheric pressure at night. The first chamber is known as the source chamber because the ions are produced in this chamber, either via laser vaporization or electrical arc discharge. The first chamber is pumped down by a Varian VHS-10 diffusion pump (6,600 liters per second of helium pumping speed). The high pumping speed is needed in order to remove the large amounts of buffer gas that is pulsed in the system which is used to collisionally cool the molecular beam. The “mass spec”

chamber is pumped by a Varian VHS-6 diffusion pump (3,000 liters per second of helium pumping speed). This is under constant vacuum to keep the system as clean as possible along with keeping as low a pressure as possible, which is important to keep impurities out of the mass spectrum and so that the ions produced do not interact with other molecules during the flight distance of the mass spectrometer.

Protonated hydrocarbon ions of interest are produced in the first chamber via an arc discharge source. This configuration is typically used when the precursor for the ions of interest has high enough vapor pressure to be seeded into the buffer gas, which is typically a mix of around 30% hydrogen and 70% argon. The high percentage of hydrogen in the buffer gas is to maximize the production of protonated ions. With the large amounts of hydrogen, most positive ions in the molecular beam are protonated, and so it minimizes the corresponding unprotonated cations, which are just one a.m.u. away in the mass spectrum.¹⁹⁻²⁴

In our experiment, the desired mixture of gas is stored in a mixing tank which flows into a stainless steel reservoir and entrains some precursor vapor with it into a pulsed gas driver (General Valve Series 9 pulse driver). If the vapor pressure of the precursor is too high or too low, the reservoir can be cooled in an ice bath or heated with heating tape. A number of different precursors that have been studied in this apparatus and their corresponding vapor pressures can be seen in Table 1. In most situations, a few drops of water are added into the gas line, which act as an electron scavenger. To maximize the formation of cations in the molecular beam, excess electrons are removed to minimize the ion-electron recombination process and subsequent neutralization of the cations with electrons.

Protonation of these complexes mostly occurs via a proton “hop” migration of H_3^+ . H_3^+ is formed by a two stage process that has been studied extensively.²⁵ First, ionization of neutral H_2 through electrical discharge removes an electron from the precursor as shown in the following equation



H_2^+ then interacts with neutral hydrogen in a secondary ion reaction to form H_3^+



Because of the low proton affinity of H_3^+ (P.A.= , the transfer of the proton occurs readily to other molecules to form neutral H_2 . In most instances, all the H_3^+ that is formed reacts and little or no H_3^+ is seen in the mass spectrum.

After the gas with the desired precursor is formed, it is pulsed into the source side vacuum chamber. Typical running conditions for hydrocarbons vary greatly depending on the system being studied, anywhere from 50 to 300 psi backing pressure with the nozzle being open for times between 180 to 320 us. In all of the protonated complexes that have been studied, a free expansion into the source is used. The use of a growth channel and other modifications to change the expansion dynamics were tested, however these modifications did not positively change the production of the desired ions.

In the arc discharge source configuration, two needles are mounted between Teflon pieces to a modified face plate. A schematic of this configuration is shown in Figure 2. The needle points are positioned at the throat of the gas expansion and are separated from one another, by about 0.5 mm. Practically, the needles are separated with the use of a razor blade,

which is placed in the middle of the discharge source and the needles are placed in position with the tips of the needles touching the razor blade. This process keeps the needles closely separated without touching. One of the needles is connected to the output of a DEI PVX 4140 Pulse generator connected to a Bertan Model 205A-03R power supply. Discharge conditions also vary depending on type of buffer gas, the backing pressure, and on the precursor. These conditions typically vary anywhere between 800 V to 2300 V with discharge timing from 5-100 μ s. In this configuration, the source produces a variety of cations, neutrals, and anions. Once the ions are produced, they are entrained in a molecular beam, which is then skimmed (Beam Dynamics model 40.5 with a 3 mm nozzle) into the second chamber, where the Wiley and McLaren type mass spectrometer is used.²⁶

In these experiments, a home-built Wiley and McLaren reflectron time-of-flight mass spectrometer is operated in the “ions out of the jet” configuration to study positive ions that are formed by arc discharge. The protonated complexes are pulse extracted into the time of flight tube with three plates known as the repeller, the draw-out grid (DOG), and a ground plate. The two-field acceleration of the ions helps resolve energy differences in the ions. The repeller and DOG are pulsed at 1000 and 900 volts respectively (Behlke HTS-50 with a 50 ns rise time pulse powered by a Stanford Research Systems DG 535). The deflection plates, usually around +40-50 volts, help neutralize the perpendicular momentum of the ions to the flight tube that comes from the initial formation of the molecular beam. An Einzel lens is used to help focus the ions towards the detector, and is usually a constant voltage of around +400 V. Once the ions enter the first flight tube, they enter a field-free region where they are separated according to mass.

The separation of the ions in relation to their mass is based on the difference in flight time down the field-free region of the mass spectrometer. Based on how much kinetic energy they have, the velocity of the ions can be described by the following equation:

$$\text{K.E.} = \frac{1}{2}mv^2 \quad (\text{Eq. 3})$$

Where K.E. is the kinetic energy, m is the mass, and v is the velocity. The kinetic energy given to all ions is the same because they are in the acceleration field of the mass spectrometer. Thus, heavier mass ions have a lower velocity than lighter mass ions, leading to a difference in time for the ions to travel a set distance. A known ion whose reference time and corresponding mass has been previously measured is used to calibrate the mass spectrum. This is usually done with protonated water, with a mass of 19 a.m.u., and a known flight time of around 33 us. For an unknown peak in the mass spectrum, the relationship between the two can be described as

$$m_u v_u^2 = m_r v_r^2 \quad (\text{Eq. 4})$$

and

$$m_u = m_r (t_u/t_r)^2 \quad (\text{Eq. 5})$$

where m_u is the unknown mass, m_r is the reference mass, and t_u and t_r are the times for two different ions to hit the detector, respectively. With this information, the mass spectrum can be calibrated to match peaks with their corresponding assignments.

Near to the end of the first flight tube, the ions encounter a mass gate, which can be used to select ions of only a certain mass. The mass gate consists of a pulsed deflection plate connected to a +400 V pulse generator (Avtech AVR-G2-C-UGA) with variable time widths, which can be used to deflect ions out of the trajectory to hit the detector. When the mass gate is

off, no voltage is applied, and all ions pass through, obtaining a full mass spectrum. To select an ion of interest, the mass gate is turned on so that the plates have the positive voltage and pulsed to ground when the ion of interest enters the mass gate. In this way, all other ions besides the mass selected one would not be detected since they would be deflected using the pulsed deflection plates.

After the ions travel down the first leg of the flight tube, they enter a reflectron. Reflectrons have been known to help increase the resolution of a time of flight mass spectrum by minimizing differences in the kinetic energy of similar ions. This is done by changing the travel path, depending on the internal energy of the ions. If two ions of the same mass but with different energies enter the reflectron, the one with more energy travels further into the reflectron and back out, giving the ion a further path to travel. This helps compensate for some of the time variation when the ions hit the detector. In our experiment, we also use the reflectron for a second purpose. At the turning region of the reflectron, the ion velocity is slowed down before being reaccelerated out of the reflectron. The ions are in the turning region of the reflection for about 1 μ s, and this extended period of time aids in the timing of the laser to intersect with the ion. Also, mass separation of the parent and fragment can be seen during the reacceleration of the ions out of the reflectron. During the reacceleration out of the reflectron and into the second field-free flight tube, separation of the fragment and parent occur similar to the first leg of the time of flight, with the lighter fragment having a higher velocity than the parent. If fragmentation occurs within the reflectron, the separate mass peaks are observed for the fragment compared to the parent.

After the ions exit the reflectron, they enter the second flight tube. This flight tube also houses the post-accelerator, which consists of a long inner tube which can be pulsed with a

positive voltage on when the ions of interest are inside the tube. Upon exiting the tube, the desired ions are accelerated with higher velocities into the detector, increasing the signal of the fragment. The ions are detected using an electron multiplier tube (EMT) (Hamamatsu Model R595). This signal is amplified (Stanford Research Systems SR445A), and connected to an oscilloscope (LeCroy Waverunner LT352), which is connected to a PC with an IEEE-488 digital card. A typical mass spectrum can be seen on Figure 3. In a typical mass spectrum, fragmentation and clustering of the precursor can be seen.

Because of the low density of ions in the molecular beam, absorption spectroscopy is not feasible. According to Beer's law, absorption is related to the sample density, along with the path length and absorption coefficient. Instead of absorption spectroscopy, action spectroscopy in the form of infrared photodissociation (IRPD) is done instead, because of the increased sensitivity. For IRPD to occur, a tunable infrared laser is needed along with dissociation of the ion being studied. This only happens when the dissociation energy of the ion is lower than the energy of the incident photon. Since most complexes have bonds much stronger than the energy of an IR photon, a technique called "rare-gas tagging" is employed.²⁸⁻⁴² For the protonated hydrocarbon complexes, the rare gas used is typically Ar, but other noble gases such as He, Ne, and Kr along with other inert gases like N₂ have been used before. In all cases of tagging, the tagged molecule binds weakly to the complexes, and then its bond energy is low enough that a single infrared photon can dissociate the complex. The effect of the Ar on the structure of the complex can be studied using theoretical computations to compare the structure with and without the Ar. In most cases for protonated hydrocarbons, rare-gas tagging does not significantly influence either the structure or spectrum of the complex.

Tunable infrared light is produced from a *LaserVision* Infrared Optical Parametric Oscillator/Amplifier (OPO/OPA) system pump by a Spectra Physics PRO 230 Nd:YAG laser.²⁷ The schematic of the OPO/OPA system is shown in Figure 4. Approximately 480 mJ/pulse of the fundamental of the Nd:YAG (1064 nm) is used to pump the OPO/OPA system. After entering the system, the light is split into two beams via a 30/70 beamsplitter. The lower power beam is frequency doubled in a beta-barium borate (BBO) crystal to produce 532 nm. The 532 nm is subsequently split into two photons in the main OPO oscillator, which uses a potassium titanyl phosphate (KTP) crystal. This leads to two photons, one with the higher energy having more than half of the energy and one with lower energy with less than half the energy, which are known as the signal and idler respectively. The two beams can be described by the following equations:

$$\omega_s > \omega_i \quad (\text{Eq. 6})$$

$$\omega_s \neq \omega_i \quad (\text{Eq. 7})$$

$$\omega_p = \omega_s + \omega_i \quad (\text{Eq. 8})$$

where ω_p , ω_s , and ω_i is the frequency of the pump beam, signal beam, and idler beam respectively.

When the input photon is split in the KTP crystal, the ratio of the energies of the two output photons depends on the phase-matching angle of the incident light with respect to the crystal face. This angle can be changed by rotating the crystal. The tuning range for the light emitted is from 710 to 880 nm for the signal beam. The signal beam is filtered out using a silicon polarization filter, and the corresponding idler beam is sent to the OPA part of the system. The 70 percent of the 1064 nm beam from the initial pump laser is sent into four angle tuned potassium titanyl arsenate (KTA) crystals, where it mixes with the idler from the OPO for a

second stage of frequency splitting. One of the resulting photons is equal to the idler beam from the OPO while the corresponding photon is the tunable mid-IR light that we use, which ranges between 2000 to 4500 cm^{-1} . For far-IR light, the signal and idler from the OPO are sent into a Silver Gallium Selenide (AgGaSe_2) crystal, where difference frequency generation of the near-IR and mid-IR photons produces photons of energies equal to the difference between the signal and idler frequency. This process results in IR light ranging from 600-2100 cm^{-1} . The OPA power is dependent on the wavelength, and ranges from less than 100 $\mu\text{J}/\text{pulse}$ to 2 mJ/pulse in the far infrared. The relation between wavelength and output power can be seen in Figure 5. In general, as the laser wavelength moves towards higher energy, the output power of the OPO/OPA increases. At certain wavelengths, the laser light is absorbed by gas molecules in the air, such as water. To minimize the loss of power, we purge the laser pathlength is preformed with nitrogen.

An example of the IRPD process can be seen in Figure 6. The top trace shows the full mass spectrum when using ethanol vapor as the precursor. Numerous peaks can be seen in the mass spectrum, corresponding to a number of different hydrocarbons that are the result of fragmentation and clustering. In the middle trace, the ion of interest can be mass selected (protonated formaldehyde cation-Ar complex at 71 a.m.u.) with the pulsed mass gate, seen as the single peak at 71 a.m.u. On the bottom trace, the tunable output from the OPO/OPA system interacts with the mass selected ion on a resonance and fragmentation can be seen. By scanning the laser wavelength and recording the fragment ion intensity, the IR spectrum of the complex can be measured.

References

1. K. LaiHing, P. Y. Cheng, T. G. Taylor, K. F. Wiley, M. Peschke, and M. A. Duncan, *Anal. Chem.* **1989**, *61*, 1458.
2. D. S. Cornett, M. Peschke, K. LaiHing, P. Y. Cheng, K. F. Wiley, and M. A. Duncan, *Rev. Sci. Instrum.* **1992**, *63*, 2177.
3. C. S. Yeh, J. S. Pilgrim, D. L. Robbins, K. F. Wiley, and M. A. Duncan, *Int. Rev. Phys. Chem.* **1994**, *13*, 231.
4. M. A. Duncan, *Ann. Rev. Phys. Chem.* **1997**, *48*, 69.
5. M. A. Duncan, *Intl. Rev. Phys. Chem.* **2003**, *22(2)*, 407.
6. B. Bandyopadhyay, T. C. Cheng and M. A. Duncan, *Int. J. Mass Spectrom.* **297**, 124 (2010)
7. T. C. Cheng, B. Bandyopadhyay, Y. Wang, B. J. Braams, J. M. Bowman and Michael A. Duncan, *J. Phys. Chem. Lett.* **1**, 758 (2010).
8. A. M. Ricks, G. E. Douberly and M. A. Duncan, *J. Chem. Phys.* **131**, 104312 (2009).
9. G.E. Douberly, A.M. Ricks, B.W. Ticknor and M.A. Duncan, *Phys. Chem. Chem. Phys.* **10**, 77 (2008).
10. G.E. Douberly, A.D. Ricks, B.W. Ticknor and M.A. Duncan, *J. Phys. Chem. A* **112**, 950 (2008).
11. G.E. Douberly, A.M. Ricks, B.W. Ticknor, W.C. McKee, P.v.R. Schleyer and M.A. Duncan, *J. Phys. Chem. A* **112**, 1897 (2008).
12. A. M. Ricks, G. E. Douberly, P. v. R. Schleyer and M. A. Duncan *J. Chem. Phys.* **132**, 051101 (2010).

13. A. M. Ricks, G. E. Douberly, P. v. R. Schleyer and M. A. Duncan, *Chem. Phys. Lett.* **480**, 17 (2009).
14. A. M. Ricks, G. E. Douberly and M. A. Duncan, *Astrophys. J.* **702**, 301 (2009).
15. G.E. Douberly, A.M. Ricks, B.W. Ticknor, P.v.R. Schleyer and M.A. Duncan, *J. Phys. Chem. A* **112**, 4869 (2008).
16. G.E. Douberly, A.M. Ricks, P.v.R. Schleyer and M.A. Duncan, *J. Chem. Phys.* **128**, 021102 (2008).
17. G.E. Douberly, A.M. Ricks, B.W. Ticknor, W.C. McKee, P.v.R. Schleyer and M.A. Duncan, *J. Phys. Chem. A* **112**, 1897 (2008).
18. G.E. Douberly, A.M. Ricks, B.W. Ticknor, P.v.R. Schleyer and M.A. Duncan, *J. Am. Chem. Soc.* **129**, 13782 (2007).
19. N. R. Walker, R. S. Walters, E. D. Pillai and M. A. Duncan, *J. Chem. Phys.* **119**, 10471 (2003).
20. R. S. Walters and M. A. Duncan, *Austr. J. Chem.* **57**, 1145 (2004)
21. N. R. Walker, R. S. Walters, K. D. Jordan and M. A. Duncan, *J. Phys. Chem. A* **109**, 7057 (2005).
22. R. S. Walters, E. D. Pillai, and M. A. Duncan, *J. Am. Chem. Soc.* **127**, 16599 (2005).
23. T. D. Vaden, J. M. Lisy, P. D. Carnegie, E. D. Pillai, and M. A. Duncan, *Phys. Chem. Chem. Phys.* **8**, 3078 (2006).
24. N. R. Walker, G. A. Grieves, J. B. Jaeger, R. S. Walters, and M. A. Duncan, *Int. J. of Mass Spectrom.* **228**, 285 (2003).
25. T. R. Hogness and E. G. Lunn, *Phys. Rev.* **26**, 44 (1925)
26. W. C. Wiley and I. H. McLaren, *Rev. Sci. Instrum.* **26**, 1150 (1955).

27. a) G. Gregoire and M. A. Duncan, M. A. *J. Chem. Phys.* **117**, 2120 (2002). b) N. R. Walker, R. S. Walters, G. A. Grieves, and M. A. Duncan, *J. Chem. Phys.* **121**, 10498 (2004). c) N. R. Walker, R. S. Walters, and M. A. Duncan, M. A. *J. Chem. Phys.* **120**, 10037 (2004).
28. W. R. Bosenburg and D. R. Guyer, *J. Opt. Soc. Am. B*, **10**, 1716 (1993).
29. L. I. Yeh, M. Okumura, J. D. Meyers, J. M. Price and Y. T. Lee, Y. T. *J. Chem. Phys.* **91**, 7319 (1989).
30. M. Okumura, L. I. Yeh, J. D. Meyers, and Y. T. Lee, *J. Phys. Chem.* **94**, 3416 (1990).
31. T. Ebata, A. Fujii and N. Mikami, N. *Int. Rev. Phys. Chem.* **17**, 331 (1998).
32. E. J. Bieske and O. Dopfer, O. *Chem. Rev.* **100**, 3963 (2000).
33. W. H. Robertson and M. A. Johnson, *Annu. Rev. Phys. Chem.* **54**, 173 (2000).
34. M. A. Duncan, *Int. Rev. Phys. Chem.* **22**, 407 (2003).
35. R. S. Walters, T. D. Jaeger, and M. A. Duncan, *J. Phys. Chem. A* **106**, 10482 (2002).
36. R. S. Walters, C. Corminboeuf, P. v. R. Schleyer and M. A. Duncan, M. A. *J. Am. Chem. Soc.* **127**, 1100 (2005).
37. R. S. Walters, E. D. Pillai, P. v. R. Schleyer and M. A. Duncan, *J. Am. Chem. Soc.* **127**, 17030 (2005).
38. T. D. Jaeger, E. D. Pillai and M. A. Duncan, *J. Phys. Chem. A* **108**, 6605 (2004).
39. T. D. Jaeger and M. A. Duncan, *J. Phys. Chem. A* **109**, 3311 (2005).
40. J. B. Jaeger, E. D. Pillai, T. D. Jaeger and M. A. Duncan, *J. Phys. Chem. A* **109**, 2801 (2005).
41. E. D. Pillai, T. D. Jaeger and M. A. Duncan, *J. Phys. Chem. A* **109**, 3521 (2005).
42. E. D. Pillai, T. D. Jaeger and M. A. Duncan, *J. Am. Chem. Soc.* **129**, 2297 (2007).

43. J. Velasquez III, B. Njegic, M. S. Gordon and M. A. Duncan, *J. Phys. Chem. A* **112**, 1907 (2008).

Laser Vaporization Cluster Machine with Reflectron Time-of-Flight Mass Spectrometer

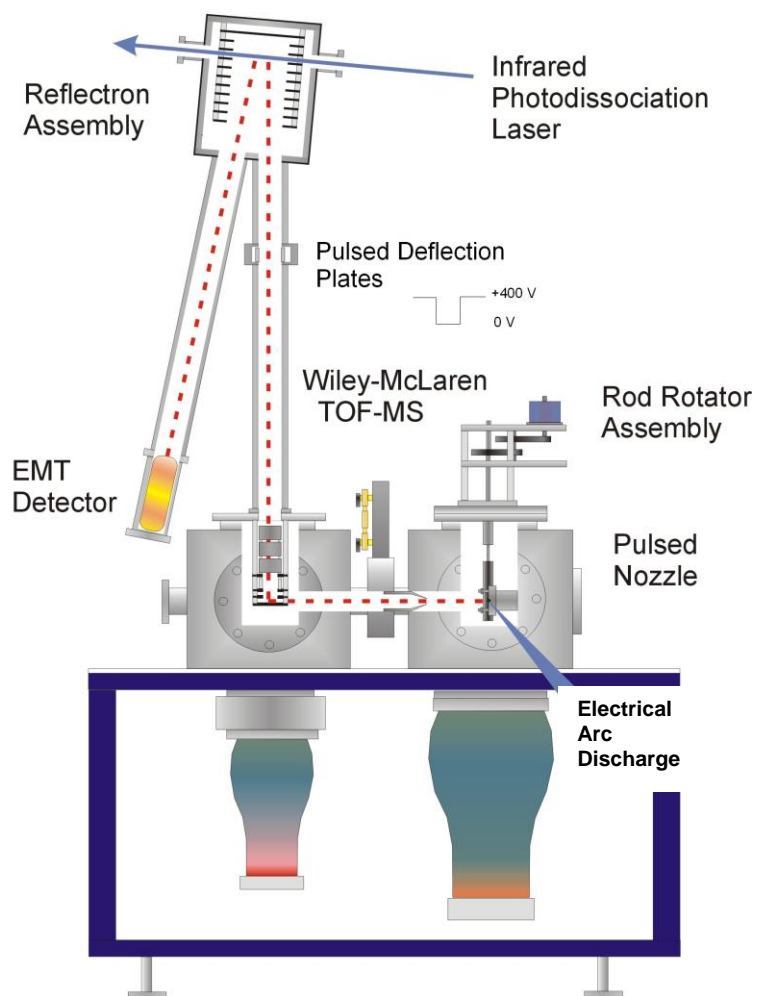


Figure 1: Schematic of the two-chamber molecular beam apparatus with a reflectron time-of-flight mass spectrometer

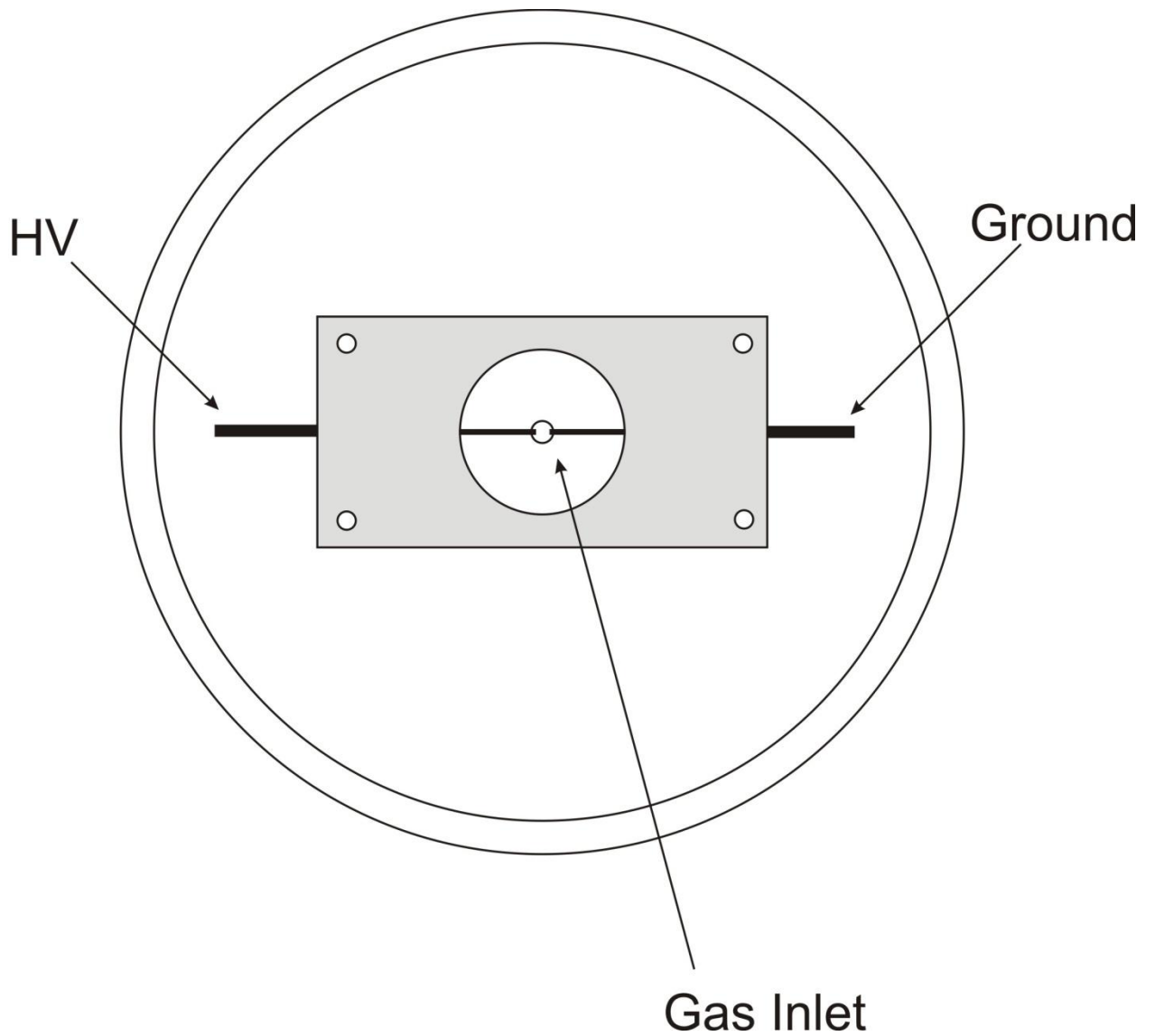


Figure 2: Blow up schematic of the arc discharge source. Two needles, one connected to a high voltage source and one grounded, are slightly separated from each other at the throat of the gas discharge.

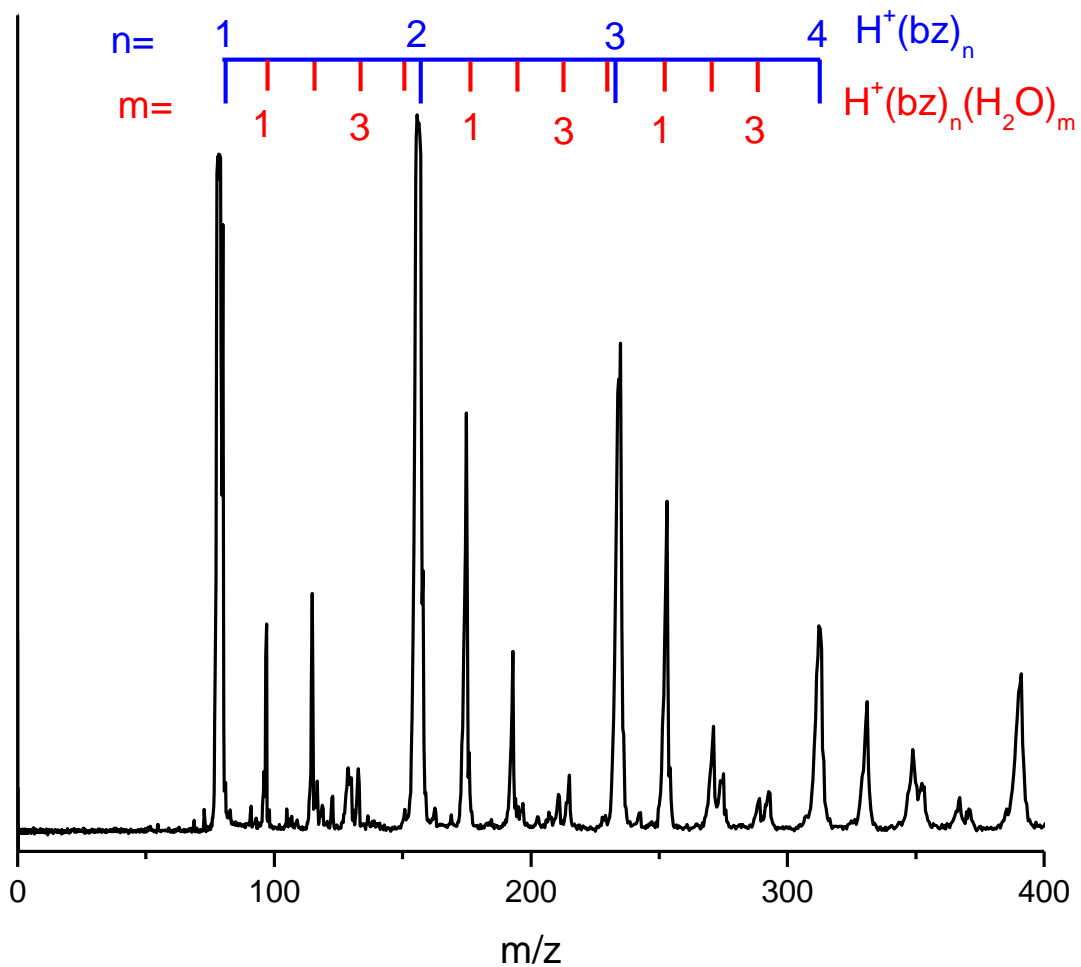


Figure 3: The mass spectrum produced from an arc discharge of water and benzene in a 30% hydrogen, 70% argon molecular beam. The mass spectrum includes many peaks corresponding to clustering of water and benzene with each other. Some argon-tagged peaks can be seen such as 137 amu ($H^+bz(H_2O)-Ar$).

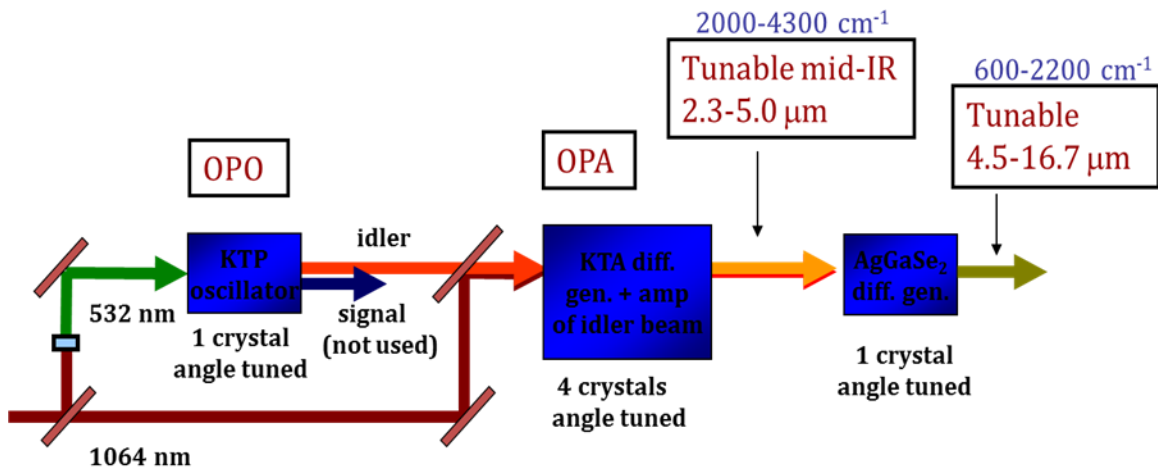


Figure 4: Schematic diagram of a *LaserVision* Infrared Optical Parametric Oscillator/Optical Parametric Amplifier

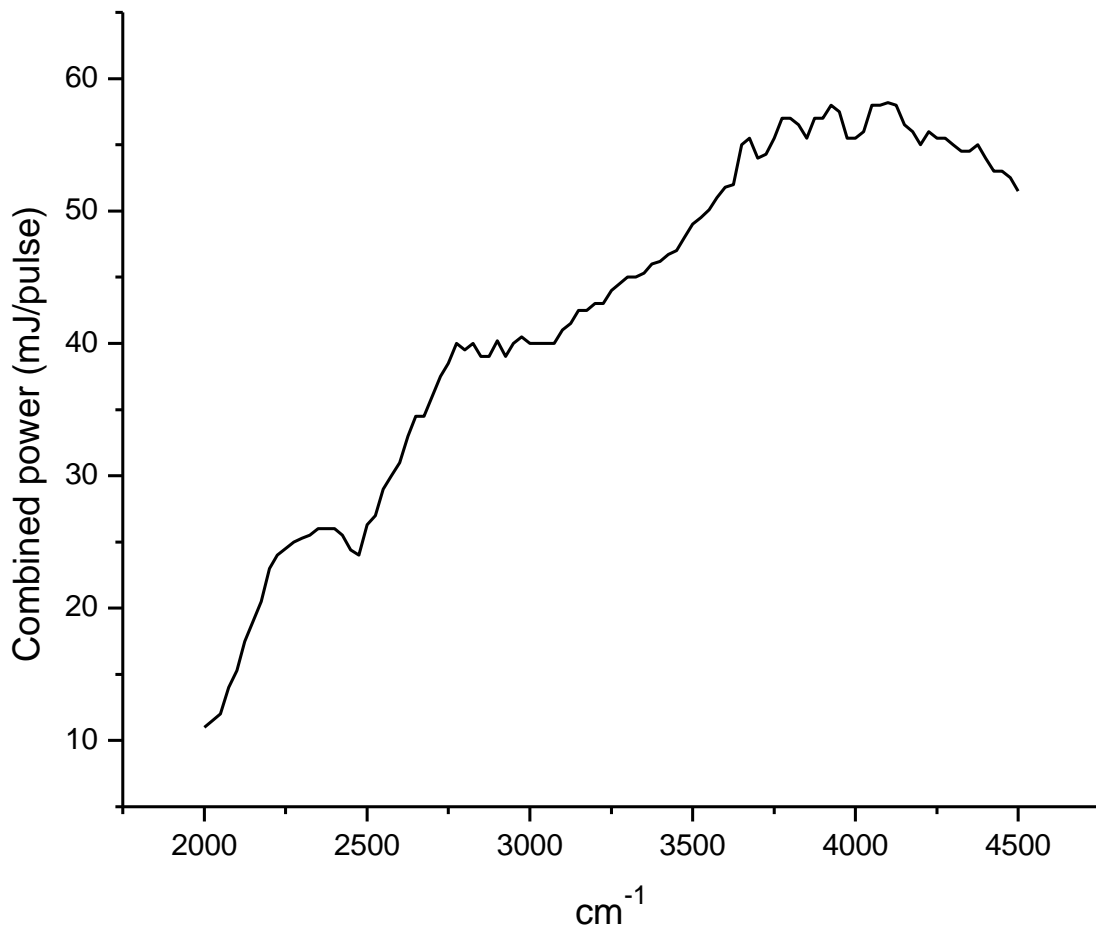


Figure 5: Output power of a *Laservision* OPO/OPA infrared laser system dependence on the wavelength. The power is of the combined signal and idler output.

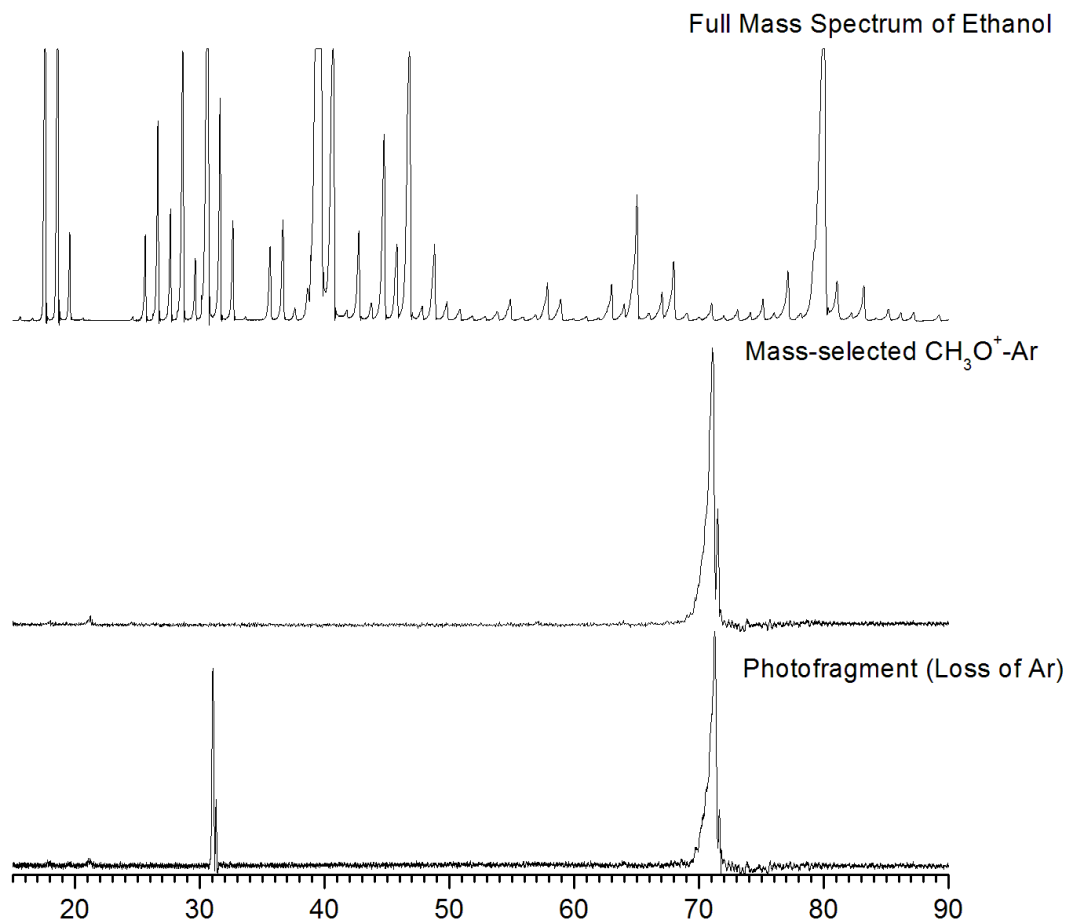


Figure 6: A full mass spectrum made with an ethanol precursor in the lines can be seen on the top trace. Upon mass selection, only one ion is detected, in this case $\text{CH}_3\text{O}-\text{Ar}^+$, as seen in the middle trace in the figure. Fragmentation of the ion is seen on the bottom trace, with the appearance of CH_3O^+ , which appears at 31 amu.

CHAPTER III

INFRARED PHOTODISSOCIATION SPECTROSCOPY

OF GLYOXAL CATION AND THEORETICAL

CALCULATIONS OF PROTONATED GLYOXAL¹

¹T. C. Cheng, B. Bandyopadhyay, and M. A. Duncan, To be submitted to *J. Phys. Chem. Lett.*

Abstract

Glyoxal cations are produced via arc discharge in a molecular beam apparatus and probed using infrared laser photodissociation spectroscopy. The spectrum suggests that the structure of glyoxal cation favors the trans-configuration over the cis configuration, similar to neutral glyoxal. The infrared spectrum of protonated glyoxal is not obtained because of a mass coincidence along with similarity in the predicted infrared bands to those of protonated water. Theory calculates that the shared proton between two oxygen atoms lowers the energy compared to the trans configuration. Calculations on the barrier of the cis-trans isomerization along with the barrier of the double well potential of the shared proton between the two oxygen atoms are performed, and the energetics differ greatly depending on the level of theory.

Introduction

Protonation of molecules is of immense chemical interest because of its occurrence in a variety of fields, including biology, atmospheric reactions, interstellar chemistry, etc.¹⁻⁴ The study of protonated carbonyls is useful in understanding many of the reactions fundamental to biology and chemistry.⁵⁻¹¹ The effects of the structural changes induced by protonation are manifested by distinct changes in the chemical properties, such as reactivity and solvation, of the molecule.

Glyoxal (C₂O₂H₂) is a di-carbonyl that has many applications both in synthetic organic chemistry and atmospheric reactions.¹²⁻²³ It is used as a building block to produce many cyclic compounds, such as imidazoles and other heterocyclic molecules. Glyoxal is a key component in cloud formation and atmospheric reactions.²³⁻²⁴ Glyoxal is also used as an indicator when studying atmospheric reactions because it is one of the by-products of certain combustion reactions.¹⁷⁻²² Glyoxal decomposes in a unimolecular reaction to form three different molecules: $\text{HCOHCO} \rightarrow \text{H}_2 + \text{CO} + \text{CO}$.²² Glyoxal is able to rotate around the C-C bond, which leads to cis-trans isomerization. The trans isomer has been experimentally measured to be lower in energy by 3.2 kcal/mol in neutral glyoxal at room temperature compared to the cis isomer.¹⁵

There have been many spectroscopic investigations using a variety of techniques on the structure of both cis and trans glyoxal.²⁴⁻³³ Both structures are stable isomers and have been detected in nature. The potential energy surface of glyoxal has been studied by theory, with particular interest focused on the barrier of the cis-trans isomerization.³⁴⁻⁴⁹ This has been an area of interest because the small size of the molecule makes it possible to perform high level quantum calculations on the structure. The barrier for the cis-trans isomerization is difficult to

model accurately, and is calculated by harmonic methods to be larger than the known value. Numerous theoretical studies have investigated the nature of the ν_7 C-C torsional motion, for which the fundamental has been measured at 127 cm^{-1} .⁴⁴ The first five overtones of this torsional motion have also been measured. It is difficult to describe these levels with harmonic models because of anharmonicity. Multimode Reaction-path Hamiltonian calculations done by Carter and coworkers have calculated the overtones of this torsion rotation while taking anharmonicity into account.⁴⁹

Protonation of glyoxal is expected to change the energy difference between the cis and trans structures. Protonation of glyoxal has been studied previously using theory, and the global minimum structure predicted favors the cis configuration using MP2/6-31G level of theory.⁵⁰ Protonated glyoxal is predicted to have a shared proton between the two oxygen atoms if the cis structure is produced. This would shift the O-H stretch to much lower frequencies than comparable O-H stretches without any shared proton characteristics.

In this report, the infrared photodissociation (IRPD) spectroscopy of argon tagged glyoxal cation is obtained for the first time. An investigation comparing different computational techniques on the structure of protonated glyoxal is performed to compare differences in calculations.

Experimental Setup

Protonated and unprotonated glyoxal cations are produced via arc discharge in a pulsed molecular beam apparatus that has been described previously.⁵¹⁻⁶⁵ Briefly, a few drops of glyoxal (Sigma Aldrich 30% glyoxal in water) at room temperature are added into the gas inlet

connected to a 30% hydrogen, 70% argon mixed buffer gas. Small amounts of water are usually added in the gas inlet to act as an electron scavenger during plasma formation. In this case, no additional water is added because the glyoxal is solvated in water. The gas is pulsed into a molecular beam apparatus through a pulsed valve with a backing pressure of around 200 psi for 200 μ s. At the throat of the expansion, an electrical discharge of around 2000 V for 20 μ s between two needles forms a plasma. Through collisional and evaporative cooling, a number of different positive, negative, and neutral clusters are produced. The ions are skimmed into the second chamber, and are pulse extracted into a reflectron time-of-flight mass spectrometer. The ions of interest are mass selected in the first leg of the time-of-flight, and then are intersected with the tunable output of an infrared OPO/OPA laser system at the turning region of the reflectron. Upon resonance absorption, photodissociation occurs if the binding energy of the ion is less than the energy of the infrared photon. By measuring the fragment intensity vs. wavelength, an infrared spectrum can be measured on a zero background. Rare gas tagging with argon is employed because the binding energy of glyoxal is too high for single photon dissociation.

Theoretical calculations for all the different isomers are done using the Gaussian 03W suite of programs.^{S1} Density functional theory (DFT) and second order Moller-Plesset perturbation theory (MP2) are used to investigate the structure, energetics, and predicted infrared spectra of glyoxal cation and protonated glyoxal. The recommended values for the scaling factors by Radom and coworkers was used.⁶⁶

Results and Discussion

The full mass spectrum of the ions produced using the glyoxal solution is shown in Figure 1. There are many peaks corresponding to fragmentation and clustering of both water and glyoxal. The peaks corresponding to glyoxal cation and protonated glyoxal can be seen at 58 and 59 amu respectively, and the argon tagged molecules occur at 98 and 99 amu. A mass coincidence occurs between argon tagged protonated glyoxal and doubly argon tagged protonated water ($\text{H}_3\text{O}^+-\text{Ar}_2$) at 99 amu. Fragmentation of both ions leads to loss of argon. The infrared spectrum of argon tagged water complexes have been studied previously. Any new bands observed are assigned to the glyoxal cation and protonated glyoxal depending on the mass selected ion.

The top trace of Figure 2 shows the infrared photodissociation spectrum of argon tagged glyoxal cation, $\text{C}_2\text{O}_2\text{H}_2^+-\text{Ar}$, measured in the mass channel corresponding to the loss of argon. The predicted spectra of two different configurations of glyoxal cation using the MP2/6311+G(p,d) level of theory are shown in the bottom two traces. The middle trace corresponds with the calculated spectrum of the *trans*-glyoxal cation configuration while the bottom trace is that of the *cis* ion. The energy difference between the two different configurations is only 0.3 kcal/mol in favor of the *cis* configuration. Four bands are observed in the mid infrared region centered at 2822, 2876, 3076, and 3320 cm^{-1} . The infrared spectrum of doubly argon tagged water cation does not have bands within this region. Therefore, the bands observed are attributed to be those of the argon tagged glyoxal cation.

Theory predicts two bands in this region corresponding to the C-H stretches for both the *cis* and *trans* configuration of glyoxal cation. The separation of the two bands is associated with

the perturbation caused by the argon atom. Definitive assignment of the glyoxal cation to the cis or the trans configurations is not possible because of the similarity between the two structures. The experimentally measured bands matches better with the trans-configuration of the glyoxal cation, predicted at 2811 and 2879 cm^{-1} . This is not a definitive assignment of the structure of the ion because the cis glyoxal has bands predicted at 2792 and 2899 cm^{-1} . There are no bands predicted in the region for the two other experimentally observed bands at 3076 and 3320 cm^{-1} . Previous experimental results on argon tagged species have observed progressions off strong bands that are spaced approximately 250 cm^{-1} off the main band. The bands at 3076 and 3320 cm^{-1} are separated from the large band at 2822 cm^{-1} by 254 and 498 cm^{-1} . These bands are therefore assigned as a progression off the 2822 cm^{-1} feature associated with combination bands of the argon-perturbed C-H stretch with a low energy argon vibration.

In the far infrared region, only one band is observed at 1791 cm^{-1} . This band is assigned to the C-O stretch of the trans configuration predicted at 1877 cm^{-1} . In the cis configuration, this band is shifted much lower in frequency to 1589 cm^{-1} . Other lower energy vibrational bands are predicted for both configurations, but are not observed in the infrared spectrum. The argon binding energy to glyoxal cation is calculated to be around 1.3 kcal/mol, so this should not be an issue leading to missing bands. One possible explanation for the absence of these bands in the experimental spectrum is that the laser power in the lower region of spectrum drops significantly. The spectrum matches better with the trans cation structure even though the cis structure is predicted to be lower in energy.

The mass spectrum of the glyoxal solution contains a band at 99 amu, corresponding to the expected mass of the protonated argon tagged glyoxal cation. The spectrum obtained for this selected mass by measuring the mass channel corresponding to the loss of argon contains strong

bands that are assigned to those of doubly argon tagged protonated water. The C-H vibrational bands of protonated glyoxal are calculated to be in the same region as the O-H stretches of protonated water. Therefore, the spectrum of protonated glyoxal is not obtained. A new technique to produce protonated glyoxal without any water present is required. Changing the precursor to glyoxal trimer dehydrate, a solid power, is currently one option being explored to remove the mass coincidence issue with argon tagged protonated glyoxal.

Theory predicts four stable energy configurations for argon tagged protonated glyoxal complex within 7 kcal/mol of the global minimum. These four isomers correspond with the *cis* and *trans* conformation of glyoxal with two different argon binding locations on each as shown in Figure 4 and 5. The argon is positioned either interacting with the protonated hydrogen or the hydrogen furthest away from the O-H bond. Protonated glyoxal without an argon adduct favors the *cis* configuration by 3.0 kcal/mol. The difference in energy between the *cis* and *trans* structure decreases with the addition of argon atom. When the argon is placed on the O-H bond, the protonated *cis*-glyoxal structure range from 0.93 to 3.51 kcal/mol lower in energy compared to the protonated *trans* structure.

The difference in energy between the four different structures depends on the level of theory performed. As shown in Table 1, with higher level basis sets, a trend of increasing energy difference between the *cis* and *trans* configuration of protonated glyoxal is found. The differences in energy are within 3 kcal/mol of the four structures with the B3LYP/631-G level of theory. The differences between the same four isomers are within 7 kcal/mol when using MP2/cc-pvtz level of theory. MP2 predicts larger differences in energy between isomers compared to DFT calculations using the same basis set. The relative energy of these structures is constant in relation to one another, with the protonated *cis* with the argon adduct close to the O-

H as the lowest energy configuration while the trans configuration with the argon attached with the C-H is the highest energy structure. Similar structures are calculated for the four different stable isomers using all five levels of theory.

There are many structural differences between the protonated cis and trans glyoxal isomers. The angle of the O-H is drastically different between the two isomers. In the trans configuration, the proton is bent away from the center of the molecule because of the repulsion from the other hydrogen atom. In the cis configuration, the O-H hydrogen is instead bent towards the center of the molecule, closer to the oxygen, forming a C-O-H⁺...O-C hydrogen bond. The distance between the hydrogen and the lone pair oxygen is 2.14 Å. This is longer than a typical hydrogen bond (1.97 Å for water), and indicates that it is a weak bond. The proton is attracted to the lone pair electrons, causing a lengthening of the O-H bond. The O-H bond is longer than in the trans configuration (1.01 vs. 0.99 Å). This difference in the two structures accounts for a 0.9 kcal/mol difference in energy. In a system without hydrogen bonding, the O-H stretch is seen to be higher in frequency. This has been observed in the protonated acetone system where the O-H vibration is observed at 3378 cm⁻¹. In the protonated cis structure, the shared O-H stretch is predicted to be lower in frequency because of this lengthening of the O-H bond.

A comparison of all four predicted infrared spectra for the four different isomers using the B3LYP/6311+G (p,d) level of theory is shown in Figure 3. In the mid infrared region, all four have a band corresponding to the O-H stretch. This band varies around 200 cm⁻¹ depending on the structure of the isomer. Cis-isomer A, which corresponds to the protonated cis configuration with the argon adduct interacting closest with the protonated hydrogen, has its O-H vibrational mode predicted at 3214 cm⁻¹. This is in good agreement with predictions that the O-

H bond would be red shifted compared to the O-H vibration of protonated acetone because of the shared proton nature of protonated glyoxal. The argon is attached to the C-H hydrogen in the cis-isomer B structure. Therefore, the O-H stretch predicted at 3271 cm^{-1} is less red-shifted compared to the cis-isomer A. The O-H stretch for trans isomer A, where the argon adduct is associated closely with the O-H hydrogen, is predicted at 3336 cm^{-1} . For trans isomer B, this O-H vibration is predicted to be at 3599 cm^{-1} .

All four isomers of argon tagged protonated glyoxal have two C-O stretch in the far infrared region around 1650 and 1800 cm^{-1} . Determining which structure is present in from looking at this C-O band would be difficult. There is a strong band predicted around 1200 cm^{-1} for the two cis structures. This band corresponds to an O-H bending mode in the plane of the molecule, and is present in both the cis and trans configuration. The cis configuration has a much larger predicted infrared intensity for this bending mode compared to the trans configuration, and should be a key spectral signature to help identify whether the cis or trans configuration is present.

The lowest energy structure of protonated glyoxal is the cis structure because of the internal shared proton between the two oxygen atoms. This shared proton has a double well potential for the proton motion in the coordinate between the two oxygen atoms. Figure 5 shows a diagram of the conformational energy of protonated cis for the proton motion between the two oxygen atoms using the MP2/cc-pVTZ level of theory. This calculation is done with a variety of different levels of theory and basis sets to examine the effects of different levels of theory in modeling this double well potential. The shared proton was first locked in position equally in between the two oxygen atoms, and the angle of the shared proton is scanned to find the minimum energy structure and position in the equally shared proton configuration. An energy

scan of the proton moving from the lowest energy structure to the transition state and then towards the other oxygen atom is shown. The barrier height of this double well potential depends on the level of theory as shown in Table 2. These values varied from 14.5 kcal/mol to 16.39 kcal/mol. A trend of increasing barrier height with increasing basis sets is observed.

Rotation of the C-C axis determines the cis-trans configuration of protonated glyoxal. Figure 6 shows a diagram of the conformational energy of protonated glyoxal as the torsional angle changes from protonated cis to trans using the MP2/cc-pVTZ level of theory. The difference in energy between the cis and trans structures is 5.6 kcal/mol using this level of theory, with a 4.5 kcal/mol barrier for the cis-trans isomerization. This value also increases with larger basis sets, ranging from 4.1 kcal/mol to 4.5 kcal/mol going from trans to cis, and 8.8 kcal/mol to 10.2 kcal/mol from cis to trans. This calculation is not entirely accurate because the O-H bond in protonated glyoxal is predicted to move away from the oxygen atom in the trans configuration. The cis configuration is the lowest energy isomer while the trans configuration is not the lowest energy isomer because the proton is known to rotate around facing away from the new hydrogen. A three dimensional potential energy surface is required to accurately model this C-C rotation along with the angle of the O-H bond. This was performed by Tomasi and coworkers using MP2/6-31G level of theory. Similar results compared to what was previously observed following a single reaction pathway are obtained where the O-H bond is fixed. The barrier for this rotation compared to the previous work shows an increase in the barrier height compared to the 6-31G level of theory. This continues the trend observed of increasing energy differences when using larger basis sets for theoretical calculations.

Future work in this project is focused on obtaining the infrared spectrum of protonated glyoxal. Producing protonated glyoxal without any water is important because of mass

coincidences along with similar predicted band positions with protonated water. Rare gas tagging with something other than neon or argon, such as nitrogen, would remove any mass coincidences with water. A calculation on the potential energy surface of protonated glyoxal in relation to the C-C bond rotation and the O-H bond angle is needed to accurately model the pathway of the cis-trans isomerization.

Conclusion

The infrared photodissociation spectrum of argon tagged glyoxal cation is measured for the first time, and is assigned to the *trans*-glyoxal cation configuration. Theory predicts the cis-configuration to be more stable by 0.3 kcal/mol over the trans configuration, compared to 3.2 kcal/mol difference in neutral glyoxal in favor of the trans structure. A progression of bands around 250 cm⁻¹ above the main C-H vibrational stretch is observed off the main C-H stretch.

The infrared spectrum of protonated glyoxal cation is not obtained because of mass coincidences in the mass spectrum. Theory predicts that the protonated glyoxal complex favors the cis configuration. The cis configuration is lower in energy because of the interaction of the proton with the other oxygen atom, forming a weak intermolecular shared proton. The difference in energy between the cis and trans configuration decreases with the addition of an argon atom. Four different isomers for argon tagged protonated glyoxal are found within 7 kcal/mol of the global minimum. While the C-O bands are predicted to be in the same region for all four isomers, the O-H bond is predicted vary in the mid infrared region, depending on the structural configuration. A strong infrared band which is predicted for the cis configuration and not for the trans configuration is the O-H bending mode around 1200 cm⁻¹.

References

1. R P. Bell, *The Proton in Chemistry*, Chapman & Hall, London, 1973.
2. E. Caldin and V. Gold, eds., *Proton Transfer Reactions*, Chapman and Hall, London, 1975.
3. J. T. Hynes, J. P. Klinman, H.-H. Limbach, R. L. Schowen, eds., *Hydrogen-Transfer Reactions*, Vols. 1-4, Wiley-VCH Publishers, Weinheim, 2006.
4. Bertini, H. B. Gray, E. I. Stiefel and J. S. Valentine, *Biological Inorganic Chemistry*, University Science Books, Sausalito, CA, 2007.
5. E. E. Ferguson, F. C. Fehsenfeld and D. L. Albritton, *Gas Phase Ion Chemistry*, edited by M. T. Bowers, Vol. 1, Academic Press, New York, 1979.
6. T. Amano and K. Tanaka, "Difference frequency laser spectroscopy of the ν_1 fundamental band of HOCO^+ ," *J. Chem. Phys.* **83**, 3721 (1985).
7. O. Dopfer, R. V. Olkhov, D. Roth, J. P. Maier, "Intermolecular interaction in proton-bound dimers.: infrared photodissociation spectra of RG-HOCO^+ ($\text{Rg} = \text{He, Ne, Ar}$) complexes," *Chem. Phys. Lett.* **296**, 585 (1998).
8. K. O. Sullivan, G. I. Gellene, "Ab initio study of Ar_n^+ ($n=0-6$): insight into size dependent cluster ion properties," *Int. J. Mass Spectrom.* **201**, 121 (2000).
9. P. Botschwina, R. Oswald, "Coupled cluster calculations for Ar-HCO^+ ," *J. Molec. Struct.* **599**, 371 (2001).
10. P. Botschwina, T. Dutoi, M. Mladenovic, R. Oswald, S. Schmatz, H. Stoll, "Theoretical investigations of proton-bound cluster ions," *Faraday Discuss.* **118**, 433 (2001).

11. B. D. Gilbert, C. S. Parmenter and D. J. Krajnovich, "Crossed beam rovibrational energy transfer from S1 glyoxal. 2. Uniform scattering characteristics from the initial levels 00, 51, and 81," *J. Phys. Chem.*, **98**, 7116 (1994).
12. C. Michel, M. Lombardi and R. Jost, "'Gate states' participation in collision-induced intersystem crossing in glyoxal: experimental evidence," *Chem. Phys.* **109**, 357 (1986).
13. J. F. Gaw and H. F. Shaefer III, "Molecular structures and energetics for the lowest triplet states of glyoxal," *J. Chem. Phys.*, **83**, 1741 (1985).
14. G. B. McDonald and E. K. C. Lee, "Fluorescence quantum yields and radiative and nonradiative lifetimes of glyoxal (1A_u)," *J. Chem. Phys.* **71**, 5049 (1979).
15. R. A. Beyer, P. F. Zittel and W. C. Lineberger, "Relaxation in the 1A_u state of glyoxal. I. collision-free lifetimes of single vibrational levels," *J. Chem. Phys.* **62**, 4016 (1975).
16. R. A. Beyer and W. C. Lineberger, "Relaxation in the 1A_u state of glyoxal. II. Collisional quenching," *J. Chem. Phys.* **62**, 4024 (1975).
17. Burak, J. W. Hepburn, N. S. Sivakumar, G. E. Hall, G. Chawla and P. L. Houston, "State-to-state photodissociation dynamics of trans-glyoxal," *J. Chem. Phys.* **86**, 1258 (1987).
18. K. Saito, T. Kakumoto, and I. Murakami, "Thermal unimolecular decomposition of glyoxal," *J. Phys. Chem.* **88**, 1182 (1984).
19. J. W. Hepburn, J. R. Buss, L. J. Butler and Y. T. Lee, "Molecular beam study of the photochemistry of S1 glyoxal," *J. Phys. Chem.*, **87**, 3638 (1983).
20. Y. Osamura, H. F. Shaefer III, W. A. Lester and M. Dupuis, "A unimolecular reaction $ABC \rightarrow A+B+C$ involving three product molecules and a single transition state. Photodissociation of glyoxal: $HCOHCO \rightarrow H_2 + CO + CO$," *J. Chem. Phys.* **75**, 5828 (1981).

21. Y. Osamura and H. F. Schaefer III, "Internal rotation barrier and transition state of glyoxal," *J. Chem. Phys.* **74**, 4576 (1981).
22. G. E. Scuseria and H. F. Schaefer III, "The unimolecular triple dissociation of glyoxal: transition-state structures optimized by configuration interaction and coupled cluster methods," *J. Am. Chem. Soc.* **111**, 7761 (1989).
23. F. Wittrock, A. Richter, H. Oetjen, J. Burrows, M. Kanakidou, S. Myriokefalitakis, R. Volkamer, S. Beirle, U. Platt and T. Wagner, "Simultaneous global observations of glyoxal and formaldehyde from space," *Geophys. Res. Lett.* **33**, L16804 (2006).
24. J. D. Blando and B. J. Turpin, "Secondary organic aerosol formation in cloud and fog droplets: a literature evaluation of plausibility," *Atmosph. Env.* **34**, 1623 (2000).
25. J. Pancif, "Cis-trans isomerization of glyoxal – a contribution to the rehabilitation of semiempirical methods," *Theoret. Chim. Acta.* **40**, 81 (1975).
26. R. Y. Dong, R. Nanes and D. A. Ramsay, "Rotational analysis of bands of the $A^1B_1-X^1A_1$ system of cis-glyoxal," *Can. J. Chem.* **71**, 1595 (1993).
27. M. Rodler, M. Oldani, G. Grassi and A. Bauder, "Rotational spectra of s-trans and s-cis glyoxal- d_1 (CHO-CDO) observed by microwave Fourier transform spectroscopy," *J. Chem. Phys.* **86**, 5365 (1987).
28. G. A. Bickel and K. K. Innes, *J. Chem. Phys.* **86**, 1572 (1987).
29. A. Kh. Mamleev, R. G. Latypova, L. N. Gunderova, V. I. Tyulin and N. M. Pozdeev, *Zh. Strukt. Khim.* **21**, 46 (1980).
30. J. R. Durig, C. C. Tong, and Y. S. Li, "Microwave spectrum of cis-glyoxal," *J. Chem. Phys.* **57**, 4425 (1972).

31. G. N. Currie and D. A. Ramsay, "The 4875 Å band system of cis-glyoxal," *Can. J. Phys.* **49**, 317 (1971).
32. J. Paldus and D. A. Ramsay, "The 4550 Å band system of glyoxal: I. rotational analyses of the (0-0) bands for C₂H₂O₂, C₂HDO₂, and C₂D₂O₂," *Can. J. Phys.* **45**, 1389 (1967).
33. G. W. King, "Excited states of glyoxal," *J. Chem. Soc.* 5054 (1957).
34. R. W. Larsen, F. Pawlowski, F. Hegelund, P. Jorgensen, J. Gauss and B. Nelander, "The equilibrium structure of trans-glyoxal from experimental rotational constants and calculated vibration-rotation interaction constants," *Phys. Chem. Chem. Phys.* **5**, 5031 (2003).
35. K. W. Butz, D. J. Krajnovich and C. S. Parmenter, "An experimental potential energy surface for internal rotation in glyoxal," *J. Chem. Phys.* **93**, 1557 (1990).
36. K. W. Butz, J. R. Johnson, D. J. Krajnovich and C. S. Parmenter, "Cis-glyoxal in effusive and supersonic beams. spectroscopy, selective pumping, and cis-trans interconversion," *J. Chem. Phys.* **86**, 5923 (1987).
37. C. E. Dyllick-Brezinger and A. Bauder, "Microwave spectrum, dipole moment and barrier to internal rotation of trans-methyl glyoxal," *Chem. Phys.* **30**, 147 (1978).
38. G. R. De Mure, Y. N. Panchenko and A. V. Abramnikov, "Effect of molecular geometry relaxation on the potential energy function of internal rotation," *J. Phys. Chem.* **96**, 2111 (1992).
39. J. Tyrell, "Internal rotation in some dicarbonyls: basis set dependence," *J. Mol. Struct. Theochem* **258**, 41 (1992).
40. G. R. De Mare, "Ab initio study of the basis set dependence of the structural parameters, relative energies and fundamental frequencies of glyoxal," *J. Mol. Struct. Theochem* **253**, 199 (1992).

41. S. Saebo, "The effect of electron correlation on the trans-cis energy difference of glyoxal," *Chem. Phys.* **113**, 383 (1987).
42. W. von Neissen, "trans- and cis-glyoxal: a green's function calculation on their photoelectron spectra," *J. Am. Chem. Soc.* **99**, 7151 (1977).
43. C. W. Bock, Y. N. Panchenko and S. V. Krasnoshchiokov, "An ab initio prediction of structures and vibrational frequencies of high-energy rotamers of glyoxal and acrolein," *Chem. Phys.* **125**, 63 (1998).
44. G. F. Musso, G. Figari and V. Magnasco, "Improved bond-orbital calculations of rotation barriers in molecules containing conjugated double bonds and/or pi lone pairs," *J. Chem. Soc., Faraday Trans. II* **81**, 1243 (1985).
45. C. V. Alsenoy, V. J. Klimkowski, L. Schafer, "Ab initio studies of structural features not easily amenable to experiment: part 37. Structural and conformational investigations of the dicarbonyls glyoxal, biacetyl, and oxalic acid," *J. Mol. Struct. Theochem* **109**, 321 (1984).
46. G. R. De Mare and D. Neisius, "Ab initio study of rotational isomerism in 1,3-butadiene. Effect of geometry optimization and basis set size on the barriers to rotation and on the stable rotamers," *J. Mol. Struct. Theochem* **109**, 103 (1984).
47. P. Pulay, G. Fogarasi, G. Pongor, J. E. Boggs and A. Vargha, "Combination of theoretical ab initio and experimental information to obtain reliable harmonic force constants. Scaled quantum mechanical (QM) force fields for glyoxal, acrolein, butadiene, formaldehyde, and ethylene," *J. Am. Chem. Soc.* **105**, 7037 (1983).
48. C. W. Bock, M. Trachtman and P. George, "An ab initio study of the geometry of the C-C(H)=O group, the f_{C-C2} stretching force constant, and the $f_{C=O,C-C}$ coupling constant in conjugated mono-substituted carbonyl compounds," *Chem. Phys.* **68**, 143 (1982).

49. D. P. Tew, N. C. Handy, and S. Carter, "Glyoxal studied with 'Multimode', explicit large amplitude motion and anharmonicity," *Phys. Chem. Chem. Phys.* **3**, 1958 (2001).
50. E. L Coitino and J. Tomasi, "Solvent effects on the internal rotation of neutral and protonated glyoxal," *Chem. Phys.* **204**, 391 (1996).
51. B. Bandyopadhyay, T. C. Cheng, and M. A. Duncan, "Proton sharing in hydronium-nitrogen clusters probed with infrared spectroscopy," *Int. J. Mass. Spec.* **124**, 120 (2010).
52. K. LaiHing, P. Y. Cheng, T. G. Taylor, K. F. Wiley, M. Peschke, and M. A. Duncan, "Photodissociation in a reflectron time-of-flight mass-spectrometer – A novel mass-spectrometry mass-spectrometry configuration for high-mass systems" *Anal. Chem.* **61**, 1458 (1989).
53. D. S. Cornett, M. Peschke, K. LaiHing, P. Y. Cheng, K. F. Wiley, and M. A. Duncan, "Reflectron time-of-flight mass-spectrometer for laser photodissociation" *Rev. Sci. Instrum.* **63**, 2177 (1992).
54. B. Bandyopadhyay, T. C. Cheng and M. A. Duncan, "Proton sharing in hydronium-nitrogen clusters probed with infrared spectroscopy" *Int. J. Mass Spectrom.* **297**, 124 (2010).
55. A. M. Ricks, G. E. Douberly and M. A. Duncan, "Infrared spectroscopy of proton-bridged nitrogen dimers: Complex vibrational dynamics of the shared proton" *J. Chem. Phys.* **131**, 104312 (2009).
56. G.E. Douberly, A.M. Ricks, B.W. Ticknor and M.A. Duncan, "Infrared spectroscopy of protonated acetone and its dimer" *Phys. Chem. Chem. Phys.* **10**, 77 (2008).
57. G.E. Douberly, A.D. Ricks, B.W. Ticknor and M.A. Duncan, "The structure of protonated carbon dioxide clusters: Infrared photodissociation spectroscopy and ab initio calculations" *J. Phys. Chem. A* **112**, 950 (2008).

58. G.E. Douberly, A.M. Ricks, B.W. Ticknor, W.C. McKee, P.v.R. Schleyer and M.A. Duncan, "Infrared photodissociation spectroscopy of protonated acetylene and its clusters" *J. Phys. Chem. A* **112**, 1897 (2008).
59. A. M. Ricks, G. E. Douberly, P. v. R. Schleyer and M. A. Duncan, "The infrared spectrum of gas phase $C_3H_3^+$: The cyclopropeny and propargyl cations" *J. Chem. Phys.* **132**, 051101 (2010).
60. A. M. Ricks, G. E. Douberly, P. v. R. Schleyer and M. A. Duncan, "Infrared spectroscopy of protonated ethylene: The nature of proton binding in the non-classical structure" *Chem. Phys. Lett.* **480**, 17 (2009).
61. A. M. Ricks, G. E. Douberly and M. A. Duncan, "The infrared spectroscopy of protonated naphthalene and its relevance for the unidentified infrared bands" *Astrophys. J.* **702**, 301 (2009).
62. G.E. Douberly, A.M. Ricks, B.W. Ticknor, P.v.R. Schleyer and M.A. Duncan, "Infrared spectroscopy of gas phase benzenium ions: Protonated benzene and protonated toluene from 750 to 3400 cm^{-1} " *J. Phys. Chem. A* **112**, 4869 (2008).
63. G.E. Douberly, A.M. Ricks, P.v.R. Schleyer and M.A. Duncan, "Infrared spectroscopy of gas phase $C_3H_5^+$: The allyl and 2-propenyl cations," *J. Chem. Phys.* **128**, 021102 (2008).
64. G.E. Douberly, A.M. Ricks, B.W. Ticknor, W.C. McKee, P.v.R. Schleyer and M.A. Duncan, "Infrared photodissociation spectroscopy of protonated acetylene and its clusters" *J. Phys. Chem. A* **112**, 1897 (2008).
65. G.E. Douberly, A.M. Ricks, B.W. Ticknor, P.v.R. Schleyer and M.A. Duncan, "The infrared spectrum of the tert-butyl cation in the gas phase" *J. Am. Chem. Soc.* **129**, 13782 (2007).

66. J. P. Marrick, D. Moran and L. Radom, "An evaluation of harmonic vibrational frequency scaling factors," *J. Phys. Chem. A* **111**, 11683 (2007)

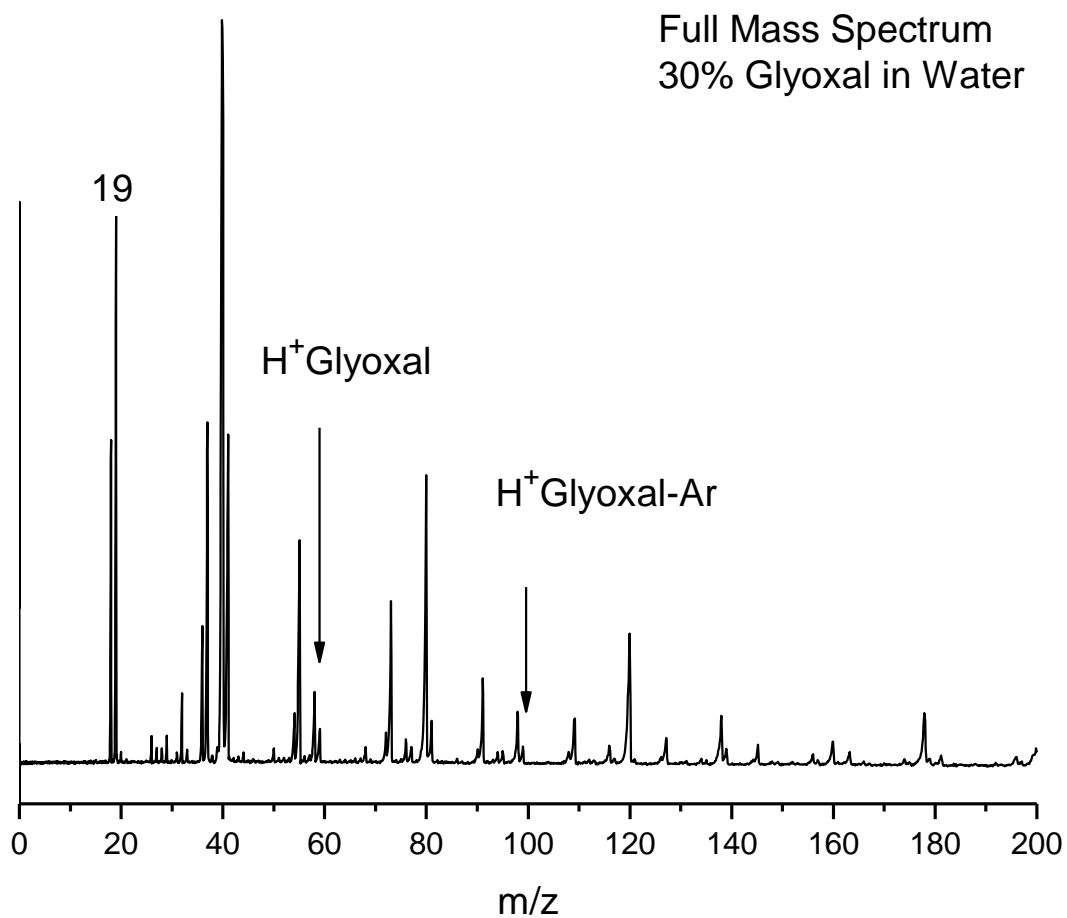


Figure 1: A full mass spectrum of 30% glyoxal in water precursor. The large progression of peaks separated by 18 amu corresponds to water clustering. Peaks assigned to mass 58 and 59 along with mass 98 and 99 amu are observed. These peaks correspond in part by glyoxal cation and protonated glyoxal along with their respective argon adducts.

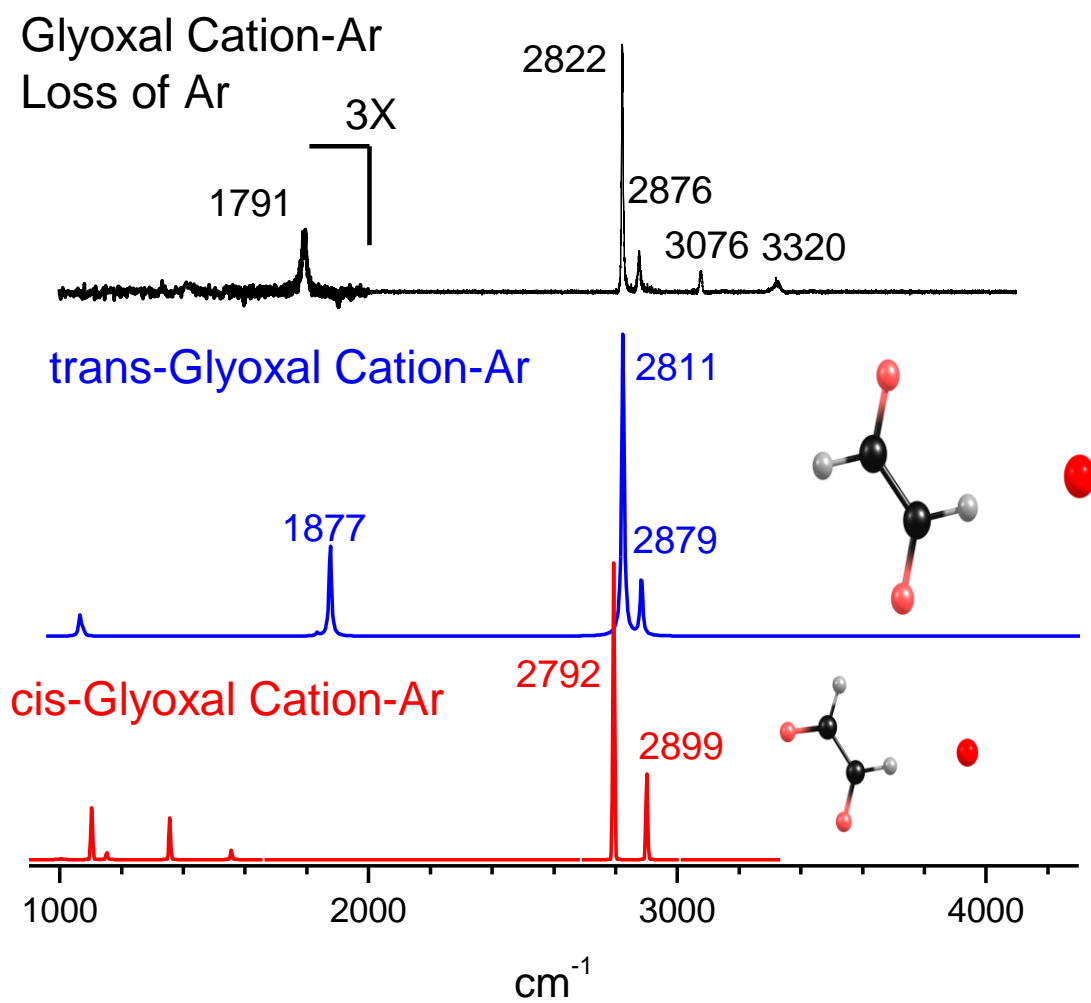


Figure 2: IRPD spectrum of Glyoxal Cation, Argon tagged, shown in black, compared to the predicted infrared spectrum using B3LYP/6311⁺G (p,d) level of theory

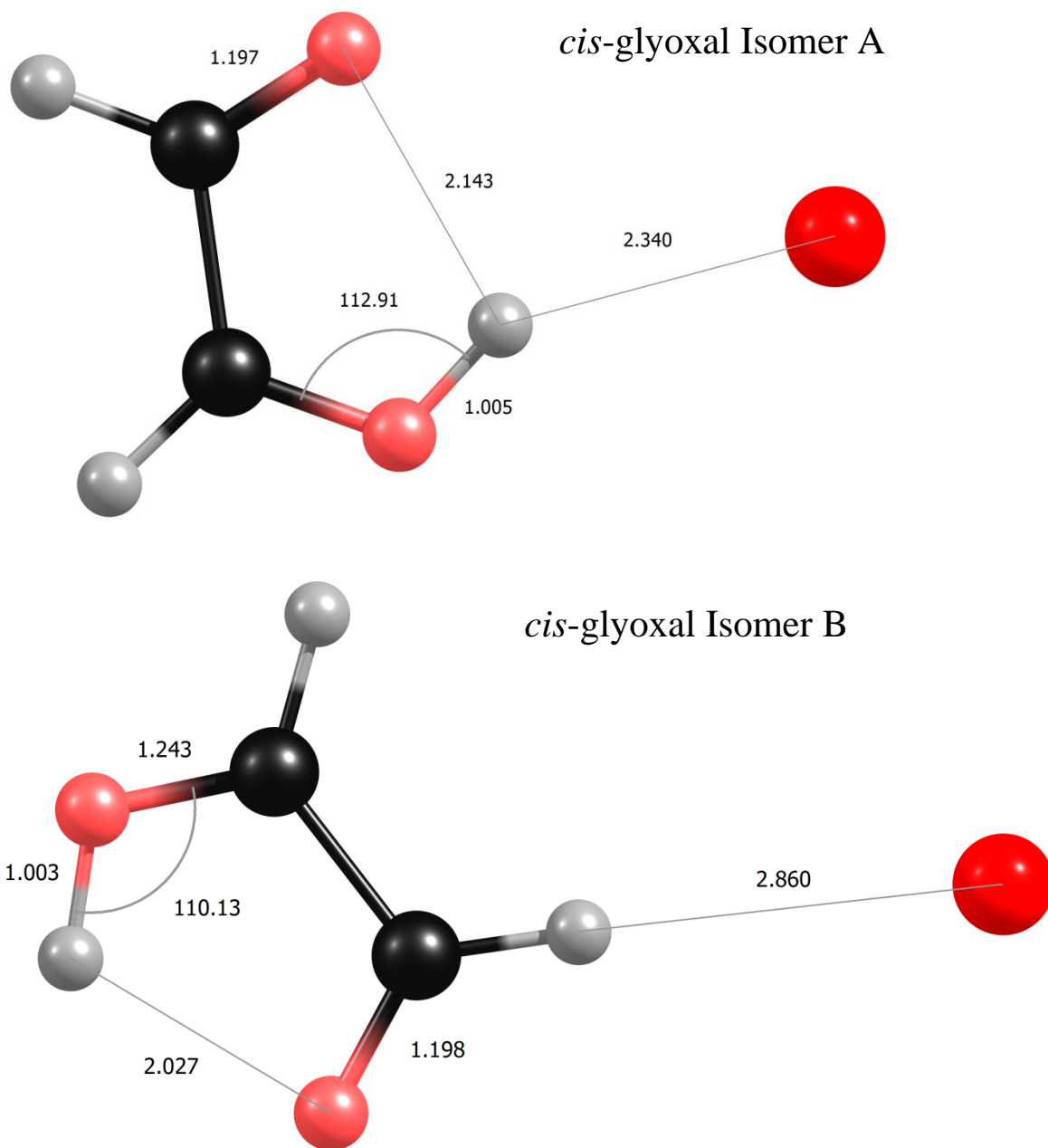


Figure 3: The structure of the two *cis*-glyoxal isomers. The top structure is labeled as *cis*-isomer A, and its predicted infrared spectrum is seen in the Figure 5 as the orange trace. The bottom structure, *cis*-isomer B, is 0.9 kcal/mol higher in energy, and its predicted spectrum is the red trace in Figure 5.

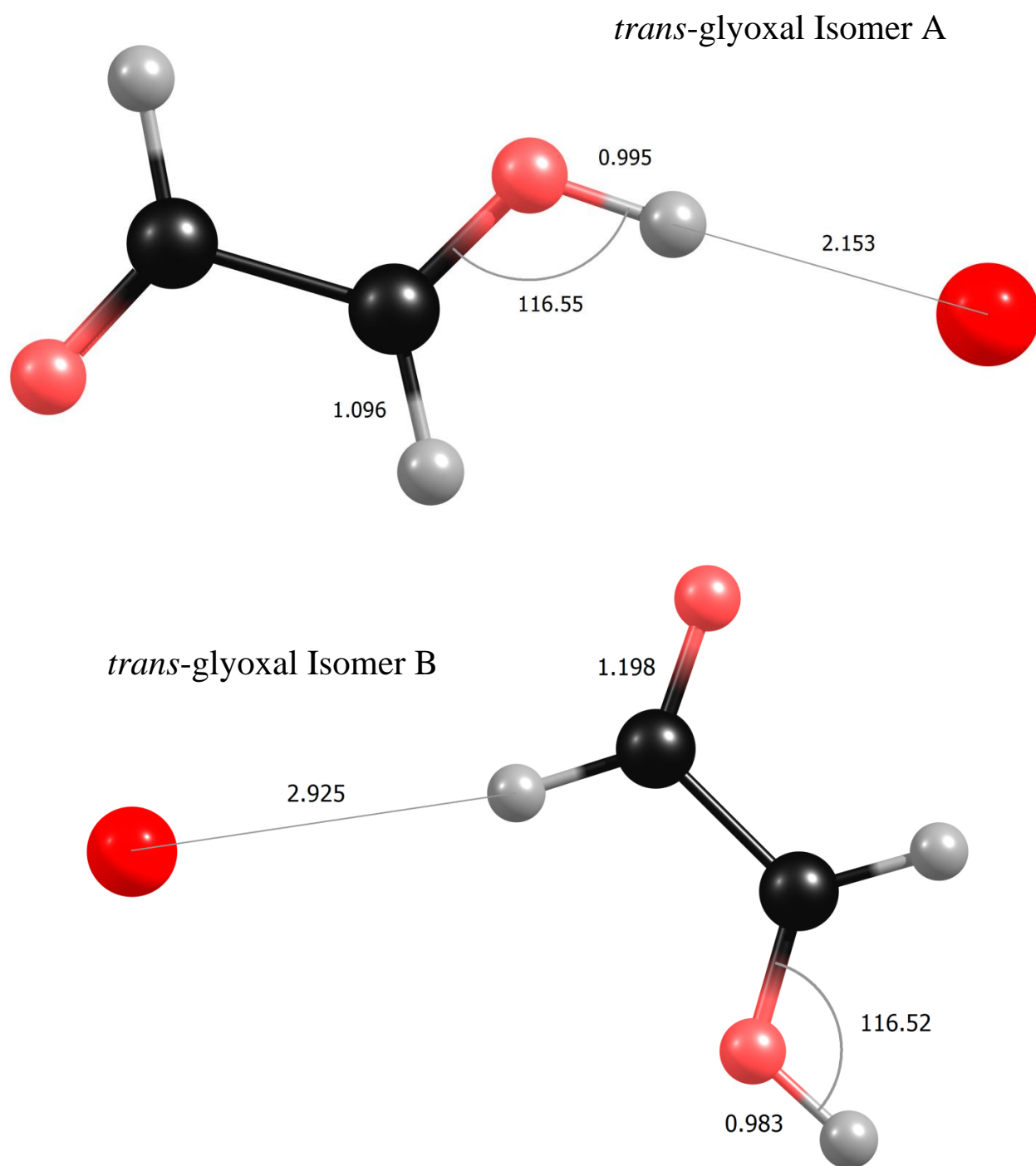


Figure 4: The structure of two *trans*-glyoxal isomers. The top structure is labeled *trans*-isomer A, and its predicted spectrum is shown as the green trace in Figure 5. The bottom structure, *trans*-isomer B, is 4.4 kcal/mol higher in energy, and its spectrum is shown in blue.

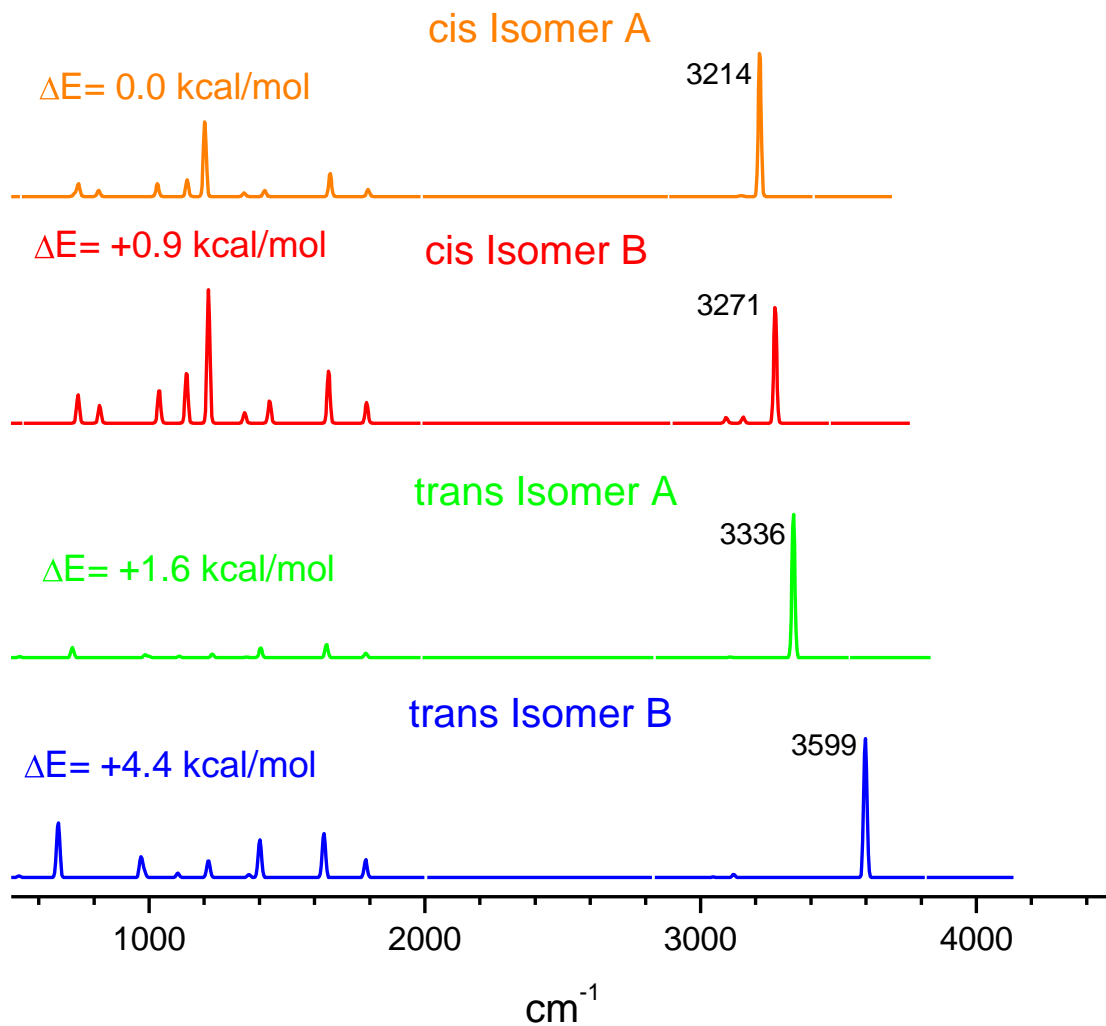


Figure 5: Predicted infrared spectrum of argon tagged protonated glyoxal of the four different isomers calculated by theory using B3LYP/6311+G (p,d). The four different isomers are labeled in Figure 4 and 5.

	B3LYP	B3LYP	B3LYP	MP2	MP2
	/6-31G	/6-311+G(p,d)	/cc-pVTZ	/6311+G(p,d)	/cc-pVTZ
cis-isomer A	0.0	0.0	0.0	0.0	0.0
cis-isomer B	+1.49	+0.98	+1.26	+0.68	+0.73
trans-isomer A	+0.93	+1.66	+1.72	+3.21	+3.51
trans-isomer B	+2.93	+4.4	+5.17	+6.45	+7.01

Table 1: Calculated relative energies in kcal/mol of protonated cis-glyoxal argon tagged vs protonated trans-glyoxal argon tagged.

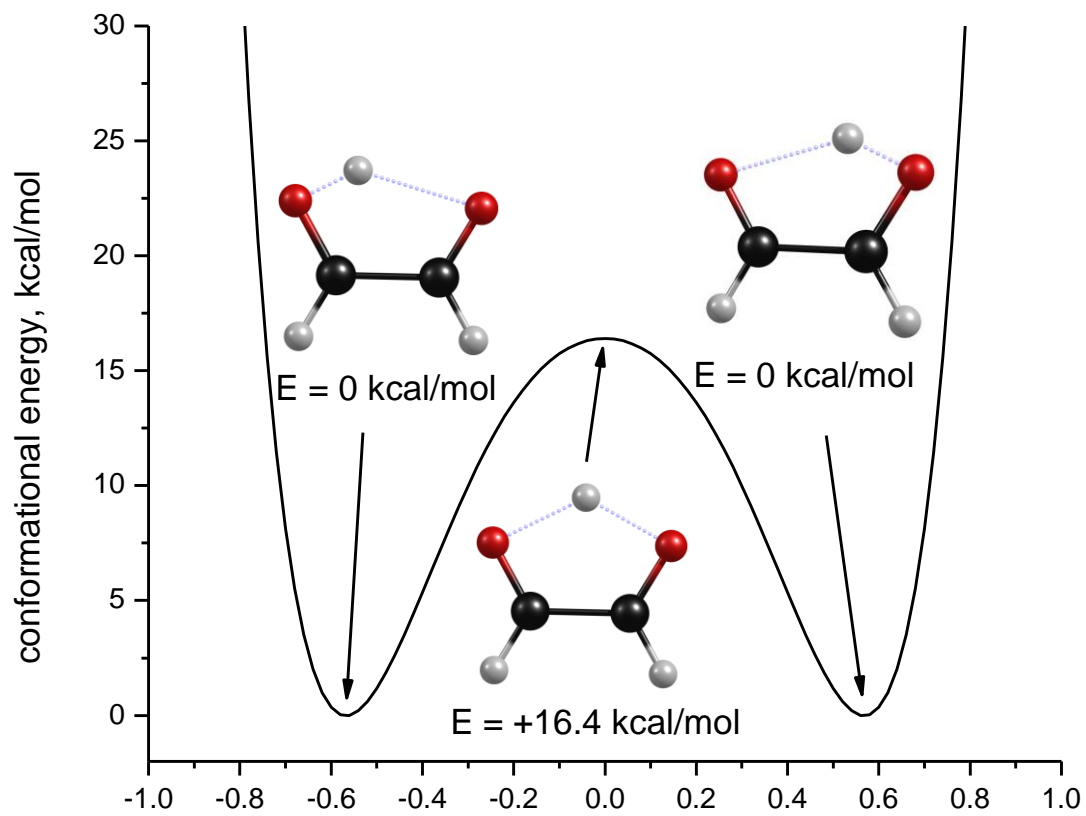


Figure 6: Diagram of the double well conformational energy of the shared proton motion between the two oxygen atoms.

	B3LYP/6-311+G(p,d)	MP2/6311+G(p,d)	MP2/cc-pVTZ
cis	0.0	0.0	0.0
trans	+15.0	+14.5	+16.39

Table 2: Calculated relative energies in kcal/mol of the barrier of the shared proton stretch between the two oxygen atoms in protonated cis-glyoxal

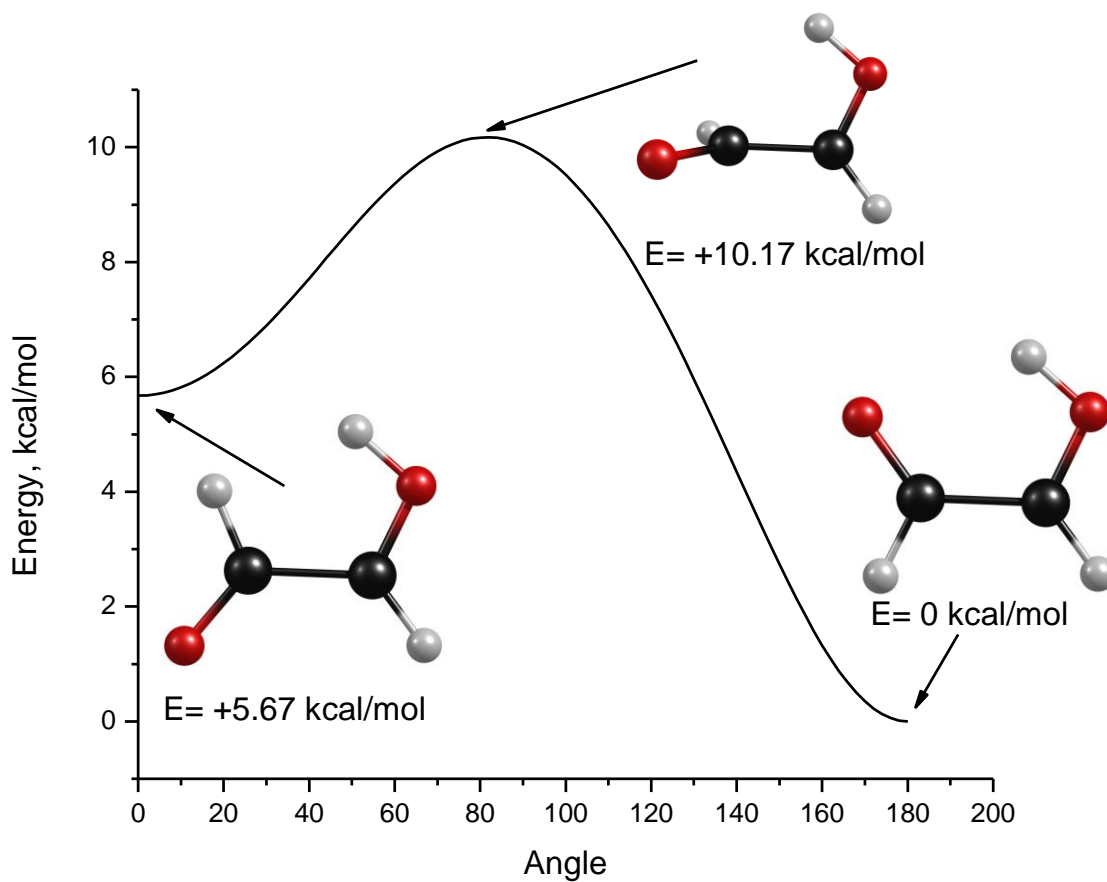


Figure 7: Diagram of the cis-trans isomerization conformational energy of protonated glyoxal. Similar profiles are obtained for the different levels of theory, with different barrier heights and relative energies of the two structures.

	B3LYP/6-311+G(p,d)	MP2/6311+G(p,d)	MP2/cc-pVTZ
cis	0.0	0.0	0.0
trans	+4.61	+5.41	+5.67
barrier	+8.80	+9.53	+10.17

Table 3: Calculated relative energies in kcal/mol of the relative energy of protonated cis glyoxal and protonated trans-glyoxal, and the barrier for the cis-trans isomerization. This is with the fixed O-H position of the protonated cis-glyoxal structure.

CHAPTER IV:
INFRARED PHOTODISSOCIATION SPECTROSCOPY
OF PROTONATED HYDROGEN CLUSTERS¹

¹T. C. Cheng, B. Bandyopadhyay, and M. A. Duncan, To be submitted to *J. Phys. Chem. Lett.*

Abstract

Protonated hydrogen clusters H_n^+ , where $n=5,7$ and 9 , are produced via arc discharge in a molecular beam apparatus and probed using infrared laser photodissociation spectroscopy. For H_5^+ , we were able to reproduce the previous data by Lee and coworkers with better resolution and to measure bands not seen before. Assignments of the observed bands correspond well with new anharmonic calculations corresponding to the shared proton structure. Because of the large oscillator strength of the shared proton stretch, combination bands involving this mode have appreciable oscillator strengths. The spectrum of the analogous deuterium clusters was also measured. For clusters larger than $n=7$, the infrared spectrum suggests a H_3^+ core solvated by neutral hydrogen molecules, unlike the shared proton structure for H_5^+ .

Introduction

Small protonated hydrogen complexes are believed to be important ingredients in interstellar chemistry. They also are ideal systems for modeling the effects of protonation because of their small size, which helps with high levels of quantum calculations. H_3^+ was first observed in the laboratory setting over a hundred years ago by J. J. Thomson while looking at a hydrogen discharge and studying its byproducts.¹ He observed that H_3^+ , not H^+ , was the major cation produced. This is because of the structural stability of H_3^+ , which consists of the positive charge shared equally by the three hydrogen atoms in an equilateral triangle configuration, first proposed by Coulson in 1935.² This H_3^+ structural configuration is the basis for the structure of many larger protonated hydrogen complexes, with neutral hydrogen molecules solvating the H_3^+ charge center.³ Multiple studies have shown H_3^+ to have an integral role in many interstellar reactions.⁴⁻⁸ In 1980, Oka and coworkers measured the infrared spectrum of H_3^+ , which was subsequently discovered in the interstellar medium in 1996.⁹⁻¹² This was done by measuring the ν_2 stretch in H_3^+ , which is the symmetric ring mode at 2521.564 cm^{-1} , and comparing these bands to absorption lines in space. Since then, H_3^+ has been discovered in a variety of different interstellar environments.¹³⁻¹⁸

Even though H_3^+ is the main positively charged ion in hydrogen plasmas, larger protonated hydrogen clusters, such as H_5^+ , have also been detected in hydrogen discharges. Dawson and Tickner first observed H_5^+ in a laboratory setting while studying a hydrogen glow discharge in 1962.¹⁹ Even larger hydrogen clusters were subsequently seen using a variety of different techniques.²⁰⁻²⁴ Using drift tube experiments, the gas-phase reaction rate coefficients of protonated hydrogen clusters have been measured. Dynamics studies have looked at the rate of reaction for many of the pure hydrogen clusters.²⁵⁻³⁶ The interaction of H_3^+ with neutral

hydrogen is believed to form H_5^+ .²⁵ Due to the abundance of both H_3^+ and H_2 in space, there is interest in the infrared spectrum of H_5^+ since it may also be present in space.^{37-39,46}

In 1988, Okumura and coworkers measured the infrared spectrum of H_5^+ in the mid-IR region, reporting three broad bands at 3532, 3910, and 4230 cm^{-1} .⁴⁰⁻⁴¹ The spectrum was assigned to the shared proton dimer structure of H_5^+ , and the bands were assigned as the second overtone of the fundamental shared proton stretch at 3532 cm^{-1} , the H-H stretch at 3904 cm^{-1} , and a combination band at 4230 cm^{-1} . These previous assignments were done with the help of harmonic calculations, which were shown to be unreliable in predicting the infrared spectrum of shared proton complexes.

H_5^+ is also a model system to study the nature of the shared proton. Numerous theoretical works have predicted the shared proton structure for H_5^+ , where the addition of H_2 to H_3^+ forms a D_{2d} structure with the proton equally shared in the center.⁴³⁻⁵⁶ Shared protons are of particular interest because of the interest in the mechanism of protonation and proton transfer, which may include a shared proton complex in the reaction process. Many different reactions involve protonation and proton transfer, including acid-base reactions, migration of protons in biological systems, and atmospheric chemistry.

Many different theoretical studies have focused on the structure of H_5^+ . The structure and energetics of H_5^+ vary greatly depending on the level of theory because of the difficulty in accurately modeling the anharmonic nature of the shared proton. While most levels of theory agree that H_5^+ is a shared proton dimer, the predicted infrared spectra has varied greatly.⁵¹⁻⁵⁶ It has been calculated that the potential energy surface for H_5^+ is extremely flat, and highly anharmonic around the global minimum with several low-lying saddle points nearby. Because of

this flat energy surface, the H_5^+ is delocalized in nature, which is problematic to accurately describe using computational methods.

Debate over the structure of even larger hydrogen clusters, such as H_7^+ and H_9^+ has been over two main configurations, one containing the H_3^+ motif, with a core H_3^+ ion solvated by multiple H_2 , and the other the shared proton structure of H_5^+ solvated by a H_2 molecules.⁴³⁻⁵¹ Theory predicts the H_7^+ structure containing the core H_3^+ to be lower in energy, and the infrared spectrum to consist of three main bands in the mid infrared region, containing an asymmetric H_3^+ ring mode similar to the ν_2 band observed by Oka and coworkers⁹, and a stretch corresponding to the H-H stretch of the H_2 molecule. The third vibrational band predicted is the symmetric stretch of the H_3^+ motif in H_7^+ . Unlike H_3^+ , the symmetric stretch of H_7^+ is predicted to be infrared active because the mode has a change in dipole from the break in symmetry coming from the addition of the two hydrogen molecules. The infrared spectrum of H_7^+ was first observed by Okumura and coworkers⁴⁰⁻⁴¹, measuring only one band in the region from 3400 to 4100 cm^{-1} . This band was assigned as the H-H stretch. The ring modes are predicted to be much lower in frequency, and the laser used at the time did not have coverage in the predicted region for the ring mode vibrations. For H_9^+ , most levels of theory agree on the H_3^+ motif with a neutral H_2 on each of the hydrogen's in the charge center. With this highly symmetric molecule, the symmetric stretch of the H_3^+ ring does not have a change in dipole. Therefore, this band is not predicted to have strong oscillator strength, and only two bands are predicted in the mid infrared region of the spectrum, the asymmetric ring mode of H_3^+ and the H-H stretch.

In this work, the single-photon infrared photodissociation spectrum for H_5^+ is measured in the mid-infrared region. Infrared multiphoton dissociation is used to measure the spectrum below 2100 cm^{-1} . The per-deuterated isotopologues are also studied to provide a deeper

understanding of the nature of the shared proton structure and to confirm their structure. In collaboration with Bowman and coworkers at Emory University, quantum Diffusion Monte Carlo (DMC) calculations, which account for the anharmonic characteristics of H_5^+ , are used to help assign the bands observed. Work on larger protonated hydrogen clusters is also presented and compared to previous results along with current theoretical models.

Experimental

Small hydrogen clusters are produced in a pure hydrogen expansion with an arc discharge ion source described previously.⁵⁷⁻⁷⁰ To form hydrogen clusters, a +2000 V discharge of 5-10 μs is used within a 300 μs gas pulse of pure hydrogen (Airgas UHP grade Hydrogen). For studying deuterium clusters, similar conditions were used except 99.9% pure deuterium (Cambridge Isotopes 99.9% pure deuterium) is used for the gas expansion. Small amounts of water are added to the gas line to act as an electron scavenger. Upon infrared absorption from a tunable infrared OPO/OPA laser, photodissociation of neutral H_2 occurs. By measuring the intensity of the smaller fragment ions in relation to the laser wavelength, the infrared spectrum of the protonated hydrogen cluster can be measured.

To get tunable infrared laser light with enough laser power for infrared multiphoton dissociation (IRMPD) below the dissociation limit, a free electron laser (FEL) is required. Similar experiments was performed by Dr. Ricks in collaboration with Dr. Asmis of FHI-Berlin at the Free Electron Laser for Infrared eXperiments (FELIX) facility at the FOM Institute for Plasma Physics “Rijnhuizen” at Nieuwegein in the Netherlands. Using the FEL, multiphoton fragmentation of H_5^+ and D_5^+ is measured from 300 to 2100 cm^{-1} .

To produce tunable infrared light with a FEL, electrons are accelerated using a linear accelerator to speeds near the speed of light. The electrons then enter a region, known as the undulator or wiggler, with alternating magnetic fields, causing the electrons to follow a sinusoidal path. The acceleration of the electrons in this alternating electric field results in synchrotron radiation. The wavelength of this radiation is related to the field strength of the magnetic field. By physically moving the magnets to change the spacing between magnets, the wavelength of synchrotron radiation can be tuned.

DMC calculations were performed by Bowman and coworkers at Emory University to provide high level anharmonic calculations on the structure and predicted spectroscopy of H_5^+ and D_5^+ . A detailed explanation of the theoretical method has been described previously.³⁹ Briefly, a 5,000-point potential energy surface (PES) was first formed with the B3LYP/aug-ccpvtz level of theory/basis set using MOLPRO. Using this constructed PES, DMC calculations to understand the energetic was done with the use of “walkers” which probed the surface at random points and directions. With 20,000 random walkers, the minimum structure is computed, and reaction path MULTIMODE calculations were performed to calculate predicted frequencies and intensity of the fundamental mode of the vibrations along with overtones and combination bands.

Results and Discussion

The mass spectrum of the ions produced in this experiment contains primarily protonated hydrogen clusters, $\text{H}_{(2n+1)}^+$ where ($n \geq 1$), as shown in Figure 1. The progression of these $\text{H}_{(2n+1)}^+$ peaks drop drastically after H_9^+ . This suggests a change in binding of hydrogen molecules after

H_9^+ . This is not surprising since this is in good agreement with numerous theoretical models where the first solvation shell has three hydrogen molecules directly interacting to H_3^+ , one on each corner. Even numbered mass peaks are also present in the mass spectrum, corresponding to even-numbered hydrogen clusters. These clusters are much smaller in intensity than the odd-numbered hydrogen clusters.

Figure 2 shows the infrared photodissociation spectrum of H_5^+ , measured in respect of the mass channel corresponding to the loss of H_2 . There are broad bands centered at 2603, 3520, 3904 and 4234 cm^{-1} in the mid-infrared region. The three higher energy bands observed correspond well with the previously measured spectrum by Okumura and coworkers.⁴⁰⁻⁴¹ There is a slight red-shift in the band positions when compared to previous results (3520 vs 3532, 3904 vs 3910 and 4232 vs 4230 cm^{-1}). The difference in band positions are attributed in part by the difference in H_5^+ formation (corona discharge vs electrical discharge), inaccuracy in picking the center of a broad band, and differences in the linewidth of the laser (5-10 cm^{-1} compared to our 1-2 cm^{-1}). The lowest frequency band observed in the mid infrared, centered at 2603 cm^{-1} , was not observed previously because of limitations in wavelength coverage in the mid-infrared region. These four bands have broad linewidths of around 50 cm^{-1} . This width is attributed mainly to predissociation. The bands are also not symmetric, with red-shading on the contours of the peaks. This suggests that there is a possibility of rotational countour that is not resolved in our spectrum.

The infrared photodissociation spectrum of D_5^+ is shown in Figure 3, measuring the appearance of D_3^+ . Three bands are present at 2546, 2815, and 3044 cm^{-1} . The deuterated isotopologue of H_5^+ is predicted to have the same vibrational modes as H_5^+ shifted lower in

frequency because of differences in molecular weight. A vibrational can be modeled by the following equation

$$\nu = \frac{1}{2\pi} \sqrt{k/\mu}$$

Where ν is the frequency, k is the bond strength, and μ is the reduced mass. The deuterated complex is expected to have the same vibrational modes shifted down in frequency by the square root of 2, since the bond strength is kept constant while the reduced mass is doubled. The three peaks in the D_5^+ spectrum correspond to the three higher-energy vibrational modes seen in H_5^+ . The band at 2603 cm^{-1} for H_5^+ is predicted to be around 1840 cm^{-1} for D_5^+ , but is not seen.

Complex computational studies are required to investigate these systems because of the highly anharmonic nature of H_5^+ . Collaboration with Bowman and coworkers utilizing Diffusion Monte Carlo (DMC) calculations provided predicted theoretical models with anharmonicity taken into account. The lowest energy conformation for H_5^+ has a structure of a charged H_3^+ with a neutral hydrogen molecule on one of the hydrogens in a C_{2v} configuration. The potential of the shared proton motion between the two hydrogens is in the form of a double well potential. The barrier between the double well has been calculated to be only 52 cm^{-1} . The zero point energy level for this molecule is already above the barrier of this double well potential. This saddle point, which has a D_{2d} configuration, is therefore very important because the ground state density is maximized in this configuration.

The dissociation limit for H_5^+ is predicted to be 6.37 kcal/mol (2227 cm^{-1}). This is higher than the harmonic estimates for the dissociation limit, which is predicted to be around 5.57 kcal/mol , and is in good agreement with previous experimental measurements. No

fragmentation is seen below 2300 cm^{-1} even though bands are predicted in this region because single photon fragmentation occurs only above the dissociation energy. Upon deuteration, the dissociation limit is predicted to shift higher in energy, to 6.87 kcal/mol (2400 cm^{-1}). This is because the zero-point energy is lowered upon deuteration, and so more energy is required to break a bond. Because of the dissociation limit of D_5^+ , the analogous band in H_5^+ at 2603 cm^{-1} is not seen.

In addition to calculating the dissociation limit for H_5^+ and D_5^+ , accurate predictions of the vibrational band positions along with its combination bands and overtones is needed to assign the bands observed. Eight fundamental vibrational modes are predicted for the shared proton structure of H_5^+ , shown in Figure 4. Assignment of the measured infrared spectrum of H_5^+ by Okumura coworkers was done with the use of harmonic calculations. The spectrum was assigned to the shared proton structure of H_5^+ , with the 3532 cm^{-1} bands identified as the second overtone of the symmetric stretch of the H_3^+ , the 3910 cm^{-1} band as the fundamental H-H stretch, and the 4230 cm^{-1} band as a combination band, possibly of the H-H stretch and the fundamental shared proton stretch.

Anharmonic factors are taken into account using DMC calculations. The fundamental shared proton stretch, ν_1 , is predicted to be around 334 cm^{-1} . This shared proton stretch has a strong oscillator strength, about eighty times stronger than the second strongest mode. This is because of the nature of the shared proton stretch, which undergoes high amplitude motion within a shallow well. This leads to a large change in dipole, which correlates to the oscillator strength of a vibration. There is only one fundamental vibrational mode in the mid-infrared region at 3560 cm^{-1} , which corresponds to ν_8 . This ν_8 vibration is analogous to the free hydrogen stretch, which has been measured at 4161 cm^{-1} , shifted down because of interactions with the

shared proton. The peak observed at 3520 cm^{-1} is assigned to this ν_8 stretch. With no other fundamental vibrational modes in this region, combination bands and overtones are required to assign the three other observed peaks.

The anharmonic nature of H_5^+ has resulted in difficulty in accurately predicting the position and oscillator strength of the combination bands and overtones of H_5^+ . In molecules that can be modeled accurately with harmonic calculations, overtones and combination bands are predicted to be close to additive in nature. For example, water has two stretches in the mid infrared region, ν_1 and ν_3 , at 3657 and 3756 cm^{-1} respectively. The combination band of $2\nu_1 + \nu_3$ has been experimentally observed at 10613 cm^{-1} , slightly less than the sum of the fundamental modes. For H_5^+ , because of the anharmonic nature of the shared proton stretch, the third overtone of the fundamental ν_1 stretch is predicted to be at 2749 cm^{-1} , over seven times the fundamental mode at 334 cm^{-1} . With the use of DMC calculations, the overtones and combination band positions along with oscillator strengths were predicted with anharmonic considerations taken into account. Because of the strong oscillator strength of the shared proton stretch, overtones and combination bands that incorporate this mode are predicted to have oscillator strengths comparable to some fundamental modes. The third overtone of the ν_1 mode is predicted to have stronger oscillator strength than that of the fundamental ν_8 mode.

Figure 5 shows the infrared photodissociation spectra of H_5^+ and D_5^+ clusters compared with the theoretical predicted spectra. Good agreement for all bands observed in H_5^+ and D_5^+ are observed. The H-H stretch is the only fundamental band in the mid infrared region of the spectrum, and this corresponds with the 3520 cm^{-1} band in H_5^+ and 2546 cm^{-1} in D_5^+ . The band at 3904 cm^{-1} is assigned to a mixed contribution from two different vibrational modes.

Assignment of the highest energy band observed is not shown because of contributions from

many different combination bands present. In H_5^+ , a fourth band is observed at 2603 cm^{-1} . This is assigned to the third overtone of the ν_1 stretch, which is the shared proton stretch. The same band is predicted to be at 1829 cm^{-1} in D_5^+ , but is not observed. This is because the dissociation limit is around 2400 cm^{-1} , so single photon absorption does not lead to dissociation.

To measure the infrared spectrum of H_5^+ and D_5^+ below the dissociation limit, single photon infrared photodissociation is not possible. Instead, infrared multiphoton photodissociation (IRMPD) is required to fragment these complexes. A larger flux of light is needed for IRMPD, which our infrared OPO/OPA system is unable to achieve. Experiments with a similar setup was performed at the Free Electron Laser for Infrared eXperiments (FELIX) facility at the FOM institute for Plasma Physics “Rijnhuizen” at Neiuwegein in the Netherlands.

Figure 6 shows the experimental spectrum of H_5^+ from 300 to 2100 cm^{-1} measured in the mass channel corresponding to loss of H_2 in the top trace, with the predicted theoretical spectrum below. The experimental spectrum has several bands with two intense ones at 940 and 1399 cm^{-1} . There are also several weaker bands that are observed. Correlation between experimentally measured peak intensity with the predicted oscillator strength is not accurate because of differences in the required absorbed photons to overcome the dissociation energy of H_5^+ . As the wavelength of the photon decreases, more photons must be simultaneously absorbed to dissociate the molecule. For example, only two photons are required to fragment H_5^+ at 1399 cm^{-1} while three photons are needed at 940 cm^{-1} . As with the mid infrared spectrum of H_5^+ , to accurately assign the observed spectrum, combination bands and overtones need to be taken into consideration.

All of the observed bands for H_5^+ appear to be slightly lower in frequency than the predicted bands from theory. The ν_1 vibration, which is the shared proton stretch, is predicted to be at 334 cm^{-1} . Three bands are seen in this region in the experimental spectrum. However, the bands at 320 and 470 cm^{-1} are known artifacts from the experimental setup which comes from certain wavelength harmonics leaking through from higher frequencies. Therefore, we assign the 379 cm^{-1} band to the shared proton stretch. This fundamental shared proton stretch is by far the strongest predicted vibrational mode in the infrared spectrum, but is seen to be quite weak in the experimental spectrum. This is in part because of the large number of photons that are required for fragmentation and because of a decrease in laser power near the edge of the tunable region of FELIX.

The other bands observed correlate well with predicted theoretical spectrum of H_5^+ . These bands observed are assigned to combination bands that all involve the ν_1 vibrational mode. This is again because of the extremely large oscillator strength of the shared proton stretch. There is red-shading present on all the bands, possibly assigned to unresolved rotational structure. This matches well with the previously seen red shading in the mid-infrared region of the spectrum. This is most prominent with the progression of bands 22 cm^{-1} to the red from the band at 1399 cm^{-1} . The strongest observed band is seen at 940 cm^{-1} . This corresponds with a strong predicted combination band. This wavelength of light in this region from FELIX is close to the maximum power through the spectrum, which contributes to strong fragmentation at this wavelength. In the predicted spectra of H_5^+ , there are many different molecular states contributing to the assignment of the combination band. Two broad features are observed centered at 1723 and 195 cm^{-1} . Even though only two photons are needed to overcome the

dissociation limit in this region, the laser power drops dramatically below 20 mJ per pulse and the linewidth of the laser broaden in this region of the spectrum.

The IRMPD spectrum of D_5^+ is shown in the top trace of Figure 6, measuring the intensity of D_3^+ as a function of wavelength. The theoretical spectrum provided by Bowman is shown in the bottom trace. The shared proton stretch for D_5^+ is predicted to be around 235 cm^{-1} . This wavelength is at the lower wavelength range of FELIX, and no fragmentation is observed. Upon deuteration, there is a shift of approximately the square root of 2 from the fundamental bands of D_5^+ compared to H_5^+ for the same reason as shown in the mid infrared region of D_5^+ vs H_5^+ . The predicted band positions are higher in energy than what is experimentally observed, opposite of what is observed for H_5^+ when compared to theory. The difference in the band positions of the experimental results compared with theoretical predictions increases as the wavelength decreases. Red-shading is not as pronounced for the bands of D_5^+ . This is not surprising because of the increase in molecular weight, which would result in more mass off-axis, decreasing the rotational constants. The predicted oscillator strengths of many of these combination bands differs from that of H_5^+ because of changes in the vibrational modes shift where combination bands coincide with one another.

Three small broad bands are observed in the lower wavenumber region of the D_5^+ spectrum. The band seen at 679 cm^{-1} corresponds with the predicted band around 791 cm^{-1} , while the two other bands centered at 886 and 1059 cm^{-1} are assigned to bands predicted around 975 and 1195 cm^{-1} . Sharp bands are present in the higher wavelength region of the far infrared for D_5^+ . Three sharp bands located at 1299 , 1357 , and 1417 cm^{-1} correlate to the predicted bands at 1473 , 1533 , and 1553 cm^{-1} . The band at 1636 cm^{-1} is assigned to the combination band predicted at 1735 cm^{-1} . The third overtone of the shared proton stretch for D_5^+ is seen at 1767

cm^{-1} . This corresponds to the predicted infrared peak at 1823 cm^{-1} . In H_5^+ , this band is seen in the mid infrared region, above the dissociation limit, and is seen previously at 2605 cm^{-1} .

Larger hydrogen clusters such as H_7^+ and H_9^+ have also been studied using the molecular beam apparatus at the University of Georgia. In these larger cluster sizes, multiple fragmentation channels are observed, corresponding to a series of peaks with the loss of two a.m.u. down to 3 a.m.u. This mass loss is from fragmentation of hydrogen molecules down to H_3^+ . For H_7^+ , only one band is observed at 3982 cm^{-1} , shown in Figure 8 with the predicted infrared spectrum below. This corresponds well with the bands seen previously at 3980 cm^{-1} by Lee and coworkers. Monitoring both loss channels resulted in the same infrared spectrum. The absence of any other peak in this whole infrared region suggests that the structure of H_7^+ greatly differs from that of H_5^+ . Harmonic theoretical calculations on the structure of H_7^+ have shown the lowest energy isomer to have a H_3^+ center with two neutral H_2 molecules on each corner in a C_{2v} configuration instead of a shared proton complex.³¹ The predicted infrared spectrum for this isomer has only one peak in this higher energy region at 3995 cm^{-1} , which matches well with the observed peak. Two other bands are predicted in the infrared region, corresponding to the asymmetric stretch of the H_3^+ center at 2303 cm^{-1} and a weaker symmetric stretch of the H_3^+ ring, at 3059 cm^{-1} . Neither of these two bands is observed in the spectrum. This may be because the peak is actually shifted below 2000 cm^{-1} , into the far-IR region. Also, binding energy considerations for these complexes may cause fragmentation not to occur.

The infrared spectrum of H_9^+ measuring the loss of neutral H_2 is shown in the top trace of Figure 9 along with the predicted infrared spectrum in the bottom trace. Multiple fragmentation channels are present corresponding to fragmentation loss of 1, 2, or 3 H_2 molecules. All three fragmentation channels result in a similar infrared spectrum. This highly symmetric molecule

has only one predicted fundamental band, corresponding to the H-H stretch of the neutral H_2 molecule, in the infrared region at 4020 cm^{-1} , which corresponds well with the band observed. Like H_7^+ , the infrared spectrum suggests that H_9^+ has the H_3^+ motif with neutral H_2 around it. The asymmetric ring mode of the core H_3^+ is predicted to shift even lower in frequency than that of H_7^+ , at 2167 cm^{-1} . This asymmetric ring mode was not observed experimentally. Unlike H_7^+ , no symmetric stretch of the H_3^+ center is predicted. Because of symmetry of H_9^+ , the symmetric stretch of H_3^+ center does not have a change in dipole, which H_7^+ has.

A comparison of the infrared spectra of H_5^+ , H_7^+ , and H_9^+ in the mid infrared region by measuring the fragmentation channels corresponding to the loss of neutral H_2 is shown in Figure 10. In all three cluster sizes the H-H stretch is observed, and the shift in the position of this band show the large difference in the structure of the H_5^+ ion compared to the other protonated hydrogen clusters. Compared to the free H_2 stretch at 4161 cm^{-1} , the H-H stretch of H_5^+ is shifted down to 3520 cm^{-1} . This shared proton structure strongly perturbs the stretches associated with the free H-H. In H_7^+ , the H_2 stretch is much closer to the free H-H stretch, at 3982 cm^{-1} , and even closer for H_9^+ at 4025 cm^{-1} . This is in good agreement with theory, which predicts that larger hydrogen clusters than H_5^+ , instead of having a shared proton structure of H_5^+ , the structure corresponds with a H_3^+ motif with neutral hydrogen attachment. The H_3^+ with neutral hydrogen molecules attached to the corners would therefore have free H-H stretches much more similar to that of neutral H-H. Okumura and coworkers have measured the H-H stretch for even larger hydrogen complexes, up to H_{15}^+ and observed the trend of higher H-H stretch vibrations upon subsequent hydrogen addition continuing.⁴⁰ With the previous assignment of the H-H stretch as the band at 3910 cm^{-1} , the band position is only a couple hundred wavenumbers from the free H-H stretch, similar to that of H_7^+ and H_9^+ even though H_5^+

was calculated not to have a free hydrogen molecule. The new assignments of bands is in good agreement with the shared proton structure of H_5^+ , with the H-H stretch being red-shifted around six hundred wavenumbers.

The infrared spectrum of D_7^+ measuring the loss of neutral D_2 is shown in Figure 11 along the comparison to H_7^+ below. Only one peak is observed, similar to the infrared spectrum of H_5^+ , at 2869 cm^{-1} . As with H_5^+ , the bands are shifted by approximately the square root of 2, from 3982 to 2869 cm^{-1} . This shift is due to the change in mass from hydrogen to deuterium into account. The ring mode of this complex is predicted to shift down to around 1700 cm^{-1} .

Future work includes measuring the low frequency of these complexes to measure the symmetric and asymmetric vibrations of the H_3^+ ring modes for the larger hydrogen clusters. If no fragmentation is seen, IRMPD may be needed if single-photon fragmentation is not possible because of binding energy considerations. Even larger hydrogen clusters, past the first solvation shell of H_3^+ , can be studied to see if the shared proton motif appears again, especially for H_{13}^+ , which corresponds with a hydrogen molecule on each of the four corners of H_5^+ . Mixed protonated clusters of H/D is also of interest to be studied. However, because of the small difference in mass along with mass coincidences, this future project would be very challenging to execute.

Conclusion

The infrared spectrum of protonated hydrogen clusters was measured using infrared photodissociation. For H_5^+ , single-photon IRPD, fragmentation above the dissociation limit showed the loss of neutral H_2 . With the increased wavelength coverage achievable with the

Laservision OPO/OPA system, the full infrared spectrum above the dissociation limit was measured, and a previously unseen peak was observed. Below the dissociation limit, IRMPD was measured using FELIX. IRPD of the deuterated clusters for all these protonated hydrogen clusters was also measured, with the bands shifted down by the square root of two, as predicted from difference in reduced mass upon deuteration. Previous assignment of the infrared spectrum corresponded to the shared proton structure. With the help of anharmonic calculations from Bowman and coworkers, the bands observed in the infrared spectrum were assigned to correspond with combination bands. Because of the large predicted oscillator strength of the fundamental shared proton stretch, combination bands involving this mode have large oscillator strengths, as seen by the predicted theoretical spectrum.

The infrared spectrum of larger protonated hydrogen clusters H_7^+ and H_9^+ and their deuterated isotopologue complex was also measured. These larger clusters showed only a single peak close to the free H_2 stretching region. This peak shifts closer to the free H_2 with the addition of each H_2 . This suggests that for H_7^+ and larger protonated hydrogen clusters, the structure of these clusters corresponds not to a shared proton structure like that of H_5^+ , but to one with a H_3^+ motif surrounded by neutral H_2 .

References

1. J. J. Thomson, "XXVI. Rays of Positive Electricity" *Philos. Mag.* **21**, 225-249 (1911).
2. C. A. Coulson, "The Electronic structure of H_3^+ " *Proc. Cambridge. Philos. Soc.* **31**, 244 (1935).
3. T. Oka. *Molecular Ions: Spectroscopy, Structure, and Chemistry*, eds T. A. Miller and V. E. Bondybey (North-Holland, Amsterdam), 73 (1983).
4. W. D. Watson, "Rate of Formation of Interstellar Molecules by Ion-Molecule Reactions" *Astrophys. J.* **183**, L17-L20 (1973).
5. E. Herbst and W. Klemperer, "Formation and Depletion of Molecules in Dense Interstellar Clouds" *Astrophys. J.* **185**, 505-533 (1973).
6. L. Trafton, D. F. Lester, K. L. Thompson, "Unidentified Emission-Lines in Jupiter's Northern and Southern 2-micron Aurorae" *Astrophys. J.* **343**, L73 (1989).
7. H. Roberts, E. Herbst, and T. J. Millar, "Enhanced Deuterium Fractionation in dense Interstellar cores resulting from multiply deuterated H_3^+ " *Astrophys. J.* **591**, L41-L44 (2003).
8. H. Roberts, E. Herbst, and T. J. Millar, "The Chemistry of multiply deuterated species in cold, dense interstellar cores" *Astron. Astrophys.* **424**, 905 (2004).
9. T. Oka, "Observation of the Infrared-Spectrum of H_3^+ " *Phys. Rev. Lett.* **45**, 531 (1980)
10. T. Oka, "Interstellar H_3^+ " *P.N.A.S.* **103**, 12235 (2006).
11. T. Oka, "The Infrared-Spectrum of H_3^+ in Laboratory and Space Plasmas" *Rev. Mod. Phys.* **64**, 1141 (1992).
12. T. R. Geballe and T. Oka, "Detection of H_3^+ in interstellar space" *Nature*, **384**, 334 (1996).

13. S. J. Kim, P. Drossart, J. Caldwell, J-P Maillard, T. Herbstshure and M. Herbstshure, "Images of Aurorae on Jupiter from H₃⁺ emission at 4 μm" *Nature*, **353**, 536 (1991).
14. J. A. Macdonald, M. A. Biondi and R. Johnsen, "Recombination of electrons with H₃⁺ and H₅⁺ Ions" *Planet Space Sci.* **32**, 651-654 (1984).
15. S. Miller, N. Achilleous, G. E. Ballestes, T. R. Geballe, R. D. Joseph, R. Prange, D. Rego, T. Stallard, J. Tennyson, L. M. Trafton and J. H. Waite Jr., "The role of H₃⁺ in planetary atmospheres" *Philos. Trans. R. Soc. London A.* **358**, 2485 (2000).
16. M. Goto, T. Usuda, T. Nagata, T. R. Geballe, B. J. McCall, N. Indriolo, H. Suto, T. Henning, C. P. Morong and T. Oka, "Absorption line survey of H₃⁺ towards the Galactic Center sources. II. Eight Infrared sources within 30 pc of the Galactic Center" *Astrophys. J.* **688**, 306 (2008).
17. S. Miller, J. Tennyson, S. Lepp, and A. Dalgarno, "Identification of features due to H₃⁺ in the Infrared spectrum of Supernova 1987A" *Nature* **355**, 420 (1992).
18. H. Suzuki, *Towards Interstellar Chemistry* University of Tokyo Press, Tokyo 1989
19. P. H. Dawson and A. W. Tickner, "Detection of H₅⁺ in Hydrogen Glow Discharge" *J. Chem. Phys.* **37**, 672-673 (1962).
20. K. Buchheit and W. Henkes, "Mass spectra of energy-analyzed Hydrogen Cluster Ions" *Z. Angew. Phys.* **24**, 191 (1968).
21. R. Clampitt and L. Gowland, "Clustering of cold hydrogen gas on protons" *Nature*, **223**, 816 (1969).
22. S. L. Anderson, T. Hirooka, P. W. Tiedemann, B. W. Mahan, and Y. T. Lee, "Photoionization of (H₂)₂ and clusters of O₂ molecules" *J. Chem. Phys.* **73**, 4779 (1980).

23. A. van Lumig and J. Reuss, "Collisions of Hydrogen Cluster Ions with a gas target at 250-900 eV energy" *Int. J. Mass Spectrom. Ion Phys.* **25**, 137 (1977).
24. A. van Lumig and J. Reuss, "Collisions of Hydrogen Cluster Ions with a gas target at 200-850 eV energy" *Int. J. Mass Spectrom. Ion Phys.* **27**, 1197 (1978).
25. K. Giles, N. G. Adams and D. Smith, "A study of the reactions of H_3^+ , H_2D^+ , HD_2^+ , and D_3^+ with H_2 , HD , and D_2 using a variable temperature selected ion flow tube" *J. Phys. Chem.* **96**, 7645-7650 (1992).
26. Y. K. Bae, "Observation of high-lying Vibrational Predissociation states of H_5^+ " *Chem. Phys. Lett.* **180**, 179-181 (1991).
27. W. Paul, S. Schlemmer, B. Lücke and D. Gerlich, "Deuteration of positive hydrogen cluster ions H_5^+ to H_{17}^+ at 10K" *Chem. Phys.* **209**, 265-274 (1996).
28. M. Cordonnier, D. Uy, R. M. Dickson, K. E. Kerr, Y. Zhang and T. Oka, "Selection rules for nuclear spin modifications in ion-neutral reactions involving H_3^+ " *J. Chem. Phys.* **113**, 3181-3193 (2000).
29. E. Hugo, O. Asvany and S. Schlemmer, " $\text{H}_3^+ + \text{H}_2$ isotopic system at low temperatures: Microcanonical model and experimental study" *J. Chem. Phys.* **130**, 164302 (2009).
30. N. J. Kirchner and M. T. Bowers, "Fragmentation dynamics of metastable hydrogen-ion cluster H_5^+ , H_7^+ , and H_9^+ - Experiment and theory" *J. Phys. Chem.* **91**, 2573 (1987).
31. A. B. Less and P. K. Rol, "Merging beams study of the $\text{H}_3^+(\text{D}_2, \text{H}_2)\text{HD}_2^+$ reaction mechanism" *J. Chem. Phys.* **63**, 5077 (1975).
32. S. L. Bennett and F. H. Field, "Reversible Reactions of Gaseous Ions .7. Hydrogen Systems" *J. Am. Chem. Soc.* **94**, 8669 (1972).

33. M. T. Elford and H. B. Milloy, "Mobility of H_3^+ and H_5^+ ions in hydrogen and equilibrium constant for reaction $\text{H}_3^+ + 2\text{H}_2 \rightleftharpoons \text{H}_5^+ + \text{H}_2$ at Gas temperatures of 195, 273 and 293K" *Aust. J. Phys.* **27**, 211 (1974).
34. R. Johnsen, C. M. Huang, and M. A. Biondi, "3-Body association reactions of H^+ and H_3^+ ions in hydrogen from 135 to 300K" *J. Chem. Phys.* **65**, 1539 (1976).
35. R. J. Beuhler, S. Ehrenson, and L. Friedman, "Hydrogen cluster ion equilibria" *J. Chem. Phys.* **79**, 5982 (1983).
36. M. T. Elford, "The heat of dissociation of H_5^+ derived from measurements of ion mobilities" *J. Chem. Phys.* **79**, 5951 (1983).
37. C. M. Lindsay and B. J. McCall, "Comprehensive evaluation and compilation of H_3^+ spectroscopy" *J. Mol. Spec.* **210**, 60 (2001).
38. T. R. Geballe and T. Oka, "A key molecular ion in the universe and in the laboratory" *Science* **312**, 1610 (2006).
39. D. Gerlich, E. Herbst and E. Roueff, " $\text{H}_3^+ + \text{HD} \rightleftharpoons \text{H}_2\text{D}^+ + \text{H}_2$: low-temperature laboratory measurements and interstellar implications" *Planet Space Sci.* **50**, 1275 (2002).
40. M. Okumura, L. I. Yeh and Y. T. Lee, "The vibrational predissociation spectroscopy of hydrogen cluster ions" *J. Chem. Phys.* **83**, 3075-3076 (1985).
41. M. Okumura, L. I. Yeh and Y. T. Lee, "Infrared-spectroscopy of the cluster ions $\text{H}_3^+(\text{H}_2)_n$ " *J. Chem. Phys.* **88**, 79-91 (1988).
42. T. C. Cheng, B. Bandyopadhyay, Y. Wang, S. Carter, B. J. Braams, J. M. Bowman and M. A. Duncan, "Shared-Proton Mode Lights up the Infrared Spectrum of Fluxional Cations H_5^+ and D_5^+ " *J. Phys. Chem. Lett.* **1**, 758-762 (2010).

43. Y. Yamaguchi, J. F. Gaw, R. B. Remington and H. F. Schaefer III, "The H_5^+ potential energy hypersurface – characterization of 10 distinct energetically low-lying stationary-points" *J. Chem. Phys.* **86**, 5072-5081 (1987).
44. Z. Xie, B. J. Braams and J. M. Bowman, "Ab initio global potential-energy surfaces for $H_5^+ \rightarrow H_3^+ + H_2$ " *J. Chem. Phys.* **122**, 224307 (2005).
45. P. H. Acioli, Z. Xie, B. J. Braams and J. M. Bowman, "Vibrational ground state properties of H_5^+ and its isotopomers from diffusion Monte Carlo calculations" *J. Chem. Phys.* **128**, 104318 (2008).
46. B. A. McGuire, Y. Wang, J. M. Bowman and S. I. Widicus-Weaver, "Do H_5^+ and its isotopologues have rotational spectra?" *J. Phys. Chem. Lett.* **2**, 1045-1047 (2011).
47. R. Prosimiti, P. Villarreal and G. Delgado-Barrio, "Structures and energetic of H_n^+ clusters (n=5-11)" *J. Phys. Chem. A* **107**, 4768-4772 (2003).
48. A. Aguado, P. Barragan, R. Prosimiti, G. Delgado-Barrio, P. Villarreal and O. Roncero, "A new accurate and full dimensional potential energy surface for H_5^+ based on a triatomics-in-molecules analytic functional form" *J. Chem. Phys.* **133**, 24306 (2010).
49. P. Barragan, R. Prosimiti, O. Roncero, A. Aguado, P. Villarreal and G. Delgado-Barrio, "Towards a realistic density functional theory potential energy surface for the H_5^+ cluster" *J. Chem. Phys.* **133**, 54303 (2010).
50. G. M. e Silva, R. Gargano, W. B. da Silva, L. F. Roncaratti and P. H. Acioli, "Quantum Monte Carlo and genetic algorithm study of the potential energy surface of the H_5^+ molecule" *Int. J. Quantum Chem.* **108**, 2318-2325 (2007).
51. Y. Ohta, K. Ohta and K. Kinugawa, "Quantum effect on the internal proton transfer and structural fluctuation in the H_5^+ cluster" *J. Chem. Phys.* **121**, 10991-10999 (2004).

52. H. Chermette and I. V. Ymmud, "Structure and stability of hydrogen clusters up to H_{21}^{+} " *Phys. Rev. B* **63**, 165427 (2001).
53. W. P. Kraemer, V. Spirko and O. Bludsky, "Extended ab-initio study of the vibrational dynamics of H_5^+ and D_5^+ including all vibrational modes" *J. Mol. Spec.* **165**, 500-509 (1994).
54. V. Spirko, T. Amano and W. P. Kraemer, "Vibrational predissociation of H_5^+ " *J. Chem. Phys.* **124**, 244303 (2006).
55. M. Barbatti, G. Jalbert and M. A. C. Nascimento, "The structure and thermochemical properties of the $H_3^+(H_2)_n$ clusters (n=8-11) *J. Chem. Phys.* **114**, 7066-7072 (2001).
56. M. Barbatti and M. A. C. Nascimento, "Vibrational analysis of small H_n^+ hydrogen clusters" *J. Chem. Phys.* **119**, 5444-5448 (2003).
57. K. LaiHing, P. Y. Cheng, T. G. Taylor, K. F. Wiley, M. Peschke, and M. A. Duncan, "Photodissociation in a reflectron time-of-flight mass-spectrometer – A novel mass-spectrometry mass-spectrometry configuration for high-mass systems" *Anal. Chem.* **61**, 1458 (1989).
58. D. S. Cornett, M. Peschke, K. LaiHing, P. Y. Cheng, K. F. Wiley, and M. A. Duncan, "Reflectron time-of-flight mass-spectrometer for laser photodissociation" *Rev. Sci. Instrum.* **63**, 2177 (1992).
59. B. Bandyopadhyay, T. C. Cheng and M. A. Duncan, "Proton sharing in hydronium-nitrogen clusters probed with infrared spectroscopy" *Int. J. Mass Spectrom.* **297**, 124 (2010).
60. A. M. Ricks, G. E. Douberly and M. A. Duncan, "Infrared spectroscopy of proton-bridged nitrogen dimers: Complex vibrational dynamics of the shared proton" *J. Chem. Phys.* **131**, 104312 (2009).

61. G.E. Douberly, A.M. Ricks, B.W. Ticknor and M.A. Duncan, "Infrared spectroscopy of protonated acetone and its dimer" *Phys. Chem. Chem. Phys.* **10**, 77 (2008).
62. G.E. Douberly, A.D. Ricks, B.W. Ticknor and M.A. Duncan, "The structure of protonated carbon dioxide clusters: Infrared photodissociation spectroscopy and ab initio calculations" *J. Phys. Chem. A* **112**, 950 (2008).
63. G.E. Douberly, A.M. Ricks, B.W. Ticknor, W.C. McKee, P.v.R. Schleyer and M.A. Duncan, "Infrared photodissociation spectroscopy of protonated acetylene and its clusters" *J. Phys. Chem. A* **112**, 1897 (2008).
64. A. M. Ricks, G. E. Douberly, P. v. R. Schleyer and M. A. Duncan, "The infrared spectrum of gas phase $C_3H_3^+$: The cyclopropeny and propargyl cations" *J. Chem. Phys.* **132**, 051101 (2010).
65. A. M. Ricks, G. E. Douberly, P. v. R. Schleyer and M. A. Duncan, "Infrared spectroscopy of protonated ethylene: The nature of proton binding in the non-classical structure" *Chem. Phys. Lett.* **480**, 17 (2009).
66. A. M. Ricks, G. E. Douberly and M. A. Duncan, "The infrared spectroscopy of protonated naphthalene and its relevance for the unidentified infrared bands" *Astrophys. J.* **702**, 301 (2009).
67. G.E. Douberly, A.M. Ricks, B.W. Ticknor, P.v.R. Schleyer and M.A. Duncan, "Infrared spectroscopy of gas phase benzenium ions: Protonated benzene and protonated toluene from 750 to 3400 cm^{-1} " *J. Phys. Chem. A* **112**, 4869 (2008).

68. G.E. Douberly, A.M. Ricks, P.v.R. Schleyer and M.A. Duncan, "Infrared spectroscopy of gas phase $C_3H_5^+$: The allyl and 2-propenyl cations," *J. Chem. Phys.* **128**, 021102 (2008).
69. G.E. Douberly, A.M. Ricks, B.W. Ticknor, W.C. McKee, P.v.R. Schleyer and M.A. Duncan, "Infrared photodissociation spectroscopy of protonated acetylene and its clusters" *J. Phys. Chem. A* **112**, 1897 (2008).
70. G.E. Douberly, A.M. Ricks, B.W. Ticknor, P.v.R. Schleyer and M.A. Duncan, "The infrared spectrum of the tert-butyl cation in the gas phase" *J. Am. Chem. Soc.* **129**, 13782 (2007).

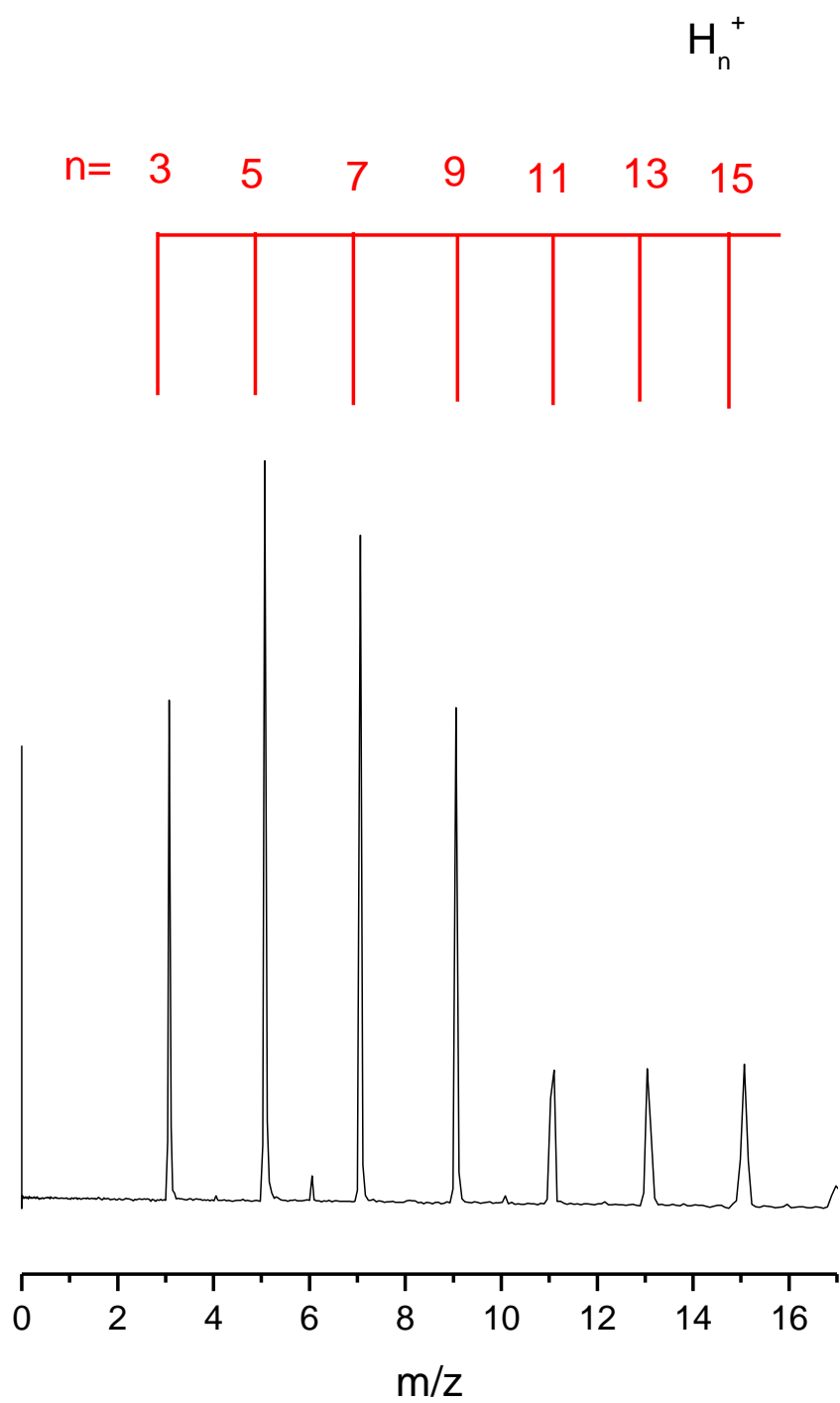


Figure 1: Mass spectrum of a pure hydrogen discharge.

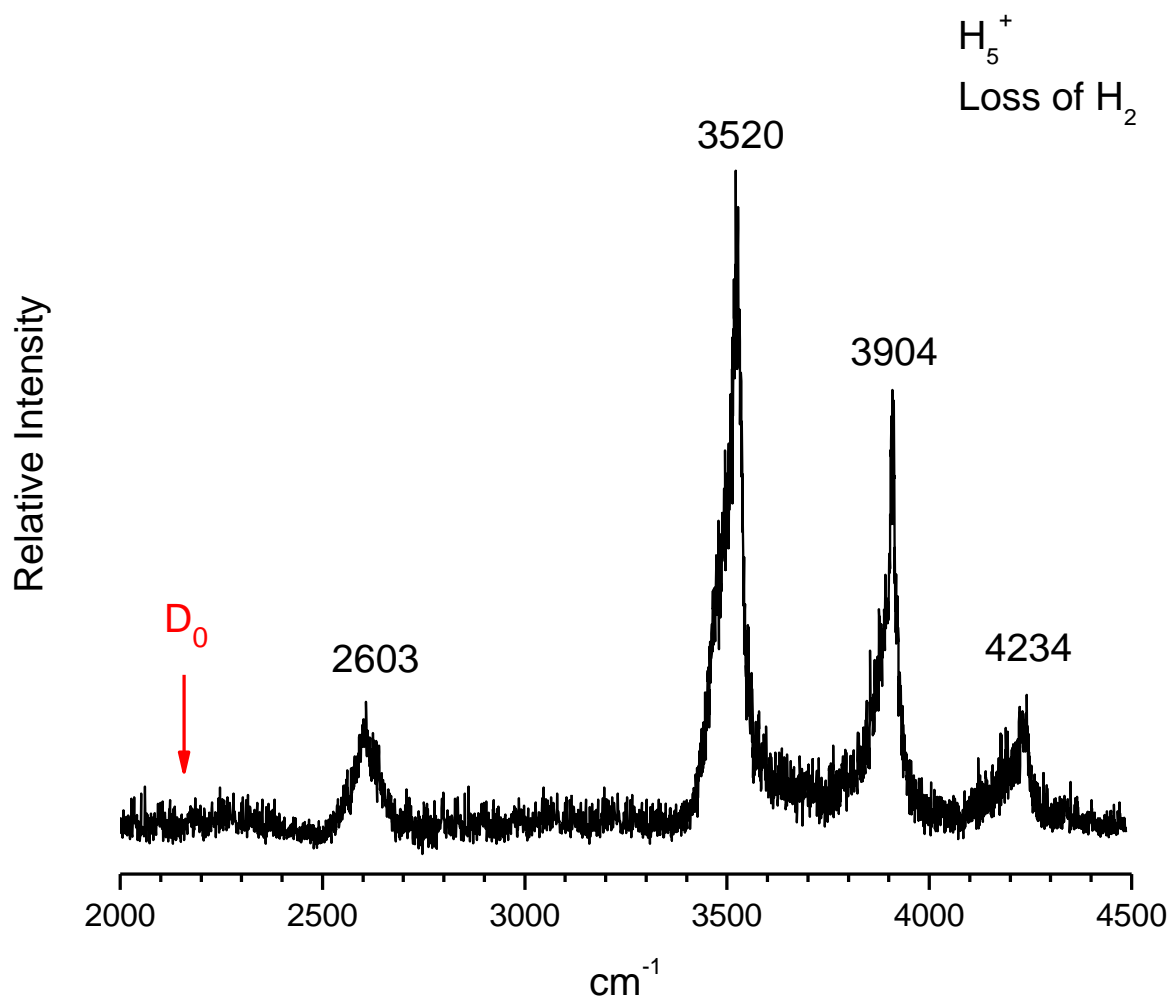


Figure 2: The infrared spectrum of H_5^+ , measuring the appearance of H_3^+ , the byproduct of photodissociation with an infrared laser. The calculated dissociation limit of 2227 cm^{-1} is labeled as D_0

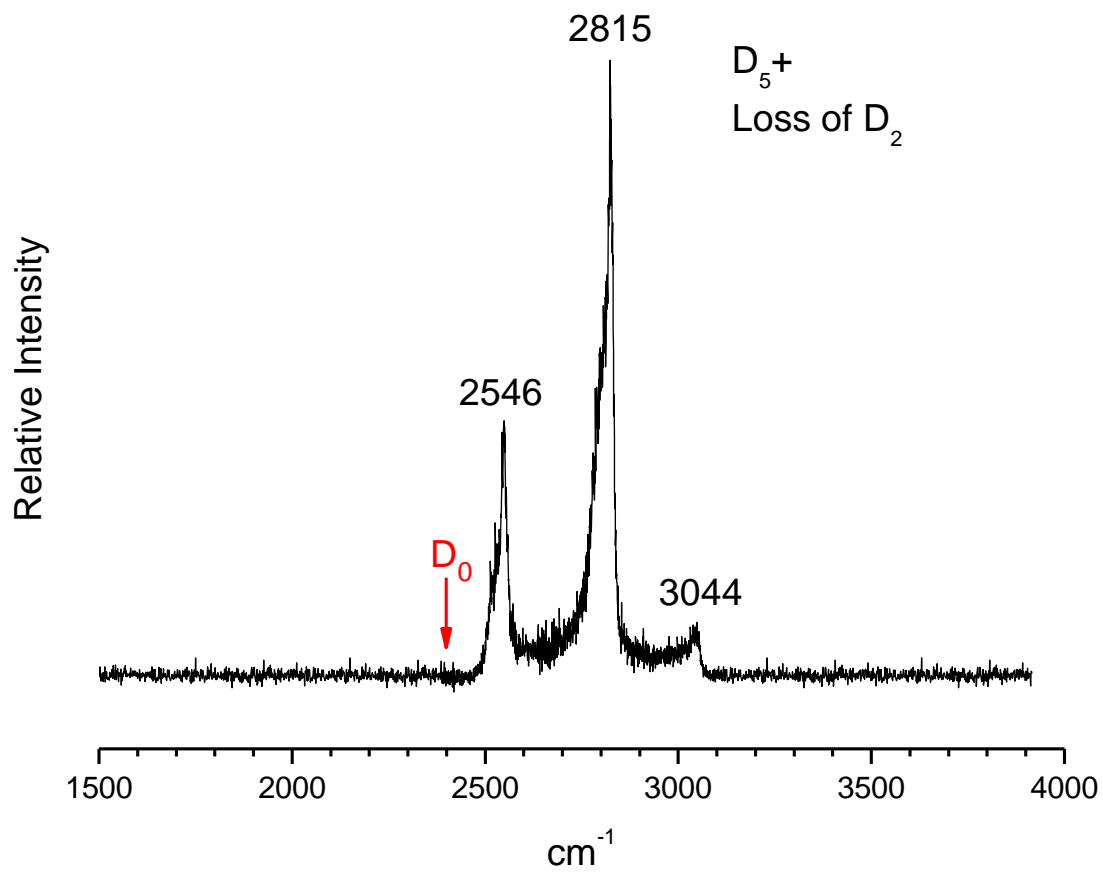


Figure 3: Infrared spectrum of D_5^+ , measuring the appearance of D_3^+ , the fragment of photodissociation of D_5^+ . The dissociation limit, D_0 , is calculated to be at 2400 cm^{-1} .

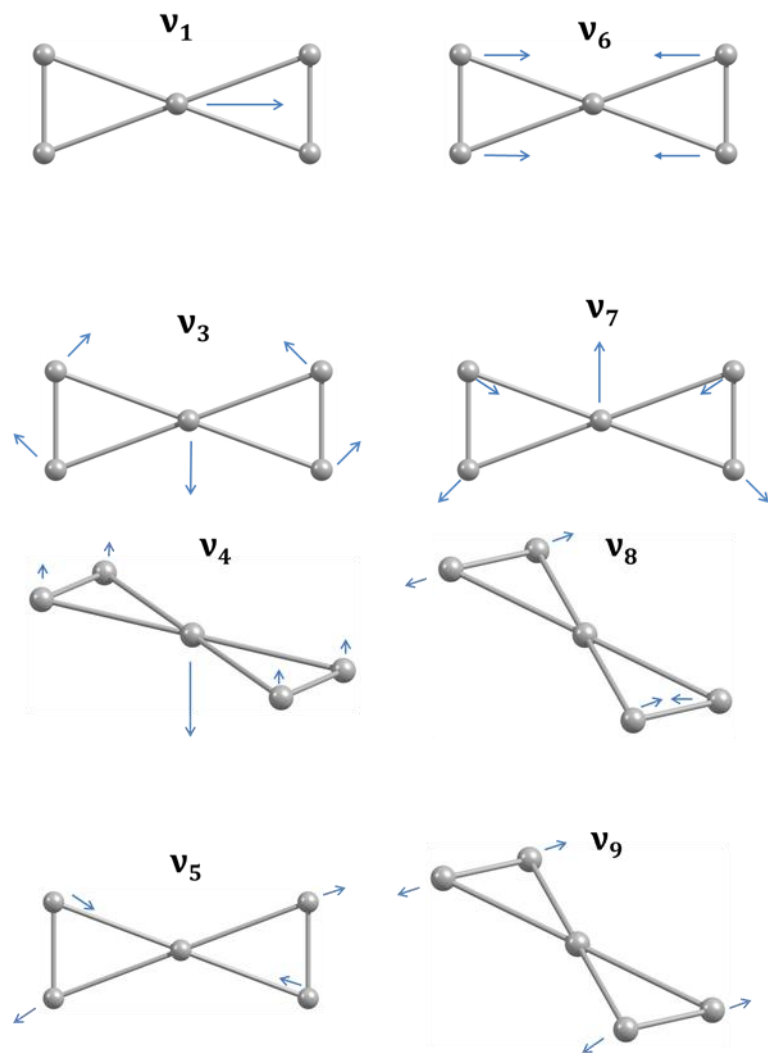


Figure 4: Important fundamental modes of the shared proton, H_5^+ . The fundamental ν_1 mode is predicted to be around 370 cm^{-1} with very strong oscillator strength.

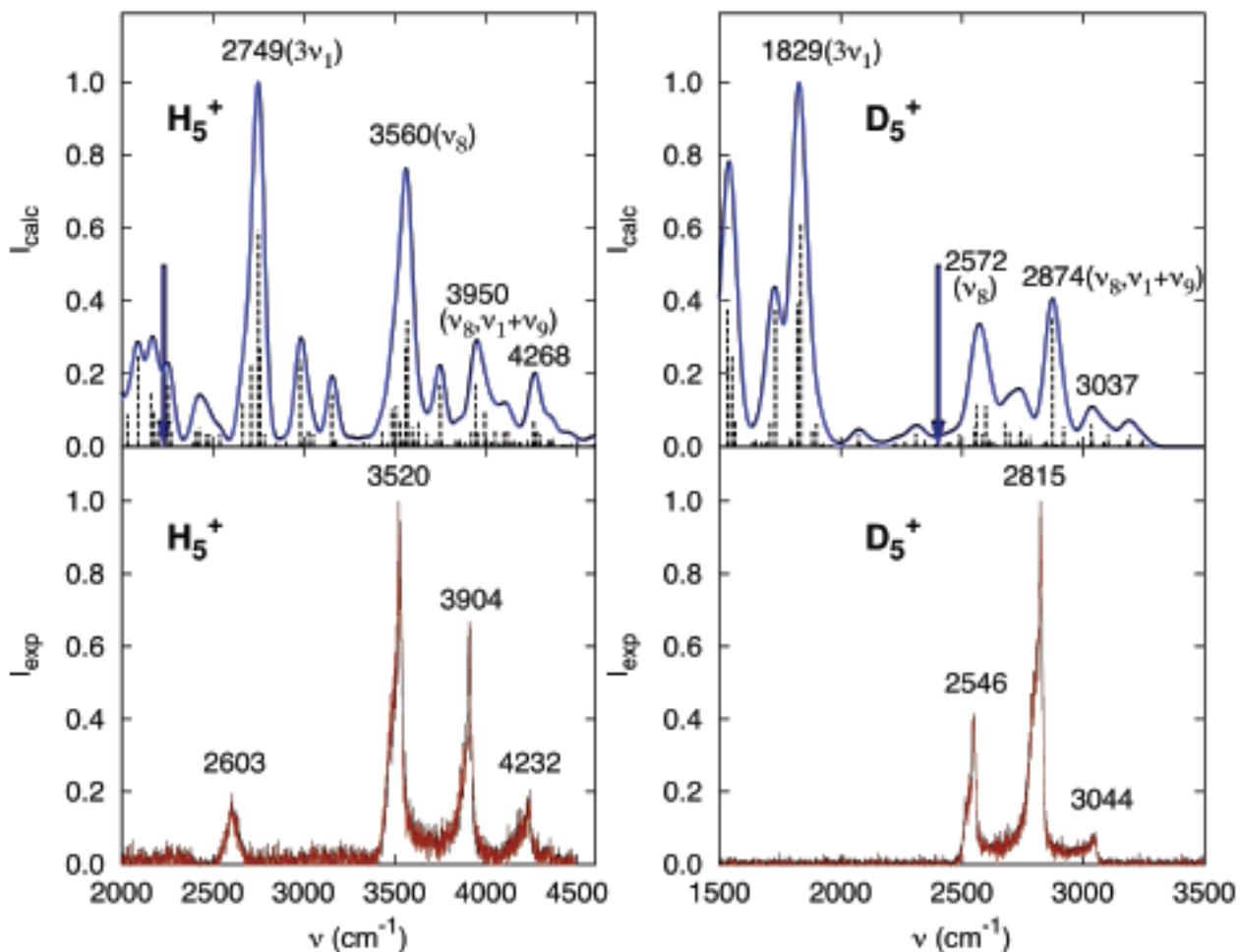


Figure 5: Comparison of the theoretical calculated spectrum, in blue, with the measured experimental spectrum, in red of H_5^+ and D_5^+ . This theory comes from the work of Dr. Bowman and coworkers at Emory University. The predicted dissociation limit for H_5^+ and D_5^+ are labeled with the arrow. Assignments of the experimentally observed bands are in good agreement with the predicted theoretical spectrum.

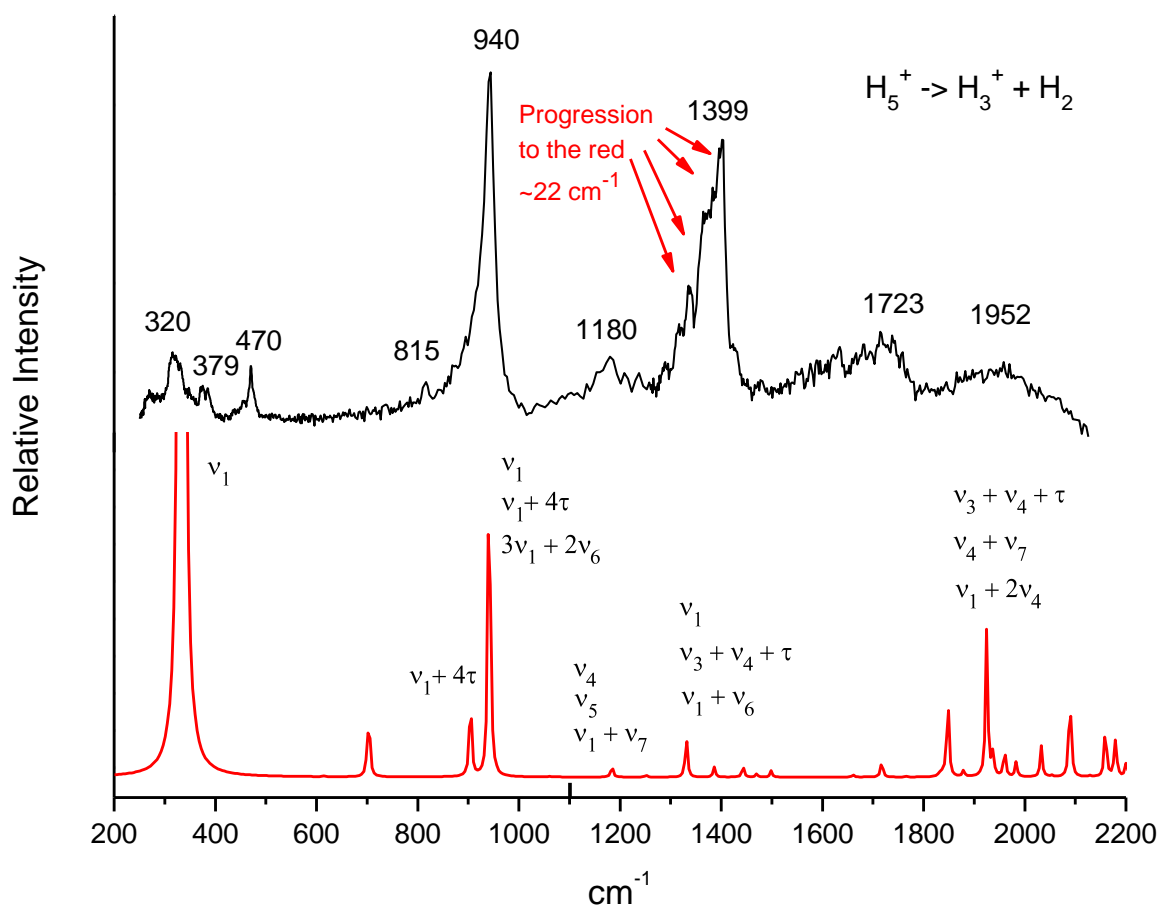


Figure 6: Infrared spectrum of H_5^+ , measured at FELIX, measured in the mass channel corresponding the loss of neutral H_2 . The top trace is the experimental results while the bottom trace is the predicted theoretical spectrum with peak assignments. Multi-photon dissociation is needed to be able to overcome the dissociation limit of these complexes.

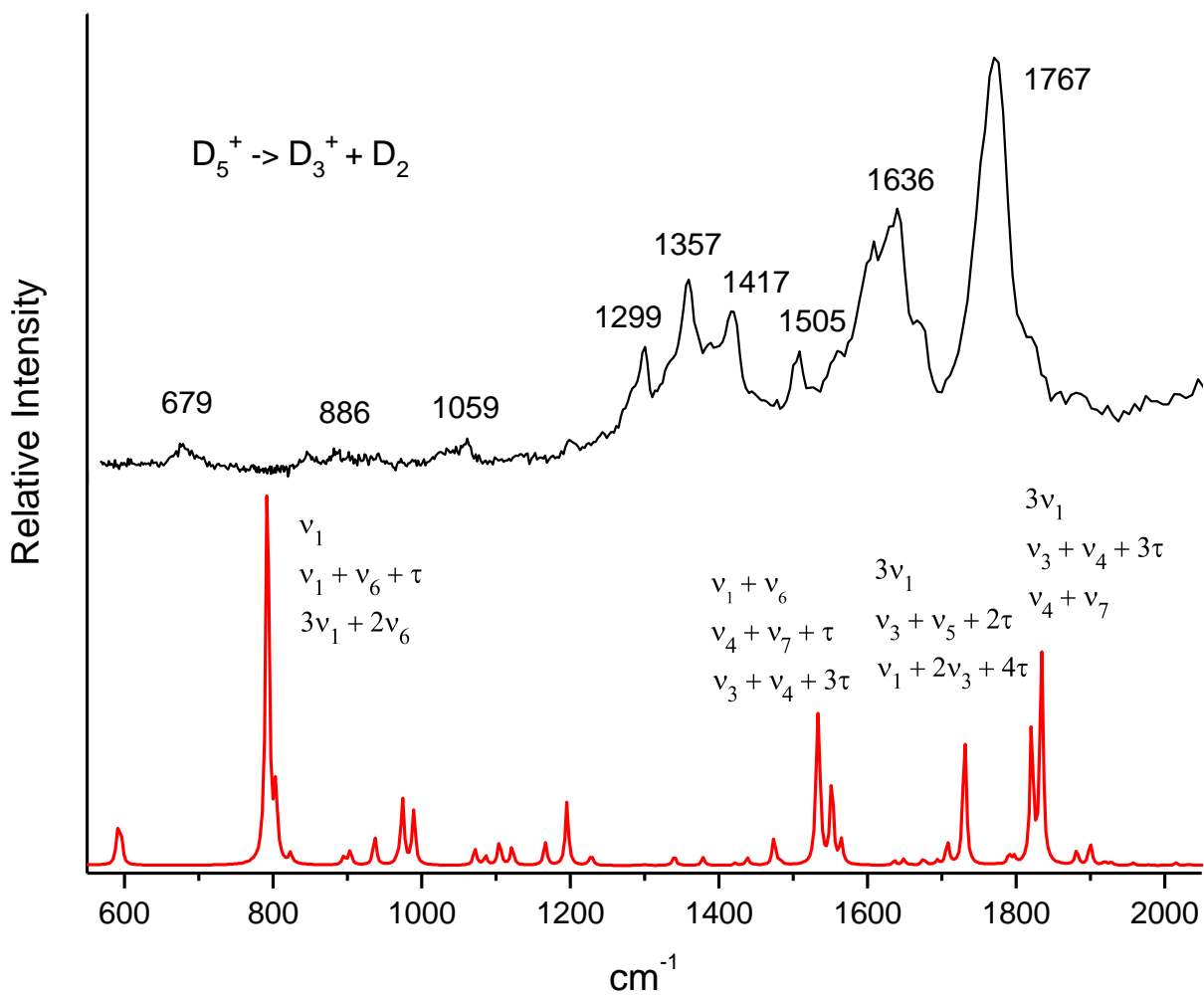


Figure 7: Infrared spectrum of D_5^+ , measured at FELIX, corresponding to the loss of neutral D_2 . The top trace is the experimental results while the bottom trace is the theoretical spectrum with peak assignments provided by Bowman and coworkers.

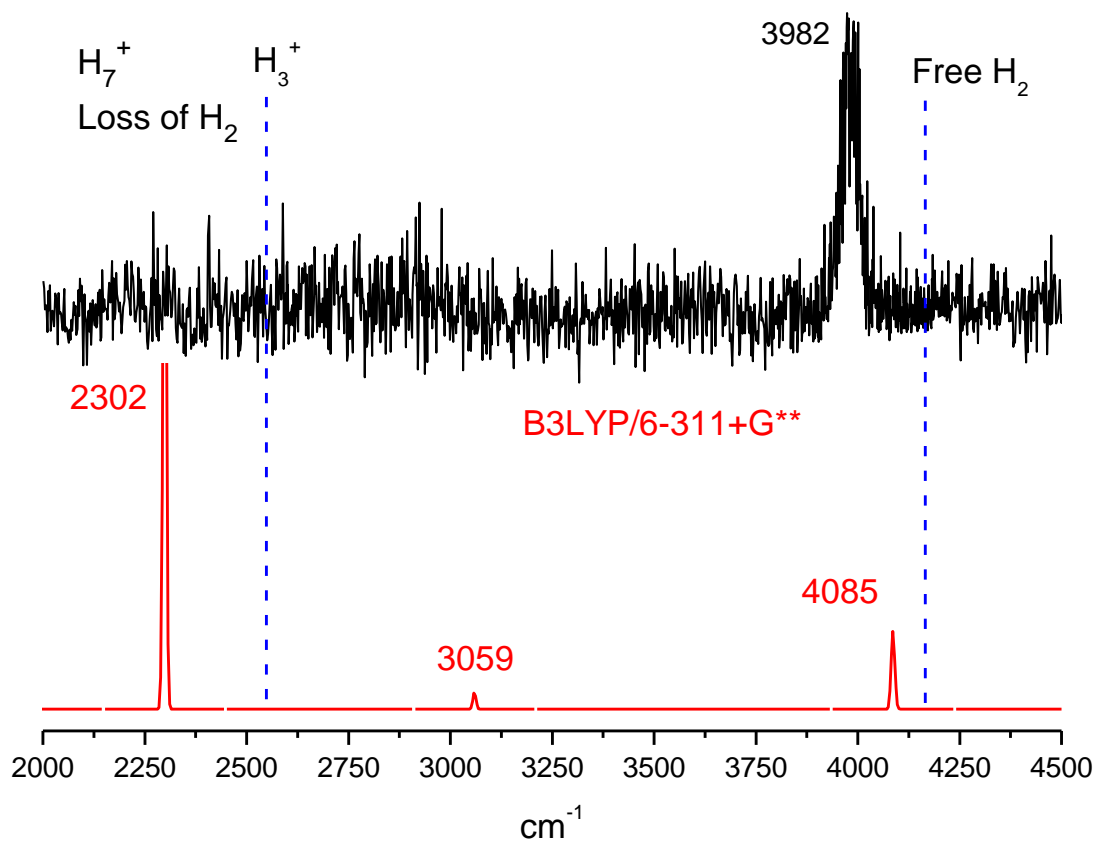


Figure 8: Infrared spectrum of H_7^+ , measured in the mass channel corresponding to the loss of neutral H_2 , shown in the top trace compared with theory shown in red on the bottom trace.

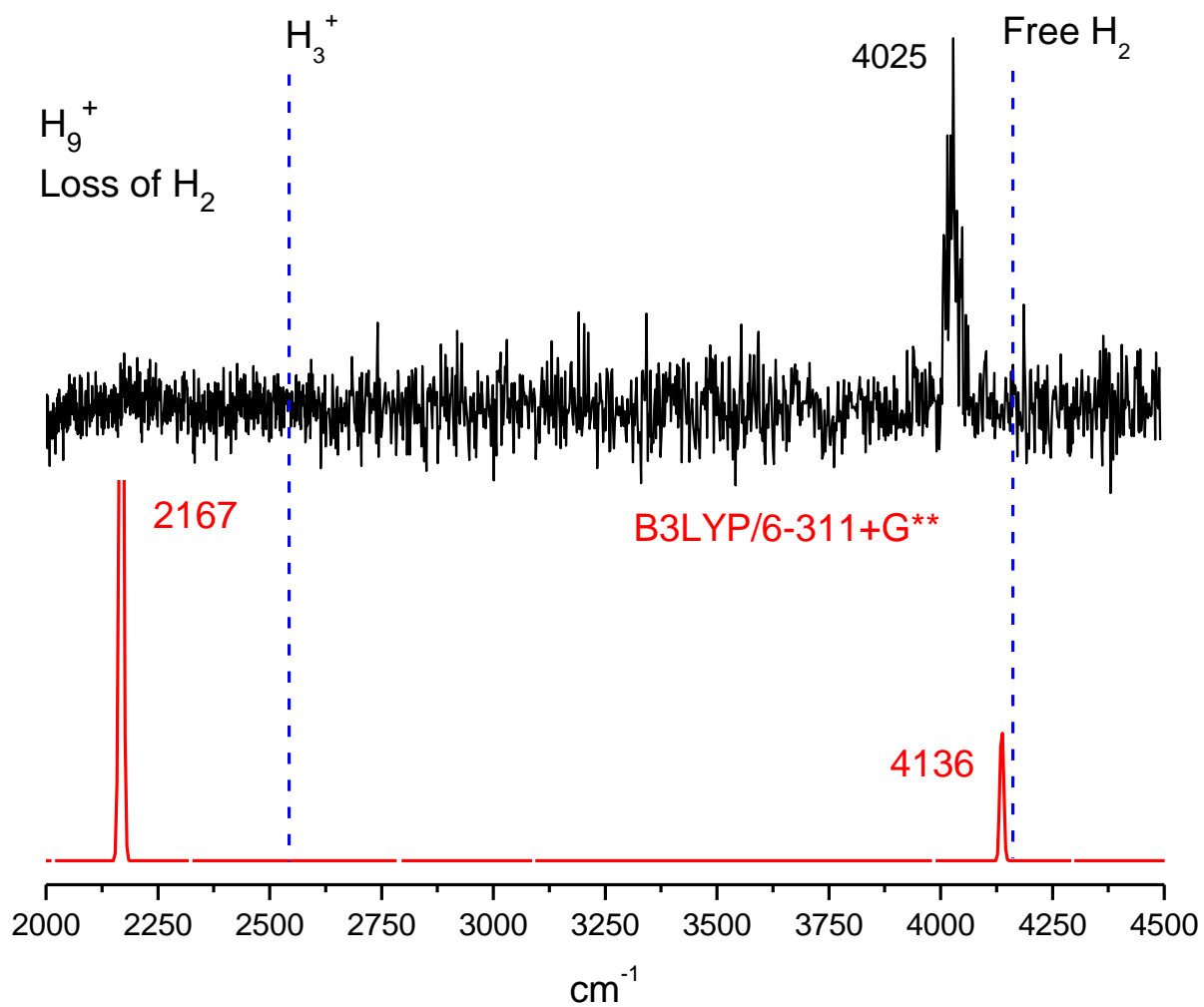


Figure 9: The infrared spectrum of H_9^+ measured in the mass channel corresponding to the appearance of H_7^+ , shown in the top trace, compared with theory below it.

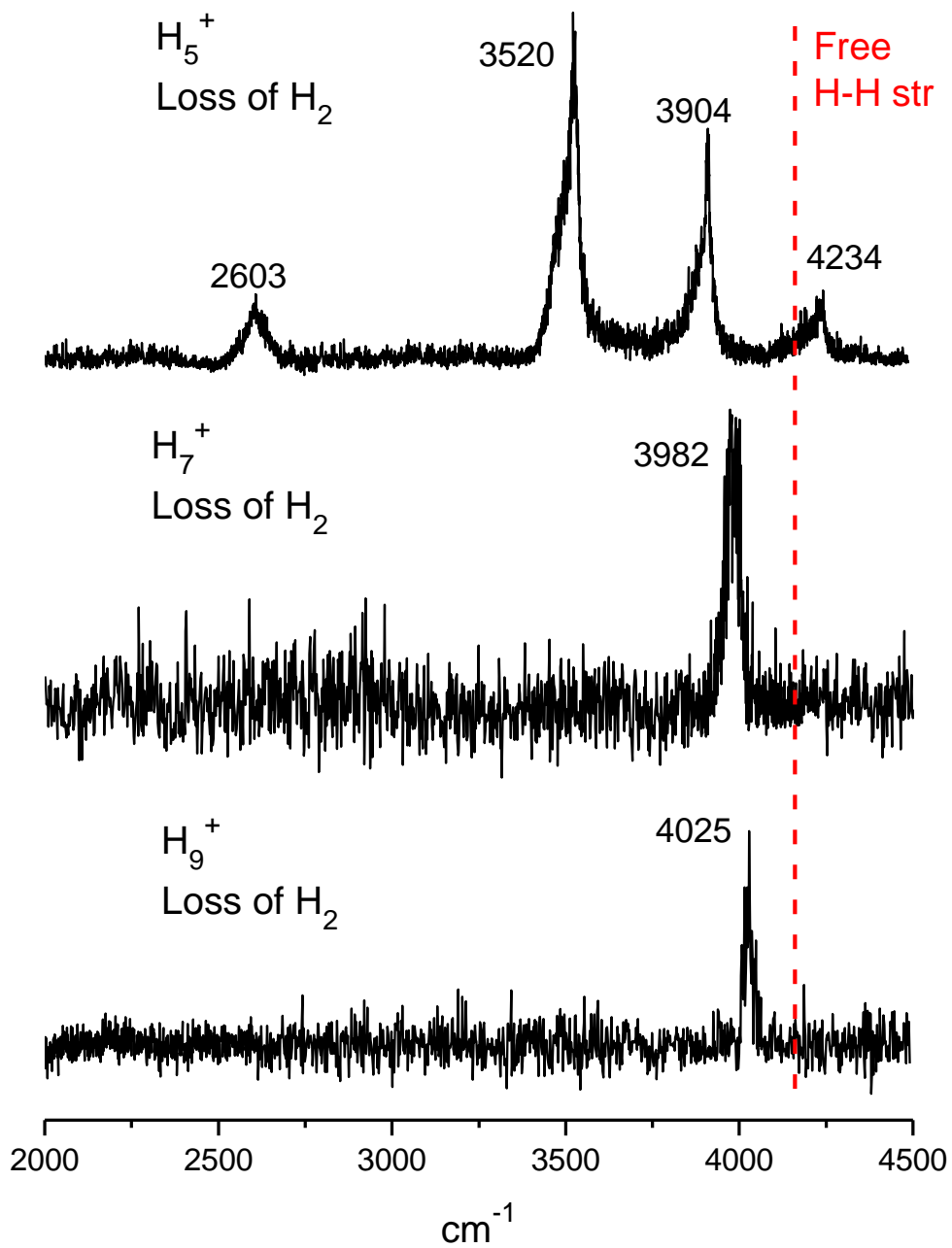


Figure 10: Infrared spectrum of H₅⁺, H₇⁺, and H₉⁺ in the mid-infrared region collected by measuring the appearance of the ion corresponding to the loss of H₂.

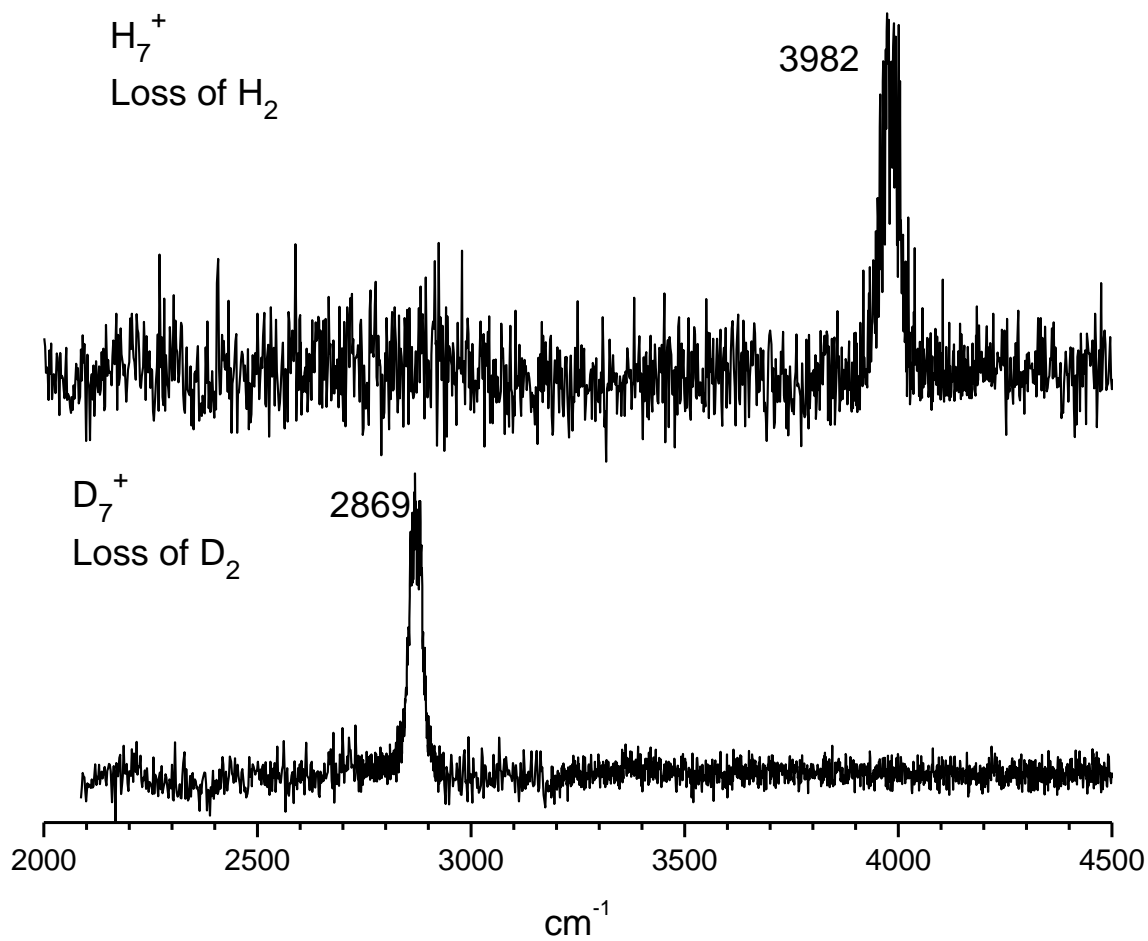


Figure 11: Comparison of the infrared spectrum of H_7^+ and D_7^+ , both collected by monitoring the mass channel corresponding to the fragmentation loss of neutral hydrogen molecule.

CHAPTER V

INFRARED PHOTODISSOCIATION SPECTROSCOPY

OF PROTONATED BENZENE-WATER CLUSTERS¹

¹ T. C. Cheng, B. Bandyopadhyay, and M. A. Duncan, To be submitted to *J. Am. Chem. Soc.*

Abstract

Protonated mixed clusters of benzene and water, $H^+(bz)_m(H_2O)_n$, where $m=1-4$ and $n=1-2$, are produced via arc discharge in a molecular beam apparatus and probed using infrared photodissociation spectroscopy. These clusters involve a shared proton stretch vibration, whose frequency is sensitive to small structural variations. For $H^+bz(H_2O)-Ar$, the infrared spectrum suggests that the proton is unequally shared between the water and benzene, favoring the water more than benzene. Solvation of the hydronium ion by multiple benzene molecules causes charge delocalization, which results in weaker blue-shifts of the benzene-bound O-H stretch with each additional benzene molecule. The solvation of the Zundel ion by benzene molecules polarizes the Zundel ion, causing unequal sharing of the proton between the two water molecules. This causes a blue-shift in the shared proton stretch in the infrared spectrum.

Introduction

Protonation and proton transfer are key aspects in many areas of chemistry, including many reactions in biology, acid-base reactions, interstellar chemistry, and atmospheric chemistry.¹⁻⁶ In many compounds, the position of the proton has not been measured, and the effects of protonation are hard to calculate because of the many intermolecular forces that are involved. Because of the importance of protonation and proton transfer, there have been many studies on the mechanism of these reactions.⁷⁻¹⁰ Many situations of proton transfer involve intermediate complexes where the proton is shared between two different molecules. Protonated benzene-water complexes are a good model system to gain a fundamental understanding of how the intermolecular interactions affect the preferred protonation site among mixed clusters.

There have been numerous studies looking into the structure of pure protonated water clusters, both with experimental and computational methods.¹¹⁻⁶⁵ Structural studies of the solvated proton in water have focused on two main isomers. The first, H_9O_4^+ , commonly known as the “Eigen” ion, was proposed in 1958, and consists of the hydronium solvated by three neutral water molecules.¹¹⁻¹⁴ The second, which consists of a proton shared between two water molecules, $\text{H}_2\text{O}-\text{H}^+-\text{H}_2\text{O}$, was proposed in 1978, and is commonly known as the “Zundel” ion.¹⁵⁻¹⁶ These two structures are important in the proton transport mechanism in water, which was first proposed by Grotthuss in 1806.¹⁷ Depending on the number of water molecules solvating the proton, theory predicts either the Eigen or the Zundel ion motif for proton solvation.³¹

Spectroscopy of pure protonated water clusters and pure protonated benzene clusters has been studied experimentally previously.¹⁸⁻²⁸ Protonated water, H_3O^+ , was first detected by high-resolution infrared spectroscopy by Saykally and coworkers in 1983, and was the focus of

numerous other theoretical and experimental studies.¹⁸ Using high resolution spectroscopy, the symmetric and asymmetric stretches of hydronium were measured at 3530.165 and 3513.840 cm⁻¹ respectively. Larger protonated water clusters H⁺(H₂O)_n, have also been studied extensively.²⁰⁻
²⁸ Protonated benzene and its clusters have also been an area of previous computation and experimental studies.⁶⁷⁻¹⁰²

In a mixed cluster species, the protonation site is hard to predict. A logical guess is that a proton would be located closer to the molecule with the higher proton affinity. Because the proton affinity of benzene (750.4 kJ/mol) is higher than that of water (691.0 kJ/mol), the proton would then be expected to bind to benzene. Johnson and coworkers have compared the location of the shared proton stretch vibration versus the difference in proton affinity between the two different molecules.¹⁰³ Recent work by Fridgen and coworkers have shown situations where the trend of the shared proton stretch position in relation to the Δ PA is not followed, specifically when the shared proton is between molecules with a high dipole moment.¹⁰⁴ This was shown by Johnson and coworkers for the shared proton between water and acetonitrile.¹⁰⁵

Previous work studying the structure of different benzene-water clusters both experimentally and with computational methods has provided a good understanding of neutral and cation mixed benzene water clusters.¹⁰⁶⁻¹²⁵ Mikami and coworkers have studied benzene-water cation clusters and saw structural changes upon photoionization for these complexes.¹⁰⁸⁻¹¹¹ Zweir and coworkers have studied the mixed benzene-water neutral clusters, and the structure of these complexes.¹¹⁷⁻¹²⁰ Chang and coworkers have studied protonated benzene with two waters in the high-frequency modes around the O-H stretch.¹²¹ Computational studies with different levels of theory have tackled the protonated 1:1 benzene water complex and have predicted

several low energy isomers. Nyugen and coworkers studied the protonated benzene water cluster computationally, predicting the proton to be associated stronger with water than benzene.¹²⁵

The solvation of protonated species is also an important chemical process. Previous work on the solvation of charged species has shown charge delocalization with the addition of subsequent molecules.¹²⁶ When water is solvated with $n=1,2,3$ nitrogen molecules, charge delocalization causes the strength of each subsequent interaction with nitrogen to decrease. This causes a smaller red-shift of the band corresponding to the nitrogen-interacting O-H stretch. In the solvation of water with benzene, charge delocalization effects are also expected to play a key role in the structures.

In this work, infrared photodissociation spectroscopy is employed on protonated mixed benzene-water clusters, $H^+(bz)_m(H_2O)_n$ where $m=1-4$ and $n=1-2$. By comparing the experimental results with computed structures, the protonation site of these complexes along with the effects of benzene solvation were examined. Solvation effects from the addition of subsequent benzene molecules were studied on the hydronium ion along with the Zundel ion.

Experimental

Mixed clusters of protonated water and benzene are formed using an arc discharge source in a home-built molecular beam apparatus. The experimental details have been described previously.¹²⁶⁻¹⁴⁰ Briefly, protonated benzene-water clusters are produced by adding both water and benzene in a chilled reservoir at the gas inlet. The gas is pulsed into a molecular beam apparatus through a pulsed valve with a backing pressure of around 150 psi for 280 μ s. At the throat of the expansion, an electrical discharge of around 1600 V for 20 μ s between two needles

forms a plasma. Within this plasma, a variety of complexes are formed including positive, negative and neutral clusters. Through collisional and evaporative cooling, protonated mixed benzene-water complexes are produced. The ions are skimmed into the second chamber, which contains the reflectron time-of-flight mass spectrometer. They are then pulse extracted into the first flight tube, where the ions are mass selected using a pulsed mass gate. After the mass gate, the ions enter the reflectron region of the time-of-flight. At the turning region of the reflectron, the ions are intersected with the tunable output of an infrared OPO/OPA system. Upon resonance absorption, photodissociation occurs if the binding energy of the ion is less than the energy of the infrared photon. The parent and fragment ions are reaccelerated out of the reflectron into a second flight tube, where separation of masses occurs. By measuring the fragment intensity vs. wavelength an infrared spectrum can be measured on a zero background.

To measure the smaller benzene-water clusters, argon tagging is required since the binding energy of these complexes is higher than the energy of the infrared photon. For the larger complexes, elimination of neutral benzene is measured. The effects of rare gas tagging can be simulated via computations using Gaussian 03W, and in most situations, tagging is found to yield a small perturbation on the structure and frequency of the infrared stretches.

Computations investigating the structure, energetics and predicted infrared spectra are done with the Gaussian 03W suite of programs.^{S1} Density functional theory (DFT) and Moller-Plesset perturbation theory (MP2) calculations are used to explore the effects of different levels of theory for the lowest isomer of all these molecules. For a scaling factor, the recommended values of 0.9575 and 0.9352 for B3LYP and MP2 calculations are used respectively. Calculated isomer energies, structures, and predicted infrared spectra are shown in the Appendix.

Results and Discussion

Figure 1 shows a full mass spectrum of protonated mixed clusters of benzene and water. In this spectrum, clustering of water and benzene can be seen with minimal amounts of fragmentation of either precursors. The main progression of peaks separated by 78 a.m.u corresponds to clustering of benzene molecules on a protonated benzene. In addition to the pure protonated benzene clusters, water clustering on the benzene clusters is present, seen by the peaks separated by 18 a.m.u. The mass spectrum can be changed to favor different ratios between benzene and water by adjusting the discharge conditions along with the ratio of benzene and water. In this particular spectrum, conditions were modified to have large amounts of water clustering with benzene, which was achieved by cooling only the benzene while keeping the water vapor pressure at room temperature. Argon tagging is required to measure photodissociation of the smaller benzene-water complexes and argon-adduct ions correspond to some of the small peaks observed in the mass spectrum. One particular problem when working with mixed benzene-water clusters is mass coincidences. This is the case for the near mass coincidence between two waters with an argon atom (76 a.m.u.) and a single benzene molecule (78 a.m.u.).

A brief background on the structure and spectral signatures of protonated water and protonated benzene is needed to understand the structure of mixed protonated benzene-water clusters. Figure 2 shows the IRPD spectrum of previously measured argon tagged hydronium ion ($\text{H}_3\text{O}^+-\text{Ar}_2$), which is shown on the top trace, and protonated benzene argon-tagged, ($\text{H}^+\text{bz}-\text{Ar}$), shown on the bottom trace, both monitoring the mass channel corresponding to the loss of Ar. Both of these clusters have been studied before and have been described in detail.^{22-27, 102} The measurement of the infrared spectrum of H_3O^+ requires tagging with two argon atoms

because the binding energy of a single argon is too strong to measure the full infrared spectrum. The infrared spectrum consists of three distinct bands in the mid-IR region, at 3187, 3266, and 3540 cm^{-1} . With two argon atoms, there is one free O-H stretch in $\text{H}_3\text{O}^+\text{-Ar}_2$, assigned to the band at 3540 cm^{-1} , which corresponds well with the known hydronium symmetric and asymmetric stretch at 3514 and 3530 cm^{-1} respectively. The two other bands, at 3187 and 3266 cm^{-1} , correspond to the O-H stretches that are interacting with Ar. In the far-IR region, two low frequency bands are seen at 1613 and 1876 cm^{-1} . These two bands are assigned to the bending mode of hydronium and a combination band on top of the bending mode respectively.

The bottom trace of Figure 2 is the infrared spectrum of $\text{H}^+\text{bz-Ar}$ measuring the fragment corresponding to the loss of Ar. One of the main spectral signatures of protonated benzene is the large band at 2820 cm^{-1} . This band is assigned to overlapping symmetric and asymmetric stretch of the sp^3 hybridized C-H₂ stretch of protonated benzene. The π electrons within the ring are redistributed, leaving a partial positive charge on the opposite side of the sp^3 hybridized CH₂. This delocalization of charge causes the ring modes of benzene, which are usually relatively weak in neutral benzene, to have increased oscillator strength because of the increase in the change in dipole upon the ring mode vibrations. This increase in oscillator strength corresponds to the ring modes observed in the infrared spectrum at 1456 and 1607 cm^{-1} , assigned to the asymmetric stretches of the C-C-C framework of protonated benzene.

An investigation into the structure of mixed benzene-water clusters is performed, using these key spectral signatures to help understand the structure of these complexes. The mass spectrum for the protonated 1:1 benzene-water complex argon tagged ($\text{H}^+\text{bz(H}_2\text{O)-Ar}$) can be seen in the top trace of Figure 3, obtained by measuring the mass channel corresponding to the loss of Ar. The bottom two traces correspond with the predicted spectra of two different

configurations of the shared proton isomer computed using B3LYP/6311⁺G (d,p) level of theory. These two calculated spectra correspond to two different structures of this complex, with the proton either associated closer with water or with benzene. Without argon tagging, no fragmentation is seen at any wavelength. This can be explained because of the binding energy for these complexes, which is calculated to be too high for fragmentation with a single photon in the infrared (see Appendix). Therefore, argon tagging is used to measure the infrared spectrum of this complex, with the binding energy of the argon being estimated to be around 300-400 cm⁻¹. This is weak enough for single photon dissociation throughout the wavelength covered by OPO.

In the infrared spectrum of the H⁺bz(H₂O)-Ar, no bands are present in the area corresponding to the protonated benzene's sp³ hybridized CH₂ stretch, which is predicted by DFT calculations to be shifted down to around 2433 cm⁻¹. The ring modes of the protonated benzene-water complex are predicted at 1224, 1417, and 1572 cm⁻¹, and they are not observed in the experimental spectrum. This suggests that the structure of this protonated complex is not one that includes the protonated benzene configuration. The other isomer, with the hydronium motif, matches better with the infrared spectrum measured. Two bands in the O-H stretching region can be seen at 3395 cm⁻¹ and 3555 cm⁻¹, corresponding with the Ar-perturbed O-H stretch and the free O-H stretch predicted at 3382 cm⁻¹ and 3553 cm⁻¹ respectively. The band at 3090 cm⁻¹ is assigned to the aromatic C-H stretch of the benzene ring, which are in the same wavelength region as the ring modes of benzene seen in water benzene cation clusters observed by Mikami and coworkers.⁶⁹⁻⁷¹ The last band that is easily assigned is the one at 1639 cm⁻¹, similar to the band at 1613 cm⁻¹ seen in the H₃O⁺-Ar complex, which is the bending mode of H₃O⁺.

Theory predicts a strong band at 2247 cm⁻¹, shown in the middle trace of Figure 3, but there are no bands observed in this region experimentally. This predicted band corresponds with

the O-H stretch interacting with the benzene, which accounts for the large red shift in frequency compared to a neutral O-H stretch. How far this O-H bond is red shifted is related to the strength of the bond, which suggests that this bond is much weaker than a normal O-H stretch, and is in the region of the bond strength of a hydrogen bond. Therefore, this O-H stretch can be thought of as a shared proton stretch between the water and benzene instead of an O-H stretch of hydronium interacting with neutral benzene. Shared proton stretch frequencies are known to be hard to model accurately using harmonic calculations. This is because the shared proton can undergo high amplitude motion within a shallow well, which results in the highly anharmonic nature of vibration. This difficulty in accurately describing the shared proton stretch is shown in Figure 4, where the differences between levels of theory (B3LYP vs MP2) drastically differ on the band position of this shared proton stretch, with B3LYP predicting the band at 2247 cm^{-1} while MP2 predicts the band at 2635 cm^{-1} using the same basis set.

Previous experimental measurements of the shared proton stretch have shown a large range in band positions depending on the difference in the proton affinity (ΔPA) between two different constituents in the shared proton complex. A systematic study of where this shared proton stretch is experimentally observed vs. the ΔPA was performed by Johnson and coworkers.¹⁰³ The shared proton stretch was found to be observed from as low as about 750 cm^{-1} for protonated nitrogen dimer to as high as $\sim 3300\text{ cm}^{-1}$ for hydronium argon ($\Delta\text{PA}=320\text{ kJ/mol}$). A correlation between the frequency of the shared proton stretch and ΔPA was observed, which is that when the difference in proton affinity increases, the frequency of the shared proton stretch shifts higher in energy. With the ΔPA between benzene and water being 60 kJ/mol , the shared proton stretch is predicted to be located between 1900 cm^{-1} and 2000 cm^{-1} . Therefore, because we know theory is unable to predict the band position of the shared proton stretch well with

harmonic calculations and because the difference in proton affinity fits well with the curve by Johnson and coworkers, the 1949 cm^{-1} band is assigned to the shared proton stretch between water and benzene.

Two stable isomers of $\text{H}^+\text{bz}(\text{H}_2\text{O})\text{-Ar}$ are used to compare the differences in theory, one where proton interacts closer to water and one with the proton interacting closer to benzene. The results of this are shown in detail in Appendix A. Depending on the level of theory, the global minimum structure of this complex differed between a protonated water and protonated benzene structure. When using DFT calculations, the protonated benzene configuration of this complex is lower in energy by 1.9 kcal/mol . With MP2 calculations, the proton interacting with water is lower in energy compared to the protonated benzene structure by 7.8 kcal/mol . By comparing the experimental results with the predicted frequencies from theory, DFT calculations are able to describe the infrared spectrum better while MP2 calculations is able to describe the lowest energy configuration better.

For a systematic study of the effects of solvation of protonated water with multiple benzene molecules, the protonated two-benzene, 1-water complex, $\text{H}^+(\text{bz})_2(\text{H}_2\text{O})\text{-Ar}$, is measured. The infrared spectrum of this complex is shown in the top trace of Figure 5, measuring the mass channel corresponding to fragmentation of argon, with two different predicted spectra corresponding with two stable conformations predicted by theory. The difference in energy between the two stable configurations is 6.6 kcal/mol in favor of the protonated water configuration. The bottom trace corresponds to the predicted spectrum which has the proton associated with benzene with a neutral water molecule. One large, sharp band is seen at 3457 cm^{-1} while another broad band is seen centered around 2740 cm^{-1} , with what seems to be a broad tailing off in intensity to higher frequency. When comparing the experimental

results with the predicted spectra of these two isomers, the measured spectrum matches better with the structure of protonated water because of the appearance of only one band in the free O-H region along with the better correlation with the frequency predicted for the O-H stretch interacting with the benzene. Two separate bands are predicted in the cis- configurations for the O-H stretch interacting with the π cloud of benzene. Two bands are likely present in the experimental spectrum, with the second band as the shoulder to the blue of the band at 2740 cm^{-1} . Two small bands in the experimental spectrum around 3000 to 3100 cm^{-1} are assigned as either the C-H ring modes of benzene or a combination band of around 250 cm^{-1} from the band at 2740 cm^{-1} . Unlike $\text{bz}(\text{H}_3\text{O}^+)\text{-Ar}$, theory is able to predict the location of the O-H stretch interacting with the benzene extremely well. This is because the structure is not a shared proton structure but a proton interacting strongly with water, which harmonic calculations can accurately describe. The effect of argon tagging on the spectrum can be seen in the Appendix.

The spectrum of $\text{H}^+(\text{bz})_2(\text{H}_2\text{O})\text{-Ar}$ contains both sharp bands and broad features. The reason for the broad bands, assigned to vibrations involving hydrogen bonding, is not well understood. This width is observed in many different hydrogen bonding systems, and a variety of different explanations have been offered, such as slight isomeric variations to the structure, a temperature effect on hydrogen bonding, predissociation lifetimes, and lifetime effects for intramolecular vibrational relaxation (IVR). Slight variations in the structure along with temperature effects can be ruled out because the spectrum contains both sharp and broad bands.

For the IRPD spectrum of protonated 3-benzene water complex, $\text{H}^+(\text{bz})_3(\text{H}_2\text{O})$, elimination of a neutral benzene fragment with a single infrared photon is possible, so argon tagging is not employed for this complex. While argon tagging is not required to fragment in the mid-IR region, no fragmentation is seen in the far-IR region. This is due to the dissociation limit

of this complex, which is calculated to be approximately 4.7 kcal/mol (1700 cm^{-1}). The argon tagged complex could not be measured because of the lack of signal for the parent complex, $\text{H}^+\text{bz}_3(\text{H}_2\text{O})\text{-Ar}$. The infrared spectrum of $\text{H}^+\text{bz}_3(\text{H}_2\text{O})$ measured in the mass channel corresponding to loss of neutral benzene is shown in the top trace of Figure 6 along with the predicted spectra of two different stable isomers. The middle trace corresponds with the global minimum structure which is a hydronium fully solvated by three benzene molecules, one on each O-H bonds. The bottom trace corresponds to the predicted spectrum of a local minimum structure which has a protonated benzene molecule solvated by neutral water and two other benzene molecules. This structure is 12.6 kcal/mol higher in energy than the global minimum. With three benzene molecules interacting with hydronium, there is no free O-H stretch since each O-H of hydronium is associated with a separate neutral benzene molecule. For the protonated benzene complex, free O-H stretches are predicted at 3643 and 3735 cm^{-1} . The lack of a strong band in the free O-H region of the experimental spectrum obtained along with the position of the broad band around 2900 cm^{-1} corresponding to the O-H stretches predicted by theory for the fully solvated hydronium complex suggests that mainly the protonated hydronium complex is produced. The O-H stretch interacting with the π cloud of benzene molecule is extremely broad, similar to that seen previously for O-H stretches interacting with benzene molecules. In this complex, since argon tagging is not employed for fragmentation, the width of these measured spectra may be caused in part by hotter cations compared to the argon tagged species.

Figure 7 shows a compilation of infrared spectra of hydronium solvated by 0-4 benzene molecules. An obvious change upon solvation is the appearance the large, broad band centered around 2740 cm^{-1} for $\text{bz}_2(\text{H}_3\text{O})\text{-Ar}$, which corresponds to the O-H stretch red shifted when

interacting with a neutral benzene molecule. With each additional benzene molecule, the frequency of this band is less red-shifted compared to a free O-H stretch. This is because with each additional benzene molecule, the charge is more delocalized, resulting in weaker interaction with benzene. The effect of the reduced red shift with subsequent addition of each solvent was observed before.¹²⁶ The absence of a band corresponding to the free O-H stretch with the addition of three benzene molecules suggests that hydronium is fully solvated, with a benzene molecule on each O-H bond. With each additional benzene molecules, the difference in energy between the protonated water isomer and the protonated benzene isomer increases. Using B3LYP/6311+G(p,d) level of theory, the difference in energy between the 1:1 benzene water complex differs only by 1.9 kcal/mol. With 2 and 3 benzene molecules, the difference increases to 6.6 and 12.6 kcal/mol respectively.

The solvation trends of the Zundel ion (H_5O_2^+) with multiple benzene molecules are studied using the same technique. The infrared spectrum of $\text{bz}(\text{H}_5\text{O}_2^+)-\text{Ar}$, obtained by measuring the mass channel corresponding to the loss of Ar is shown in the middle trace in Figure 8. The top trace is the infrared spectrum of $(\text{H}_5\text{O}_2^+-\text{Ar})$, obtained by measuring the mass channel corresponding to the loss of Ar, which was studied previously, while the bottom trace is the theoretical spectrum of the lowest energy isomer calculated using the B3LYP/6311+G (p,d) level of theory. This computed structure has both the argon atom and neutral benzene molecule interacting with the same side of the Zundel ion. There are four bands in the O-H region of the infrared spectrum in the tagged Zundel ion, caused by splitting of the symmetric and asymmetric stretch of water by argon. The bands at 3523 and 3658 cm^{-1} correspond to the symmetric and asymmetric stretches of water coupled with the argon atom, while the 3616 and 3696 cm^{-1} bands are assigned to the symmetric and asymmetric stretches of the free O-H. In the far infrared

region of the spectrum, two bands are seen at 1073 and 1764 cm^{-1} . These bands have been assigned previously as the shared proton stretch and a bending mode of the Zundel complex.²⁶

In the middle trace of Figure 8, which is the spectrum of $\text{H}^+(\text{bz})(\text{H}_2\text{O})_2\text{-Ar}$, three sharp bands along with one relatively broad peak are present in the mid infrared region of the spectrum. These three bands match up with the theoretical structure shown in the third trace and with three bands that were observed for the argon tagged Zundel ion. The 3634 and 3718 cm^{-1} bands correspond to the symmetric and asymmetric stretches of a free O-H. The free O-H stretches are shifted approximately 20 cm^{-1} to the blue compared to the argon tagged Zundel ion. This suggests that the benzene molecule has an effect even on the water molecule that is not in direct contact with it. This effect is seen in the computed structure with a decrease in the O-H bond length compared to the Zundel ion. A band at 3523 cm^{-1} is present in both the spectra of $\text{H}^+(\text{bz})(\text{H}_2\text{O})_2\text{-Ar}$ and $\text{H}^+(\text{H}_2\text{O})_2\text{-Ar}$. This band is assigned to the O-H stretch interacting with Ar. The broad band at 2970 cm^{-1} is assigned to the O-H stretch interacting with benzene.

In the far infrared region of the spectrum, two bands are present at 1488 and 1820 cm^{-1} . The spectra of $\text{H}^+(\text{bz})(\text{H}_2\text{O})_2\text{-Ar}$ and $\text{H}_5\text{O}_2^+\text{-Ar}$ are similar because both have two bands in this region corresponding with the shared proton stretch and bend of the Zundel ion. A blue-shift of these bands is logical because of the polarizing effect the addition of benzene has on the Zundel ion. This would cause the shared proton to be unequally shared between the two oxygen atoms of water. Therefore, the shared proton stretch vibration will shift higher in frequency along with the bending mode, from 1073 cm^{-1} to 1488 cm^{-1} and 1764 cm^{-1} to 1820 cm^{-1} respectively. This is seen in the predicted structure of this complex, with a decrease in the distance between the shared proton and the water molecule from 1.04 Å from 1.15 Å of the Zundel ion argon tagged.

The IRPD spectrum of $\text{bz}_2(\text{H}_5\text{O}_2^+)$ -Ar measuring the mass channel corresponding to the loss of argon is shown on the top trace of Figure 9 compared with the predicted spectra of two different stable isomers below. The structural difference between these two different isomers lies in the position of the benzene ring, located either in the cis or trans configuration in relation to one another. The difference in energy between these two isomers is predicted to be 0.9 kcal/mol in favor of the cis configuration. Two sharp bands are present at 3636 and 3717 cm^{-1} along with a broad one centered at 3110 cm^{-1} . The two sharp bands are assigned to the free O-H stretches of water while the broad band is assigned to the O-H stretch interacting with the benzene molecule. In the mid infrared region, both the cis and trans configuration have similar predicted spectra. In the far infrared region, two bands are seen, which correspond with the shared proton stretch at 1462 cm^{-1} and the bend at 1788 cm^{-1} . The vibrational frequency of the shared proton stretch is shifted drastically towards the red compared to that of the Zundel ion. This suggests that the structure of this complex is primarily the cis configuration, since the trans configuration would have equal polarization on both sides of the Zundel ion. In the trans configuration for this complex, the two benzene molecules would have similar polarization effects on both sides of the Zundel ion, which would result in the shared proton stretch being located closer to that of the argon tagged Zundel ion.

When three benzene molecule solvate the Zundel ion ($\text{bz}_3(\text{H}_5\text{O}_2^+)$), elimination of neutral benzene is used to measure the mid infrared region, as shown in the top trace of Figure 10. The predicted spectrum of the lowest energy isomer is shown in the bottom trace. No fragmentation is seen in the far infrared region of the spectrum. The dissociation energy for this complex is calculated to be 7.7 kcal/mol (2695 cm^{-1}). Therefore, fragmentation in the mid infrared region is possible while no fragmentation is observed below the dissociation limit. Argon tagging of this

and larger complexes is difficult because parent signal is too small and unstable. Three sharp bands can be seen, at 3129 , 3621 , and 3706 cm^{-1} along with a broad band centered around 3250 cm^{-1} . The bands observed at 3621 and 3706 cm^{-1} are assigned to the free O-H stretches of water. The bands at 3129 and 3250 cm^{-1} correspond with the O-H stretch interacting with the pi cloud of the benzene molecule. This assignment of bands matches well with the predicted theoretical spectrum in the O-H region. The large band predicted by theory around 2050 cm^{-1} corresponds to the shared proton stretch, which is not seen experimentally. As with the other shared proton stretches, harmonic calculations of this vibrational band are inaccurate, and bands should be red-shifted from their predicted position, probably to around 1400-1500 cm^{-1} .

The IRPD spectrum of $\text{bz}_4(\text{H}_5\text{O}_2^+)$ obtained by measuring the mass channel corresponding to elimination of neutral benzene, is shown in the top trace of Figure 11, along with the predicted theoretical spectrum of the lowest energy conformation. There are no bands in the free O-H region of the spectrum. With four benzene molecules, theory predicts that there is one on each of the O-H bonds of the Zundel ion. With the Zundel ion fully solvated by benzene, all O-H stretches are now shifted to around 3379 cm^{-1} , where a large broad band is observed. Three sharp bands at 3049, 3075, and 3100 cm^{-1} correspond to the Fermi triad of the C-H stretch in benzene. While these bands may have been present on the benzene-solvated Zundel ion, the intensity of the hydrogen stretch band interacting with the benzene is large and broad enough to hide this signal. Theory predicts two separate bands at 3330 and 3455 cm^{-1} while only one large band is seen. However, it is possible two separate bands are within the broad band, seen by the slight band at 3300 cm^{-1} .

The infrared spectra of the Zundel ion solvated by 0-4 benzene molecules are shown in Figure 12. The absence of the free O-H stretch with four benzene molecules supports a structure

of a fully solvated Zundel ion. With the addition of each additional benzene molecule, there is a blue-shift in the location of the band corresponding to the O-H stretch interacting with the π cloud of benzene, similar to what is seen in the solvation of hydronium. With each additional benzene molecule, the interaction decreases, causing a smaller red-shift in the O-H stretch.

The location of the shared proton stretch in the low frequency is measured in the bottom three traces, which correspond to having 0-2 benzene molecules solvating the Zundel ion. This stretch shifts to higher energy with the addition of one benzene, and back down a little bit when the second benzene is added. While the first shift is significant, the second shift back is pretty small, and it is hard to accurately say within the linewidth of the band it shifted. The reason for this shift is the polarization of the water by benzene. With the addition of the benzene molecule, the shared proton between the two water molecules becomes polarized, interacting more with the water than the benzene. Because of this, the proton is unequally shared, being closer to one water molecule than the other. This causes the shared proton stretch vibration to shift to the blue, towards the O-H stretch vibration of hydronium. This could be seen in the theory, shown in the Appendix, in the predicted position of the shared proton, which has the proton unequally shared upon the addition of the benzene molecule.

There are numerous projects suitable for future work continuing in this area of research. One obvious project would be to see if the shift is reduced for the shared proton stretch in the far infrared region of the Zundel ion with the addition of three and four benzene molecules. Theory predicts that with the addition of the third and fourth benzene molecule, the shared proton stretch moves back towards where the Zundel ion shared proton stretch is seen. The polarizing effect of benzene is now symmetric on both sides of the shared proton, helping cancel the effect. The solvation of the Eigen ion, (H_9O_4^+) is another area of interest because of the importance of this

ion as an intermediate in proton transfer reactions in water. Polarizing and charge dispersion effects are also predicted to be present in these complexes.

Conclusion

Protonated mixed benzene-water complexes are studied using infrared photodissociation with a tunable infrared OPO/OPA laser. The effects of subsequent solvation by benzene of small protonated water complexes are studied. While benzene has a higher proton affinity than water, none of the clusters observed at had the proton interacting strongly with the benzene molecule. Hydronium, H_3O^+ , is fully solvated by three benzene molecules, and no bands associated with free O-H stretch observed in the infrared spectrum with this complex. The Zundel ion, H_5O_2^+ , is fully solvated by four benzene molecules. The effect of the benzene on the Zundel ion includes a blue shift in the shared proton stretch between the two water molecules, seen in the far infrared region. This is because of the polarizing effect on the water molecule, causing the proton to be unequally shared. Charge delocalization can be seen in the change in the shift of the O-H stretch interacting with benzene.

References

1. R P. Bell, *The Proton in Chemistry*, Chapman & Hall, London, 1973.
2. E. Caldin and V. Gold, eds., *Proton Transfer Reactions*, Chapman and Hall, London, 1975.
3. J. T. Hynes, J. P. Klinman, H.-H. Limbach, R. L. Schowen, eds., *Hydrogen-Transfer Reactions*, Vols. 1-4, Wiley-VCH Publishers, Weinheim, 2006.
4. I. Bertini, H. B. Gray, E. I. Stiefel and J. S. Valentine, *Biological Inorganic Chemistry*, University Science Books, Sausalito, CA, 2007.
5. E. E. Ferguson, F. C. Fehsenfeld and D. L. Albritton, "Ion chemistry of the earth's atmosphere," in *Gas Phase Ion Chemistry*, edited by M. T. Bowers, Vol. 1, Academic Press, New York, 1979.
6. S. T. Ceyer, P. W. Tiedemann, B. H. Mahan, and Y. T. Lee "Energetics of gas-phase proton solvation by NH_3 " *J. Chem. Phys.* **70**, 14 (1979).
7. H. C. Chang, J. C. Jiang, I. Hahndorf, S. H. Lin, and Y. T. Lee "Migration of an excess proton upon asymmetric hydration: $\text{H}^+[(\text{CH}_3)_2\text{O}](\text{H}_2\text{O})_n$ as a model system" *J. Am. Chem. Soc.* **121**, 4443 (1999).
8. K. Wu, M. J. Iedema, and J. P. Cowin "Ion penetration of the water-oil interface" *Science* **286**, 2482 (1999).

9. C.-T. Chiang, K. S. Shores, M. Freindorf, T. Furlani, R. L. DeLeon, and J. F. Garvey
"Size-Restricted Proton Transfer within Toluene-Methanol Cluster Ions" *J Phys. Chem. A* **112**, 11559 (2008).
10. H. P. Cheng, "The motion of protons in water-ammonia clusters" *J. Chem. Phys* **105**
6844 (1996).
11. M. Eigen, "Uber die kinetik sehr schnell verlaufender ionen reaktionen in wasseriger
losung," *Z. Phys. Chem. (N.F. Frankfurt)* **1**, 176 (1954).
12. M. Eigen, "Protonennubertragung sauer-base-katalyse und enzymatische hydrolyse. I.
Elementarvorgange," *Angew. Chem.* **75**, 489 (1963).
13. M. Eigen, "Proton transfer acid-base catalysis + enzyme hydrolysis. I. Elementary
processes," *Angew. Chem. Int. Ed. Eng.* **3**, 1 (1964)
14. M. Eigen, W. Kruse, G. Maass, L. DeMaeyer, "Rate constants of protolytic reactions in
aqueous solution," *Prog. React. Kinet. & Mech.* **2**, 285 (1964).
15. G. Zundel, H. Z. Metzger, "Energy bands of excess tunneling protons in fluid acids. IR
spectroscopy of H_5O_2^+ groups," *Z. Phys. Chem. (N.F. Frankfurt)* **58**, 225 (1968).
16. G. Zundel, "Hydrogen bonds with large proton polarizability and proton transfer
processes in electrochemistry and biology," *Adv. Chem. Phys.* **111**, 1 (2000).
17. C. T. J. de Grotthuss, "Sur la décomposition de l'eau et des corps qu'elle tient en
dissolution à l'aide de l'électricité galvanique," *Ann. Chim.* **58**, 54 (1806)

18. P. B. Petersen and R. J. Saykally, "Evidence for an Enhanced Hydronium Concentration at the Liquid Water Surface" *J. Phys. Chem. B* **109**, 7976 (2005).
19. P. B. Petersen and R. J. Saykally, "Is the liquid water surface basic or acidic? Macroscopic vs. molecular-scale investigations" *Chem. Phys. Lett.* **458**, 255 (2008).
20. T. D. Fridgen, T. B. McMahon, L. MacAleese, J. Lemaire, and P. Maitre, "Infrared spectrum of the protonated water dimer in the gas phase," *J. Phys. Chem. A* **108**, 1089 (2004)
21. L. I. Yeh, M. Okumura, J. D. Myers, J. M. Price and Y. T. Lee, "Vibrational spectroscopy of the hydrated hydronium cluster ions $\text{H}_3\text{O}^+(\text{H}_2\text{O})_n$ ($n=1,2,3$)," *J. Chem. Phys.* **91**, 7319 (1989)
22. J. M. Headrick, J. C. Bopp, and M. A. Johnson, "Predissociation spectroscopy of the argon-solvated H_5O_2^+ "zundel" cation in the 1000-1900 cm^{-1} region," *J. Chem. Phys.* **121**, 11523 (2004)
23. J.-W. Shin, N.I. Hammer, E.G. Diken, M.A. Johnson, R.S. Walters, T.D. Jaeger, M.A. Duncan, R.A. Christie and K.D. Jordan, "Infrared signature of structural motifs associated with the $\text{H}^+(\text{H}_2\text{O})_n$, $n=6-27$, clusters," *Science* **304**, 1137 (2004).
24. J. Headrick, E.G. Diken, R.S. Walters, N.I. Hammer, R.A. Christie, J. Cui, E.M. Myshakin, M.A. Duncan, M.A. Johnson and K.D. Jordan, "Spectral signatures of hydrated proton vibrations in water clusters," *Science* **308**, 1765 (2005).

25. G. E. Douberly, R. S. Walters, J. Cai, K. D. Jordan and M. A. Duncan, "Infrared spectroscopy of small protonated water clusters $H^+(H_2O)_n$ ($n=2-5$): Isomers, argon tagging and deuteration," *J. Phys. Chem. A* **114**, 4570 (2010).
26. L. R. McCunn, J. R. Roscioli, B. M. Elliott, and A. B. McCoy, "Why does argon bind to deuterium? Isotope effects and structure of $Ar-H_5O_2^+$ complexes," *J. Phys. Chem. A* **112**, 6074 (2008)
27. L. R. McCunn, J. M. Headrick and M. A. Johnson, "An H/D isotopic substitution study of the $H_5O_2^+$ -Ar vibrational predissociation spectra: exploring the putative role of Fermi resonances in the bridging proton fundamentals," *J. Phys. Chem. B*, **112**, 321 (2007)
28. M. Miyazaki, A. Fujii, T. Ebata, and N. Mikami, "Infrared Spectroscopic evidence for protonated water clusters forming nanocrystal cages" *Science* **21**, 1137 (2004).
29. E. S. Stoyanov, I. V. Stoyanova, F. S. Tham, and C. A. Reed, "The nature of the hydrated proton $H-(aq)(+)$ in organic solvents" *J. Am. Chem. Soc.* **130**, 12128 (2008).
30. T. Schindler, C. Berg, G. Niedner-Schatteburg and V. E. Bondybey, "Protonated water clusters and their black body radiation induced fragmentation," *Chem. Phys. Lett.* **250**, 301 (1996).
31. G. Niedner-Schatteburg and V. E. Bondybey, " FT-ICR studies of solvation effects in ionic water cluster reactions," *Chem. ReV.* **100**, 4059 (2000).

32. K. Honma and P. B. Armentrout, "The mechanism of proton exchange: Guided ion beam studies of the reactions, $\text{H}(\text{H}_2\text{O})_n^+$ ($n=1-4$) + D_2O and $\text{D}(\text{D}_2\text{O})_n^+$ ($n=1-4$)+ H_2O ," *J. Chem. Phys.* **121**, 8307 (2004).
33. M. Meot-Ner, "The ionic hydrogen bond," *Chem. Rev.* **105**, 213 (2005).
34. P. U. Andersson, M. J. Ryding, O. Sekiguchi and E. Uggerud, "Isotope exchange and structural rearrangements in reactions between size-selected ionic water clusters: $\text{H}_3\text{O}^+(\text{H}_2\text{O})_n$ and $\text{NH}_4^+(\text{H}_2\text{O})_n$, and D_2O ," *Phys. Chem. Chem. Phys.* **10**, 6127 (2008).
35. Y. Xie, R. B. Remington and H. F. Schaefer III, "The protonated water dimer: extensive theoretical studies of H_5O_2^+ ," *J. Chem. Phys.* **101**, 4878 (1994).
36. D. Wei and D. R. Saluhub, "Hydrated proton clusters, solvent effects on the proton transfer barrier: a density functional study," *J. Chem. Phys.* **101**, 7633 (1994).
37. G. Corongiu, R. Kelterbaum and E. Kochanski, "Theoretical studies of $\text{H}^+(\text{H}_2\text{O})_5$," *J. Phys. Chem.* **99**, 8038 (1995).
38. D. J. Wales and M. P. Hodges, "Global minima of water clusters $(\text{H}_2\text{O})_n$, $n \leq 21$, described by an empirical potential," *Chem. Phys. Lett.* **286**, 65 (1998).
39. M. P. Hodges and D. J. Wales, "Global minima of protonated water clusters," *Chem. Phys. Lett.* **324**, 279 (2000).
40. T. James and D. J. Wales, "Protonated water clusters described by an empirical valence bond potential," *J. Chem. Phys.* **122**, 134306 (2005).

41. M. Svanberg and J. B. C. Pettersson, "Structure, thermodynamics of $\text{H}^+(\text{H}_2\text{O})_n$ ($n=9, 21, 40$) clusters between 0, 300 K: A Monte Carlo study," *J. Phys. Chem. A* **102**, 1865 (1998).
42. I. Kusaka and D. W. Oxtoby, "Evaluating free energy, enthalpy, entropy of protonated water clusters by a grand canonical Monte Carlo simulation," *J. Chem. Phys.* **113**, 10100 (2000).
43. S. J. Singer, S. McDonald and L. Ojamae, "Topology versus temperature: Thermal behavior of $\text{H}^+(\text{H}_2\text{O})_8$, $\text{H}^+(\text{H}_2\text{O})_{16}$," *J. Chem. Phys.* **112**, 710 (2000).
44. A. L. Sobolewski and W. Domcke, "Ab initio investigation of the structure and spectroscopy of hydronium-water clusters," *J. Phys. Chem. A* **106**, 4158 (2002).
45. X. Huang, H. M. Cho, S. Carter, L. Ojamae, J. M. Bowman and S. J. Singer, "Full dimensional quantum calculations of vibrational energies of H_5O_2^+ ," *J. Phys. Chem. A* **107**, 7142 (2003).
46. M. Mella and D. C. Clary, "Zero temperature quantum properties of small protonated water clusters $\text{H}^+(\text{H}_2\text{O})_n$ ($n=1-5$)," *J. Chem. Phys.* **119**, 10048 (2003).
47. X. Huang, H. M. Cho, S. Carter, L. Ojamae, J. M. Bowman and S. J. Singer, "Full dimensional quantum calculations of vibrational energies of H_5O_2^+ ," *J. Phys. Chem. A* **107**, 7142 (2003).
48. J. Dai, Z. Bacic, X. Huang, S. Carter and J. M. Bowman, "A theoretical study of vibrational mode coupling in H_5O_2^+ ," *J. Chem. Phys.* **119**, 6571 (2003).

49. X. Huang, S. Carter and J. M. Bowman, "Ab initio potential energy surface and rovibrational energies of H_3O^+ and its isotopomers," *J. Chem. Phys.* **118**, 5431 (2003).
50. X. Huang, B. J. Braams and J. M. Bowman, "Ab initio potential energy and dipole moment surfaces for H_5O_2^+ ," *J. Chem. Phys.* **122**, 044308 (2005).
51. A. B. McCoy, X. Huang, S. Carter, M. Y. Landeweer and J. M. Bowman, "Full-dimensional vibrational calculations for H_5O_2^+ using an *ab initio* potential energy surface," *J. Chem. Phys.* **122**, 061101 (2005).
52. M. Kaledin, A. L. Kaledin and J. M. Bowman, "Vibrational analysis of H_5O_2^+ infrared spectrum using molecular and driven molecular dynamics," *J. Phys. Chem. A* **110**, 2933 (2006).
53. M. Kaledin, A. L. Kaledin, J. M. Bowman, J. Ding and K. D. Jordan, "Calculation of the vibrational spectra of H_5O_2^+ and its deuterium-substituted isotopologues by molecular dynamics simulations," *J. Phys. Chem. A* (2009).
54. R. Ludwig, "Protonated water clusters: the third dimension," *Chem. Phys. Chem.* **5**, 1495 (2004).
55. J.-L. Kuo and M. L. Klein, "Structure of protonated water clusters: low-energy structures, finite temperature behavior," *J. Chem. Phys.* **122**, 024516 (2005).
56. F. C. Pickard, IV, E. K. Pokon, M. D. Liptak and G. C. Shields, "Comparison of CBS-QB3, CBS-APNO, G2, G3 thermochemical predictions with experiment for the

- formation of ionic clusters of hydronium and hydroxide ions complexed with water," *J. Chem. Phys.* **122**, 024302 (2005).
57. J. P. Devlin, M. W. Severson, F. Mohamed, J. Sadlej, V. Buch and M. Parrinello, "Experimental and computational study of isotopic effects within the Zundel ion," *Chem. Phys. Lett.* **408**, 439 (2005).
58. N. J. Singh, M. Park, S. K. Min, S. B. Suh and K. S. Kim, "Magic and antimagic protonated water clusters: exotic structures with unusual dynamics effects," *Angew. Chem. Int. Ed.* **45**, 3795 (2006).
59. I. Shin, M. Park, S. K. Min, E. C. Lee, S. B. Suh and K. S. Kim, "Structure and spectral features of $\text{H}^+(\text{H}_2\text{O})_7$: Eigen versus Zundel forms," *J. Chem. Phys.* **125**, 234305 (2006).
60. M. Park, I. Shin, N. J. Singh and K. S. Kim, "Eigen and Zundel forms of small protonated water clusters: structures, infrared spectra," *J. Phys. Chem. A* **111**, 10692 (2007).
61. S. Karthikeyan, M. Park, I. Shin and K. S. Kim, "Structure, stability, thermodynamic properties and infrared spectra of the protonated water octamer $\text{H}^+(\text{H}_2\text{O})_8$," *J. Phys. Chem. A* **112**, 10120 (2008).
62. Y. Luo, S. Maeda and K. Ohno, "Quantum chemistry study of $\text{H}^+(\text{H}_2\text{O})_8$: A global search for its isomers by the scaled hypersphere method and its thermal behavior," *J. Phys. Chem. A* **111**, 10732 (2007).

63. H. Yu and Q. Cui, "The vibrational spectra of protonated water clusters: A benchmark for self-consistent-charge density-functional tight binding," *J. Chem. Phys.* **127**, 234504 (2007).
64. O. Vendrell, F. Gatti and H. D. Meyer, "Dynamics, infrared spectroscopy of the protonated water dimer," *Angew. Chem. Int. Ed.* **46**, 6918 (2007).
65. O. Vendrell and H. D. Meyer, "A proton between two waters: Insight from full-dimensional quantum-dynamics simulations of the $[\text{H}_2\text{O}-\text{H}^+-\text{H}_2\text{O}]$ clusters," *Phys. Chem. Chem. Phys.* **10**, 4692 (2008).
66. O. Vendrell, F. Gatti and H. D. Meyer, "Strong isotope effects in the infrared spectrum of the Zundel Cation," *Angew. Chem. Int. Ed.* **48**, 352 (2009).
67. M. N. Glukhovtsev, A. Pross, A. Nicolaides, and L. Radom, "Is the most stable gas-phase isomer of the benzenium cation a face-protonated pi-complex?" *J. Chem. Soc.-Chem. Commun.* 2347 (1995).
68. M. O. Sinnokrot, E. F. Valeev, and C. D. Sherrill, "Estimates of the ab initio limit for pi-pi interactions: The benzene dimer" *J. Am. Chem. Soc.* **124**, 10887 (2002).
69. N. J. Singh, S. K. Min, D. Y. Kim, and K. S. Kim, "Comprehensive Energy Analysis for Various Types of pi-Interaction" *J. Chem. Theory Comput.* **5**, 515 (2009).
70. M. Schauer and E. R. Bernstein, "Calculations of the Geometry and Binding-energy of Aromatic Dimers - Benzene, Toluene, and Toluene Benzene" *J. Chem. Phys.* **82**, 3722 (1985).

71. P. A. Pieniazek, A. I. Krylov, and S. E. Bradforth, "Electronic structure of the benzene dimer cation" *J. Chem. Phys* **127**, 044317 (2007).
72. Y. Nakai, K. Ohashi, and N. Nishi, "Electronic structures and photoevaporation dynamics of benzene cluster ions" *J. Phys. Chem. A* **101**, 472 (1997).
73. N. Muller, L. W. Pickett, and R. S. Mulliken, "Hyperconjugation and Spectrum of the Benzenium ion, Prototype of Aromatic Carbonium ions" *J. Am. Chem. Soc.* **76**, 4770 (1954).
74. M. Mine, H. Mori, M. Ogata, S. Tanaka, T. Tsutsui, and E. Miyoshi, "Computational research of the electronic structure of benzene trimer cation by ab initio method" *Chem. Phys. Lett.* **438**, 157 (2007).
75. C. A. Hunter and J. K. M. Sanders, "The nature of pi-pi interactions" *J. Am. Chem. Soc.*, **112**, 5525(1990).
76. D. M. Hudgins, C. W. Bauschlicher and L. J. Allamandola, "Closed-shell polycyclic aromatic hydrocarbon cations: a new category of interstellar polycyclic aromatic hydrocarbons" *Spectrochimica Acta A-Molecular and Biomolecular Spectroscopy* **57**, 907 (2001).
77. P. Hobza, H. L. Selzle, and E. W. Schlag, "Structure and properties of benzene-containing molecular clusters – nonempirical ab-initio calculations and experiments" *Chem. Rev.* **94**, 1767 (1994).

78. H. Tachikawa, and M. Igarashi, "Dynamics of the ionization processes of benzene-H₂O clusters: A direct ab initio dynamics study" *J. Phys. Chem. A* **102**, 8648 (1998).
79. W. C. Ermler, R. S. Mulliken, and E. Clementi, "Ab-initio SCF computations on benzene and benzenium ion using a large contracted Gaussian basis set" *J. Am. Chem. Soc.* **98**, 388 (1976).
80. S. J. Kim, H. I. Seo, and B. H. Boo, "Theoretical investigations for the molecular structures and binding energies for C₆H₆(H₂O)_n, (n=1-7) complexes" *Mol. Phys.* **107**, 1261 (2009).
81. C. Chaudhuri, C. C. Wu, J. C. Jiang, and H. C. Chang, "In comparative studies of H⁺(C₆H₆)(H₂O)_(1,2) and H⁺(C₅H₅N)(H₂O)_(1,2) by DFT calculations and IR spectroscopy" *Aus. J. Chem.* **57**, 1153 (2004).
82. K. S. Kim, J. Y. Lee, H. S. Choi, J. S. Kim, and J. H. Jang, "Quantum mechanical probabilistic structure of the benzene-water complex" *Chem. Phys. Lett.* **265**, 497 (1997).
83. B. S. Freiser and J. L. Beauchamp, "Photochemistry of organic ions in gas-phase – comparison of gas-phase photodissociation and solution absorption-spectra of benzoyl cation, protonated benzene, and protonated mesitylene." *J. Am. Chem. Soc.* **98**, 3136 (1976).
84. P. Carcabal, R. T. Kroemer, L. C. Snoek, J. P. Simons, J. M. Bakker, I. Compagnon, G. Meijer, and G. von Helden, "Hydrated complexes of tryptophan: ion dip infrared spectroscopy in the 'molecular fingerprint' region, 100-2000 cm⁻¹" *Phys. Chem. Chem. Phys.* **6**, 4546 (2004).

85. S. K. Burley, and G. A. Petsko, "Aromatic-aromatic interaction – A mechanism of protein structure stabilization" *Science* **229**, 23 (1985).
86. K. O. Bornsen, H. L. Selzle, and E. W. Schlag, "Spectra of isotopically mixed benzene dimers – Details on the interaction in the VDW VDW bond" *J. Chem. Phys.* **85**, 1726 (1986).
87. P. Andries, and N. M. M. N. Bruins, "Hydrogen scrambling in the long-lived protonated benzene ion generated from benzyl amine in the I.C.R. spectrometer" *Org. Mass Spectrom.* **11**, 950 (1976).
88. K. S. Kim, P. Tarakeshwar, and J. Y. Lee, "Molecular clusters of pi-systems: Theoretical studies of structures, spectra, and origin of interaction energies" *Chem. Rev.* **100**, 4145 (2000).
89. J. Y. Lee, J. Kim, H. M. Lee, P. Tarakeshwar, and K. S. Kim, "Structures, vibrational frequencies, and infrared spectra of the hexa-hydrated benzene clusters" *J. Chem. Phys.* **113**, 6160 (2000).
90. D. A. Rodham, S. Suzuki, R. D. Suenram, F. J. Lovas, S. Dasgupta, W. A. Goddard, and G. A. Blake, "Hydrogen-bonding in the benzene ammonia dimer" *Nature* **362**, 735 (1993).
91. J. A. Stone, "H-D exchange at low-energy in a collision cell between protonated aromatic-hydrocarbons and D₂O, CD₃OD, and C₆D₆" *Org. Mass Spectrom.* **28**, 1119 (1993).

92. J. M. Steed, T. A. Dixon, and W. Klemperer, "Molecular-beam studies of Benzene dimer, Hexafluorobenzene dimer, and Benzene-Hexafluorobenzene." *J. Chem. Phys.* **70**, 4940 (1979).
93. A. J. Stace, D. M. Bernard, J. J. Crooks, and K. L. Reid, "Benzene Clusters – Liquid or Solid state". *Mol. Phys.* **60**, 671 (1987).
94. V. Spirko, O. Engvist, P. Soldan, H. L. Selzle, E. W. Schlag, and P. Hobza, "Structure and vibrational dynamics of the benzene dimer." *J. Chem. Phys.* **111**, 572 (1999).
95. S. Tsuzuki, T. Uchimaru, K. Sugawara, and M. Mikami, "Energy profile of the interconversion path between T-shape and slipped-parallel benzene dimers." *J. Chem. Phys.* **117**, 11216 (2002).
96. K. Ohashi and N. Nishi, "Photodissociation dynamics of $(C_6H_6)_3^+$: Role of the extra benzene molecule weakly bound to the dimer core." *J. Chem. Phys.* **109**, 3971 (1998).
97. K. Ohashi and N. Nishi, "Photodissociation Spectroscopy of Benzene Cluster Ions - $(C_6H_6)_2^+$ and $(C_6H_6)_3^+$." *J. Chem. Phys.* **95**, 4002 (1991).
98. P. R. R. Langridgesmith, D. V. Brumbaugh, C. A. Haynam, and D. H. Levy, "Ultraviolet-spectra of benzene clusters." *J. Phys. Chem.* **85**, 3742 (1981).
99. M. Y. Hahn, K. E. Schriver, and R. L. Whetten, "Multiple ionization of benzene clusters by ultraviolet-radiation" *J. Chem. Phys.* **88**, 4242 (1988).
100. J. R. Grover, E. A. Walters, and E. T. Hui, "Dissociation-energies of the benzene dimer and dimer cation" *J. Phys. Chem.* **91**, 3233 (1987).

101. K. H. Fung, H. L. Selzle, and E. W. Schlag, "Study of isotope effects in benzene dimers in a seeded supersonic jet" *J. Phys. Chem.* **87**, 5113 (1983).
102. G. E. Douberly, A. M. Ricks, and M. A. Duncan "Infrared Spectroscopy of gas phase benzenium ions: protonated benzene and protonated toluene, from 750 to 3400 cm^{-1} " *J. Phys. Chem. A.* **112**, 22 (2008).
103. J. R. Roscioli, L. R. McCunn, and M. A. Johnson, "Quantum Structure of the Intermolecular Bond" *Science*, **316**, 249 (2007).
104. T. D. Fridgen, T. B. McMahon, L. MacAleese, J. Lemaire, and P. Maitre, "Infrared spectrum of the protonated water dimer in the gas phase," *J. Phys. Chem. A* **108**, 1089 (2004)
105. G. H. Gardenier, J. R. Roscioli and M. A. Johnson, "Intermolecular proton binding in the presence of a large electric dipole: Ar-tagged vibrational predissociation spectroscopy of the $\text{CH}_3\text{CN-H}^+\text{-OH}_2$ and $\text{CH}_3\text{CN-H}^+\text{-OD}_2$ complexes," *J. Phys. Chem. A* **112**, 12022 (2008).
106. B. J. Berne, J. D. Weeks and R. Zhou, "Dewetting and hydrophobic interactions in physical and biological systems," *Annu. Rev. Phys. Chem.* **60**, 85 (2009).
107. S. Iuchi, H. Chen, F. Paesani and G. A. Voth, "Hydrated excess proton at water-hydrophobic interfaces," *J. Phys. Chem. B* **113**, 4017 (2009).
108. T. Ebata, A. Fujii, and N. Mikami, "Vibrational spectroscopy of small-sized hydrogen-bonded clusters and their ions" *Int. Rev. Phys. Chem.* **17**, 331 (1998).

109. M. Miyazaki, A. Fujii, T. Ebata, and N. Mikami, "Infrared spectroscopy of hydrated benzene cluster cations, $[\text{C}_6\text{H}_6-(\text{H}_2\text{O})_n]^+$ ($n=1-6$): Structural changes upon photoionization and proton transfer reactions" *Phys. Chem. Chem. Phys.* **5**, 1137 (2003).
110. M. Miyazaki, A. Fujii, and N. Mikami, "Binding Energy of the Benzene-Water Cluster Cation: An Ar-Mediated IR Photodissociation Study" *J. Phys. Chem. A* **108**, 8272 (2004).
111. M. Miyazaki, A. Fujii, T. Ebata, and N. Mikami, "Infrared Spectroscopy of Size-Selected Benzene-Water Cluster Cations $[\text{C}_6\text{H}_6-(\text{H}_2\text{O})_n]^+$ ($n=1-23$): Hydrogen Bond Network Evolution and Microscopic Hydrophobicity" *J. Phys. Chem.* **108**, 10656 (2004).
112. N. Solca and O. Dopfer, "Interaction of the benzenium ion with inert ligands: IR spectra of $\text{C}_6\text{H}_7^+-\text{L}-n$ cluster cations ($\text{L} = \text{Ar}, \text{N}_2, \text{CH}_4, \text{H}_2\text{O}$)." *Chem. Eur. J.* **9**, 3154 (2003).
113. O. Dopfer, N. Solca, J. Lemaire, P. Maitre, M. E. Crestoni, and S. Fornarini, "Protonation sites of isolated fluorobenzene revealed by IR spectroscopy in the fingerprint range" *J. Phys. Chem. A* **109**, 7881 (2005).
114. N. Solca, and O. Dopfer, "IR spectrum of the benzene-water cation: direct evidence for the hydrogen-bonded charge-dipole complex" *Chem. Phys. Lett.* **347**, 59 (2001).
115. Chiavarino, M. E. Crestoni, S. Fornarini, J. Lemaire, P. Maitre, and L. MacAleese, "Pi-complex structure of gaseous benzene-NO cations assayed by IR multiple photon dissociation spectroscopy" *J. Am. Chem. Soc.* **128**, 12553 (2006).

116. W. Jones, P. Boissel, B. Chiavarino, M. E. Crestoni, S. Fornarini, J. Lemaire, and P. Maitre, "Infrared Fingerprint of Protonated Benzene in the Gas Phase" *Angew. Chem. Int. Ed.* **42**, 2057, (2003).
117. R. N. Pribble, and T. S. Zwier, "Size-specific infrared-spectra of benzene-(H₂O)_n clusters (n=1 through 7) – evidence for noncyclic (H₂O)_n structures" *Science* **265**, 75 (1994).
118. T. S. Zwier, "The spectroscopy of solvation in hydrogen-bonded aromatic clusters" *Annu. Rev. Phys. Chem.* **47**, 205 (1996).
119. A. W. Garrett, and T. S. Zwier, "Multiphoton ionization studies of clusters of immiscible liquids .2 C₆H₆-(H₂O)_N, N=3-8 and (C₆H₆)₂-(H₂O)₁," *J. Chem. Phys.* **96**, 3402 (1992).
120. C. J. Gruenloh, R. J. Carney, C. A. Arrington, T. S. Zwier, S. Y. Fredericks, and K. D. Jordan, "Infrared spectrum of a molecular ice cube: The S-4 and D-2d water octamers in benzene-(water)₈" *Science* **276**, 1678 (1997).
121. T. Tassaing, "A vibrational spectroscopic study of water confined in benzene from ambient conditions up to high temperature and pressure" *Vib. Spectrosc.* **24**, 15 (2000).
122. R. Souda, "Interactions of water with pyridine and benzene studied by TOF-SIMS" *J. Phys. Chem. B* **108**, 283 (2004).
123. P. M. Maxton, M. W. Schaeffer, and P. M. Felker, "Nonlinear Raman-spectroscopy of intermolecular vibrations in benzene-(water)_n clusters" *Chem. Phys. Lett.* **241**, 603 (1995).

124. D. Feller, "Strength of the benzene-water hydrogen bond" *J. Phys. Chem. A* **103**, 7558 (1999).
125. E. S. Kryachko and M. T. Nguyen, "Low energy barrier proton transfer in protonated benzene-water complex". *J. Phys. Chem. A* **105**, 153 (2001).
126. B. Bandyopadhyay, T. C. Cheng, and M. A. Duncan, "Proton sharing in hydronium-nitrogen clusters probed with infrared spectroscopy," *Int. J. Mass. Spec.* **124**, 120 (2010).
127. K. LaiHing, P. Y. Cheng, T. G. Taylor, K. F. Wiley, M. Peschke, and M. A. Duncan, "Photodissociation in a reflectron time-of-flight mass-spectrometer – A novel mass-spectrometry mass-spectrometry configuration for high-mass systems" *Anal. Chem.* **61**, 1458 (1989).
128. D. S. Cornett, M. Peschke, K. LaiHing, P. Y. Cheng, K. F. Wiley, and M. A. Duncan, "Reflectron time-of-flight mass-spectrometer for laser photodissociation" *Rev. Sci. Instrum.* **63**, 2177 (1992).
129. B. Bandyopadhyay, T. C. Cheng and M. A. Duncan, "Proton sharing in hydronium-nitrogen clusters probed with infrared spectroscopy" *Int. J. Mass Spectrom.* **297**, 124 (2010).
130. A. M. Ricks, G. E. Douberly and M. A. Duncan, "Infrared spectroscopy of proton-bridged nitrogen dimers: Complex vibrational dynamics of the shared proton" *J. Chem. Phys.* **131**, 104312 (2009).

131. G.E. Douberly, A.M. Ricks, B.W. Ticknor and M.A. Duncan, "Infrared spectroscopy of protonated acetone and its dimer" *Phys. Chem. Chem. Phys.* **10**, 77 (2008).
132. G.E. Douberly, A.D. Ricks, B.W. Ticknor and M.A. Duncan, "The structure of protonated carbon dioxide clusters: Infrared photodissociation spectroscopy and ab initio calculations" *J. Phys. Chem. A* **112**, 950 (2008).
133. G.E. Douberly, A.M. Ricks, B.W. Ticknor, W.C. McKee, P.v.R. Schleyer and M.A. Duncan, "Infrared photodissociation spectroscopy of protonated acetylene and its clusters" *J. Phys. Chem. A* **112**, 1897 (2008).
134. A. M. Ricks, G. E. Douberly, P. v. R. Schleyer and M. A. Duncan, "The infrared spectrum of gas phase $C_3H_3^+$: The cyclopropeny and propargyl cations" *J. Chem. Phys.* **132**, 051101 (2010).
135. A. M. Ricks, G. E. Douberly, P. v. R. Schleyer and M. A. Duncan, "Infrared spectroscopy of protonated ethylene: The nature of proton binding in the non-classical structure" *Chem. Phys. Lett.* **480**, 17 (2009).
136. A. M. Ricks, G. E. Douberly and M. A. Duncan, "The infrared spectroscopy of protonated naphthalene and its relevance for the unidentified infrared bands" *Astrophys. J.* **702**, 301 (2009).
137. G.E. Douberly, A.M. Ricks, B.W. Ticknor, P.v.R. Schleyer and M.A. Duncan, "Infrared spectroscopy of gas phase benzenium ions: Protonated benzene and protonated toluene from 750 to 3400 cm^{-1} " *J. Phys. Chem. A* **112**, 4869 (2008).

138. G.E. Douberly, A.M. Ricks, P.v.R. Schleyer and M.A. Duncan, "Infrared spectroscopy of gas phase $C_3H_5^+$: The allyl and 2-propenyl cations," *J. Chem. Phys.* **128**, 021102 (2008).
139. G.E. Douberly, A.M. Ricks, B.W. Ticknor, W.C. McKee, P.v.R. Schleyer and M.A. Duncan, "Infrared photodissociation spectroscopy of protonated acetylene and its clusters" *J. Phys. Chem. A* **112**, 1897 (2008).
140. G.E. Douberly, A.M. Ricks, B.W. Ticknor, P.v.R. Schleyer and M.A. Duncan, "The infrared spectrum of the tert-butyl cation in the gas phase" *J. Am. Chem. Soc.* **129**, 13782 (2007).

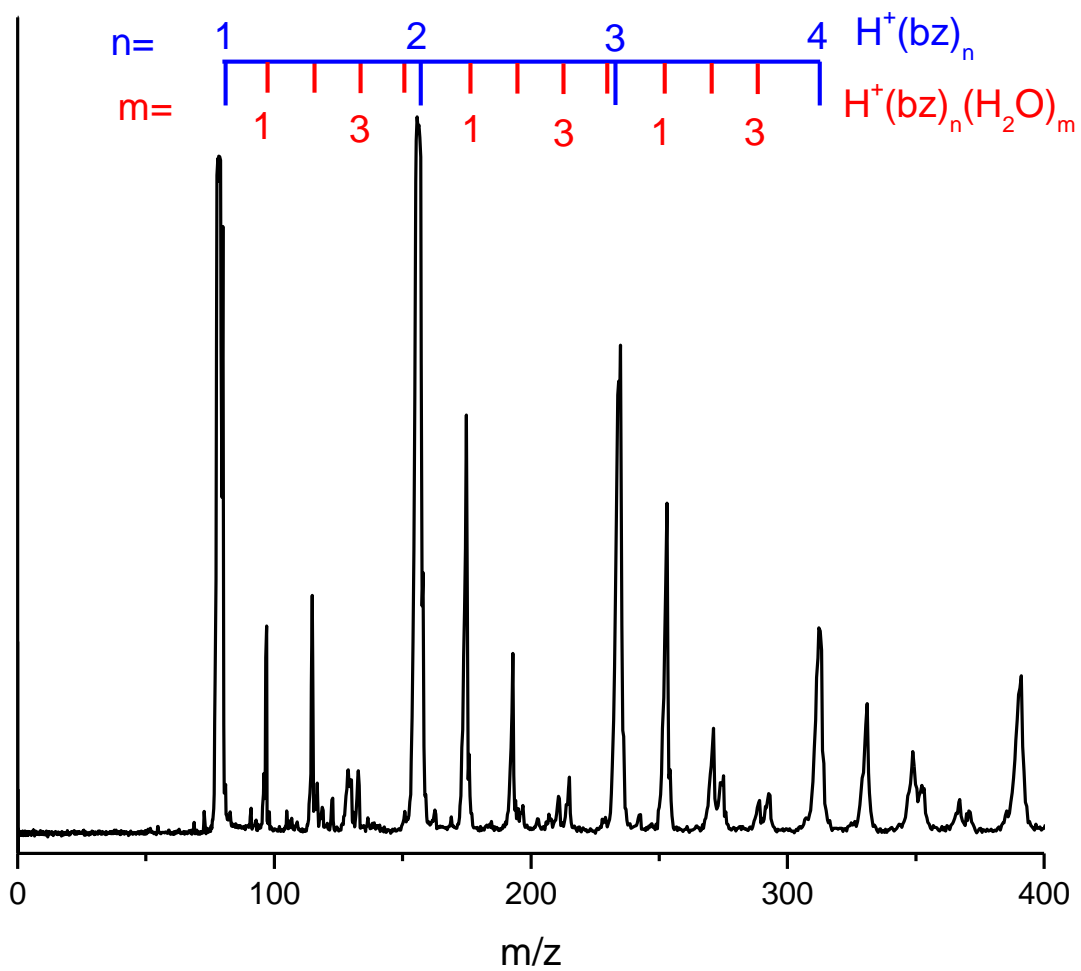


Figure 1: Full mass spectrum of clusters of protonated benzene and water.

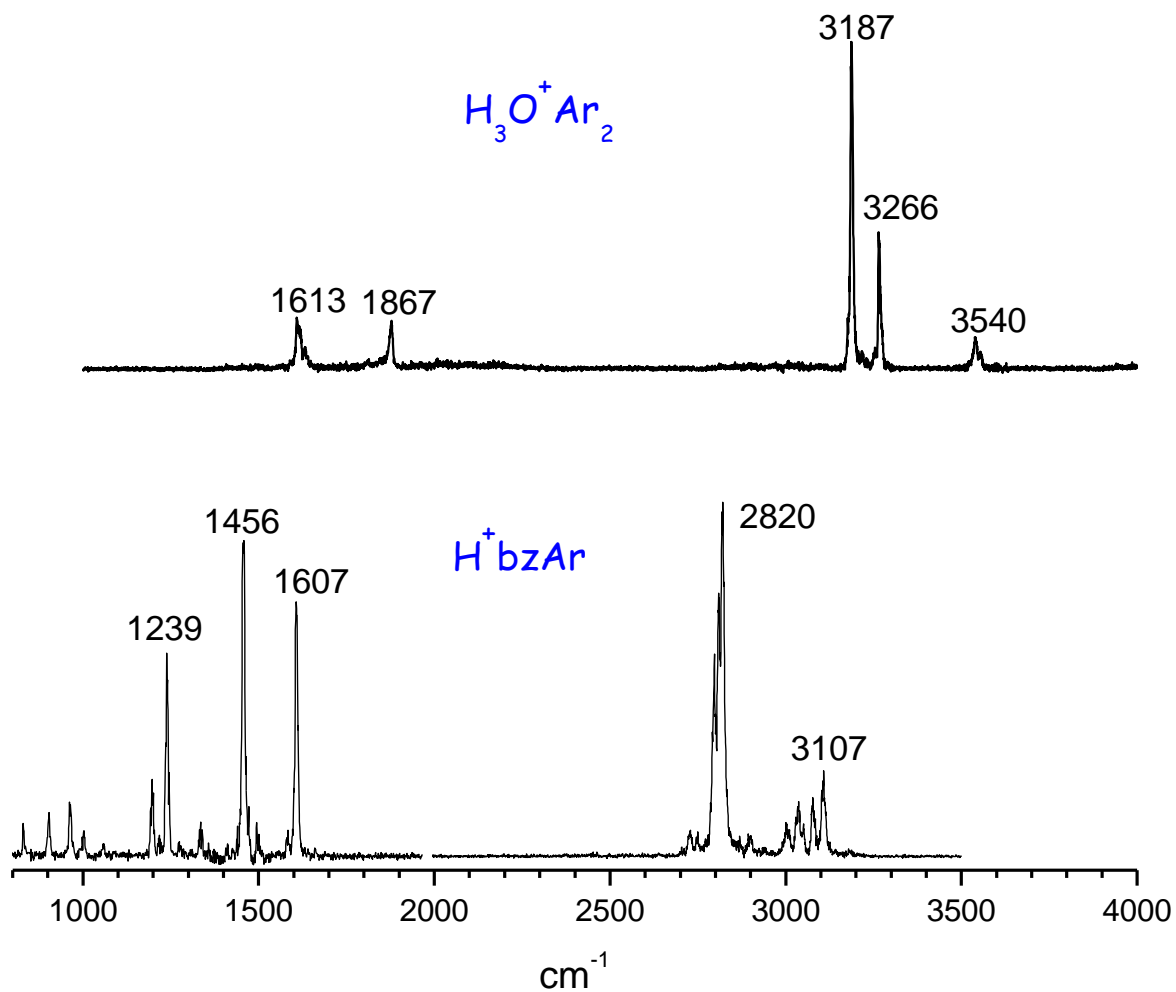


Figure 2: Infrared spectrum of $H_3O^+Ar_2$ and H^+bzAr measuring the mass channel corresponding to the loss of Ar. Key spectral signatures of the proton interacting with water and benzene is used to help understand the spectrum of protonated mixed benzene-water clusters.

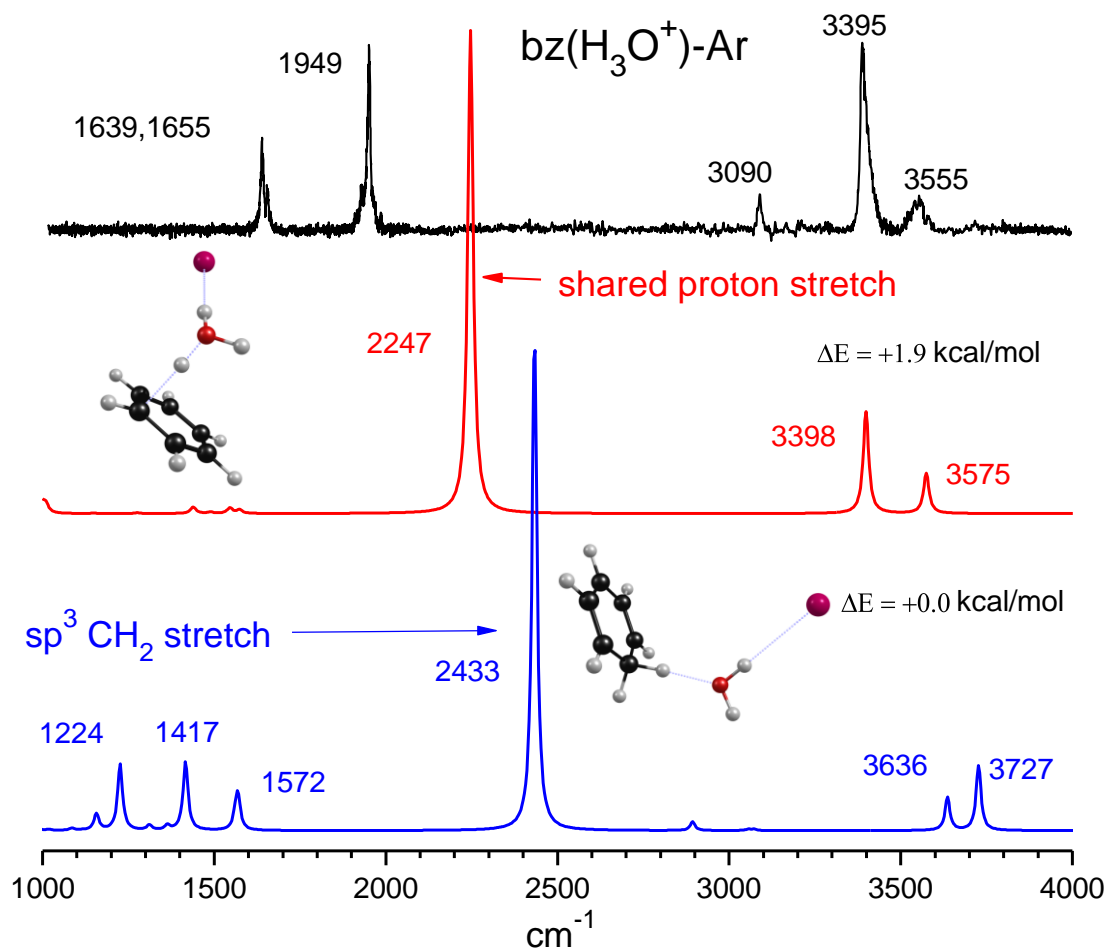


Figure 3: Comparison of the IRPD of $\text{bz}(\text{H}_3\text{O}^+)\text{-Ar}$, shown in the top trace, with two stable isomers calculated using B3LYP/6311+G (p,d) level of theory.

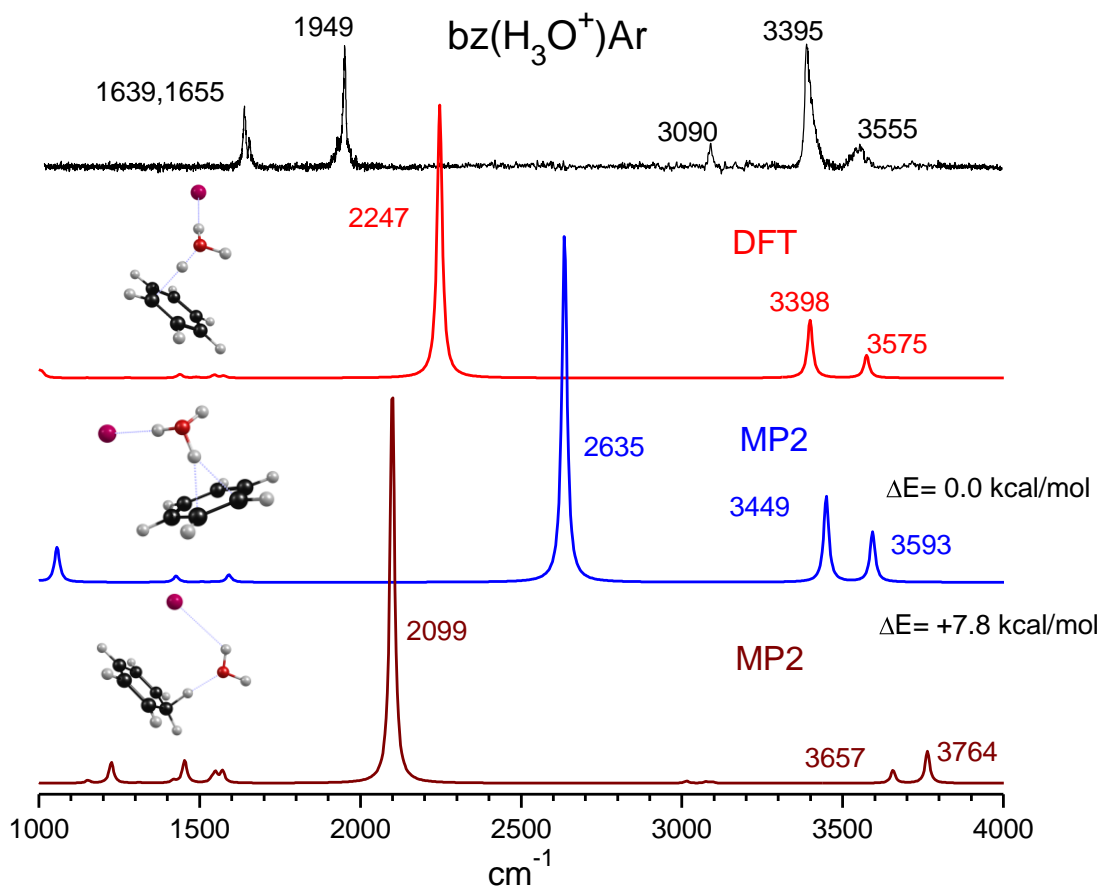


Figure 4: Comparison of the IRPD of $\text{bz}(\text{H}_3\text{O}^+)\text{Ar}$, shown in the top trace, with the predicted spectra of two isomers calculated with MP2/6311+G(d,p) level of theory along with the lowest isomer from DFT.

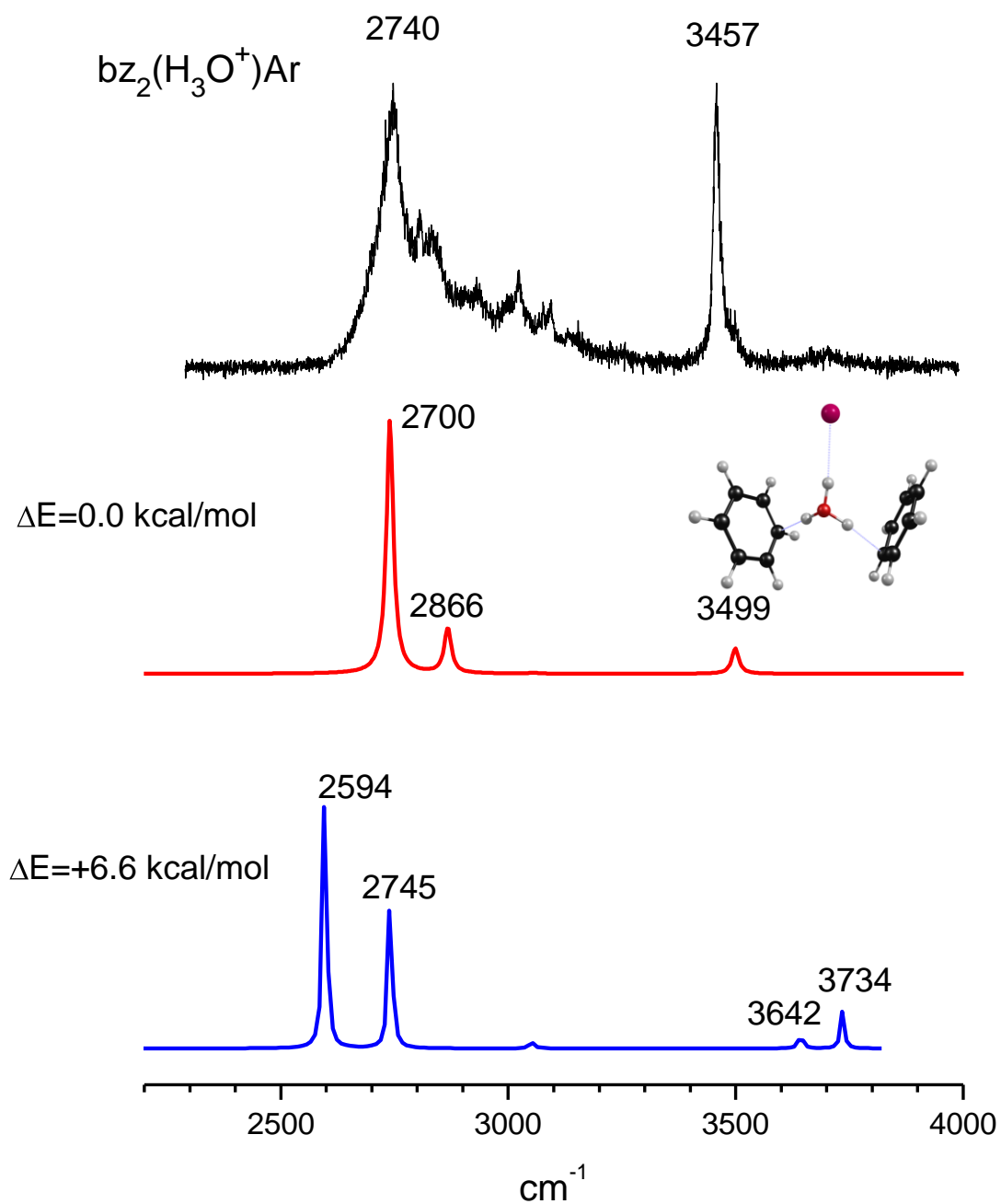


Figure 5: Comparison of the infrared Spectra of $\text{bz}_2(\text{H}_3\text{O}^+)\text{Ar}$, obtained by measuring the mass channel corresponding to the loss of argon, with the predicted spectra of two different configurations calculated using the B3LYP/6311+G (p,d) below.

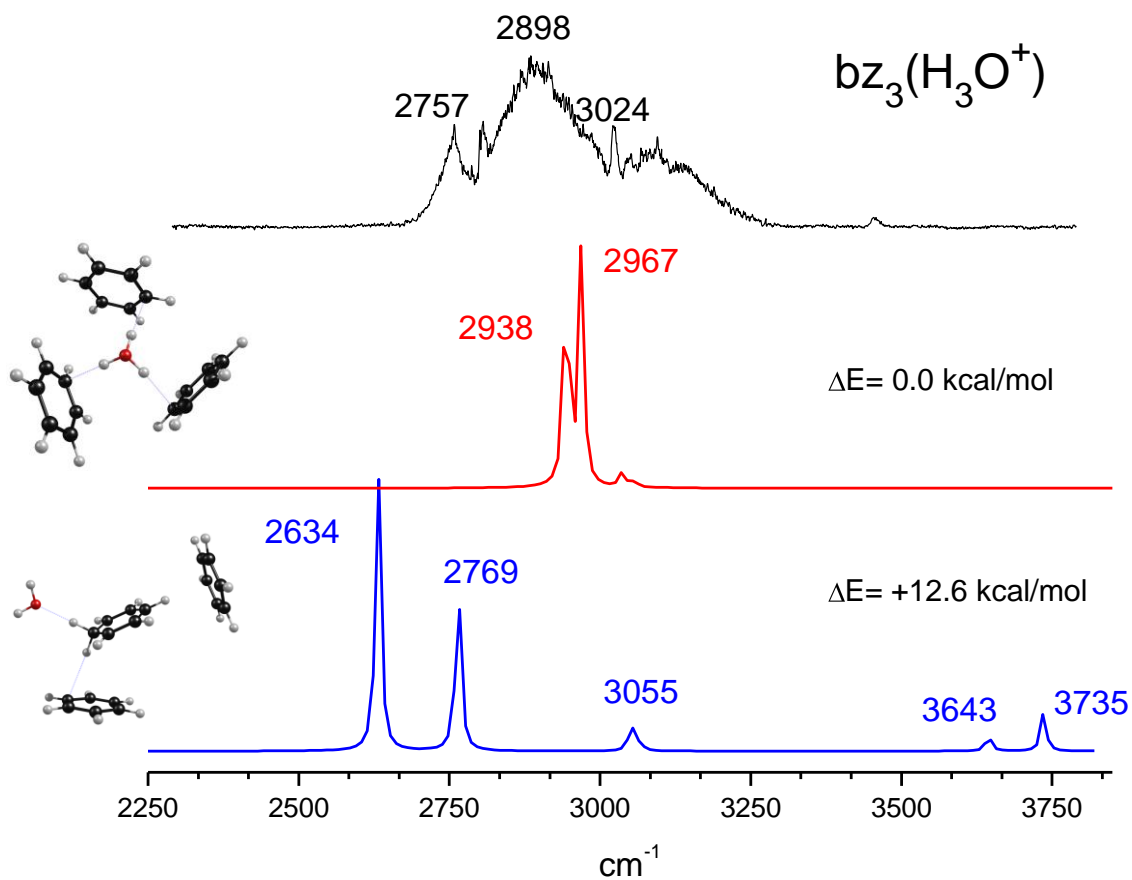


Figure 6: The infrared spectrum of $\text{bz}_3(\text{H}_3\text{O}^+)$, obtained by measuring the mass channel corresponding to the loss of a neutral benzene molecule, compared to two different isomers calculated by B3LYP/6311+G (d,p) level of theory.

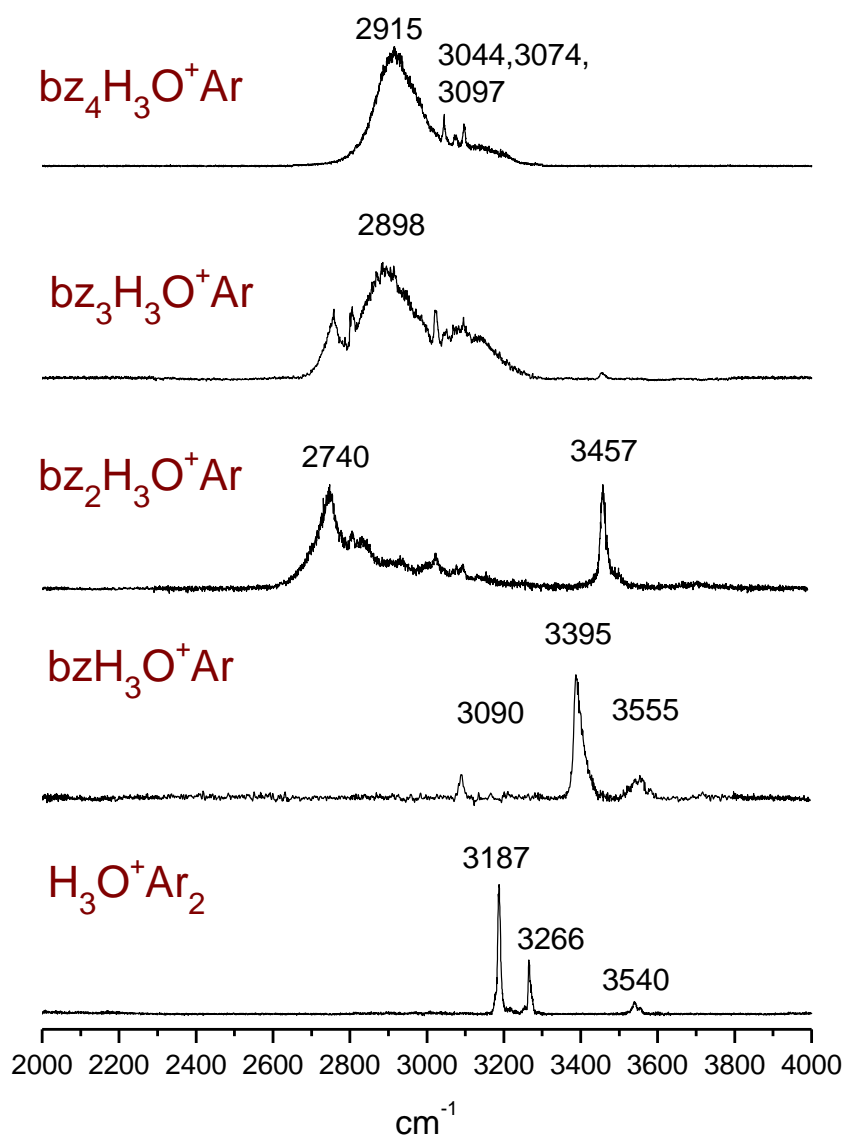


Figure 7: Comparison of IRPD spectra showing the effect of solvation of 0-4 benzene on hydronium. Each spectrum was obtained by measuring the mass channel corresponding to the loss of Ar.

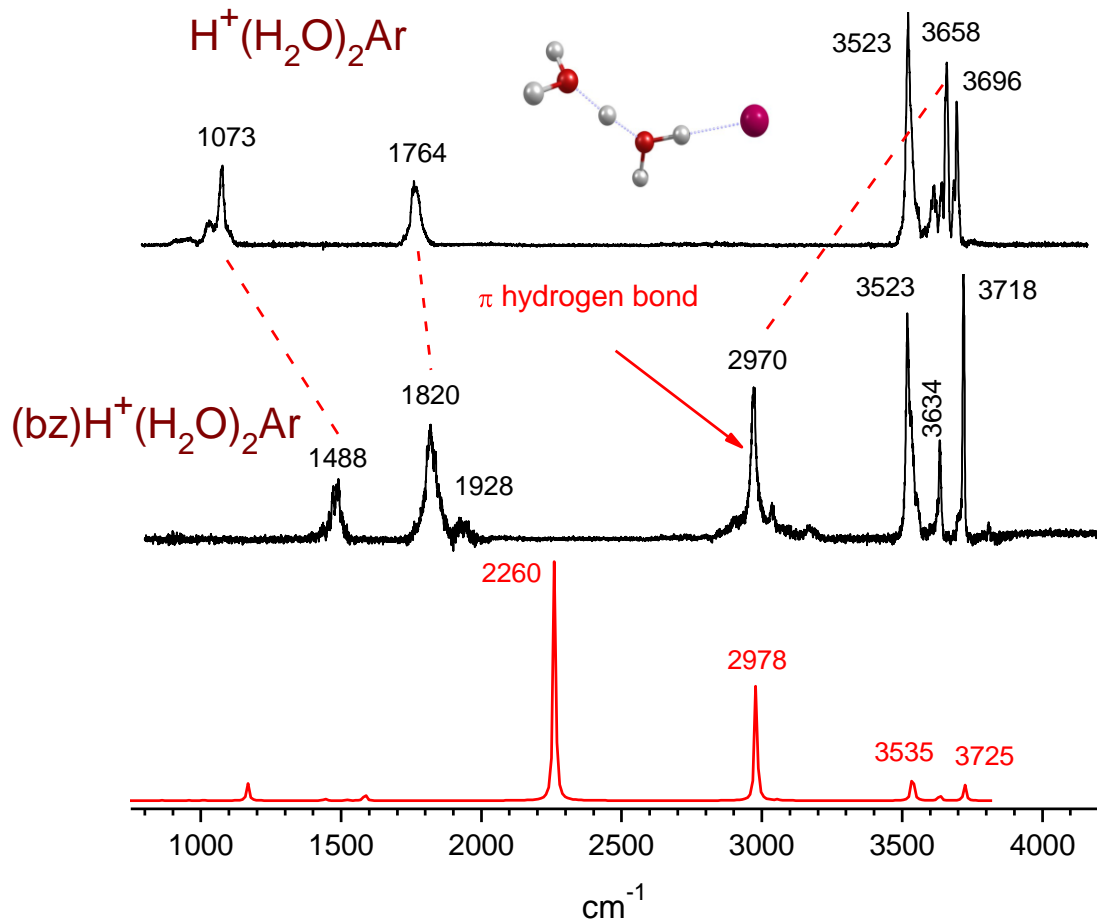


Figure 8: The IRPD spectra of $(\text{H}_5\text{O}_2^+)\text{Ar}$, shown in the top trace, $(\text{bz})\text{H}^+(\text{H}_2\text{O})_2\text{Ar}$, shown in the middle trace, and the predicted spectrum using B3LYP/6311+G (p,d) level of theory of the lowest energy isomer.

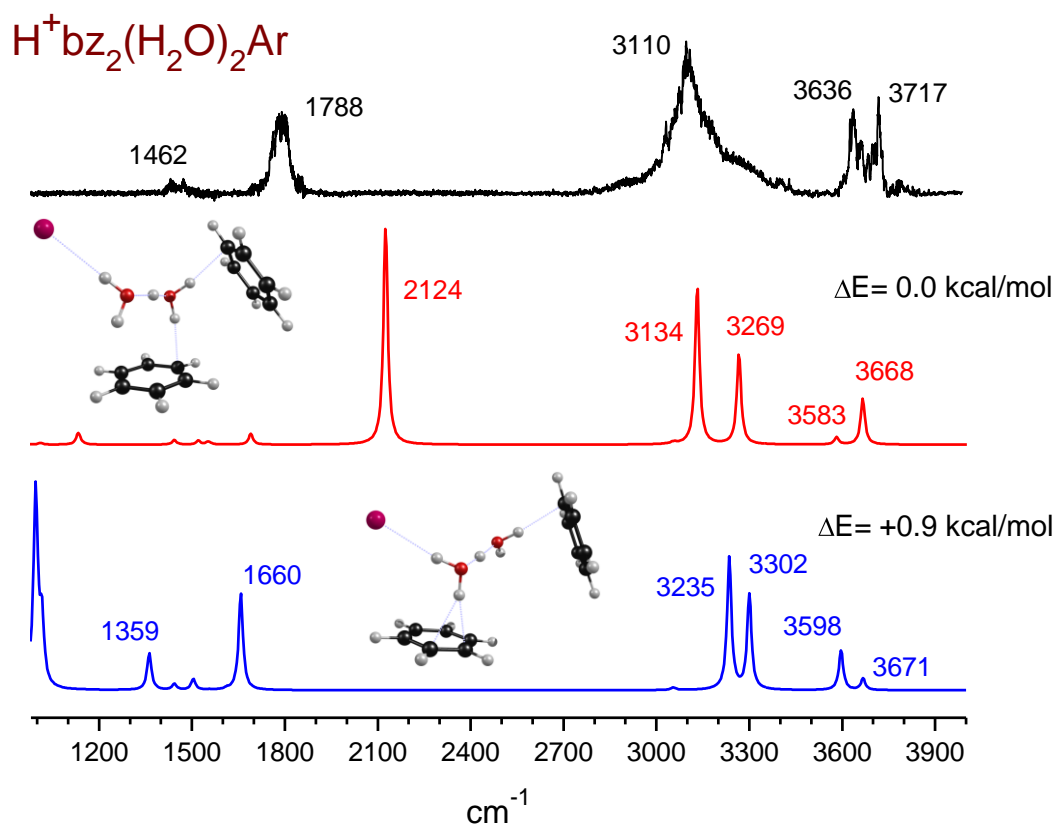


Figure 9: IRPD spectrum of $bz_2(H_5O_2^+)_2-Ar$, obtained by measuring the mass channel corresponding to the loss of Ar, compared to the predicted spectrum of two different stable isomers calculated using B3LYP/6311+G (p,d)

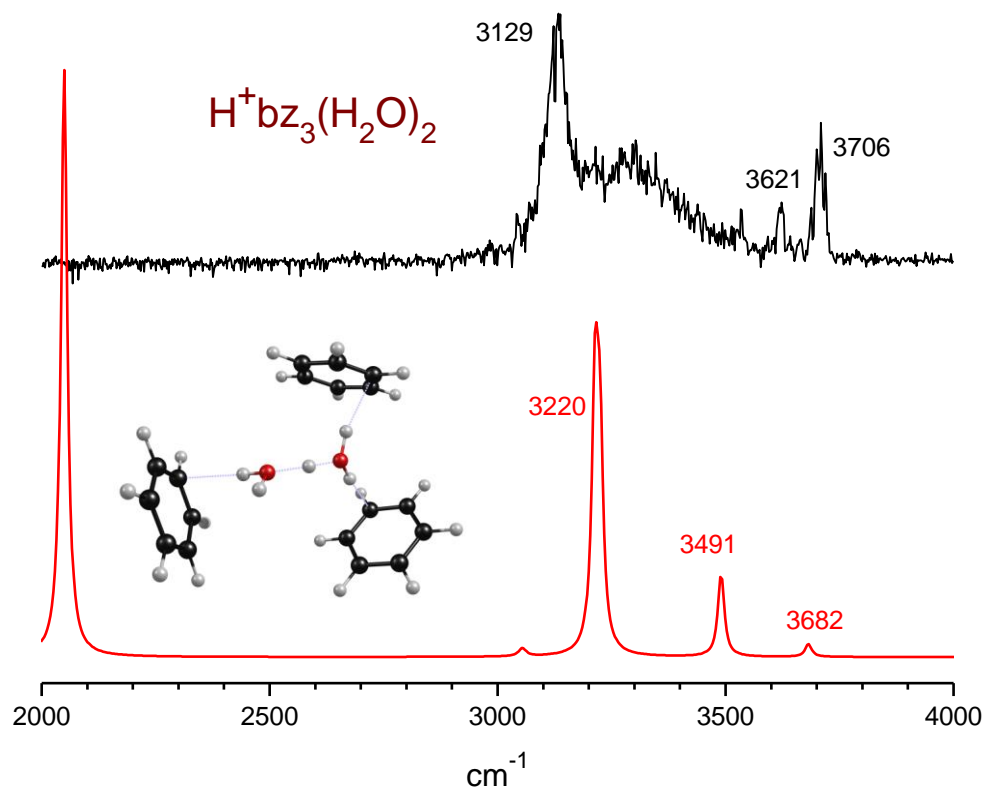


Figure 10: IRPD spectrum of $Bz_3(H_5O_2^+)$ obtained by measuring the mass channel corresponding to the loss of benzene. The predicted structure and corresponding spectra is below in red, calculated using B3LYP/6311+G (p,d)

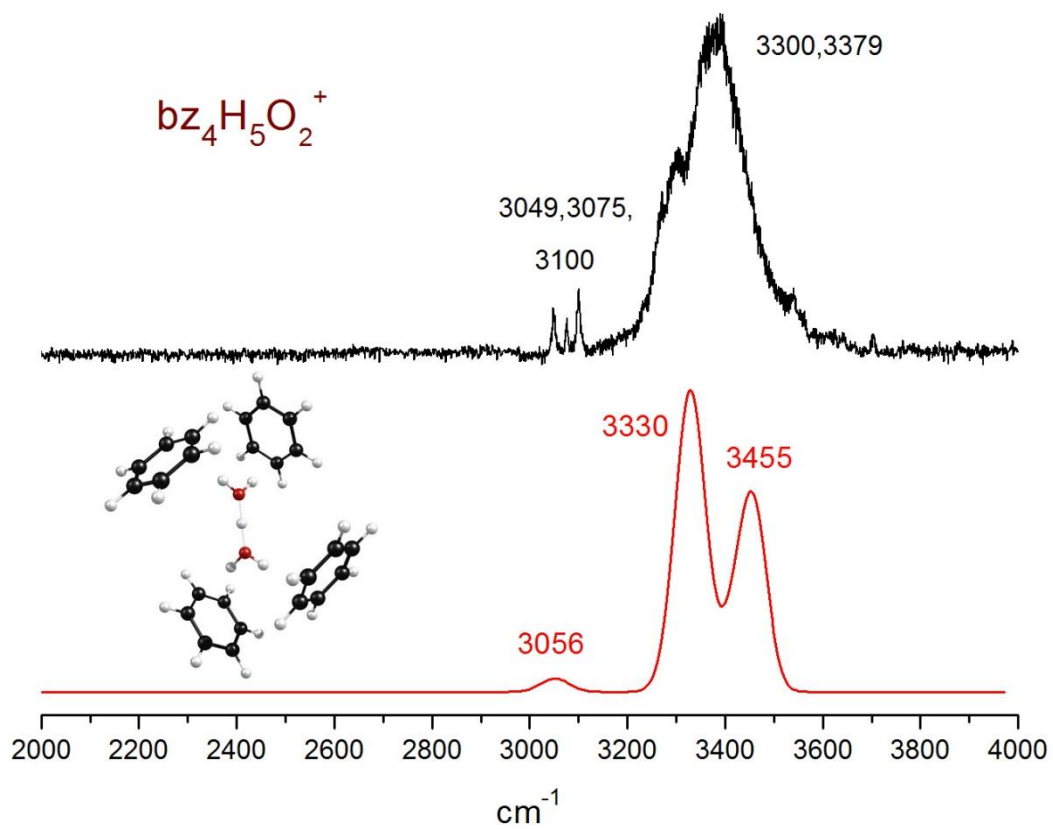


Figure 11: Infrared spectrum of $\text{bz}_4(\text{H}_5\text{O}_2^+)$ measured from the mass channel corresponding to the loss of neutral benzene. The predicted theoretical spectrum using B3LYP/6311+G (d, p) can be seen on the bottom trace

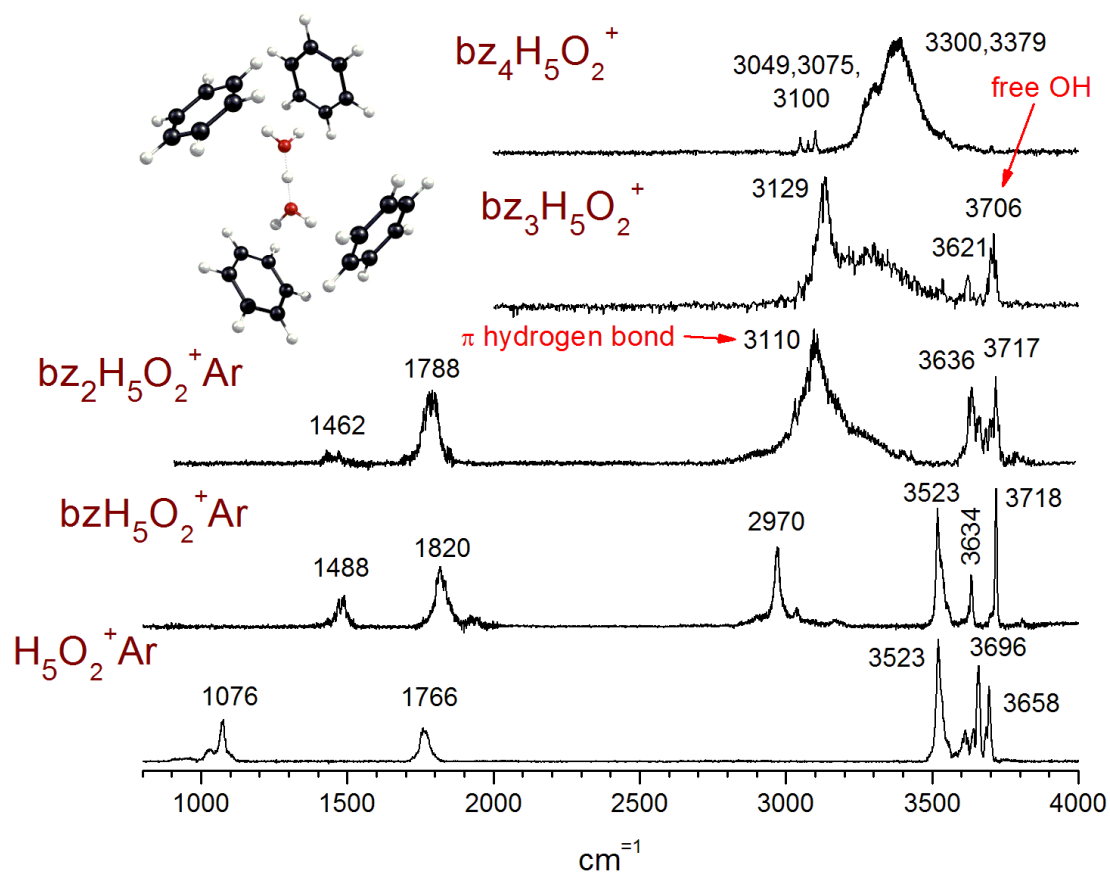


Figure 12: Comparison IRPD spectra of the Zundel ion with sequential addition of 0-4 benzene molecules.

CHAPTER VI

CONCLUSION

Protonation is a key process in different areas of research. Using infrared laser photodissociation spectroscopy on mass-selected ions, the spectra of a variety of different protonated complexes are investigated and compared with theoretical models. By choosing three model systems, the effects of protonation, the shared proton structure, and solvation effects are studied.

In Chapter III, the infrared spectrum of glyoxal cation is obtained for the first time. The spectrum matches well with the infrared spectrum of the trans configuration, similar to the most abundant conformation found naturally in the atmosphere, even though the cis structure is calculated to be lower in energy by 0.3 kcal/mol. Theory predicts the global minimum structure of protonated glyoxal to be the protonated cis configuration with an intermolecular shared proton between two oxygen atoms. The energy difference between the cis and trans configuration for protonated glyoxal increases as larger basis sets are used, ranging from 3 to 7 kcal/mol depending on the level of theory.

Chapter IV discussed the structure of protonated hydrogen clusters H_n^+ , where $n=5,7,9$. The spectra for all three cluster sizes along with their fully deuterated isotopologues are measured. Below the dissociation limit, IRMPD spectra were obtained for both H_5^+ and D_5^+ using the free electron laser at FELIX. The infrared spectrum for H_5^+ matches well with the

predicted infrared spectrum by Bowman and coworkers using DMC calculations, which take into account the anharmonic nature of H_5^+ . The structure of H_5^+ is assigned to the D_{2d} structure where the proton is shared equally in the structure. Many of the combination bands that include the shared proton stretch are observed because of its strong oscillator strength. Bands corresponding to the same modes in H_5^+ are red-shifted down because of the change in mass in D_5^+ . The infrared spectrum of larger hydrogen clusters agree well with structures of H_3^+ solvated by neutral hydrogen molecules.

In Chapter V, the solvation of protonated water and protonated water dimer clusters with benzene molecules is studied. The infrared spectrum suggests a shared proton structure, with the proton interacting closer to the water than the benzene, for protonated 1:1 benzene water. The structure corresponds with the hydronium motif solvated by neutral benzene molecules when additional benzene molecules are added to protonated water. Charge delocalization reduces the red-shift of the O-H stretch interacting benzene with each additional benzene molecule. For the Zundel ion, H_5O_2^+ , the solvation of benzene polarizes the Zundel ion, causing unequal sharing of the proton. This is seen by a blue-shift in the shared proton stretch. The Zundel ion is fully solvated by benzene with four benzene molecules. The protonation of benzene is not observed for any of the mixed complexes studied.

APPENDIX

Full citation of Gaussian03

Frisch, M. J.; Trucks, G. W.; Schlegel, H. B.; Scuseria, G. E.; Robb, M. A.; Cheeseman, J. R.; Montgomery, J. A. Jr.; Vreven, T.; Kudin, K. N.; Burant, J. C.; Millam, J. M.; Iyengar, S. S.; Tomasi, J.; Barone, V.; Mennucci, B.; Cossi, M.; Scalmani, G.; Rega, N.; Petersson, G. A.; Nakatsuji, H.; Hada, M.; Ehara, M.; Toyota, K.; Fukuda, R.; Hasegawa, J.; Ishida, M.; Nakajima, T.; Honda, Y.; Kitao, O.; Nakai, H.; Klene, M.; Li, X.; Knox, J. E.; Hratchian, H. P.; Cross, J. B.; Adamo, C.; Jaramillo, J.; Gomperts, R.; Stratmann, R. E.; Yazyev, O.; Austin, A. J.; Cammi, R.; Pomelli, C.; Ochterski, J. W.; Ayala, P. Y.; Morokuma, K.; Voth, G. A.; Salvador, P.; Dannenberg, J. J.; Zakrzewski, V. G.; Dapprich, S.; Daniels, A. D.; Strain, M. C.; Farkas, O.; Malick, D. K.; Rabuck, A. D.; Raghavachari, K.; Foresman, J. B.; Ortiz, J. V.; Cui, Q.; Baboul, A. G.; Clifford, S.; Cioslowski, J.; Stefanov, B. B.; Liu, G.; Liashenko, A.; Piskorz, P.; Komaromi, I.; Martin, R. L.; Fox, D. J.; Keith, T.; Al-Laham, M. A.; Peng, C. Y.; Nanayakkara, A.; Challacombe, M.; Gill, P. M. W.; Johnson, B.; Chen, W.; Wong, M. W.; Gonzalez, C.; Pople, J. A. *Gaussian 03 (Revision B.02)*; Gaussian, Inc.: Pittsburgh, PA, 2003.

All calculations are done with either DFT-B3LYP or MP2 level of theory with 6-311+G (d, p) basis set.

- a. Total binding energy in the complex relative to separated molecules as specified (in kcal/mol). The energies are not ZPVE and BSSE corrected.
- b. Dissociation energy in kcal/mol for the elimination of benzene, water or argon as specified.
- c. Intensities are in Km/mol. Frequencies are scaled by a factor of 0.9575 for DFT and 0.9523 for MP2.

Total energies are in atomic units.

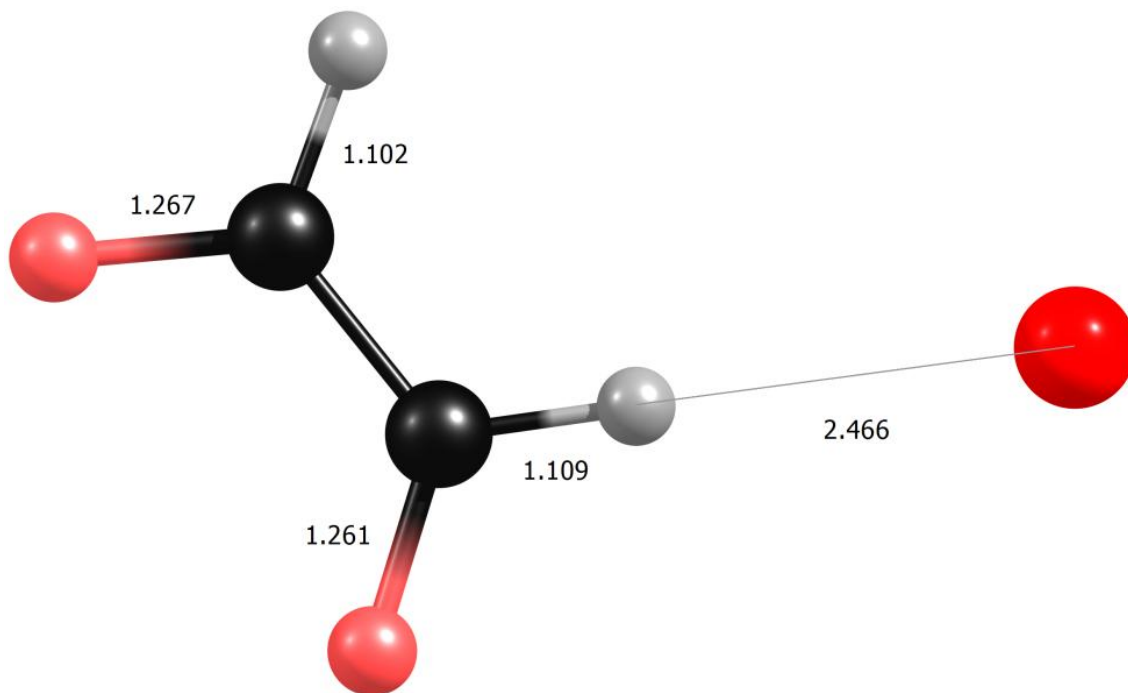
cis-glyoxal cation-Ar DFT

State: $^1A(C_s)$

Total Energy = - 754.985026

$\Delta E = 0.0$

D.E^b (Ar) = 1.4



Unscaled Frequency (Intensity) Scaled Frequency /Symmetry of vibration

36 (11.6) 34/a, 57 (26.4)55/a, 65 (12.5)63/a, 235 (5.2)227/a, 381 (0.1)368/a, 636 (30.0)614/a, 732 (37.9)707/a, 807(1.1)779/a,
1036 (1.6) 1000/a, 1140 (97.9)1100/a, 1191 (12.0)1149/a, 1402 (73.6)1353/a, 1608 (16.2)1551/a, 2888 521.7)2787/a,
2998 (148.9)2894/a

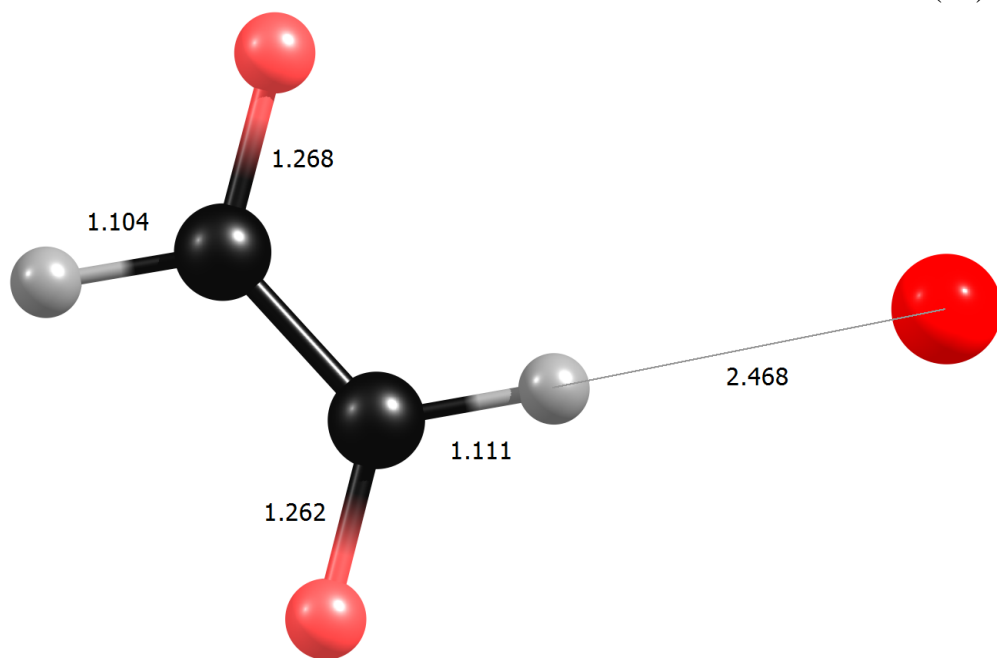
trans-glyoxal-Ar DFT

State: $^1A(C_s)$

Total Energy = - 754.983928

$\Delta E = +0.7$

D.E^b (Ar) = 1.4



Unscaled Frequency (Intensity) Scaled Frequency /Symmetry of vibration

33 (1.9) 32/a, 69 (13.9) 67/a, 103 (0.4) 100/a, 273 (18.6) 264/a, 303 (32.1) 293/a, 503 (0.2) 485/a, 775 (22.9) 748/a, 814 (28.7) 785/a, 1121 (1.9) 1082/a, 1139 (36.4) 1099/a, 1203 (0.0) 1161/a, 1362 (160.3) 1314/a, 1613 (8.1) 1557/a, 2867 (551.4) 2767/a, 2973 (107.6) 2869/a.

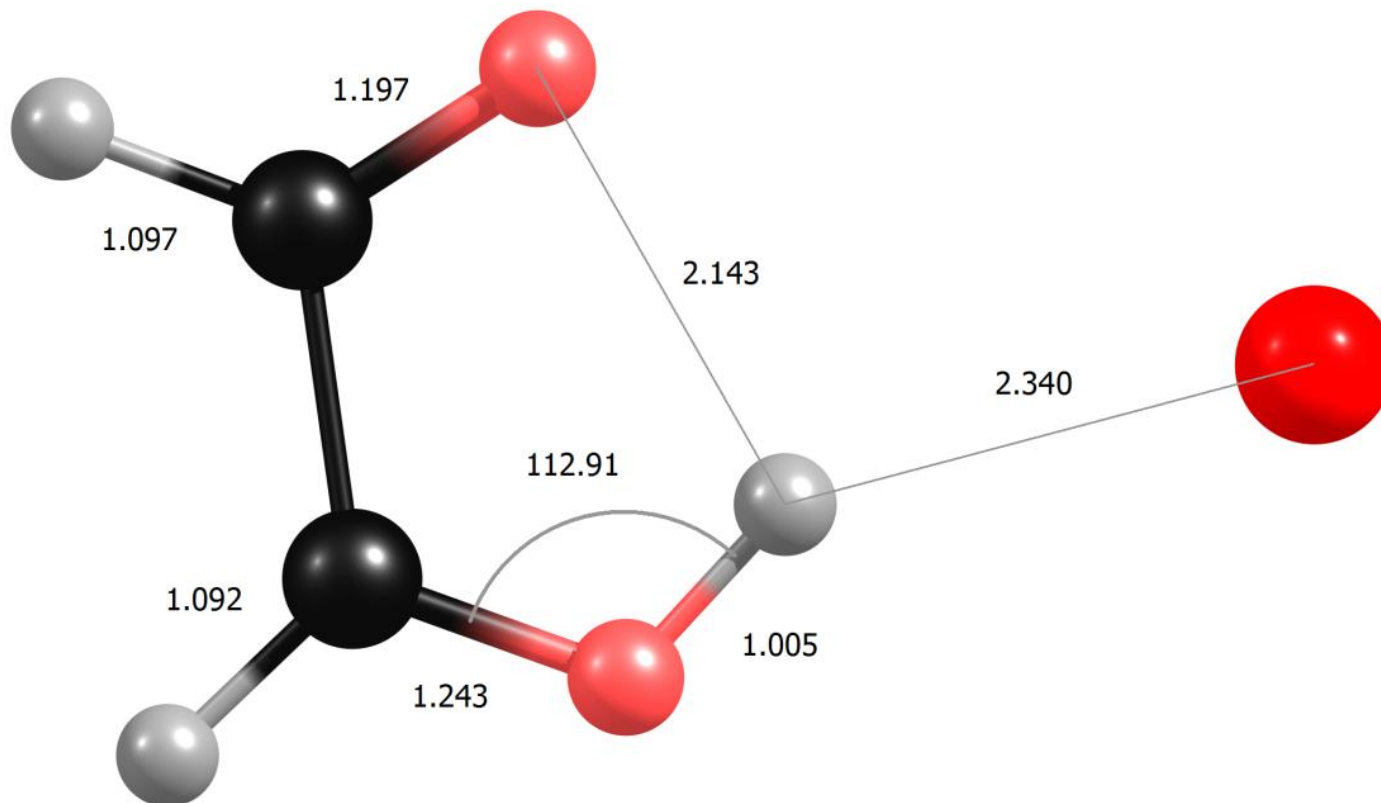
cis-H⁺glyoxal-Ar isomer-a DFT

State: ¹A(C_s)

Total Energy = - 755.7267498

ΔE = +0.0

D.E^b (Ar) = 1.5



Unscaled Frequency (Intensity) Scaled Frequency /Symmetry of vibration

53 (2.0) 51/a, 54 (13.2) 53/a, 88 (22.0) 85/a, 243 (6.5) 234/a, 280 (43.3) 271/a, 730 (11.9) 705/a, 744 (48.9) 718/a, 817 (23.6) 788/a, 1030 (48.7) 994/a, 1138 (63.8) 1098/a, 1202 (290.6) 1160/a, 1345 (13.5) 1298/a, 1419 (23.6) 1369/a, 1656 (88.2) 1599/a, 1794 (27.2) 1731/a, 3078 (0.1) 2971/a, 3147 (3.2) 3037/a, 3214 (553.4) 3102/a.

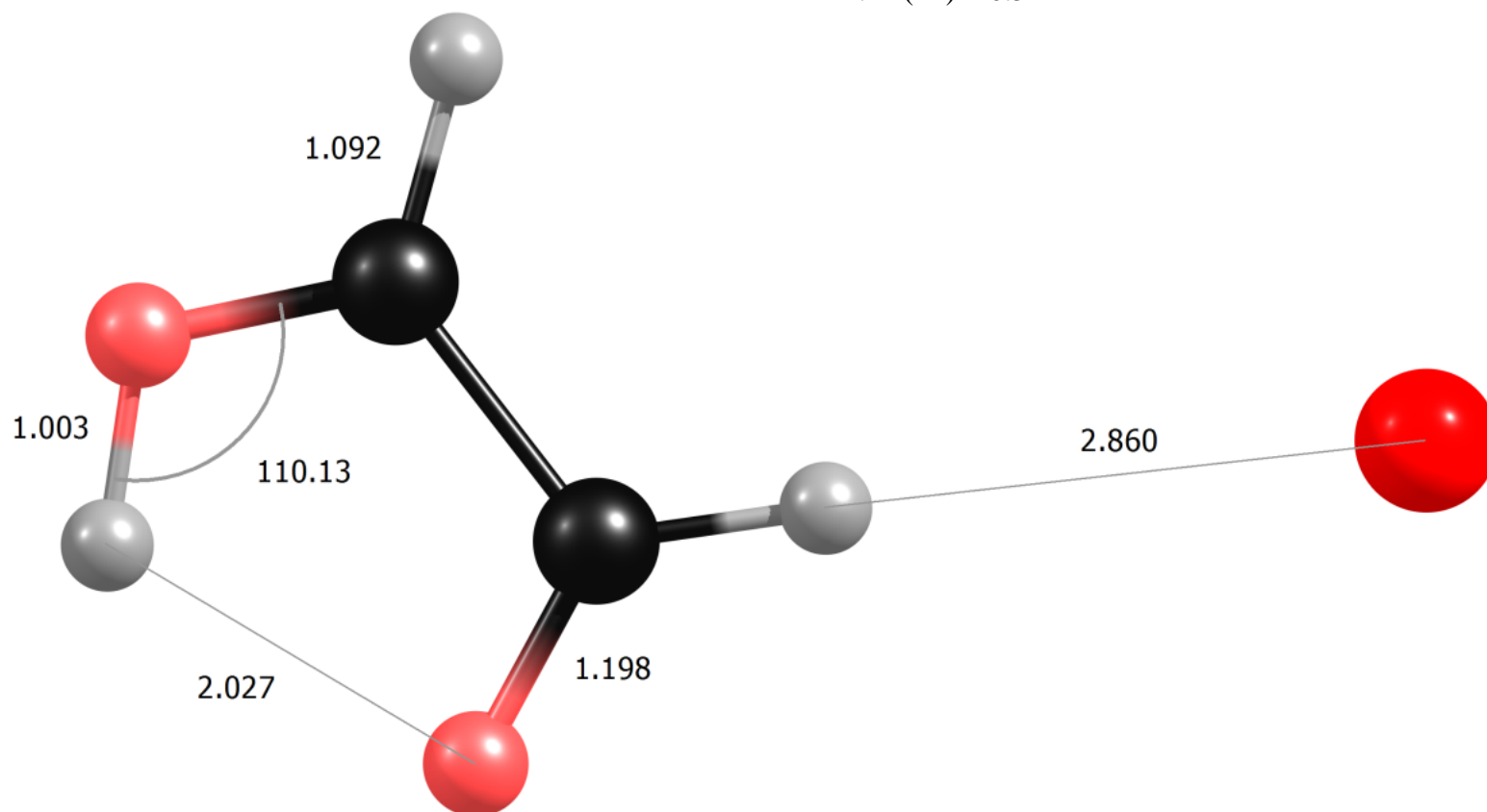
cis-H⁺glyoxal-Ar isomer-b DFT

State: ¹A(C_s)

Total Energy = - 755.7251893

ΔE = +0.9

D.E^b (Ar) = 0.5



Unscaled Frequency (Intensity) Scaled Frequency /Symmetry of vibration

30 (9.1) 29/a, 44 (10.6) 42/a, 57 (6.2) 55/a, 262 (10.1) 253/a, 292 (49.1) 282/a, 741 (26.0) 716/a, 743 (19.3) 717/a, 821 (28.0) 792/a,
 1036 (53.6) 1000/a, 1136 (81.6) 1096/a, 1215 (214.2) 1173/a, 1347 (17.0) 1300/a, 1437 (36.1) 1387/a, 1651 (84.0) 1593/a,
 1789 (32.5) 1726/a, 3093 (9.0) 2985/a, 3154 (9.4) 3044/a, 3270 (187.6) 3156/a

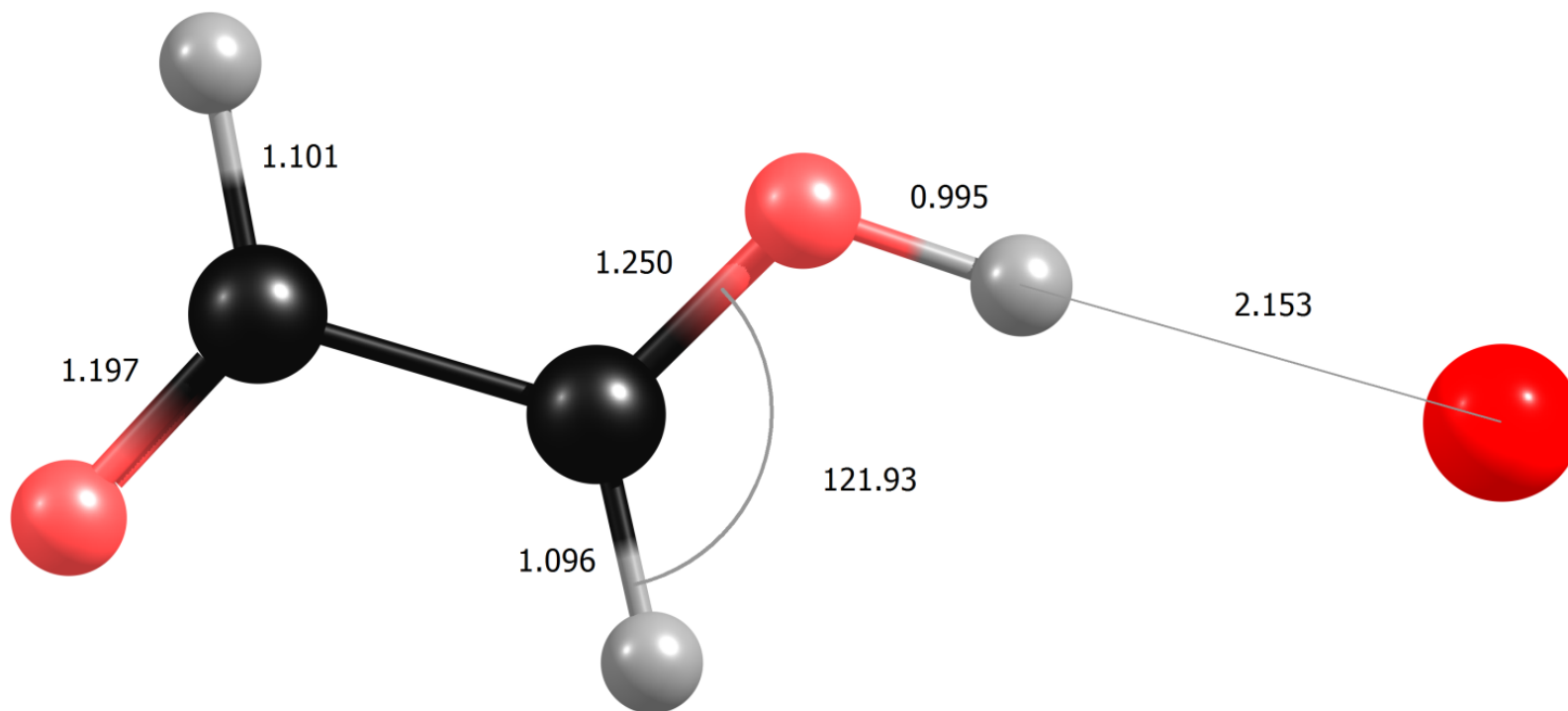
trans-H⁺ glyoxal-Ar isomer-a DFT

State: ¹A(C_s)

Total Energy = - 755.724097

$\Delta E = +1.7$

D.E^b (Ar) = 3.1



Unscaled Frequency (Intensity) Scaled Frequency /Symmetry of vibration

45 (9.5) 43/a, 55 (35.9) 53/a, 90 (3.4) 87/a, 109 (26.2) 105/a, 329 (27.7) 318/a, 530 (11.1) 512/a, 722 (98.9) 697/a, 986 (29.8) 951/a, 999 (12.3) 965/a, 1110 (13.3) 1071/a, 1229 (33.7) 1186/a, 1355 (6.9) 1307/a, 1405 (97.7) 1355/a, 1643 (131.8) 1586/a, 1785 (44.9) 1723/a, 3035 (1.7) 2930/a, 3107 (5.7) 2999/a, 3337 (1424.3) 3220/a.

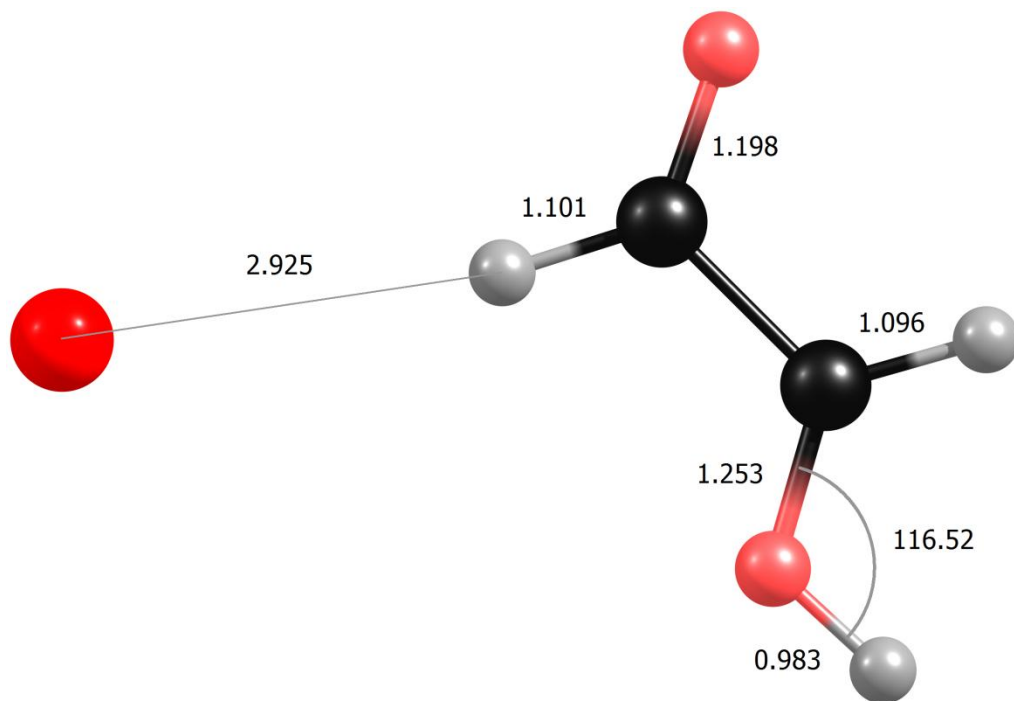
trans-H⁺ glyoxal-Ar isomer-b DFT

State: ¹A(C_s)

Total Energy = - 754.983928

$\Delta E = +4.4$

D.E^b (Ar) = 1.4



Unscaled Frequency (Intensity) Scaled Frequency /Symmetry of vibration

-39 (4.0) -38/a, 15 (7.7) 14/a, 24 (8.4) 23/a, 63 (23.0) 61/a, 317 (42.6) 306/a, 525 (4.2) 507/a, 668 (145.1) 645/a, 968 (52.5) 934/a, 979 (15.2) 945/a, 1101 (11.7) 1063/a, 1211 (45.6) 1169/a, 1357 (8.5) 1310/a, 1397 (99.6) 1348/a, 1629 (116.8) 1572/a, 1780 (47.4) 1718/a, 3037 (1.8) 2931/a, 3110 (8.5) 3002/a, 3587 (365.6) 3462/a.

BW-1, 1 isomer-a (bz-H₃O)⁺ DFT

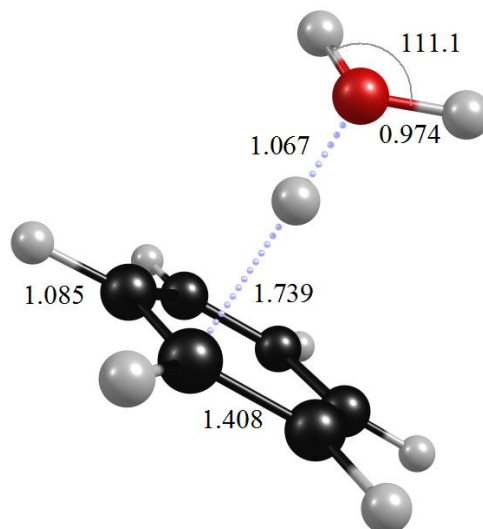
State: ¹A(C₁)

Total Energy = -309.082267

$\Delta E = +3.5$

B.E.^a = E (complex) - E (H₃O⁺ + bz) = 25.0

D.E.^b (H₃O⁺, bz) = 25.0



Unscaled Frequency (Intensity) Scaled Frequency /Symmetry of vibration

45 (8.8) 43/a, 62 (5.8) 60/a, 101(52.6) 97/a, 267 (89.8) 255/a, 289 (1.8) 277/a, 407 (0.1) 389/a, 408(10.7) 391/a, 487 (246.6) 467/a, 616(0.1) 589/a, 617 (1.6) 590/a, 683 (21.3) 654/a, 733 (87.6) 702/a, 882 (14.2) 845/a, 891 (0.1) 853/a, 970 (7.3) 928/a, 1000(4.8)957/a, 1015 (0.1) 972/a, 1022 (0.4) 979/a, 1033 (0.3) 989/a, 1049 (0.6) 1004/a, 1056 (3.0) 1011/a, 1066 (144.7) 1021/a, 1182 (0.8) 1132/a, 1201 (3.7) 1150/a, 1202 (0.4) 1151/a, 1331 (8.0) 1275/a, 1383 (0.0) 1324/a, 1499 (22.9) 1435/a, 1500 (32.6) 1437/a, 1535(2.9)1469/a, 1602 (110.1)1534/a, 1614(0.4) 1546/a, 1635 (14.9) 1565/a, 2137 (3139) 2046/a, 3165 (0.2) 3030/a, 3180 (0.0) 3045/a, 3181(0.1) 3046/a, 3189 (0.2) 3054/a, 3196 (0.1) 3060/a, 3203 (0.1) 3067/a, 3677 (133.3) 3521/a, 3762 (258.9) 3602/a.

BW-1, 1 isomer-b (bzH-H₂O)⁺ DFT

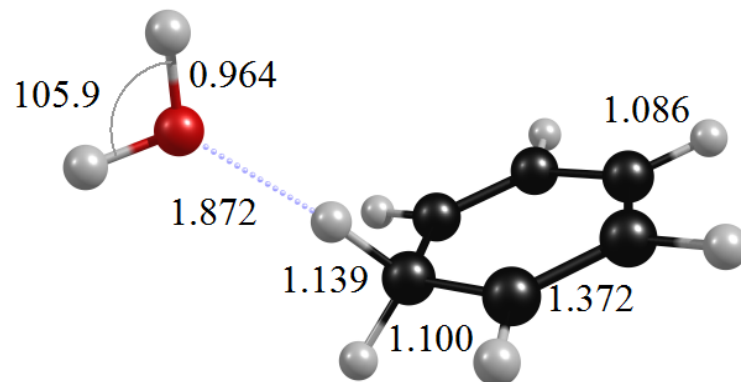
State: ¹A(C₁)

Total Energy = -309.0878769

ΔE = +0.0

B.E.^a = E (complex)-E (H₂O+bzH⁺) = 11.4

D.E^b (H₂O) = 11.4



Unscaled Frequency (Intensity) Scaled Frequency /Symmetry of vibration

41 (3.5) 40/a, 46 (1.4) 44/a, 83(0.1)79/a, 166(35.5)159/a, 235 (271.4) 225/a, 281 (29.0) 269/a, 342 (0.6) 328/a, 366(37.0) 351/a, 490 (16.3) 469/a, 595 (4.0) 570/a, 600 (2.7) 574/a, 665 (62.9) 637/a, 820 (0.3) 785/a, 839 (21.2) 804/a, 922(13.0)883/a, 1001 (18.4) 958/a, 1006 (0.3) 964/a, 1012 (1.9) 969/a, 1020 (0.3) 976/a, 1040 (0.8) 996/a, 1061 (2.5) 1016/a, 1135 (5.1) 1087/a, 1166 (0.8) 1116/a, 1205(13.2) 1154/a, 1209 (31.3) 1158/a, 1277 (172.2)1223/a, 1369 (12.8)1311/a, 1425 (11.5)1364/a, 1479 (150.9) 1416/a, 1482 (24.5)1419/a, 1575(0.0)1508/a, 1632 (30.6) 1563/a, 1639(86.6) 1569/a, 2565 (1146.7) 2456/a, 3018(22.6) 2889/a, 3181 (0.0) 3046/a, 3191 (1.0) 3055/a, 3192 (2.8) 3057/a, 3208 (2.7) 3072/a, 3211 (0.6) 3074/a, 3800 (55.8) 3639/a, 3895 (119.6) 3730/a.

BW-1, 1 isomer-a (bz-H₃O)⁺ MP2

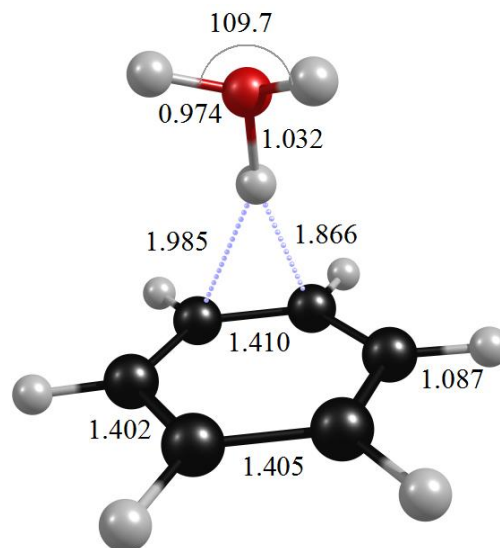
State: ¹A(C₁)

Total MP2 Energy = -308.1764399

ΔE = 0.0

B.E.^a = E (complex)-E (H₃O⁺+bz) = 28.7

D.E^b (H₃O⁺, bz) = 28.7



Unscaled Frequency (Intensity) Scaled Frequency /Symmetry of vibration

45(8.8) 43/a, 82 (20.8) 78/a, 96 (57.0) 92/a, 191 (0.1)182/a, 259 (68.5) 246/a, 375 (0.8) 358/a, 388(0.1) 369/a, 437(29.1) 416/a, 463 (167.5) 440/a, 604(0.3)575/a, 605(0.0)576/a, 722 (84.7) 688/a, 876(0.4) 834/a,886(1.3) 844/a,942(0.4)897/a, 948(0.1) 903/a, 966(1.9) 920/a, 998(1.1) 951/a, 1006 (0.1) 958/a, 1052 (2.6) 1002/a, 1056 (2.9)1006/a, 1099 (190.7) 1047/a, 1183 (0.2) 1126/a, 1203 (0.3) 1146/a, 1204 (0.6) 1147/a, 1371(0.0)1306/a, 1440 (1.1) 1371/a, 1497(22.6) 1426/a, 1498 (16.0)1427/a, 1571(7.6)1496/a, 1618(3.8)1541/a, 1627(1.8)1549/a, 1649 (53.8) 1571/a, 2660 (2143.1) 2533/a,3208 (0.0)3055/a, 3217(0.1)3064/a, 3218(0.2)3065/a,3 2280.8) 3074/a, 3231(0.3) 3077/a, 3238 (0.3) 3083/a, 3711(149.5)3534/a, 3798 (259.5) 3617/a.

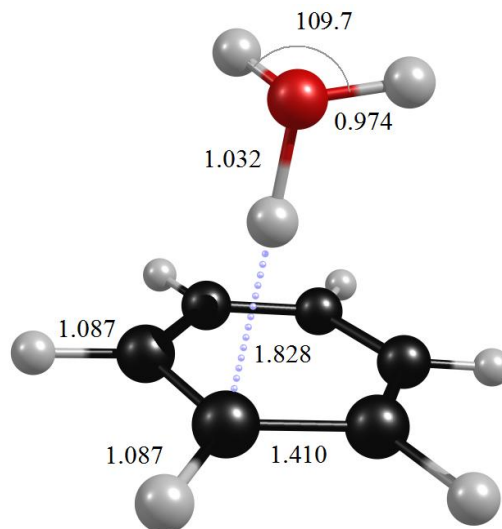
BW-1, 1 (bz-H₃O)⁺ transition state MP2

State: ¹A(C₁) Total MP2 Energy = -308.1764186

$\Delta E = 0.0$

B.E.^a = E (complex) - E (H₃O⁺ + bz) = 28.7

D.E.^b (H₃O⁺, bz) = 28.7



Unscaled Frequency (Intensity) Scaled Frequency /Symmetry of vibration

-47 (3.0) -45/a, 82 (76.4) 78/a, 88 (9.5) 84/a, 186 (0.7) 177/a, 258 (65.7) 246/a, 378 (0.0) 360/a, 389 (1.1) 370/a, 445 (102.9) 424/a, 472 (100.8) 450/a, 604(0.0) 575/a, 605 (0.2) 576/a, 723 (84.7) 688/a, 877 (0.2) 835/a, 886 (1.3) 843/a, 947 (0.6) 901/a, 950(0.0)905/a, 963 (2.6) 918/a, 998 (1.2) 951/a, 1007 (0.2) 959/a, 1052(1.4)1002/a, 1056(2.7)1006/a, 1105(186.4)1052/a, 1183(0.1)1126/a,1204(1.1) 1146/a,1204 (0.0) 114/a, 1371(0.0) 1306/a,1439(2.0)1370/a, 1497(24.1)1426/a,1498 (15.3)1427/a, 1567(5.1)1492/a, 1622(1.2)1544/a, 1623 (5.9) 1545/a, 1651 (52.3) 1572/a, 2665 (2145.8) 2537/a, 3208 (0.1) 3055/a, 3217 (0.1) 3064/a, 3218(0.2) 3065/a, 3228 (0.9) 3074/a, 3231 (0.3) 3077/a, 3238 (0.3) 3083/a, 3711 (150.3) 3534/a, 3798 (257.6) 3617/a.

BW-1, 1 isomer-b (bzH-H₂O)⁺ MP2

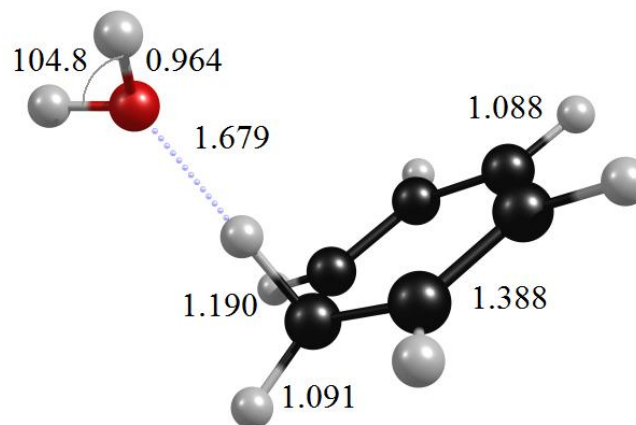
State: ¹A(C₁)

Total MP 2 Energy = -308.1666288

ΔE = +6.2

B.E.^a = E (complex)-E (H₂O+bzH⁺) =13.6

D.E^b (H₂O) = 13.6



Unscaled Frequency (Intensity) Scaled Frequency /Symmetry of vibration

30 (8.1) 28/a, 61 (7.4) 58/a, 89 (4.2) 85/a, 131 (105.7) 125/a, 299 (229.9) 284/a, 345 (23.9) 328/a, 357 (10.4) 340/a, 378 (25.9) 360/a, 573 (33.8) 546/a, 591 (3.7) 563/a, 597 (1.2) 569/a, 656 (33.8) 624/a, 800 (44.0) 762/a, 821 (24.4) 782/a, 931 (47.8) 886/a, 964 (18.9) 918/a, 1009 (0.6) 961/a, 1016 (6.4) 967/a, 1020 (2.8) 972/a, 1040 (1.8) 991/a, 1050 (0.4) 999/a, 1062 (0.0) 1011/a, 1185 (0.1) 1128/a, 1209 (8.3) 1151/a, 1212 (2.1) 1154/a, 1273 (60.7) 1212/a, 1379 (2.2) 1313/a, 1463 (0.2) 1393/a, 1489 (15.0) 1418/a, 1524 (91.2) 1452/a, 1616 (12.0) 1539/a, 1625 (72.7) 1547/a, 1651 (40.5) 1573/a, 2078 (2056.8) 1979/a, 3181 (8.9) 3029/a, 3219 (0.0) 3065/a, 3226 (1.8) 3073/a, 3228 (3.9) 3074/a, 3247 (4.0) 3093/a, 3250 (1.4) 3095/a, 3833 (73.2) 3650/a, 3943 (134.2) 3755/a.

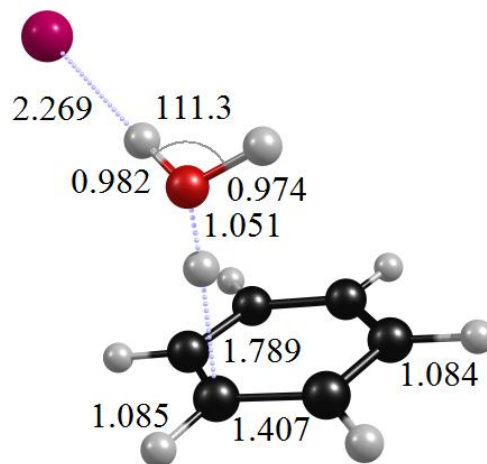
BW-1, 1-Ar isomer-a (bz-H₃O-Ar)⁺ DFT

State: ¹A(C₁) Total Energy = -836.639238

$\Delta E = +1.9$

B.E.^a = E (complex) - E (H₃O⁺ + bz + Ar) = 27.0

D.E.^b (Ar) = 1.9



Unscaled Frequency (Intensity) Scaled Frequency /Symmetry of vibration

14 (4.0) 13/a, 26 (3.2) 25/a, 55 (0.8) 53/a, 62 (6.3) 60/a, 110 (21.5) 105/a, 240 (63.1) 230/a, 252 (86.4) 241/a, 319 (4.8) 306/a, 407 (0.1) 390/a, 409 (7.7) 391/a, 517 (194.3) 495/a, 617 (0.1) 591/a, 618 (0.8) 591/a, 686 (12.4) 656/a, 733 (90.3) 702/a, 888 (10.3) 850/a, 891 (1.3) 853/a, 971 (19.4) 930/a, 1000 (5.0) 958/a, 1013 (0.8) 970/a, 1022 (2.5) 979/a, 1032 (3.3) 988/a, 1041 (69.2) 997/a, 1054 (36.2) 1009/a, 1057 (17.8) 1012/a, 1182 (0.5) 1132/a, 1201 (1.2) 1150/a, 1202 (0.9) 1151/a, 1332 (4.5) 1276/a, 1383 (0.0) 1324/a, 1502 (17.5) 1438/a, 1503 (23.5) 1439/a, 1555 (8.9) 1489/a, 1614 (32.5) 1546/a, 1616 (2.1) 1548/a, 1644 (23.2) 1574/a, 2346 (3015.8) 2247/a, 3166 (0.1) 3032/a, 3180 (0.1) 3045/a, 3181 (0.0) 3046/a, 3189 (0.4) 3054/a, 3196 (0.2) 3060/a, 3202 (0.1) 3066/a, 3550 (635.8) 3399/a, 3733 (250.3) 3575/a.

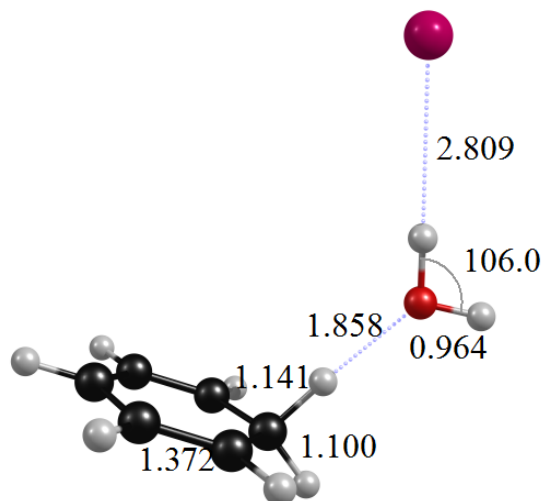
BW-1,1-Ar isomer-b (bzH-H₂O-Ar)⁺ DFT

State: ¹A(C₁) Total Energy = -836.6422875

$\Delta E = 0.0$

B.E.^a = E (complex) - E (H₂O + bzH⁺ + Ar) = 11.8

D.E.^b (Ar) = 0.3



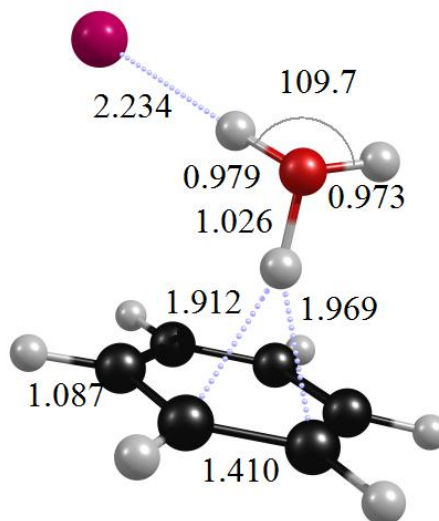
Unscaled Frequency (Intensity) Scaled Frequency /Symmetry of vibration

10 (1.3) 10/a, 17 (0.2) 16/a, 44 (6.7) 42/a, 48 (3.3) 46/a, 52 (0.9) 50/a, 131 (6.2) 125/a, 173 (38.2) 165/a, 251 (246.9) 240/a, 293 (27.8) 280/a, 342 (0.9) 328/a, 374 (37.2) 358/a, 498 (18.3) 477/a, 596 (3.9) 570/a, 600 (2.6) 575/a, 666 (64.6) 637/a, 820 (0.4) 785/a, 839 (21.1) 804/a, 924 (12.7) 885/a, 1001 (18.0) 958/a, 1007 (0.3) 964/a, 1012 (2.5) 969/a, 1020 (0.3) 976/a, 1040 (0.9) 996/a, 1062 (2.5) 1017/a, 1133 (5.4) 1085/a, 1167 (0.9) 1117/a, 1206 (12.8) 1155/a, 1209 (29.0) 1158/a, 1280 (164.2) 1226/a, 1369 (12.1) 1311/a, 1424 (12.0) 1364/a, 1479 (147.5) 1416/a, 1482 (24.3) 1419/a, 1575 (0.0) 1508/a, 1632 (33.0) 1562/a, 1639 (78.0) 1570/a, 2541 (1227.1) 2433/a, 3022 (21.7) 2894/a, 3181 (0.0) 3046/a, 3191 (1.0) 3055/a, 3192 (2.7) 3056/a, 3208 (2.6) 3072/a, 3210 (0.6) 3074/a, 3798 (82.2) 3636/a, 3892 (161.0) 3727/a.

BW-1, 1-Ar isomer-a (bz-H₃O-Ar)⁺ MP2

State: ¹A(C₁) Total MP2 Energy = -835.1367415 ΔE = 0.0

B.E.^a = E (complex)-E (H₃O⁺+bz+Ar) = 32.3 D.E.^b (Ar) = 3.5



Unscaled Frequency (Intensity) Scaled Frequency /Symmetry of vibration

11 (3.9) 10/a, 38 (3.0) 36/a, 75 (5.3) 71/a, 92 (6.7) 87/a, 117 (23.5) 111/a, 236 (62.9) 225/a, 251 (56.9) 239/a, 255 (26.4) 243/a, 375 (1.6) 357/a, 388 (0.1) 370/a, 450 (0.4) 429/a, 484 (146.4) 461/a, 605 (0.1) 576/a, 606 (0.0) 577/a, 721 (86.4) 687/a, 875 (0.3) 833/a, 885 (0.8) 843/a, 947 (0.1) 902/a, 949 (0.0) 904/a, 968 (0.6) 922/a, 999 (1.3) 951/a, 1008 (0.0) 960/a, 1053 (1.8) 1003/a, 1056 (3.0) 1006/a, 1109 (200.5) 1056/a, 1183 (0.2) 1126/a, 1203 (0.0) 1146/a, 1204 (0.7) 1147/a, 1371 (0.0) 1305/a, 1441 (0.8) 1373/a, 1498 (19.7) 1427/a, 1499 (16.3) 1427/a, 1582 (2.4) 1507/a, 1618 (1.5) 1541/a, 1629 (1.1) 1551/a, 1671 (43.0) 1591/a, 2767 (1978.3) 2635/a, 3208 (0.0) 3055/a, 3217 (0.1) 3064/a, 3218 (0.1) 3064/a, 3228 (0.7) 3074/a, 3230 (0.2) 3076/a, 3237 (0.5) 3083/a, 3622 (488.9) 3449/a, 3773 (286.1) 3593/a.

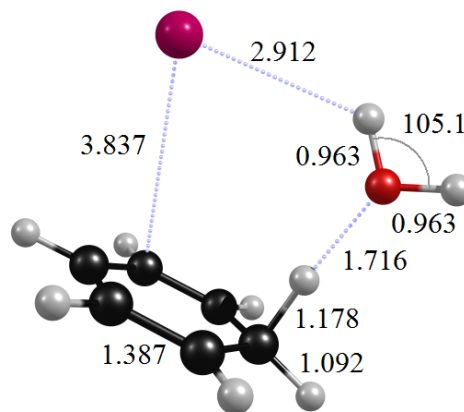
BW-1, 1-Ar isomer-b (bzH-H₂O-Ar)⁺ MP2

State: ¹A(C₁) Total MP2 Energy = -835.124332

$\Delta E = +7.8$

$B.E^a = E(\text{complex}) - E(\text{H}_2\text{O} + \text{bzH}^+ + \text{Ar}) = 15.5$

$D.E^b(\text{Ar}) = 1.9$



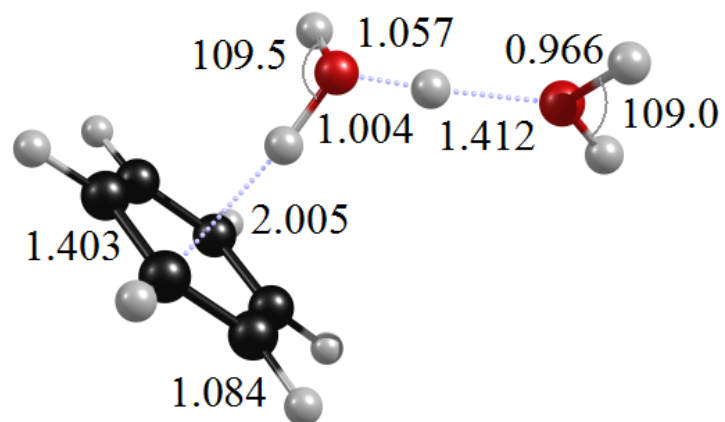
Unscaled Frequency (Intensity) Scaled Frequency /Symmetry of vibration

14 (0.7) 13/a, 29 (2.9) 27/a, 47 (3.1) 45/a, 58 (9.9) 55/a, 68 (4.5) 65/a, 108 (27.7) 103/a, 147 (70.1) 140/a, 226 (222.3) 215/a, 323 (41.2) 308/a, 350 (0.9) 333/a, 378 (28.0) 360/a, 583 (15.8) 555/a, 590 (3.3) 562/a, 605 (8.9) 576/a, 657 (55.1) 625/a, 762 (27.3) 726/a, 820 (30.0) 781/a, 912 (29.0) 869/a, 961 (17.3) 916/a, 1010 (0.6) 961/a, 1012 (4.6) 963/a, 1020 (2.5) 971/a, 1036 (2.0) 987/a, 1044 (0.1) 994/a, 1062 (0.0) 1012/a, 1182 (0.2) 1125/a, 1209 (10.0) 1152/a, 1213 (2.7) 1155/a, 1287 (94.5) 1225/a, 1377 (2.7) 1311/a, 1462 (0.0) 1393/a, 1490 (11.8) 1418/a, 1526 (103.7) 1453/a, 1615 (13.9) 1538/a, 1627 (43.5) 1549/a, 1650 (52.3) 1571/a, 2204 (1825.2) 2099/a, 3166 (10.4) 3015/a, 3216 (0.0) 3063/a, 3228 (2.1) 3074/a, 3229 (4.2) 3075/a, 3248 (4.8) 3093/a, 3250 (0.9) 3095/a, 3840 (58.5) 3657/a, 3952 (146.2) 3764/a.

BW-1, 2 isomer-a (bz-H₅O₂)⁺ DFT

State: ¹A(C₁) Total Energy = -385.5831972 ΔE = 0.0

B.E.^a = E (complex)-E (H₃O⁺+H₂O+bz) = 51.7 D.E.^b (H₂O, bz) = (26.7, 15.0)



Unscaled Frequency (Intensity) Scaled Frequency /Symmetry of vibration

10 (2.0) 9/a, 35 (4.7) 34/a, 47 (11.7) 45/a, 56 (4.9) 54/a, 92 (94.7) 88/a, 165 (139.8) 158/a, 189 (82.5) 181/a, 324 (132.6) 310/a, 390 (137.8) 373/a, 408 (0.5) 391/a, 412 (1.2) 395/a, 430 (26.4) 412/a, 489 (8.8) 469/a, 619 (0.3) 592/a, 619 (0.1) 593/a, 695 (24.9) 665/a, 710 (82.5) 680/a, 740 (65.0) 709/a, 889 (0.5) 852/a, 900 (4.2) 862/a, 1002 (4.5) 959/a, 1003 (0.8) 960/a, 1009 (0.1) 967/a, 1019 (0.1) 976/a, 1031 (0.1) 987/a, 1054 (5.0) 1009/a, 1056 (4.6) 1011/a, 1180 (0.1) 1130/a, 1200 (0.2) 1149/a, 1201 (0.1) 1150/a, 1242 (249.6) 1189/a, 1331 (0.8) 1275/a, 1383 (0.0) 1324/a, 1505 (13.0) 1441/a, 1506 (13.1) 1442/a, 1594 (5.4) 1526/a, 1619 (0.3) 1550/a, 1623 (3.8) 1554/a, 1649(36.3)1579/a, 1660(47.1)1590/a, 2294 (3235.4) 2197/a, 3106 (1391.1) 2974/a, 3169 (0.2) 3034/a, 3178 (0.0) 3043/a, 3179 (0.2) 3044/a, 3190 (4.9) 3054/a, 3193 (2.7) 3057/a, 3200 (2.1) 3064/a, 3774 (156.5) 3614/a, 3794 (80.4) 3633/a, 3887 (205.4) 3722/a.

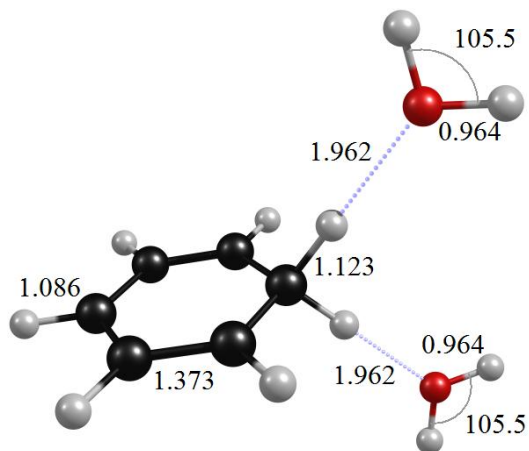
BW-1, 2 isomer-b (bzH-H₂O)⁺ DFT

State: ¹A(C₁) Total Energy = -385.5612877

$\Delta E = +13.7$

B.E.^a = E (complex)-E (bzH⁺+2*H₂O) = 20.8

D.E^b (H₂O) = 9.4



Unscaled Frequency (Intensity) Scaled Frequency /Symmetry of vibration

33 (0.2) 32/a, 36 (2.1) 35/a, 37 (0.5) 35/a, 42 (2.9) 40/a, 71 (0.2) 68/a, 78 (0.3) 75/a, 141 (14.7) 135/a, 161 (5.1) 154/a, 228 (28.7) 218/a, 242 (389.4) 232/a, 255 (141.0) 244/a, 313 (68.5) 300/a, 343 (0.9) 328/a, 372 (43.1) 357/a, 506 (32.4) 485/a, 598 (3.8) 573/a, 602 (7.8) 576/a, 675 (76.8) 646/a, 827 (0.0) 792/a, 844 (12.4) 808/a, 926 (13.4) 887/a, 1004 (0.6) 962/a, 1011 (0.0) 968/a, 1013 (18.8) 970/a, 1022 (0.5) 978/a, 1038 (0.3) 994/a, 1060 (2.3) 1015/a, 1154 (1.8) 1105/a, 1172 (0.8) 1122/a, 1204 (13.8) 1153/a, 1207 (49.7) 1155/a, 1267 (221.4) 1213/a, 1371 (17.5) 1312/a, 1431 (21.6) 1370/a, 1474 (132.0) 1412/a, 1484 (27.8) 1421/a, 1578 (0.2) 1511/a, 1635 (65.6) 1566/a, 1636 (8.8) 1567/a, 1640 (97.8) 1570/a, 2720 (555.8) 2605/a, 2768 (899.4) 2650/a, 3180 (0.1) 3045/a, 3189 (0.4) 3054/a, 3191 (1.5) 3055/a, 3207 (0.8) 3070/a, 3209 (0.1) 3073/a, 3805 (45.0) 3643/a, 3805 (40.0) 3643/a, 3900 (104.5) 3734/a, 3900 (108.1) 3734/a.

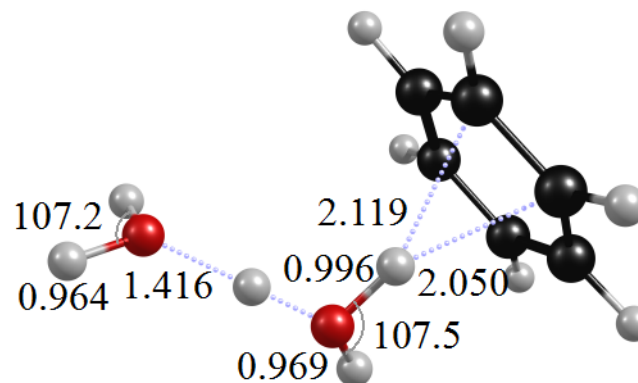
BW-1, 2 isomer-a (bz-H₅O₂)⁺ MP2

State: ¹A(C₁) Total MP2 Energy = -384.4948164

ΔE = 0.0

B.E.^a = E (complex)-E (H₃O⁺+H₂O+bz) = 56.5

D.E.^b (bz) = 18.7



Unscaled Frequency (Intensity) Scaled Frequency /Symmetry of vibration

8 (1.9) 7/a, 37 (4.0) 35/a, 78 (13.9) 74/a, 89 (1.0) 85/a, 130 (24.0) 123/a, 194 (32.8) 185/a, 253 (204.7) 241/a, 299 (145.3) 285/a, 380 (0.6) 362/a, 390 (0.5) 372/a, 393 (115.7) 374/a, 439 (40.1) 418/a, 483 (3.3) 460/a, 505 (3.7) 480/a, 606 (0.0) 577/a, 607 (0.1) 578/a, 708 (120.4) 674/a, 773 (43.3) 736/a, 873 (0.7) 831/a, 883 (2.4) 841/a, 947 (0.0) 901/a, 958 (0.1) 912/a, 965 (0.4) 919/a, 1000 (2.2) 952/a, 1008 (0.0) 960/a, 1055 (3.4) 1005/a, 1057 (3.8) 1006/a, 1181 (0.0) 1124/a, 1202 (0.1) 1145/a, 1203 (0.0) 1145/a, 1333 (276.4) 1270/a, 1370 (0.0) 1305/a, 1441 (0.8) 1372/a, 1500 (13.4) 1428/a, 1501 (12.8) 1429/a, 1613 (27.5) 1536/a, 1622 (2.0) 1544/a, 1624 (1.3) 1547/a, 1657 (26.2) 1578/a, 1724 (40.1) 1641/a, 2408 (2803.9) 2293/a, 3207 (0.0) 3054/a, 3215 (0.1) 3062/a, 3216 (0.3) 3062/a, 3228 (1.4) 3074/a, 3229 (0.7) 3075/a, 3235 (7.0) 3081/a, 3269 (1069.2) 3113/a, 3816 (146.6) 3634/a, 3837 (88.2) 3654/a, 3944 (196.7) 3756/a.

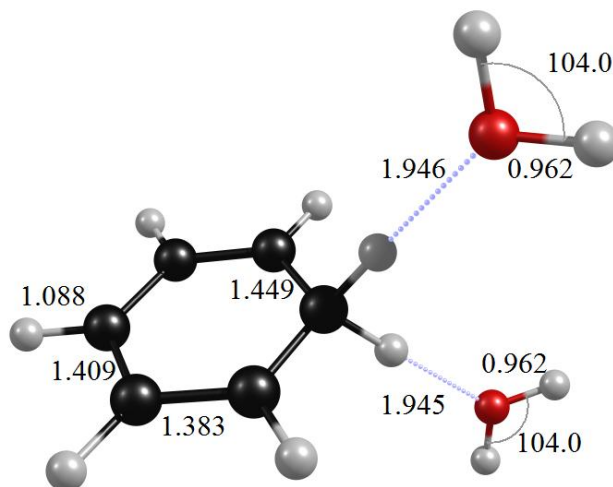
BW-1, 2 isomer-b (bzH-H₂O)⁺ MP2

State: ¹A(C₁) Total MP2 Energy = -384.4560766

ΔE = +24.3

B.E.^a = E (complex)-E (bzH⁺+2*H₂O) = 23.2

D.E.^b (Ar) = 9.6



Unscaled Frequency (Intensity) Scaled Frequency /Symmetry of vibration

-32 (3.4) -30/a, 25 (4.2) 24/a, 27 (0.0) 26/a, 36 (0.9) 34/a, 61 (0.8) 58/a, 82 (0.0) 78/a, 138 (16.7) 131/a, 159 (2.6) 151/a, 210 (40.2) 200/a, 215 (466.4) 205/a, 238 (46.5) 226/a, 307 (57.9) 292/a, 323 (4.9) 308/a, 344 (14.1) 328/a, 418 (66.4) 398/a, 589 (4.5) 561/a, 594 (5.6) 66/a, 647 (70.3) 616/a, 804 (21.8) 766/a, 817 (0.0) 778/a, 936 (43.3) 892/a, 977 (2.0) 930/a, 978 (0.0) 931/a, 985 (1.1) 938/a, 1018 (23.2) 969/a, 1023 (1.7) 974/a, 1033 (2.6) 983/a, 1134 (1.5) 1080/a, 1148 (6.7) 1094/a, 1193 (222.8) 1136/a, 1212 (5.4) 1154/a, 1221 (89.1) 1163/a, 1363 (11.6) 1298/a, 1463 (11.3) 1393/a, 1490 (19.7) 1419/a, 1530 (140.8) 1457/a, 1610 (17.6) 1533/a, 1648 (13.6) 1570/a, 1651 (65.2) 1572/a, 1654 (74.0) 1575/a, 2772 (530.1) 2640/a, 2803 (977.0) 2670/a, 3213 (0.0) 3060/a, 3225 (0.8) 3071/a, 3225 (3.1) 3072/a, 3250 (2.4) 3095/a, 3251 (0.6) 3096/a, 3855 (42.9) 3671/a, 3855 (39.8) 3671/a, 3966 (116.7) 3777/a, 3966 (103.2) 3777/a.

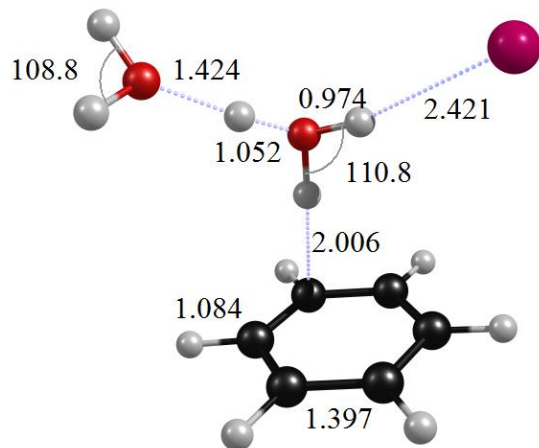
BW-1, 2-Ar isomer-a (bz-H₅O₂-Ar)⁺ DFT (Argon is “cis” to benzene)

State: ¹A(C₁) Total Energy = -913.1387812

ΔE = 0.0

B.E.^a = E (complex)-E (H₃O⁺+H₂O+bz+Ar) = 52.8

D.E.^b (Ar) = 1.1



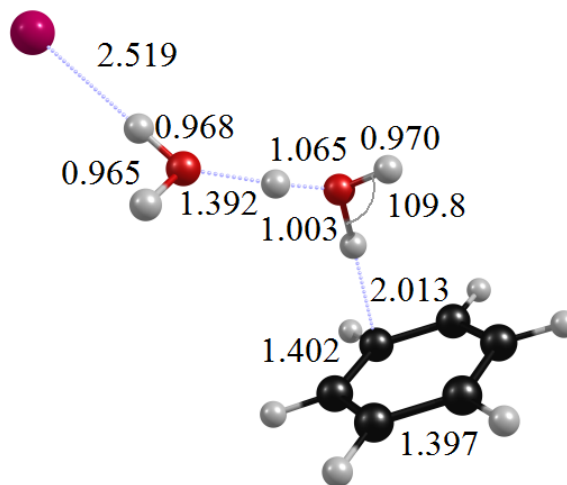
Unscaled Frequency (Intensity) Scaled Frequency /Symmetry of vibration

20 (2.2) 19/a, 24 (1.3) 23/a, 32 (1.7) 30/a, 36 (5.1) 34/a, 57 (1.9) 55/a, 63 (5.5) 60/a, 86 (3.4) 82/a, 118 (80.4) 113/a, 166 (149.3) 159/a, 189 (107.9) 181/a, 375 (138.6) 359/a, 388 (110.9) 371/a, 411 (3.0) 393/a, 412 (0.1) 395/a, 429 (24.6) 411/a, 515 (7.2) 493/a, 619 (0.2) 593/a, 620 (0.1) 593/a, 698 (17.2) 668/a, 710 (110.3) 680/a, 747 (46.1) 715/a, 888 (0.4) 850/a, 900 (4.3) 862/a, 1000 (1.8) 958/a, 1003 (3.1) 960/a, 1009(0.2) 967/a, 1019 (0.1) 976/a, 1031 (0.0) 987/a, 1055 (4.9) 1010/a, 1057 (4.6) 1012/a, 1180 (0.1) 1130/a, 1200 (2.6) 1149/a, 1201 (0.1) 1150/a, 1219 (211.6) 1168/a, 1333 (0.5) 1276/a, 1384 (0.0) 1325/a, 1506 (12.8) 1442/a, 1507 (11.9) 1443/a, 1588 (9.0) 1521/a, 1621 (0.6) 1552/a, 1624 (3.1) 1555/a, 1650 (28.9) 1580/a, 1659 (54.8) 1589/a, 2361 (3011.7) 2261/a, 3112 (1523.4) 2979/a, 3168 (0.4) 3033/a, 3178 (0.2) 3043/a, 3179 (0.1) 3044/a, 3190 (7.2) 3054/a, 3193 (3.5) 3057/a, 3201 (2.7) 3065/a, 3695 (439.9) 3538/a, 3796 (85.1) 3635/a, 3889 (198.5) 3724/a.

BW-1, 2-Ar isomer-b (bz-H₅O₂-Ar)⁺ DFT (Argon is “trans” to benzene)

State: ¹A(C₁) Total Energy = -913.1383365 ΔE = +0.3

B.E.^a = E (complex)-E (H₃O⁺+H₂O+bz+Ar) = 52.5 D.E.^b (Ar) = 0.8



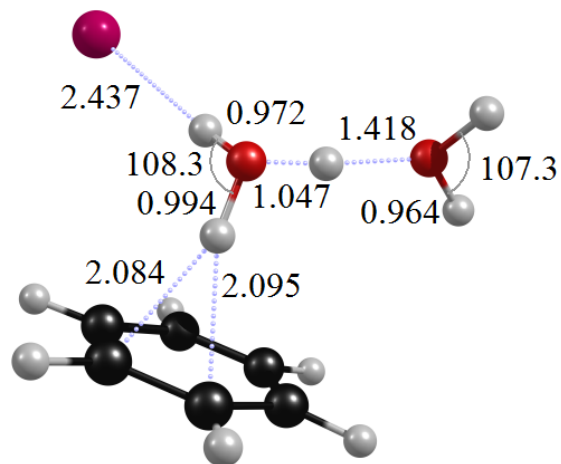
Unscaled Frequency (Intensity) Scaled Frequency /Symmetry of vibration

11 (3.0) 11/a, 14 (3.2) 14/a, 25 (1.8) 24/a, 29 (2.9) 28/a, 53 (1.4) 51/a, 58 (4.4) 55/a, 79 (15.2) 75/a, 124 (136.3) 118/a, 184 (53.1) 176/a, 261 (76.6) 250/a, 333 (165.3) 319/a, 403 (147.0) 386/a, 408 (0.2) 391/a, 412 (6.9) 395/a, 457 (27.7) 437/a, 495 (9.9) 474/a, 619 (0.2) 592/a, 619 (0.0) 593/a, 697 (15.6) 667/a, 710 (100.9) 680/a, 747 (60.3) 715/a, 888 (0.4) 850/a, 900 (5.7) 862/a, 1000 (2.6) 958/a, 1002 (2.9) 960/a, 1008 (0.3) 966/a, 1019 (0.1) 976/a, 1030 (0.1) 986/a, 1054 (5.3) 1009/a, 1056 (4.6) 1012/a, 1180 (0.1) 1130/a, 1200 (0.1) 1149/a, 1201 (0.1) 1150/a, 1265 (233.6) 1211/a, 1332 (0.5) 1275/a, 1383 (0.0) 1324/a, 1505 (13.4) 1441/a, 1507 (11.3) 1442/a, 1574 (54.8) 1507/a, 1619 (0.8) 1551/a, 1623 (3.0) 1554/a, 1650 (44.5) 1579/a, 1655 (33.0) 1585/a, 2194 (3332.0) 2101/a, 3121 (1451.4) 2988/a, 3168 (0.3) 3033/a, 3178 (0.1) 3043/a, 3179 (0.1) 3044/a, 3190 (7.7) 3054/a, 3192 (3.2) 3057/a, 3200 (2.8) 3064/a, 3764 (266.2) 3604/a, 3781 (132.2) 3620/a, 3871 (262.7) 3706/a.

BW-1, 2-Ar isomer-a (bz-H₅O₂-Ar)⁺ MP2 (Argon is “cis” to benzene)

State: ¹A(C₁) Total MP2 Energy = -911.45386 ΔE = 0.0

B.E.^a = E (complex)-E (H₃O⁺+H₂O+bz+Ar) = 59.2 D.E.^b (Ar) = 2.7



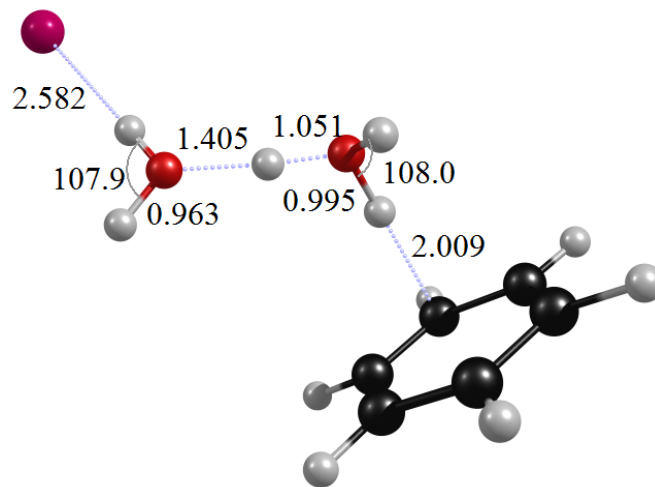
Unscaled Frequency (Intensity) Scaled Frequency /Symmetry of vibration

10(0.9)10/a, 22(5.1) 21/a, 30(4.2)28/a, 35(4.9)33/a, 70 (5.6) 66/a, 87 (4.7) 83/a, 98 (14.5) 93/a, 111 (12.9) 106/a, 186 (27.2) 177/a, 217 (205.2) 207/a, 342 (108.9) 326/a, 380 (1.7) 362/a, 389 (8.8) 371/a, 396 (122.6) 377/a, 427 (30.5) 407/a, 502 (2.7) 478/a, 535 (31.9) 509/a, 606 (0.0) 577/a, 607 (0.1) 578/a, 706 (116.4) 673/a, 790 (51.4) 752/a, 872 (0.6) 831/a, 883 (4.1) 841/a, 948 (0.1) 902/a, 959 (0.1) 913/a, 964 (0.3) 918/a, 1000 (2.1) 953/a, 1009 (0.0) 961/a, 1056 (3.8) 1006/a, 1057 (3.2) 1006/a, 1181 (0.1) 1124/a, 1202 (0.1) 1144/a, 1203 (0.0) 1146/a, 1302 (243.2) 1240/a, 1371 (0.0) 1305/a, 1442 (0.3) 1373/a, 1500 (13.8) 1429/a, 1501 (12.0) 1429/a, 1612 (8.3) 1535/a, 1622 (0.3) 1545/a, 1626 (2.9) 1549/a, 1667 (51.0) 1587/a, 1734 (38.8) 1651/a, 2426 (2544.5) 2310/a, 3205 (0.1) 3052/a, 3214 (0.1) 3060/a, 3215 (0.3) 3062/a, 3226 (1.2) 3072/a, 3228 (0.7) 3074/a, 3235 (1.5) 3080/a, 3302 (1069.7) 3145/a, 3767 (383.3) 3587/a, 3844 (79.5) 3661/a, 3952 (194.8) 3763/a.

BW-1, 2-Ar isomer-b (bz-H₅O₂-Ar)⁺ MP2 (Argon is “trans” to benzene)

State: ¹A(C₁) Total Energy = -911.4514554 ΔE = +1.5

B.E.^a = E (complex)-E (H₃O⁺+H₂O+bz+Ar) = 57.7 D.E.^b (Ar) = 1.2



Unscaled Frequency (Intensity) Scaled Frequency /Symmetry of vibration

12 (4.1) 11/a, 17 (4.7) 16/a, 21 (1.5) 20/a, 31 (6.6) 30/a, 56 (115.1) 53/a, 69 (15.7) 66/a, 89 (46.0) 84/a, 92 (28.8) 87/a, 197 (43.4) 188/a, 262 (21.8) 249/a, 331 (154.3) 315/a, 383 (0.4) 364/a, 390 (3.5) 372/a, 401 (128.9) 382/a, 456 (36.3) 434/a, 482 (0.5) 459/a, 496 (9.4) 472/a, 606 (0.0) 577/a, 607 (0.2) 578/a, 710 (118.7) 676/a, 754 (50.7) 718/a, 873 (0.6) 832/a, 887 (1.9) 845/a, 949 (0.1) 904/a, 958 (0.1) 913/a, 966 (0.2) 920/a, 997 (2.4) 949/a, 1007 (0.0) 959/a, 1053 (3.7) 1003/a, 1056 (3.5) 1006/a, 1181 (0.0) 1125/a, 1201 (0.1) 1143/a, 1204 (0.0) 1146/a, 1326 (264.5) 1263/a, 1371 (0.0) 1306/a, 1435 (0.3) 1367/a, 1499 (12.5) 1428/a, 1500 (13.1) 1428/a, 1605 (10.2) 1528/a, 1619 (0.5) 1542/a, 1621 (0.2) 1544/a, 1671 (45.9) 1592/a, 1698 (41.5) 1617/a, 2369 (3085.0) 2256/a, 3195 (0.1) 3043/a, 3200 (0.1) 3048/a, 3211 (0.2) 3058/a, 3216 (0.4) 3063/a, 3225 (1.2) 3071/a, 3229 (1.7) 3075/a, 3290 (1124.8) 3133/a, 3802 (166.9) 3621/a, 3821 (157.3) 3639/a, 3934 (261.5) 3746/a.

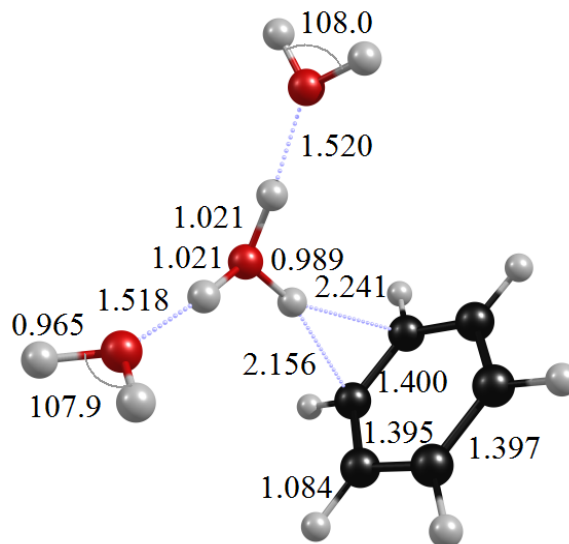
BW-1, 3 isomer-a (bz-H₇O₃)⁺ DFT

State: ¹A(C₁) Total Energy = -462.0750758

ΔE = 0.0

B.E.^a = E (complex) - E (H₃O⁺ + 2*H₂O + bz) = 72.7

D.E.^b(H₂O, bz) = (21, 11.4)



Unscaled Frequency (Intensity) Scaled Frequency /Symmetry of vibration

19 (0.2) 18/a, 21 (0.1) 21/a, 37 (5.0) 35/a, 54 (2.2) 51/a, 64 (0.4) 62/a, 83 (5.8) 80/a, 88 (14.0) 84/a, 131 (19.0) 126/a, 158 (11.6) 151/a, 161 (79.5) 154/a, 207 (464.1) 198/a, 317 (91.1) 304/a, 337 (96.9) 323/a, 368 (2.6) 352/a, 400 (60.5) 383/a, 411 (0.3) 393/a, 413 (0.1) 396/a, 596 (2.6) 571/a, 620 (0.1) 594/a, 621 (0.0) 595/a, 659 (89.5) 631/a, 704 (0.1) 674/a, 724 (81.5) 693/a, 884 (0.1) 847/a, 893 (1.5) 855/a, 987 (41.8) 945/a, 1004 (2.8) 962/a, 1005 (8.5) 962/a, 1007 (6.7) 964/a, 1017 (0.0) 974/a, 1030 (0.2) 986/a, 1056 (4.2) 1011/a, 1057 (5.5) 1012/a, 1167 (265.6) 1117/a, 1179 (0.2) 1129/a, 1200 (0.5) 1149/a, 1200 (0.3) 1149/a, 1333 (0.3) 1276/a, 1383 (0.0) 1324/a, 1507 (11.4) 1443/a, 1508 (11.2) 1444/a, 1611 (8.5) 1542/a, 1623 (1.0) 1554/a, 1627 (9.4) 1558/a, 1639 (24.6) 1569/a, 1661 (71.5) 1590/a, 1685 (37.6) 1613/a, 2768 (2718.1) 2650/a, 2864 (1441.5) 2743/a, 3167 (0.0) 3032/a, 3176 (0.0) 3041/a, 3176 (0.1) 3041/a, 3188 (4.8) 3052/a, 3190 (7.7) 3055/a, 3198 (1.6) 3062/a, 3365 (1168.3) 3222/a, 3805 (98.8) 3643/a, 3806 (33.2) 3645/a, 3899 (57.2) 3733/a, 3900 (277.1) 3734/a.

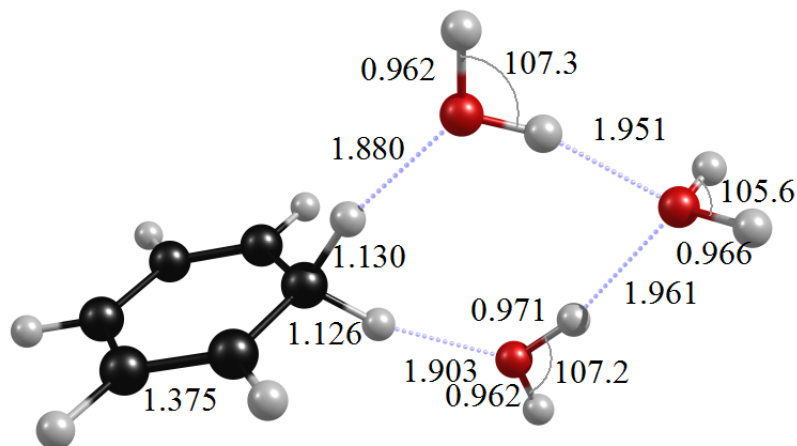
BW-1, 3 isomer-b (bzH-H₆O₃)⁺ DFT

State: ¹A(C₁) Total Energy = -462.0417494

ΔE = +21.0

B.E.^a = E (complex)-E (bzH⁺+3*H₂O) = 34.6

D.E.^b = -



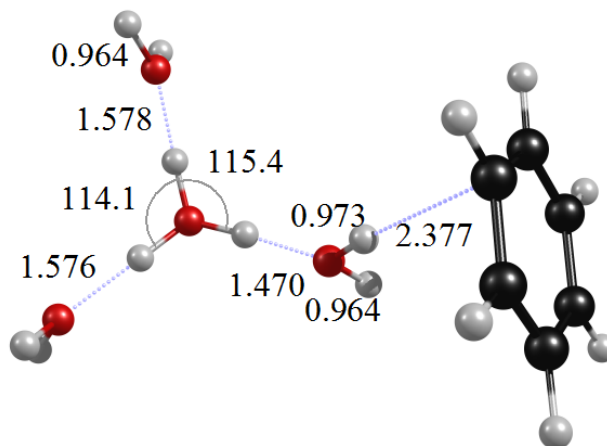
Unscaled Frequency (Intensity) Scaled Frequency /Symmetry of vibration

28 (0.4) 26/a, 30 (2.1) 28/a, 31 (3.7) 30/a, 44 (17.3) 42/a, 75 (1.3) 72/a, 142 (48.0) 136/a, 146 (0.3) 140/a, 155 (43.7) 148/a, 161 (135.0) 154/a, 180 (11.8) 172/a, 203 (1.0) 194/a, 227 (95.5) 218/a, 261 (0.3) 250/a, 340 (1.5) 326/a, 348 (0.0) 333/a, 401 (0.1) 384/a, 476 (13.0) 456/a, 480 (311.1) 459/a, 580 (53.8) 555/a, 601 (4.2) 575/a, 605 (26.1) 579/a, 608 (0.2) 582/a, 672 (241.3) 643/a, 680 (89.2) 651/a, 834 (0.1) 798/a, 843 (13.8) 807/a, 938 (17.3) 898/a, 1005 (3.3) 962/a, 1011 (0.8) 968/a, 1017 (18.0) 974/a, 1024 (1.7) 981/a, 1035 (0.1) 991/a, 1059 (2.1) 1014/a, 1152 (2.5) 1103/a, 1165 (0.7) 1115/a, 1187 (484.0) 1137/a, 1203 (11.9) 1152/a, 1219 (137.7) 1167/a, 1370 (17.7) 1311/a, 1431 (37.4) 1370/a, 1476 (99.1) 1413/a, 1487 (34.2) 1424/a, 1581 (0.5) 1513/a, 1621 (19.3) 1552/a, 1627 (124.0) 1558/a, 1638 (51.3) 1568/a, 1659 (0.0) 1589/a, 2613 (531.3) 2502/a, 2728 (1345.0) 2612/a, 3180 (0.2) 3045/a, 3190 (0.2) 3054/a, 3191 (1.0) 3056/a, 3206 (0.2) 3070/a, 3209 (0.0) 3073/a, 3670 (188.6) 3514/a, 3694 (618.7) 3537/a, 3788 (18.3) 3627/a, 3877 (126.1) 3712/a, 3880 (237.1) 3715/a, 3883 (27.2) 3718/a.

BW-1, 4 isomer-a (bz-H₉O₄)⁺ DFT

State: ¹A(C₁) Total Energy = -538.5595123 ΔE = 0.0

B.E.^a = E (complex) - E (H₃O⁺ + 3*H₂O + bz) = 89.0 D.E.^b(H₂O, bz) = (16.3, 7.0)



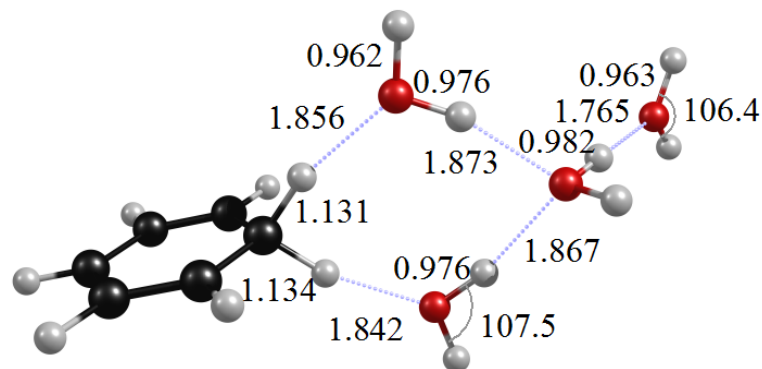
Unscaled Frequency (Intensity) Scaled Frequency /Symmetry of vibration

8 (0.1) 7/a, 11 (0.2) 11/a, 24 (0.8) 23/a, 33 (0.2) 32/a, 41 (5.0) 40/a, 64 (0.9) 61/a, 69 (2.4) 66/a, 84 (4.0) 80/a, 102 (8.9) 98/a, 110 (17.7) 105/a, 122 (5.5) 116/a, 158 (5.6) 151/a, 197 (152.1) 189/a, 232 (354.1) 223/a, 268 (63.1) 256/a, 319 (76.4) 305/a, 351 (52.4) 337/a, 359 (74.4) 343/a, 377 (68.4) 361/a, 390 (192.8) 373/a, 411 (0.7) 394/a, 412 (1.2) 395/a, 457 (60.9) 438/a, 621 (0.0) 594/a, 621 (0.0) 595/a, 706 (37.2) 676/a, 710 (86.0) 680/a, 720 (0.8) 689/a, 879 (0.3) 842/a, 882 (0.6) 845/a, 953 (60.0) 912/a, 998 (0.2) 956/a, 1001 (0.1) 958/a, 1006 (4.0) 963/a, 1014 (130.1) 970/a, 1016 (0.2) 973/a, 1027 (0.0) 984/a, 1056 (5.5) 1011/a, 1058 (5.5) 1013/a, 1177 (1.6) 1127/a, 1179 (261.3) 1129/a, 1199 (0.0) 1148/a, 1200 (0.3) 1149/a, 1332 (0.2) 1275/a, 1382 (0.0) 1324/a, 1507 (10.0) 1443/a, 1508 (11.0) 1444/a, 1625 (0.2) 1556/a, 1627 (1.4) 1558/a, 1633 (81.0) 1564/a, 1634 (63.8) 1565/a, 1645 (10.1) 1575/a, 1687 (13.6) 1616/a, 1701 (15.9) 1629/a, 2600 (3708.7) 2490/a, 3029 (2555.3) 2900/a, 3090 (703.5) 2958/a, 3164 (0.5) 3030/a, 3173 (0.3) 3038/a, 3176 (0.3) 3041/a, 3187 (11.6) 3051/a, 3190 (12.0) 3055/a, 3198 (0.3) 3062/a, 3669 (412.3) 3513/a, 3808 (77.4) 3646/a, 3809 (28.2) 3647/a, 3856 (79.2) 3692/a, 3902 (61.1) 3736/a, 3902 (257.9) 3736/a.

BW-1, 4 isomer-b (bzH-H₈O₄)⁺ DFT

State: ¹A(C₁) Total Energy = -538.5197066 ΔE = +25.0

B.E.^a = E (complex)-E (bzH⁺+4*H₂O) =46.9 D.E^b (H₂O) = 12.2



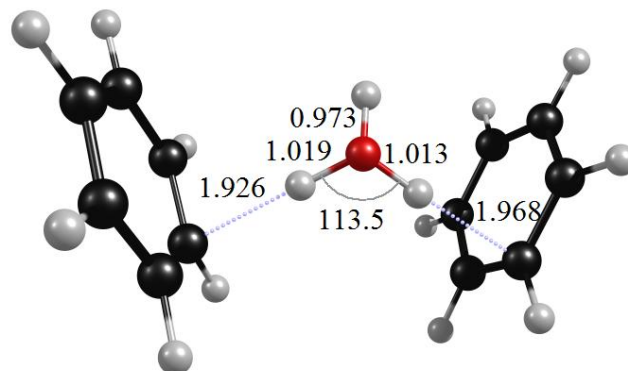
Unscaled Frequency (Intensity) Scaled Frequency /Symmetry of vibration

17 (0.8) 16/a, 20 (5.7) 19/a, 29 (1.1) 28/a, 42 (2.8) 40/a, 44 (0.1) 43/a, 52 (11.1) 50/a, 79 (3.4) 76/a, 91 (0.4) 87/a, 156 (83.2) 149/a, 159 (17.1) 152/a, 160 (45.7) 153/a, 174 (17.5) 166/a, 194 (72.8) 186/a, 200 (102.4) 192/a, 204 (304.5) 196/a, 280 (12.5) 268/a, 296 (45.9) 284/a, 351 (0.0) 336/a, 356 (2.9) 341/a, 384 (17.0) 367/a, 400 (7.6) 383/a, 459 (93.2) 439/a, 513 (11.6) 491/a, 602 (3.6) 577/a, 604 (20.5) 578/a, 607 (34.7) 582/a, 662 (64.5) 634/a, 689 (107.7) 660/a, 757 (204.7) 725/a, 836 (0.1) 801/a, 844 (13.2) 808/a, 882 (127.2) 845/a, 943 (18.0) 903/a, 1005 (4.8) 963/a, 1010 (0.3) 967/a, 1020 (19.9) 976/a, 1025 (2.3) 982/a, 1033 (0.3) 989/a, 1056 (2.0) 1011/a, 1152 (4.0) 1103/a, 1163 (44.1) 1113/a, 1179 (587.1) 1129/a, 1203 (11.0) 1152/a, 1215 (84.8) 1163/a, 1370 (18.6) 1311/a, 1429 (42.1) 1368/a, 1477 (85.4) 1414/a, 1488 (35.9) 1425/a, 1582 (0.7) 1515/a, 1622 (14.8) 1553/a, 1637 (77.7) 1567/a, 1638 (75.4) 1568/a, 1642 (53.2) 1572/a, 1675 (14.5) 1604/a, 2543 (582.5) 2435/a, 2676 (1705.4) 2562/a, 3179 (0.2) 3044/a, 3190 (0.1) 3054/a, 3191 (0.6) 3056/a, 3206 (0.0) 3070/a, 3209 (0.0) 3072/a, 3491 (1277.0) 3342/a, 3573 (318.9) 3421/a, 3622 (546.5) 3468/a, 3816 (34.4) 3653/a, 3853 (93.0) 3689/a, 3881 (180.8) 3716/a, 3884 (37.6) 3719/a, 3912 (124.5) 3746/a.

BW-2, 1 isomer-a (bz₂-H₃O)⁺ DFT

State: ¹A(C₁) Total Energy = -541.4190482 ΔE = 0.0

B.E.^a = E (complex)-E (H₃O⁺+2*bz) = 41.1 D.E.^b (bz) = 16.0



Unscaled Frequency (Intensity) Scaled Frequency /Symmetry of vibration

13 (1.7) 12/a, 16 (1.0) 15/a, 30 (2.6) 29/a, 39 (2.4) 38/a, 49 (1.0) 47/a, 51 (0.5) 49/a, 64 (1.1) 61/a, 178 (4.9) 170/a, 233 (126.0) 223/a, 265 (36.4) 254/a, 356 (24.4) 340/a, 408 (0.8) 391/a, 410 (0.1) 393/a, 412 (4.5) 394/a, 413 (2.0) 395/a, 571 (43.9) 547/a, 618 (0.3) 592/a, 619 (0.3) 593/a, 619 (0.3) 593/a, 620 (0.3) 593/a, 696 (10.2) 666/a, 700 (20.0) 671/a, 723 (213.8) 693/a, 730 (44.8) 699/a, 884 (3.5) 847/a, 889 (2.5) 851/a, 892 (13.2) 854/a, 902 (1.4) 864/a, 977 (45.6) 936/a, 1000 (4.1) 957/a, 1001 (14.2) 959/a, 1003 (0.9) 960/a, 1006 (13.1) 963/a, 1011 (0.2) 968/a, 1018 (39.0) 974/a, 1020 (0.2) 977/a, 1024 (2.3) 980/a, 1031 (1.4) 987/a, 1033 (2.0) 989/a, 1053 (5.6) 1009/a, 1054 (9.1) 1009/a, 1057 (3.7) 1012/a, 1058 (14.7) 1013/a, 1180 (0.0) 1130/a, 1181 (0.1) 1131/a, 1200 (0.1) 1149/a, 1201 (0.2) 1150/a, 1201 (0.2) 1150/a, 1201 (0.9) 1150/a, 1332 (0.9) 1275/a, 1336 (1.5) 1279/a, 1383 (0.0) 1324/a, 1383 (0.0) 1324/a, 1504 (6.8) 1440/a, 1505(10.1) 1441/a, 1506 (18.4) 1442/a, 1507 (20.8) 1443/a, 1595 (8.4) 1527/a, 1616 (2.5) 1547/a, 1621 (1.0) 1552/a, 1621 (2.0) 1552/a, 1626 (5.2) 1557/a, 1640 (45.1) 1570/a, 2819 (4224.4) 2700/a, 2977 (725.9) 2851/a, 3164 (0.6) 3029/a, 3169 (0.1) 3034/a, 3178 (0.9) 3043/a, 3179 (0.0) 3044/a, 3181 (0.2) 3046/a, 3181 (0.1) 3046/a, 3189 (3.1) 3053/a, 3190 (2.0) 3055/a, 3194 (1.6) 3058/a, 3195 (1.8) 3059/a, 3201 (0.7) 3065/a, 3203 (0.3) 3067/a, 3744 (114.8) 3585/a.

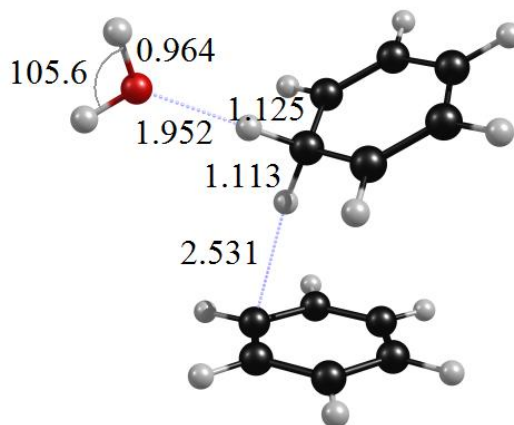
BW-2, 1 isomer-b ($\text{bz}_2\text{H-H}_2\text{O}^+$)⁺ DFT

State: $^1\text{A}(\text{C}_1)$ Total Energy = -541.4084667

$\Delta E = +6.6$

B.E.^a = E (complex) - E ($\text{bzH}^+ + \text{H}_2\text{O} + \text{bz}$) = 17.3

D.E.^b (bz) = 5.8



Unscaled Frequency (Intensity) Scaled Frequency /Symmetry of vibration

10 (0.0) 9/a, 23 (0.5) 22/a, 34 (4.0) 33/a, 37 (1.5) 36/a, 43 (3.5) 41/a, 58 (0.3) 56/a, 65(0.6) 62/a, 82 (0.4) 79/a, 90 (5.8) 86/a, 157 (19.5) 150/a, 234 (245.6) 224/a, 261 (24.6) 250/a, 344 (1.3) 329/a, 351 (47.5) 336/a, 409 (0.6) 392/a, 411 (0.0) 393/a, 476 (24.1) 456/a, 597 (4.0) 571/a, 599 (5.7) 574/a, 619 (0.0) 593/a, 620 (0.8) 593/a, 669 (60.6) 641/a, 707 (53.9) 677/a, 709 (83.6) 679/a, 818 (1.8) 783/a, 842 (10.6) 806/a, 878 (0.2) 840/a, 882 (0.6) 845/a, 920 (9.3) 881/a, 1000 (1.0) 958/a, 1002 (1.6) 960/a, 1004 (7.4) 962/a, 1005 (1.6) 962/a, 1006 (5.1) 963/a, 1008 (4.4) 966/a, 1016 (0.0) 972/a, 1021 (0.1) 977/a, 1029 (0.0) 986/a, 1035 (1.8) 991/a, 1055 (3.1) 1010/a, 1058 (1.7) 1013/a, 1059 (4.7) 1014/a, 1150 (1.5) 1101/a, 1163 (4.5) 1113/a, 1178 (0.0) 1128/a, 1198 (0.7) 1147/a, 1199 (4.2) 1148/a, 1203 (14.0) 1152/a, 1207 (30.6) 1156/a, 1270 (122.7) 1216/a, 1337 (0.3) 1280/a, 1369 (13.0) 1310/a, 1383 (0.0) 1324/a, 1425 (22.2) 1365/a, 1471 (130.7) 1409/a, 1482 (28.8) 1419/a, 1507 (11.6) 1443/a, 1510 (9.7) 1446/a, 1575 (0.5) 1508/a, 1622 (0.3) 1553/a, 1626 (11.3) 1557/a, 1634 (24.8) 1565/a, 1638 (101.1) 1568/a, 2712 (761.9) 2597/a, 2862 (471.0) 2741/a, 3164 (0.0) 3029/a, 3172 (0.1) 3037/a, 3173 (0.0) 3038/a, 3180 (0.2) 3045/a, 3186 (10.2) 3050/a, 3187 (10.7) 3052/a, 3190 (0.7) 3055/a, 3195 (0.8) 3059/a, 3200 (0.6) 3064/a, 3208 (0.8) 3072/a, 3212 (0.4) 3076/a, 3805 (44.3) 3643/a, 3900 (101.4) 3734/a.

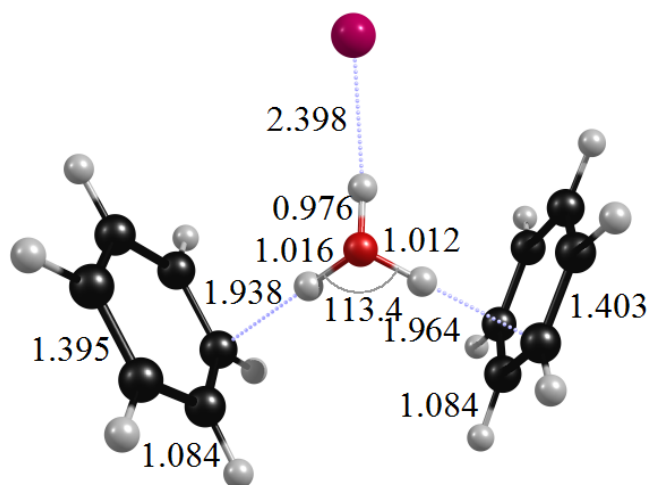
BW-2, 1-Ar isomer-a (bz₂-H₃O-Ar)⁺ DFT

State: ¹A(C₁) Total Energy = -1068.9744595

$\Delta E = 0.0$

B.E.^a = E (complex) - E (H₃O⁺ + 2*bz + Ar) = 42.0

D.E.^b (Ar) = 1.0



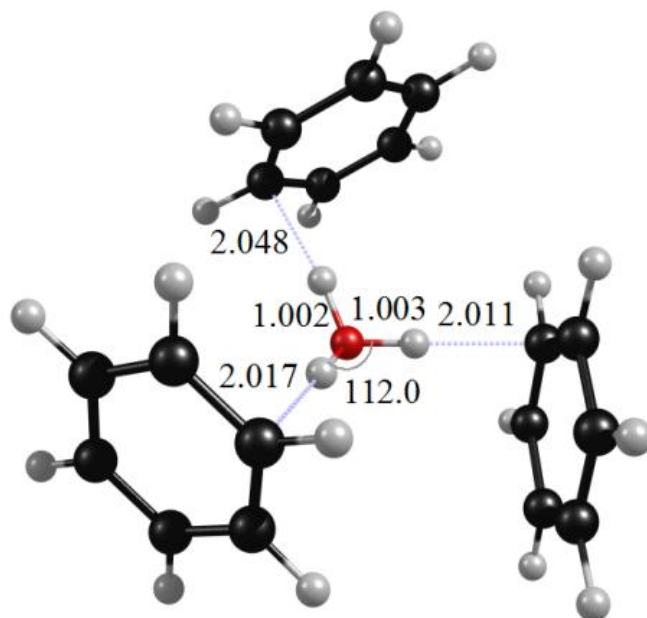
Unscaled Frequency (Intensity) Scaled Frequency /Symmetry of vibration

12 (0.0) 12/a, 16 (0.1) 15/a, 19 (0.5) 19/a, 22 (0.3) 21/a, 29 (1.9) 28/a, 40 (0.2) 38/a, 43 (1.0) 41/a, 49 (0.5) 47/a, 63 (6.0) 60/a, 93 (5.0) 89/a, 179 (13.7) 171/a, 224 (110.9) 215/a, 332 (15.5) 318/a, 380 (46.5) 364/a, 409 (2.4) 392/a, 410 (2.3) 393/a, 411 (0.1) 394/a, 412 (2.5) 395/a, 603 (43.2) 577/a, 618 (0.2) 592/a, 619 (0.1) 593/a, 620 (0.3) 593/a, 620 (3.8) 594/a, 697 (14.7) 667/a, 701 (15.7) 671/a, 721 (211.4) 690/a, 729 (48.4) 698/a, 883 (8.3) 845/a, 886 (2.9) 848/a, 888 (4.9) 850/a, 902 (2.7) 864/a, 966 (42.0) 925/a, 1000 (0.7) 957/a, 1002 (13.2) 959/a, 1003 (0.3) 961/a, 1008 (7.2) 965/a, 1010 (0.4) 967/a, 1017 (41.8) 974/a, 1021 (1.0) 977/a, 1023 (4.0) 980/a, 1031 (0.9) 987/a, 1033 (3.2) 989/a, 1054 (5.1) 1009/a, 1054 (12.8) 1010/a, 1057 (5.1) 1012/a, 1058 (7.9) 1013/a, 1180 (0.1) 1129/a, 1180 (0.2) 1130/a, 1200 (0.2) 1149/a, 1200 (0.4) 1149/a, 1201 (0.5) 1150/a, 1201 (0.3) 1150/a, 1332 (1.4) 1276/a, 1335 (1.3) 1279/a, 1383 (0.0) 1324/a, 1383 (0.0) 1324/a, 1504 (11.1) 1441/a, 1505 (3.3) 1441/a, 1506 (24.1) 1442/a, 1507 (14.7) 1443/a, 1583 (4.7) 1515/a, 1615 (1.7) 1546/a, 1621 (2.0) 1552/a, 1622 (2.1) 1553/a, 1624 (3.4) 1555/a, 1634 (13.4) 1565/a, 2862 (4105.0) 2740/a, 2994 (731.7) 2867/a, 3164 (0.4) 3030/a, 3167 (0.1) 3033/a, 3178 (0.6) 3043/a, 3179 (0.1) 3044/a, 3180 (0.6) 3045/a, 3180 (0.2) 3045/a, 3188 (4.4) 3053/a, 3190 (2.5) 3054/a, 3194 (2.4) 3058/a, 3195 (2.6) 3059/a, 3201 (0.8) 3065/a, 3202 (0.4) 3066/a, 3654 (409.4) 3499/a.

BW-3, 1 isomer-a (bz₃-H₃O)⁺ DFT

State: ¹A(C₁) Total Energy = -773.7472826 ΔE = 0.0

B.E.^a = E (complex) - E (H₃O⁺ + 3*bz) = 51.7 D.E.^b (bz) = 10.6



Unscaled Frequency (Intensity) Scaled Frequency /Symmetry of vibration

8 (0.1) 7/a, 11 (0.0) 11/a, 15 (0.1) 14/a, 22 (0.2) 21/a, 27 (0.1) 26/a, 31 (0.3) 30/a, 33 (0.7) 31/a, 41 (0.5) 39/a, 43 (0.3) 41/a, 46 (0.4) 44/a, 54 (0.6) 52/a, 64 (1.2) 62/a, 136 (1.1) 130/a, 198 (53.1) 189/a, 202 (60.8) 193/a, 400 (20.2) 383/a, 408 (0.5) 391/a, 410 (0.2) 392/a, 411 (1.0) 393/a, 412 (3.8) 394/a, 414 (2.4) 397/a, 425 (19.2) 407/a, 481(38.9) 460/a, 548 (15.4) 525/a, 619 (0.3) 593/a, 619 (0.0) 593/a, 620 (0.2) 593/a, 620 (0.1) 593/a, 620 (0.2) 594/a, 621 (0.1) 594/a, 701 (39.1) 671/a, 702 (29.9) 672/a, 703 (9.9) 673/a, 716 (187.8) 686/a, 718 (180.7) 687/a, 722 (19.5) 692/a, 865 (24.0) 828/a, 880 (1.0) 843/a, 881 (0.2) 844/a, 888 (7.5) 850/a, 893 (11.1) 855/a, 896 (0.9) 858/a, 917 (30.3) 878/a, 996 (9.4) 954/a, 997 (6.9) 955/a, 1003 (7.4) 961/a, 1004 (3.3) 961/a, 1004 (3.4) 961/a, 1005 (0.7) 963/a, 1007 (0.7) 964/a, 1007 (1.0) 965/a, 1009 (2.6) 966/a, 1020 (0.0) 976/a, 1021 (0.1) 978/a, 1022 (0.1) 978/a, 1030 (0.3) 986/a, 1031 (0.1) 987/a, 1032 (0.3) 988/a, 1054 (6.0) 1009/a,

1054 (7.1) 1010/a, 1055 (6.1) 1011/a, 1057 (3.6) 1012/a, 1058 (0.7) 1013/a, 1059 (10.1) 1014/a, 1178 (0.4) 1128/a, 1179 (0.1) 1129/a, 1180 (0.1) 1129/a, 1199 (0.4) 1148/a, 1200 (0.4) 1149/a, 1200 (0.4) 1149/a, 1201 (0.6) 1150/a, 1201 (0.1) 1150/a, 1201 (0.3) 1150/a, 1334 (1.6) 1277/a, 1335 (0.3) 1278/a, 1336 (1.1) 1279/a, 1382 (0.0) 1323/a, 1383 (0.0) 1324/a, 1383 (0.0) 1325/a, 1506 (10.7) 1442/a, 1506 (10.9) 1442/a, 1507 (3.8) 1443/a, 1508 (7.7) 1444/a, 1509 (2.7) 1445/a, 1509 (27.2) 1445/a, 1615 (6.7) 1547/a, 1622 (0.2) 1553/a, 1622 (0.8) 1553/a, 1624 (3.1) 1555/a, 1626 (4.3) 1557/a, 1627 (1.3) 1557/a, 1632 (4.1) 1562/a, 1659 (9.2) 1588/a, 3075 (2728.9) 2944/a, 3101 (2626.6) 2969/a, 3163 (5.5) 3029/a, 3164 (4.2) 3030/a, 3165 (2.9) 3031/a, 3172 (154.1) 3037/a, 3176 (0.3) 3041/a, 3176 (4.9) 3041/a, 3177 (1.3) 3042/a, 3179 (7.8) 3044/a, 3179 (1.1) 3044/a, 3180 (0.4) 3044/a, 3188 (12.8) 3053/a, 3188 (16.8) 3053/a, 3189 (10.6) 3054/a, 3193 (4.1) 3057/a, 3193 (6.1) 3057/a, 3193 (7.1) 3058/a, 3200 (8.3) 3064/a, 3200 (3.1) 3064/a, 3201 (1.6) 3065/a.

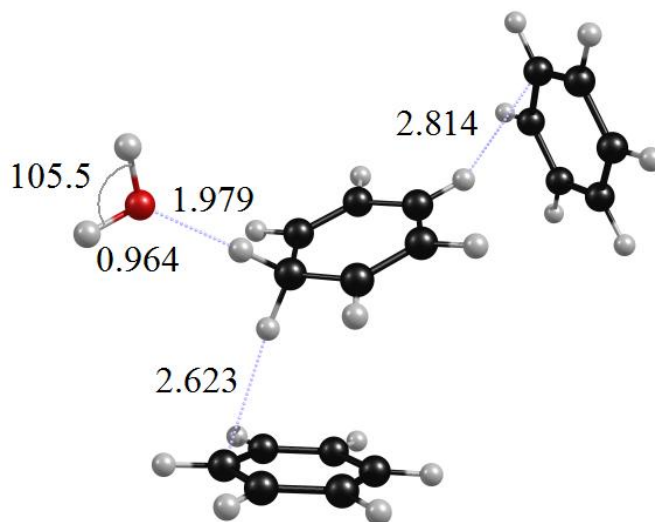
BW-3, 1 isomer-b ($\text{bz}_3\text{H-H}_2\text{O}^+$)⁺ DFT

State: $^1\text{A}(\text{C}_1)$ Total Energy = -773.7272378

$\Delta E = +12.6$

$\text{B.E.}^{\text{a}} = E(\text{complex}) - E(\text{bzH}^+ + \text{H}_2\text{O} + 2*\text{bz}) = 22.0$

$\text{D.E}^{\text{b}}(\text{bz}) = 4.7$



Unscaled Frequency (Intensity) Scaled Frequency /Symmetry of vibration

9 (0.6) 9/a, 12 (0.5) 12/a, 14 (0.8) 14/a, 20 (0.3) 19/a, 22 (0.2) 21/a, 34 (3.9) 32/a, 38 (0.9) 36/a, 43 (0.4) 41/a, 52 (5.0) 49/a, 58 (0.2) 56/a, 60 (1.2) 58/a, 64 (0.2) 61/a, 65 (2.5) 62/a, 81 (0.2) 78/a, 90 (9.6) 86/a, 153 (19.8) 147/a, 231 (243.3) 221/a, 256 (23.2) 246/a, 342 (44.7) 328/a, 344 (0.6) 330/a, 409 (0.2) 392/a, 411 (0.0) 393/a, 412 (0.1) 394/a, 413 (0.0) 395/a, 468 (21.1) 448/a, 597 (3.1) 571/a, 598 (0.9) 573/a, 620 (0.7) 594/a, 620 (0.0) 594/a, 620 (0.1) 594/a, 621 (0.3) 595/a, 665 (45.9) 637/a, 704 (198.5) 674/a, 706 (92.1) 676/a, 709 (3.1) 679/a, 712 (0.0) 682/a, 815 (1.3) 780/a, 846 (7.2) 810/a, 877 (0.2) 840/a, 877 (0.1) 840/a, 878 (0.1) 840/a, 880 (0.5) 843/a, 917 (17.1) 878/a, 999 (0.1) 957/a, 1000 (1.2) 957/a, 1001 (0.0) 958/a, 1001 (1.1) 958/a, 1004 (4.2) 961/a, 1005 (7.8) 962/a, 1007 (3.6) 964/a, 1007 (2.3) 964/a, 1010 (2.3) 967/a, 1016 (0.0) 973/a, 1017 (0.0) 974/a, 1019 (1.6) 976/a, 1028 (0.0) 984/a, 1029 (0.0) 985/a, 1035 (0.4) 991/a, 1055 (7.5) 1010/a, 1056 (3.6) 1011/a, 1057 (4.1) 1012/a, 1058 (0.9) 1013/a, 1059 (4.1) 1014/a, 1151 (1.5) 1102/a, 1167 (3.7) 1117/a, 1177 (0.0) 1127/a, 1178 (0.1) 1128/a, 1198 (1.3) 1147/a, 1198 (3.3) 1147/a, 1198 (1.2) 1147/a, 1198 (2.5) 1147/a, 1199 (0.2) 1148/a, 1205 (30.7) 1154/a, 1280 (160.1) 1225/a, 1334 (0.0) 1278/a, 1336 (0.2) 1279/a, 1368 (10.9) 1310/a, 1382 (0.0) 1323/a, 1383 (0.0) 1324/a,

1427 (8.6) 1366/a, 1477 (136.2) 1414/a, 1479 (42.9) 1416/a, 1508 (10.5) 1444/a, 1508 (10.0) 1444/a, 1509 (9.2) 1445/a,
1510 (9.2) 1446/a, 1572 (0.6) 1505/a, 1624 (6.3) 1555/a, 1626 (8.7) 1557/a, 1627 (1.4) 1558/a, 1627 (0.8) 1558/a, 1635 (43.8) 1565/a,
1638 (157.9) 1568/a, 2749 (692.2) 2632/a, 2887 (434.6) 2765/a, 3163 (0.1) 3028/a, 3163 (0.0) 3029/a, 3171 (0.0) 3036/a,
3171 (0.1) 3037/a, 3173 (0.0) 3038/a, 3173 (0.0) 3038/a, 3185 (12.0) 3050/a, 3185 (13.3) 3050/a, 3187 (13.5) 3051/a,
3187 (6.7) 3051/a, 3187 (8.4) 3052/a, 3192 (21.7) 3057/a, 3195 (0.5) 3059/a, 3195 (0.7) 3060/a, 3200 (9.6) 3064/a,
3208 (2.3) 3072/a, 3212 (3.2) 3076/a, 3806 (41.8) 3644/a, 3902 (97.1) 3736/a.

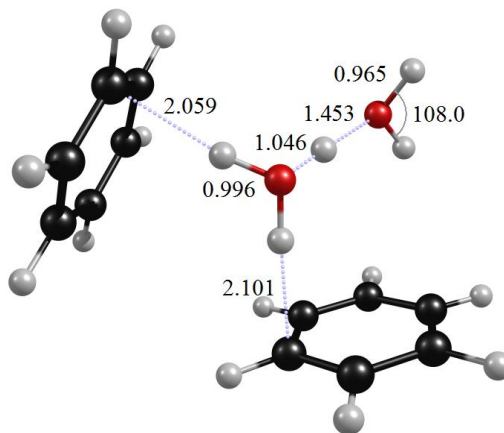
BW-2, 2 isomer-a (bz₂-H₅O₂)⁺ (benzenes are in “cis” position) DFT

State: ¹A(C₁) Total Energy = -617.9115719

ΔE = 0.0

B.E.^a = E (complex)-E (H₃O⁺+H₂O+2*bz) = 62.4

D.E.^b (bz) = 10.7



Unscaled Frequency (Intensity) Scaled Frequency /Symmetry of vibration

8 (0.8) 7/a, 21 (3.1) 20/a, 26 (5.6) 25/a, 27 (0.9) 26/a, 35 (1.8) 33/a, 45 (0.0) 43/a, 49 (0.7) 47/a, 58 (1.4) 56/a, 65 (0.0) 63/a, 141 (5.2) 135/a, 142 (29.2) 136/a, 184 (41.5) 176/a, 322 (145.1) 309/a, 380 (172.9) 364/a, 410 (0.4) 393/a, 411 (0.5) 393/a, 412 (0.5) 395/a, 415 (3.1) 397/a, 421 (16.5) 403/a, 477 (75.5) 456/a, 607 (55.4) 581/a, 619 (0.1) 593/a, 620 (0.3) 594/a, 620 (0.1) 594/a, 621 (8.3) 595/a, 700 (16.9) 670/a, 702 (11.3) 672/a, 715 (66.7) 684/a, 718 (183.2) 688/a, 748 (20.3) 716/a, 883 (0.4) 846/a, 884 (0.6) 847/a, 892 (6.2) 854/a, 895 (0.7) 857/a, 997 (3.4) 955/a, 999 (3.7) 957/a, 1004 (2.1) 961/a, 1004 (2.2) 962/a, 1007 (0.2) 964/a, 1007 (0.1) 965/a, 1017 (0.0) 974/a, 1019 (0.0) 976/a, 1030 (0.1) 986/a, 1031 (0.3) 987/a, 1054 (5.7) 1009/a, 1055 (4.3) 1010/a, 1057 (2.8) 1012/a, 1058 (3.8) 1013/a, 1154 (125.5) 1105/a, 1178 (0.6) 1128/a, 1179 (0.1) 1129/a, 1198 (0.0) 1147/a, 1200 (0.1) 1149/a, 1201 (0.9) 1150/a, 1201 (0.4) 1150/a, 1332 (0.6) 1276/a, 1334 (0.6) 1277/a, 1383 (0.0) 1324/a, 1383 (0.0) 1324/a, 1506 (7.1) 1442/a, 1507 (11.2) 1442/a, 1507 (8.9) 1443/a, 1508 (18.3) 1444/a, 1607 (10.0) 1539/a, 1620 (13.5) 1551/a, 1622 (14.0) 1553/a, 1624 (22.4) 1555/a, 1626 (0.6) 1557/a, 1630 (7.9) 1560/a, 1749 (69.7) 1675/a, 2432 (2004.3) 2329/a, 3164 (0.4) 3030/a, 3164 (0.5) 3030/a, 3170 (0.2) 3035/a, 3175 (0.1) 3040/a, 3178 (0.1) 3043/a, 3179 (0.6) 3044/a, 3186 (4.2) 3050/a, 3187 (9.7) 3052/a, 3192 (4.8) 3056/a, 3193 (2.4) 3057/a, 3199 (16.3) 3063/a, 3199 (1.1) 3063/a, 3245 (1893.2) 3107/a, 3326 (921.1) 3185/a, 3781 (47.8) 3620/a, 3873 (211.8) 3709/a.

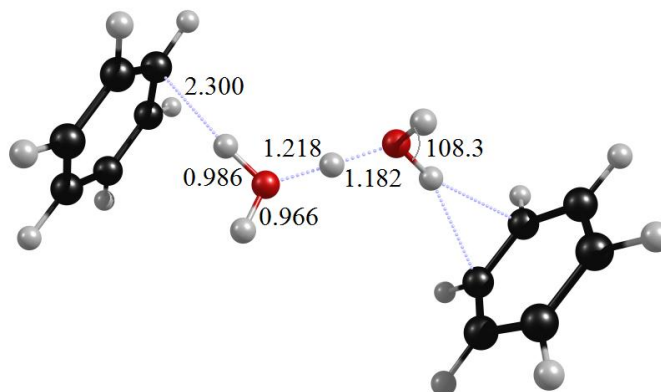
BW-2, 2 isomer-b ($\text{bz}_2\text{-H}_5\text{O}_2^+$)⁺ (benzenes are in “trans” position) DFT

State: $^1\text{A}(\text{C}_1)$ Total Energy = -617.9092657

$\Delta E = +1.4$

B.E.^a = E (complex) - E ($\text{H}_3\text{O}^+ + \text{H}_2\text{O} + 2*\text{bz}$) = 61.0

D.E.^b (bz) = 9.3



Unscaled Frequency (Intensity) Scaled Frequency /Symmetry of vibration

1 (2.8) 1/a, 9 (3.7) 9/a, 19 (0.8) 18/a, 22 (2.0) 21/a, 27 (0.6) 26/a, 40 (5.9) 38/a, 46 (4.3) 44/a, 57 (4.7) 55/a, 61 (12.8) 59/a, 121 (275.4) 116/a, 149 (2.3) 142/a, 197 (73.6) 188/a, 294 (42.7) 281/a, 401 (135.6) 384/a, 410 (0.6) 393/a, 411 (3.0) 394/a, 413 (0.4) 396/a, 420 (54.5) 402/a, 524 (87.8) 502/a, 565 (169.3) 541/a, 611 (52.7) 585/a, 619 (0.3) 593/a, 620 (0.1) 593/a, 620 (0.5) 593/a, 621 (0.0) 594/a, 657 (51.7) 629/a, 703 (4.4) 673/a, 705 (0.3) 675/a, 720 (368.3) 689/a, 721 (34.3) 690/a, 882 (400.8) 844/a, 885 (24.1) 847/a, 889 (142.9) 851/a, 892 (0.7) 854/a, 941 (2701.2) 901/a, 1000 (1.8) 958/a, 1003 (0.3) 960/a, 1003 (1.8) 961/a, 1005 (39.7) 962/a, 1006 (0.4) 964/a, 1008 (125.2) 965/a, 1017 (2.1) 974/a, 1020 (1.4) 976/a, 1029 (0.4) 986/a, 1030 (0.4) 986/a, 1054 (3.5) 1009/a, 1055 (12.7) 1010/a, 1056 (10.4) 1011/a, 1057 (4.3) 1012/a, 1179 (0.3) 1129/a, 1179 (0.2) 1129/a, 1199 (0.1) 1148/a, 1200 (0.2) 1149/a, 1200 (0.5) 1149/a, 1201 (0.2) 1150/a, 1329 (0.7) 1273/a, 1330 (2.6) 1273/a, 1383 (0.0) 1324/a, 1383 (0.0) 1324/a, 1429 (97.4) 1368/a, 1505 (12.9) 1441/a, 1506 (10.8) 1442/a, 1507 (16.5) 1443/a, 1507 (16.7) 1443/a, 1575 (570.2) 508/a, 1619 (0.2) 1551/a, 1620 (0.4) 1552/a, 1624 (3.7) 1555/a, 1624 (1.4) 1555/a, 1671 (17.9) 1600/a, 1729 (931.5) 1655/a, 3161 (0.0) 3026/a, 3165 (0.0) 3031/a, 3170 (0.6) 3035/a, 3174 (0.9) 3039/a, 3174 (0.1) 3040/a, 3175 (0.2) 3040/a, 3184 (4.7) 3049/a, 3185 (6.0) 3050/a, 3186 (4.8) 3051/a, 3189 (4.9) 3053/a, 3196 (1.9) 3061/a, 3196 (0.8) 3061/a, 3371 (1490.8) 3228/a, 3421 (757.8) 3276/a, 3804 (118.6) 3642/a, 3834 (122.7) 3671/a.

BW-2, 2-Ar isomer-a (bz₂-H₅O₂Ar)⁺ (benzenes are in “cis” position, Argon on the other OH) DFT

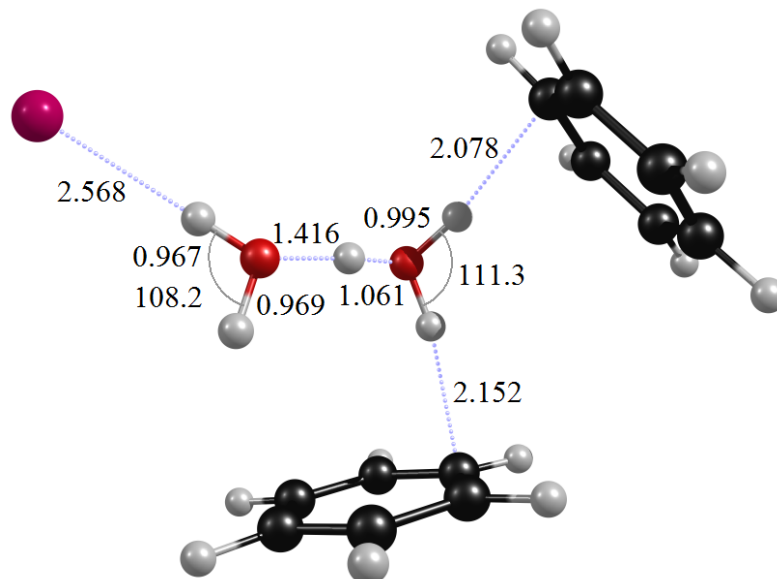
State: ¹A(C₁)

Total Energy = -1145.466415

ΔE = +0.0

B.E.^a = E (complex) - E (H₃O⁺ + H₂O + 2*bz + Ar) = 63.0

D.E.^b (Ar) = 0.6



Unscaled Frequency (Intensity) Scaled Frequency /Symmetry of vibration

-12 (0.1) -12/a, 13 (0.3) 12/a, 19 (0.3) 18/a, 24 (2.5) 23/a, 27 (0.4) 25/a, 29 (0.5) 28/a, 34 (0.8) 32/a, 48 (0.5) 46/a, 50 (0.4) 48/a, 58 (2.1) 56/a, 72 (0.6) 69/a, 84 (13.0) 80/a, 132 (8.8) 126/a, 175 (41.5) 167/a, 240 (32.7) 230/a, 366 (90.3) 351/a, 410 (3.7) 392/a, 410 (2.6) 393/a, 412 (0.2) 395/a, 415 (1.2) 398/a, 426 (205.9) 408/a, 439 (15.5) 420/a, 478 (78.3) 457/a, 616 (15.5) 590/a, 619 (0.1) 593/a, 620 (0.0) 593/a, 620 (0.0) 594/a, 628 (47.4) 602/a, 700 (11.4) 670/a, 702 (6.7) 672/a, 717 (70.3) 686/a, 718 (192.3) 687/a, 748 (25.2) 716/a, 884 (0.2) 846/a, 885 (0.4) 847/a, 892 (4.5) 855/a, 894 (1.3) 856/a, 999 (3.9) 956/a,

1000 (4.3) 958/a, 1004 (0.9) 961/a, 1005 (2.3) 962/a, 1007 (0.1) 964/a, 1008 (0.1) 965/a, 1015 (0.1) 972/a, 1018 (0.0) 975/a, 1030 (0.1) 986/a, 1031 (0.1) 987/a, 1054 (4.9) 1009/a, 1055 (4.9) 1010/a, 1057 (3.3) 1012/a, 1057 (3.8) 1012/a, 1178 (7.3) 1128/a, 1179 (2.8) 1129/a, 1184 (109.6) 1133/a, 1197 (0.6) 1146/a, 1200 (0.4) 1149/a, 1201 (3.0) 1150/a, 1201 (1.7) 1150/a, 1332 (0.7) 1275/a, 1333 (0.4) 1277/a, 1382 (0.0) 1324/a, 1383 (0.0) 1324/a, 1506 (8.1) 1442/a, 1506 (9.3) 1442/a, 1507 (9.4) 1443/a, 1508 (20.0) 1444/a, 1588 (39.1) 1521/a, 1619 (13.2) 1550/a, 1622 (4.1) 1553/a, 1623 (9.3) 1554/a, 1626 (1.0) 1557/a, 1628 (6.5) 1559/a, 1765 (108.6) 1690/a, 2220 (2194.0) 2125/a, 3162 (1.1) 3028/a, 3164 (0.3) 3030/a, 3166 (0.4) 3032/a, 3175 (0.0) 3040/a, 3179 (0.1) 3044/a, 3180 (0.1) 3045/a, 3185 (3.8) 3050/a, 3187 (6.1) 3052/a, 3192 (4.7) 3056/a, 3194 (3.0) 3058/a, 3198 (0.5) 3062/a, 3199 (5.1) 3063/a, 3271 (1597.1) 3132/a, 3412 (918.0) 3267/a, 3741 (72.6) 3582/a, 3829 (461.6) 3666/a.

BW-2, 2-Ar (bz₂-H₅O₂Ar)⁺ (benzenes are in “trans” position, Argon on the other OH) DFT

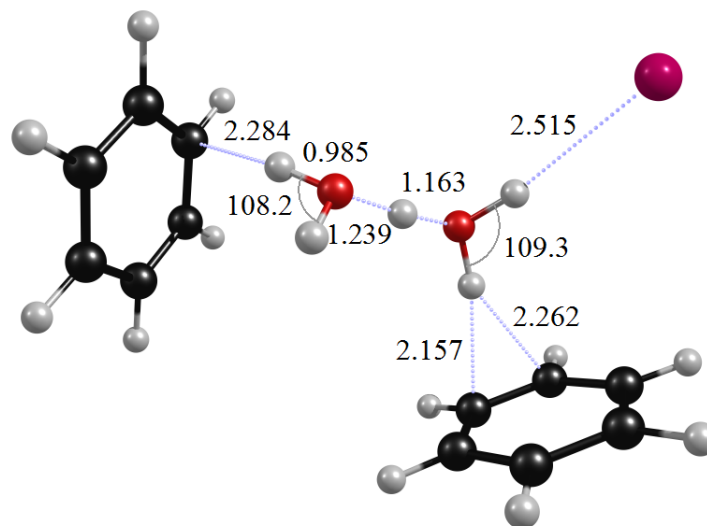
State: ¹A(C₁)

Total Energy = -1145.4649879

ΔE = +0.9

B.E.^a = E (complex)-E (H₃O⁺+H₂O+2*bz+Ar) = 62.1

D.E^b (Ar) = 1.2



Unscaled Frequency (Intensity) Scaled Frequency /Symmetry of vibration

10 (0.3) 10/a, 11 (0.5) 10/a, 14 (1.4) 14/a, 19 (1.5) 18/a, 20 (0.4) 19/a, 26 (0.2) 25/a, 28 (3.4) 26/a, 46 (0.4) 44/a, 48 (4.0) 46/a, 62 (2.4) 59/a, 64 (7.4) 61/a, 78 (6.3) 74/a, 136 (109.9) 130/a, 153 (27.6) 146/a, 260 (71.5) 249/a, 340 (75.8) 326/a, 410 (2.3) 393/a, 411 (1.0) 393/a, 413 (1.0) 395/a, 413 (0.2) 395/a, 491 (124.3) 470/a, 521 (63.4) 499/a, 562 (149.4) 538/a, 611 (91.5) 585/a, 620 (0.1) 593/a, 620 (0.1) 594/a, 620 (0.2) 594/a, 622 (9.8) 595/a, 672 (41.0) 644/a, 703 (0.1) 673/a, 703 (4.9) 673/a, 717 (244.9) 687/a, 723 (107.5) 692/a, 884 (25.3) 846/a, 885 (1.3) 847/a, 888 (87.0) 850/a, 892 (3.2) 854/a, 995 (450.9) 953/a, 1001 (59.8) 959/a, 1003 (3.6) 960/a, 1004 (1.5) 962/a, 1005 (6.8) 962/a, 1006 (0.9) 963/a, 1017 (2.2) 974/a, 1018 (2.0) 975/a, 1029 (0.3) 985/a, 1030 (24.3) 986/a, 1040 (1775.9) 995/a, 1056 (6.0) 1011/a, 1057 (1.0) 1012/a, 1057 (5.8) 1012/a, 1061 (584.6) 1015/a, 1179 (0.2) 1129/a, 1179 (0.1) 1129/a, 1199 (0.6) 1148/a, 1200 (1.3) 1149/a, 1200 (0.1) 1149/a, 1201 (0.5) 1150/a, 1332 (1.4) 1275/a, 1332 (0.3) 1276/a, 1383 (0.0) 1324/a, 1383 (0.0) 1324/a, 1423 (334.5) 1362/a, 1507 (13.1) 1443/a, 1507 (10.0) 1443/a, 1507 (15.9) 1443/a, 1508 (14.1) 1444/a, 1571 (97.6) 1504/a,

1623 (0.4) 1554/a, 1623 (0.5) 1554/a, 1625 (1.8)1556/a, 1626 (0.8) 1557/a, 1684 (10.2) 1613/a, 1731 (879.3) 1658/a,
3166 (0.0) 3032/a, 3167 (0.0) 3033/a, 3176 (0.3) 3041/a, 3176 (0.1) 3041/a, 3177 (0.2) 3042/a, 3177 (0.1) 3042/a,
3188 (3.9) 3053/a, 3189 (5.3) 3053/a, 3190 (6.4) 3054/a, 3191 (6.8) 3055/a, 3198 (0.8) 3062/a, 3199 (1.1) 3063/a,
3379 (1204.6) 3235/a, 3447 (861.4) 3300/a, 3756 (363.1) 3596/a, 3830 (104.7) 3667/a.

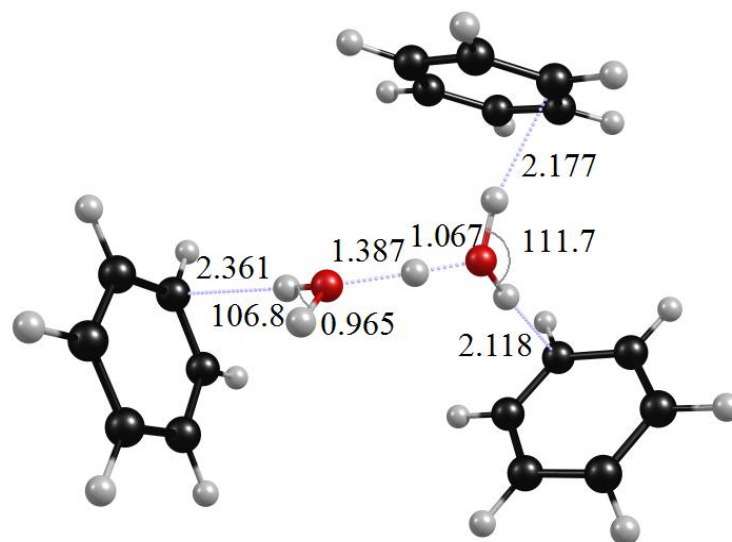
BW-3, 2 (bz₃-H₅O₂)⁺ DFT

State: ¹A(C₁) Total Energy = -850.2350923

ΔE = 0.0

B.E.^a = E (complex) - E (H₃O⁺ + H₂O + 3*bz) = 70.1

D.E.^b (bz) = 7.7



Unscaled Frequency (Intensity) Scaled Frequency /Symmetry of vibration

10 (0.2) 10/a, 13 (0.3) 12/a, 14 (0.2) 14/a, 17 (0.1) 17/a, 18 (0.1) 18/a, 24 (1.0) 23/a, 29 (0.6) 27/a, 31 (0.2) 30/a, 37 (0.8) 36/a, 42 (0.3) 40/a, 44 (1.0) 42/a, 52 (2.5) 50/a, 61 (0.5) 58/a, 90 (4.1) 86/a, 105 (10.3) 100/a, 135 (18.9) 129/a, 178 (37.3) 170/a, 202 (34.2) 194/a, 366 (90.8) 350/a, 409 (0.9) 392/a, 410 (0.2) 393/a, 412 (11.1) 394/a, 412 (1.7) 394/a, 412 (0.7) 395/a, 412 (0.6) 395/a, 422 (114.0) 404/a, 461 (62.0) 441/a, 505 (20.9) 483/a, 593 (34.5) 568/a, 620 (0.1) 594/a, 620 (0.2) 594/a, 620 (0.0) 594/a, 621 (0.1) 594/a, 621 (0.2) 594/a, 621 (0.1) 595/a, 694 (106.8) 665/a, 704 (4.2) 674/a, 705 (6.9) 675/a, 707 (25.8) 677/a, 711 (137.5) 681/a, 718 (52.5) 688/a, 729 (135.6) 698/a, 879 (0.2) 842/a, 881 (0.6) 844/a, 882 (0.1) 844/a,

884 (1.2) 847/a, 890 (8.2) 852/a, 892 (5.0) 854/a, 996 (1.7) 954/a, 1000 (0.5) 958/a, 1000 (1.6) 958/a, 1003 (0.1) 960/a, 1004 (0.1) 961/a, 1005 (4.5) 962/a, 1005 (0.3) 962/a, 1005 (4.8) 962/a, 1006 (0.1) 963/a, 1016 (0.0) 973/a, 1018 (0.0) 975/a, 1020 (0.0) 976/a, 1028 (0.0) 985/a, 1029 (0.1) 985/a, 1029 (0.0) 986/a, 1056 (5.5) 1011/a, 1056 (1.2) 1011/a, 1056 (8.7) 1011/a, 1057 (2.7) 1013/a, 1058 (3.8) 1013/a, 1058 (8.1) 1013/a, 1178 (0.1) 1127/a, 1178 (0.1) 1128/a, 1179 (0.2) 1129/a, 1198 (0.4) 1148/a, 1199 (0.1) 1148/a, 1200 (0.0) 1149/a, 1200 (0.1) 1149/a, 1200 (0.1) 1149/a, 1201 (0.0) 1150/a, 1268 (103.3) 1214/a, 1332 (0.1) 275/a, 1333 (0.9) 1277/a, 1334 (0.5) 1278/a, 1382 (0.0) 1324/a, 1383 (0.0) 1324/a, 1383 (0.0) 1324/a, 1506 (8.1) 1442/a, 1507 (4.1) 1443/a, 1507 (9.9) 1443/a, 1508 (13.9) 1444/a, 1508 (1.6) 1444/a, 1509 (15.1) 1445/a, 1561 (146.0) 1495/a, 1620 (51.9) 1551/a, 1624 (1.2) 1555/a, 1624 (0.3) 1555/a, 1625 (0.3) 1556/a, 1626 (1.8) 1557/a, 1628 (0.6) 1558/a, 1634 (58.8) 1564/a, 1679 (27.1) 1608/a, 2140 (3384.2) 2049/a, 3164 (0.2) 3030/a, 3165 (0.2) 3031/a, 3166 (0.0) 3032/a, 3174 (0.1) 3039/a, 3176 (0.6) 3041/a, 3176 (0.4) 3041/a, 3176 (0.1) 3041/a, 3177 (0.1) 3042/a, 3178 (0.8) 3043/a, 3187 (7.9) 3052/a, 3188 (7.5) 3052/a, 3188 (3.6) 3052/a, 3190 (8.3) 3055/a, 3191 (7.0) 3055/a, 3192 (10.3) 3056/a, 3198 (0.1) 3062/a, 3199 (2.3) 3063/a, 3200 (2.0) 3064/a, 3356 (1432.4) 3214/a, 3367 (1168.7) 3224/a, 3645 (471.2) 3490/a, 3845 (74.6) 3682/a.

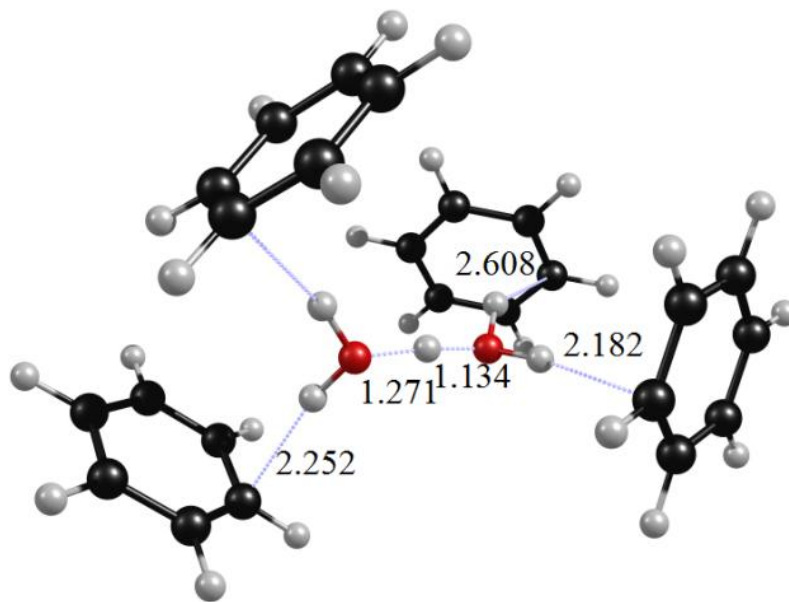
BW-4, 2 isomer-a ($\text{bz}_4\text{-H}_5\text{O}_2^+$)⁺ DFT

State: $^1\text{A}(\text{C}_1)$ Total Energy = -1082.5554622

$\Delta\text{E} = 0.0$

B.E.^a = E (complex) - E ($\text{H}_3\text{O}^+ + \text{H}_2\text{O} + 4*\text{bz}$) = 75.8

D.E.^b (bz) = 5.7



Unscaled Frequency (Intensity) Scaled Frequency /Symmetry of vibration

-8 (0.5) -7/a, -3 (0.0) -3/a, 11 (0.2) 11/a, 18 (0.2) 17/a, 19 (0.0) 18/a, 20 (0.2) 19/a, 22 (0.3) 21/a, 25 (0.9) 24/a, 28 (1.2) 27/a, 31 (0.5) 30/a, 32 (0.1) 30/a, 32 (0.4) 31/a, 34 (0.1) 32/a, 36 (0.1) 35/a, 39 (0.1) 37/a, 43 (3.3) 41/a, 47 (0.2) 45/a, 53 (5.8) 51/a, 59 (0.4) 57/a, 98 (25.0) 94/a, 114 (45.1) 109/a, 149 (13.5) 143/a, 164 (26.5) 157/a, 385 (24.9) 369/a, 409 (3.4) 392/a, 410 (1.6) 392/a, 410 (0.2) 393/a, 411 (6.3) 394/a, 412 (9.6) 395/a, 412 (1.4) 395/a, 414 (10.1) 396/a, 414 (1.3) 397/a, 425 (100.8) 407/a, 446 (110.6) 427/a, 516 (250.6) 495/a, 583 (79.6) 558/a, 607 (7.7) 581/a, 620 (0.3) 594/a, 621 (0.0) 594/a, 621 (0.2) 595/a,

621 (0.1) 595/a, 622 (0.2) 595/a, 622 (0.2) 595/a, 622 (0.4) 595/a, 622 (0.1) 596/a, 647 (24.7) 620/a, 704 (112.1) 674/a, 704 (107.9) 674/a, 705 (122.3) 675/a, 707 (18.8) 677/a, 710 (96.0) 680/a, 711 (83.7) 680/a, 711 (74.8) 681/a, 715 (14.0) 685/a, 875 (0.4) 838/a, 875 (0.7) 838/a, 877 (3.1) 840/a, 879 (0.1) 842/a, 882 (11.7) 845/a, 882 (6.0) 845/a, 885 (5.1) 848/a, 886 (6.9) 848/a, 995 (6.3) 952/a, 996 (13.9) 954/a, 996 (3.7) 954/a, 998 (5.3) 955/a, 1001 (1.4) 958/a, 1001 (0.1) 959/a, 1002 (0.7) 959/a, 1003 (0.3) 960/a, 1005 (37.6) 962/a, 1006 (2.4) 963/a, 1006 (2.6) 963/a, 1007 (0.1) 964/a, 1017 (0.2) 974/a, 1018 (0.0) 974/a, 1018 (0.0) 975/a, 1019 (0.1) 975/a, 1027 (0.2) 984/a, 1028 (0.2) 984/a, 1028 (0.1) 984/a, 1029 (0.1) 985/a, 1056 (36.4) 1011/a, 1056 (5.2) 1012/a, 1057 (2.4) 1012/a, 1057 (4.3) 1012/a, 1058 (4.6) 1013/a, 1058 (2.0) 1013/a, 1058 (5.2) 1013/a, 1059 (6.4) 1014/a, 1168 (2836.6) 1118/a, 1177 (8.7) 1127/a, 1177 (0.5) 1127/a, 1177 (0.2) 1127/a, 1178 (25.9) 1128/a, 1198 (4.8) 1147/a, 1198 (8.9) 1147/a, 1199 (0.5) 1148/a, 1199 (2.6) 1148/a, 1199 (3.5) 1148/a, 1199 (6.7) 1149/a, 1200 (2.1) 1149/a, 1200 (14.0) 1149/a, 1334 (1.6) 1277/a, 1334 (0.9) 1278/a, 1335 (1.8) 1278/a, 1335 (2.4) 1278/a, 1382 (0.0) 1323/a, 1382 (0.0) 1323/a, 1382 (0.0) 1323/a, 1382 (0.0) 1324/a, 1415 (157.7) 1355/a, 1508 (8.2) 1444/a, 1508 (5.5) 1444/a, 1508 (14.6) 1444/a, 1508 (6.1) 1444/a, 1509 (13.8) 1445/a, 1509 (13.9) 1445/a, 1509 (10.7) 1445/a, 1510 (10.6) 1446/a, 1587 (158.1) 1519/a, 1625 (0.2) 1556/a, 1626 (0.3) 1556/a, 1626 (0.1) 1557/a, 1627 (0.1) 1558/a, 1627 (1.6) 1558/a, 1628 (0.4) 1559/a, 1629 (1.6) 1560/a, 1629 (0.6) 1560/a, 1675 (6.9) 1604/a, 1761 (910.6) 1686/a, 3161 (0.5) 3027/a, 3161 (0.5) 3027/a, 3162 (0.1) 3028/a, 3164 (0.2) 3030/a, 3171 (0.2) 3037/a, 3172 (0.4) 3037/a, 3173 (0.3) 3038/a, 3175 (0.4) 3040/a, 3175 (0.5) 3040/a, 3175 (0.5) 3040/a, 3176 (0.4) 3041/a, 3177 (0.8) 3042/a, 3185 (13.3) 3050/a, 3185 (7.1) 3050/a, 3186 (7.2) 3050/a, 3188 (7.8) 3052/a, 3188 (10.1) 3053/a, 3189 (11.3) 3054/a, 3190 (8.3) 3055/a, 3191 (12.2) 3055/a, 3197 (1.3) 3061/a, 3197 (0.5) 3061/a, 3198 (1.0) 3062/a, 3199 (1.1) 3063/a, 3457 (550.0) 3310/a, 3483 (1525.9) 3335/a, 3565 (330.0) 3414/a, 3610 (1169.8) 3457/a.

Table S1: Computed binding energies and relative energies (with respect to the most stable isomer) of $(\text{benzene})_m\text{H}^+(\text{H}_2\text{O})_n\text{Ar}_x$ complexes in kcal/mol. Calculations are done with MP2 and/or B3LYP levels of theory with 6-311+G (d, p) basis set. Energies are not ZPVE or BSSE corrected.

Complex	DFT		MP2	
	B.E.	ΔE	B.E.	ΔE
BW-1, 1 isomer-a ($\text{bz-H}_3\text{O}^+$)	25.0	+3.5	28.7	0.0
BW-1, 1 isomer-b ($\text{bzH-H}_2\text{O}^+$)	11.4	0.0	13.6	+6.2
BW-1, 1-Ar isomer-a ($\text{bz-H}_3\text{O-Ar}^+$)	27.0	+1.9	32.3	0.0
BW-1, 1-Ar isomer-b ($\text{bzH-H}_2\text{O-Ar}^+$)	11.8	0.0	15.5	+7.8
BW-1, 2 isomer-a ($\text{bz-H}_5\text{O}_2^+$)	51.7	0.0	56.5	0.0
BW-1, 2 isomer-b ($\text{bzH-H}_2\text{O}_4^+$)	20.8	+13.7	23.2	+24.3
BW-1, 2-Ar isomer-a ($\text{bz-H}_5\text{O}_2\text{-Ar}^+$) (Argon is "cis" to benzene)	52.8	0.0	59.2	0.0
BW-1, 2-Ar isomer-b ($\text{bz-H}_5\text{O}_2\text{-Ar}^+$) (Argon is "trans" to benzene)	52.5	+0.3	57.7	+1.5
BW-1, 3 isomer-a ($\text{bz-H}_7\text{O}_3^+$)	72.7	0.0	--	--
BW-1, 3 isomer-b ($\text{bzH-H}_6\text{O}_3^+$)	34.6	+21.0	--	--
BW-1, 4 isomer-a ($\text{bz-H}_9\text{O}_4^+$)	89.0	0.0	--	--
BW-1, 4 isomer-b ($\text{bzH-H}_8\text{O}_4^+$)	46.9	+25.0	--	--
BW-2, 1 isomer-a ($\text{bz}_2\text{-H}_3\text{O}^+$)	41.1	0.0	--	--
BW-2, 1 isomer-b ($\text{bz}_2\text{H-H}_2\text{O}^+$)	17.3	+6.6	--	--
BW-2, 2 isomer-a ($\text{bz}_2\text{-H}_5\text{O}_2^+$) bz-cis	62.4	0.0	--	--
BW-2, 2 isomer-a ($\text{bz}_2\text{-H}_5\text{O}_2^+$) bz-trans	61.0	+1.4	--	--
BW-3, 1 isomer-a ($\text{bz}_3\text{-H}_3\text{O}^+$)	51.7	0.0	--	--
BW-3, 1 isomer-b ($\text{bz}_3\text{H-H}_2\text{O}^+$)	22.0	+12.6	--	--